

**Investigation of wear in cervical total disc
replacement under loads and motions that
represent activities of daily living**

Mohamad Faizal Bin Kamarol Zaman

Submitted in accordance with the requirements for the degree of
Doctor of Philosophy

The University of Leeds
School of Mechanical Engineering

December 2023

I confirm that the work submitted is my own and that appropriate credit has been given where reference has been made to the work of others.

This copy has been supplied on the understanding that it is copyright material and that no quotation from the thesis may be published without proper acknowledgement.

© 2023 The University of Leeds and Mohamad Faizal Bin Kamarol Zaman

Acknowledgements

It has been my privilege to be the apprentice for all my supervisors, who are the great masters of their individual crafts. On top of their immeasurable support in this research project, I wish to express my gratitude for their unique contribution in shaping me as a person. Professor Richard M Hall – thank you very much for nuggets of wisdom you gave that I wish I had when I was younger. Professor Anthony Redmond – I am grateful for our fortnightly session, which calmed my anxiety and stopped me from overthinking. Professor Michael Bryant – thank you very much for constantly checking on me and all the philosophical answers to some of scientific inquiries I had, which have instilled in me the true meaning of being a philosophical doctor. Dr Rob Beadling – thank you very much for the lab banter, which has put me at ease from a bag of nerves. Beyond their scientific guidance, they all also have provided me strength during some of the testing times in my personal life – losing my loved ones, suffering from a heart attack, and enduring a global pandemic alone, far from my family.

I also would like to thank all my research colleagues, PGRs and PDRAs, from 2019 to 2023, in Leeds (Rooms X1.01, 3.39A, 3.39, 3.32A, 3.44), Zurich, Uppsala, and Luleå (NuSpine and BioTrib), as well as all the researchers at FASTER in LIRMM for their scientific inputs, given directly or indirectly, as well as words of encouragement that has helped me in many ways. There are too many of you to mention here. I also would like to thank all the technicians (Camille, Mick, Jordan, Graham, *et al.*) as well as the admin support (Judith, Sharif, Alexandra, and Fiona) for their assistance. I should like to acknowledge the European Commission's Horizon 2020 as well as the European community in general for generously funding this research project.

Last but certainly not the least, a big thank you to my family for always supporting me in whatever I do, although they might never understand the work nor content of this thesis. And for bearing the brunt of me, yet still loves me, every time.

“So, surely with hardship comes ease. Surely with that hardship comes more ease.”

Abstract

There are several articulating cervical disc implants available commercially with different mechanical properties. Although their short- and medium-term clinical outcomes have been positive, the long-term impact of this innovation is still unknown, given it has only been introduced into clinical practice relatively recently. Protocols for wear simulation in testing the device do not adequately reflect the loading and motion of the cervical spine in daily life. This two-phase research project aims to investigate the wear of the implant under the loads and motions during activities of daily living.

Ethical approval was granted to recruit research participants performing daily activities involving neck using motion capture equipment. Data were processed and simulated using musculoskeletal multibody modelling to estimate the cervical intervertebral joint angles and contact forces. These outputs were fashioned into a novel wear testing profile and fed into a mechanical joint implant simulator. Wear simulation, based on activities of daily living, was carried out for five million cycles, on top of a separate standard wear test recommended by ISO18192-1. Gravimetric wear rate and surface roughness were assessed.

Results from Phase I have shown that, on average, cervical joint excursions are less than the prescribed angles in ISO18192-1 but joint loading is higher, in general, for all activities studied. Outcomes from Phase II revealed that the wear rate based on parameters from activities of daily living is comparable to wear rate under ISO18192-1 parameters, and the difference is statistically insignificant. Nonetheless, tribological regime during activities of daily living is harsher than the standard test condition based on the wear coefficient estimation. To truly evaluate implant's wear performance *in vivo*, several wear profiles based on activities of daily living must be employed in tandem with an appropriately considered duty cycle, which is estimated between three to five million cycles per year.

Contents

| | |
|---|-------------|
| Acknowledgements | iii |
| Abstract | iv |
| Contents | v |
| List of Figures | xiii |
| List of Tables..... | xxi |
| List of Equations..... | xxiv |
| Abbreviations | xxv |
| Standards | xxvi |
| Chapter 1 Introduction | 1 |
| 1.1 Background and Motivations..... | 1 |
| 1.2 Research Aims..... | 3 |
| 1.3 Research Hypotheses..... | 3 |
| 1.4 Research Scope | 4 |
| 1.5 Thesis Outline | 4 |
| Chapter 2 Literature Review..... | 6 |
| 2.1 Cervical Spinal Disc Implant in Clinical Context..... | 6 |
| 2.1.1 Description of Structure and Function of the Spine..... | 6 |
| 2.1.2 Cervical Spine and its Pathologies..... | 9 |
| 2.1.3 Cervical Total Disc Replacement | 12 |
| 2.1.4 Unwanted Complications | 14 |
| 2.1.5 Financial Incentives | 15 |
| 2.1.6 Short Summary..... | 16 |
| 2.2 Innovation in Spinal Intervertebral Disc Implants | 16 |
| 2.2.1 Evolution of the Technology..... | 16 |
| 2.2.2 Biomaterials for Spinal Intervertebral Disc Implants..... | 19 |

| | |
|---|----|
| 2.2.3 Contemporary Cervical Disc Prostheses | 20 |
| 2.2.4 Short Summary | 22 |
| 2.3 Tribological Performance of the Articulating Spinal Disc Devices | 23 |
| 2.3.1 Wear Testing on Cervical Spinal Disc Implants | 23 |
| 2.3.2 Lubrication Regime within the Spinal Disc Implants..... | 28 |
| 2.3.3 Frictional Torque Subjected to Spinal Disc Implants..... | 31 |
| 2.3.4 Mechanisms of Wear in Spinal Disc Implants | 32 |
| 2.3.5 Surface Analysis Methodology..... | 33 |
| 2.3.6 Consequences from Wear of Spinal Disc Implants and Biological Responses..... | 38 |
| 2.3.7 Short Summary | 40 |
| 2.4 ISO18192-1 Wear Testing Equipment, Parameters, and Protocols | 40 |
| 2.4.1 Spinal Disc Implant Wear Testing Protocols | 41 |
| 2.4.2 Motion Profiles and Cross Shear | 43 |
| 2.4.3 Axial Load Profile | 44 |
| 2.4.4 Angular Displacement Profiles..... | 46 |
| 2.4.5 Duty Cycle | 48 |
| 2.4.6 Degree of Freedom Coverage | 49 |
| 2.4.7 Frequency of Load and Motion | 49 |
| 2.4.8 Cyclical Motion Conundrum | 50 |
| 2.4.9 Short Summary | 51 |
| 2.5 Cervical Spine Biomechanics | 52 |
| 2.5.1 Spinal Kinematics and Soft Tissue Artefacts | 54 |
| 2.5.2 Tracking the Movement of Cervical Spinal Vertebrae | 55 |
| 2.5.3 Other Methods of Cervical Kinematics Study..... | 56 |
| 2.5.4 Estimation of Biomechanical Forces..... | 57 |
| 2.5.5 Inverse Dynamics Study | 57 |

| | |
|---|-----------|
| 2.5.6 Muscle Recruitment Algorithm | 59 |
| 2.5.7 Muscle Modelling | 59 |
| 2.5.8 Biomechanical Modelling of the Cervical Spine | 60 |
| 2.5.9 Musculoskeletal Multibody Modelling..... | 61 |
| 2.5.10 Other Methods for Predicting Cervical Spinal Loading..... | 63 |
| 2.5.11 Activities of Daily Living in the Context of Cervical Spine | 63 |
| 2.5.12 Short Summary..... | 65 |
| 2.6 Summary of Literature Review..... | 66 |
| 2.7 Hypotheses..... | 67 |
| 2.8 Aims and Objectives | 68 |
| 2.9 Overall Research Project Workflow | 70 |
| Chapter 3 Study of Cervical Spine Biomechanics During Activities of Daily Living | 71 |
| 3.1 Methods | 73 |
| 3.1.1 Ethics and Covid-safety Measures..... | 73 |
| 3.1.2 Definition for Activities of Daily Living Involving Cervical Spine | 74 |
| 3.1.3 Recruitment of Study Participants for Cervical Biomechanics Study..... | 75 |
| 3.1.4 Motion Capture Method and Equipment | 76 |
| 3.1.5 Kinematics and Inverse Dynamic Data Processing | 78 |
| 3.1.5.1 Folder Setup | 78 |
| 3.1.5.2 Model Configuration..... | 80 |
| 3.1.5.3 Environment and Lab Setup | 81 |
| 3.1.5.4 Subject Setup | 82 |
| 3.1.5.5 Trial Setup | 82 |
| 3.1.5.6 Simulation Studies and Output | 82 |
| 3.1.6 Simulation Output Data Extraction | 84 |

| | |
|---|-----|
| 3.1.7 Cervical Biomechanics Data Analysis | 85 |
| 3.1.8 Formulation of New Wear Test Profile | 86 |
| 3.2 Results | 87 |
| 3.2.1 Selection of Activities Daily Living Involving the Cervical Spine | 87 |
| 3.2.2 Motion Capture Data Processing | 89 |
| 3.2.3 Multibody Modelling Simulation | 89 |
| 3.2.4 Cervical Joint Kinematics | 94 |
| 3.2.5 Cervical Joint Loading | 101 |
| 3.2.7 Newly Formulated Wear Test Profiles for Cervical Disc Implant | 114 |
| 3.3 Discussion | 118 |
| 3.3.1 Selection of Activities of Daily Living Involving the Cervical Spine | 118 |
| 3.3.2 Participants' Demographic for Cervical Biomechanics Study .. | 118 |
| 3.3.3 Skin Marker and Soft Tissue Artefact in Study of Cervical Spine | 119 |
| 3.3.4 Unsuccessful Multibody Modelling Simulations | 119 |
| 3.3.5 Kinematics Analysis | 120 |
| 3.3.5.1 Kinematics Validation | 120 |
| 3.3.5.2 Kinematics Variations | 127 |
| 3.3.6 Inverse Dynamics | 128 |
| 3.3.6.1 Verification of Cervical Muscle Modelling | 128 |
| 3.3.6.2 Cervical Muscle Recruitment Validation | 131 |
| 3.3.6.3 Cervical Intervertebral Joint Loading Validation | 135 |
| 3.3.6.4 Variation in Cervical Joint Loading | 138 |
| 3.3.7 Phase I: Cervical Biomechanics Study Limitations | 139 |
| 3.3.8 ADL Wear Testing Profiles | 143 |

| | |
|---|------------|
| 3.4 Summary | 145 |
| Chapter 4 Study of Mechanical Wear Simulation on Articulating Cervical Disc Implants | 146 |
| 4.1 Methods..... | 148 |
| 4.1.1 Replica Design of Cervical Spinal Disc Implant Bearing Surfaces..... | 148 |
| 4.1.1.1 Replica's Convex Bearing Surface | 148 |
| 4.1.1.2 Replica's Concave Bearing Surface | 149 |
| 4.1.1.3 Radial Clearance and Nominal Contact Area | 149 |
| 4.1.2 Joint Simulator for Cervical Disc Implant Wear Testing | 150 |
| 4.1.3 Parameters for Wear Tests | 151 |
| 4.1.3.1 Standard Wear Test and Settings for Simulator | 152 |
| 4.1.3.2 ADL Wear Test and Settings for Simulator | 152 |
| 4.1.4 Wear Test Protocol | 155 |
| 4.1.4.1 Preparations of Implant Replica's Convex and Concave Bearing Parts..... | 155 |
| 4.1.4.2 Test Cell Setup | 156 |
| 4.1.4.3 Fluid Test Medium | 157 |
| 4.1.4.4 Pilot Test for Simulation Output Verification | 158 |
| 4.1.4.5 Wear Test Simulation | 158 |
| 4.1.5 Gravimetric Analysis | 158 |
| 4.1.6 Estimation of Sliding Distance and Aspect Ratio from Wear Profiles for the Simulation..... | 159 |
| 4.1.6.1 Estimation of Sliding Distance, L | 160 |
| 4.1.6.2 Estimation of Aspect Ratio for Individual Point's Motion Path | 162 |
| 4.1.7 Surface Roughness Measurement..... | 163 |
| 4.2 Results | 165 |

| | | |
|---------|--|-----|
| 4.2.1 | ISO18192-1 Wear Test on Cervical Disc Replicas..... | 165 |
| 4.2.1.1 | Pre-simulation UHMWPE Fluid Sorption | 165 |
| 4.2.1.2 | ISO18192-1 Pilot Test Output Verification..... | 166 |
| 4.2.1.3 | UHMWPE Gravimetric Wear Rate..... | 167 |
| 4.2.1.4 | Analysis of Variance | 169 |
| 4.2.1.5 | Motion Path, Sliding Distance, and Aspect Ratio..... | 170 |
| 4.2.1.6 | UHMWPE Bearing Surface Analysis | 173 |
| 4.2.2 | ADL Flexion/Extension Wear Test on Cervical Disc Replicas | 179 |
| 4.2.2.1 | Pre-simulation UHMWPE Fluid Sorption | 179 |
| 4.2.2.2 | ADL Flexion/Extension Pilot Test Output Verification .. | 180 |
| 4.2.2.3 | UHMWPE Gravimetric Wear Rate..... | 182 |
| 4.2.2.4 | Analysis of Variance | 184 |
| 4.2.2.5 | Motion Path, Sliding Distance, and Aspect Ratio..... | 185 |
| 4.2.2.6 | UHMWPE Bearing Surface Analysis | 188 |
| 4.3 | Discussion | 194 |
| 4.3.1 | Cervical Spinal Disc Implant Replica Design | 196 |
| 4.3.2 | Output Verification During Pilot Simulations..... | 197 |
| 4.3.3 | Bedding-in Phase..... | 198 |
| 4.3.4 | ISO18192-1 Gravimetric Wear Rate Validation..... | 198 |
| 4.3.5 | Statistical Comparison of Wear Rate between ISO18192- 1 and ADL Flexion/Extension Simulations | 199 |
| 4.3.6 | Tribological Regime | 202 |
| 4.3.6.1 | Normal (Axial) Load Applied, W | 202 |
| 4.3.6.2 | Sliding Distance, L | 203 |
| 4.3.6.3 | Estimation of Wear Coefficients..... | 204 |
| 4.3.6.4 | Estimation of Aspect Ratio for Individual Motion Path .. | 206 |
| 4.3.7 | Surface Roughness Analysis | 209 |

| | | |
|--|--|------------|
| 4.3.8 | Phase II: Mechanical Wear Simulation Study Limitations ... | 211 |
| 4.4 | Summary | 212 |
| Chapter 5 Overall Discussion and Conclusion | | 214 |
| 5.1 | Review of the Achievement on the Research Objectives..... | 214 |
| 5.2 | Hypotheses Validation | 216 |
| 5.3 | Scientific Advancements | 223 |
| 5.3.1 | Catalogue of Cervical Intervertebral Joint Loadings and Motion during Different Activities of Daily Living..... | 223 |
| 5.3.2 | Mechanical Wear Simulation of Articulating Cervical Disc Implant under Loading and Motion that Represent Activities of Daily Living..... | 224 |
| 5.4 | Discussion and Review on the Overall Aims of the Research Project | 224 |
| 5.5 | Limitations of Current Research Project | 228 |
| 5.6 | Potential Publications..... | 230 |
| 5.7 | Consideration for Future Research | 231 |
| 5.8 | Final Conclusions..... | 232 |
| 5.8.1 | Conclusions from Study of Cervical Spine Biomechanics During Activities of Daily Living | 232 |
| 5.8.2 | Conclusion from Study of Mechanical Wear Simulation on Articulating Cervical Disc Implants | 233 |
| 5.8.3 | Overall Conclusion..... | 234 |
| References..... | | 236 |
| Appendices..... | | 262 |
| Appendix A | Ethics Approval from Engineering and Physical Sciences Ethics Committee (MEEC) | 262 |
| Appendix B | PPIE Notes from Cervical/Neck Problem Focus Group (ADL discussed are highlighted in grey) | 263 |

| | | |
|-------------------|--|-----|
| Appendix C | Programming Codes for Musculoskeletal Modelling in AnyBody Modeling System..... | 264 |
| (a) | Simulation output pathway definition..... | 264 |
| (b) | C3D file input pathway definition..... | 264 |
| (c) | Configuration of the body model..... | 264 |
| (d) | Configuration of weak drivers for the mannequin..... | 265 |
| (e) | Settings for LumpedHyoid muscle strength parameters..... | 265 |
| (f) | Setting for direction of gravity..... | 265 |
| (g) | Setup for force plates..... | 266 |
| (h) | Input setup for individual subject's height and weight..... | 266 |
| (i) | Setup for trial file of the captured task..... | 266 |
| (j) | Optimisation setup for anthropometric measurement..... | 267 |
| (k) | Setup for MarkerFilterIndex value during Parameter Identification simulation study..... | 267 |
| Appendix D | Engineering Drawings for Replica of Cervical Disc Implant | 268 |
| (a) | Design for CoCrMo concave part..... | 268 |
| (b) | Design for UHMWPE convex part..... | 269 |
| Appendix E | 128-point Wear Profiles for LifeLongJoint Hip Simulator Input..... | 270 |
| (a) | <i>ISO18192-1 Cervical.txt</i> | 270 |
| (b) | <i>ADL Flex/Ext Cervical.txt</i> | 271 |
| Appendix F | Estimation of Lubrication Regime Based on Replica of Implant during Worst-case Scenarios..... | 272 |
| Appendix G | Permissions for Reproduction of Copyrighted Images | 276 |

List of Figures

| | |
|--|----|
| Figure 1.1 The national incidence of (a) lumbar and (b) cervical total disc replacements in the United States between 2005 to 2017 [6] | 1 |
| Figure 2.1 Regions of vertebral column in human..... | 6 |
| Figure 2.2 Superior view of lumbar vertebra depicting typical feature of neural arch..... | 8 |
| Figure 2.3 Example of a functional spinal unit from thoracic region | 8 |
| Figure 2.4 Rotational motion of the head in three main axes | 9 |
| Figure 2.5 Different permutations of articulating disc prostheses..... | 17 |
| Figure 2.6 Constraining classification for cervical disc implants; unconstrained device can be further split into (a) non-conformal gliding surfaces, (b) different articulating couplings, and (c) deformable core [67]..... | 18 |
| Figure 2.7 Commercially available cervical disc implants [66, 76] | 22 |
| Figure 2.8 Stribeck Diagram (reproduced from [105])..... | 29 |
| Figure 2.9 Modified Stribeck Curve (reproduced from [108]) | 29 |
| Figure 2.10 An example of profile surface topography (top line) when filtered through according to its wavelength to reveal surface waviness (middle line, after low-pass filter) and surface roughness (bottom line, after high-pass filter) (reproduced from [127])..... | 36 |
| Figure 2.11 Representation of centre line average, R_a , calculation over L measurement length where the area shaded blue is equal to the area shaded red (reproduced from [127]) | 37 |
| Figure 2.12 Phasing, including its tolerances (shaded region), of the load and displacement curves for cervical intervertebral disc prostheses (reproduced from ISO18192-1 [1]) | 42 |
| Figure 2.13 Box-and-whisker plot of statistical analysis between ISO and ASTM wear testing protocols [121] | 44 |

| | |
|---|-----|
| Figure 2.14 Intradiscal load at C5-C6 disc level from a kinematic simulation with superimposed ISO18192 [1] axial load input parameters in red (x-axis not to scale) [100]..... | 45 |
| Figure 2.15 Average of total force at C2 level from 16 subjects during head movement from full flexion to full extension and vice versa [158]..... | 46 |
| Figure 2.16 An illustration of linked-segment model as a representation for lower limb of a human (adapted and reproduced from [173]) | 53 |
| Figure 2.17 Schematic diagram that represent Hill's muscle model (reproduced from [174]) | 60 |
| Figure 2.18 General workflow of activities involved in the current research project..... | 70 |
| Figure 3.1 Workflow for activities involved in Phase I | 72 |
| Figure 3.2 Conventional full body reflective marker set developed by Vicon..... | 77 |
| Figure 3.3 AnyBody programming class structure for data processing | 79 |
| Figure 3.4 Axes definitions set by International Society of Biomechanics (left) and ISO18192-1 [1] (right). Positive direction of motion indicated by the direction of arrows [1, 224]..... | 86 |
| Figure 3.5 An example of a successful simulation from Subject 6's WAT trial..... | 90 |
| Figure 3.6 Motion capture data processing where markers were 'labelled' and 'linked' to form body segments..... | 91 |
| Figure 3.7 Assessment of processed motion capture data from a WAT trial where the trajectories were checked for 'completeness' | 92 |
| Figure 3.8 Normalised cervical joint excursions for all trials for all ADL tasks | 97 |
| Figure 3.9 Normalised cervical joint loading for all trials for all tasks | 106 |
| Figure 3.10 Combined overall normalised cervical joint kinematics and loading | 110 |
| Figure 3.11 ADL Looking before Crossing (TRA) Wear Test Profile | 115 |

| | |
|---|-----|
| Figure 3.12 ADL Bending Down (BND) Wear Test Profile | 115 |
| Figure 3.13 ADL Stand-sit-stand (StS+SiS) Wear Test Profile | 116 |
| Figure 3.14 ADL Flexion/Extension (MOB+WAT) Wear Test Profile | 117 |
| Figure 3.15 ADL Adverse Condition Wear Test Profile | 117 |
| Figure 3.16 Mean cervical intervertebral joint excursion during flexion/extension compared against normal cervical kinematics prediction bands between C1 to C4 [185]...... | 124 |
| Figure 3.17 Mean cervical intervertebral joint excursion during flexion/extension compared against normal cervical kinematics prediction bands between C4 to C7 [185]...... | 125 |
| Figure 3.18 Mean cervical intervertebral joint excursion during axial rotation compared against normal cervical kinematics prediction bands between C3 to C7 [185] | 126 |
| Figure 3.19 Graphical representation of left and right 'LumpedHyoidT1C0', which is highlighted in the multibody modelling, without any intervening hyoid bone. | 129 |
| Figure 3.20 Muscle force contribution from 'LumpedHyoidT1C0' and cervical joint contact force at C5-C6 vertebral level during neck extension motion (WAT) in Subject 5 Trial 2..... | 130 |
| Figure 3.21 Muscle force contribution and cervical joint contact force at C5-C6 vertebral level during neck extension motion (WAT) in Subject 5 Trial 2 with the omission of 'LumpedHyoidT1C0' | 131 |
| Figure 3.22 Activation of deep cervical flexor (DCF, longi colli and longi capitis) during head flexion from neutral position as seen in EMG study [235] (bottom diagram) and the corresponding muscle recruitment seen in this study (top diagram). In the EMG study by Falla <i>et al.</i> [235], data were collected whilst subject was supine. Subjects were required to lift their heads off the bed for cervical flexion (CF) and only nodding their head without lifting their heads off the bed for cranio-cervical flexion (CCF). Other activities are jaw-clenching (JC), jaw-opening (JO), and head rotation to right (R-ROT) and left (L-ROT). | 133 |

| | |
|---|-----|
| Figure 3.23 Activation of sternocleidomastoids (SCM _{l & r}) during head flexion from neutral position and return as seen in EMG study [236] (bottom diagram, top two lines) and the corresponding muscle recruitment seen in this study (top diagram, red lines). Eccentric contraction by the sternocleidomastoids is also observed in both diagrams in the second half of the trial. Extensor components (splenii and semispinales capitis; SPL _{l & r} , SSC _{l & r} , green and purple lines) were eccentrically contracting during the first half and concentrically contracting during the second half in both studies. | 134 |
| Figure 3.24 Co-contraction ratio during head flexion from neutral position (left dashed box, 0.9) compared to flexed head back to neutral position (right dashed box, 0.1) [236]. | 135 |
| Figure 3.25 Comparison of cervical axial joint loading at C1-C2 vertebral level from this study (dash lines) superimposed over results from Anderst <i>et al.</i> [158] (solid lines). | 136 |
| Figure 4.1 Workflow for activities involved in Phase II | 147 |
| Figure 4.2 Design features of UHMWPE convex bearing part | 148 |
| Figure 4.3 Design features of CoCrMo concave bearing part | 149 |
| Figure 4.4 3-station, electromechanical LLJ hip joint simulator..... | 151 |
| Figure 4.5 Comparison of axis orientation for kinematics and loadings between a typical left hip (blue) and cervical vertebra (red) wear simulation in ISO18192-1 [1] (top) and ADL Flexion/Extension (bottom) wear tests | 154 |
| Figure 4.6 Schematic diagram of test cell assembly (top) and its cross-section (bottom) | 157 |
| Figure 4.7 Location of thirteen discrete points on concave surface of CoCrMo part for calculation of motion path (top: inferior view, bottom: cross-section view) | 160 |

| | |
|---|-----|
| Figure 4.8 An illustration of a conversion from index coordinate point to the next incremental coordinate based on angular displacement of flexion/extension, lateral bending, axial rotation given in wear profile | 162 |
| Figure 4.9 Illustration of the location of the scanned area from the UHMWPE convex bearing surface | 164 |
| Figure 4.10 Percentage of incremental mass change of UHMWPE convex parts over 24 hours during soaking protocol prior to ISO18192-1 [1] wear simulation..... | 165 |
| Figure 4.11 Sample of load cells' angular displacement readings during pilot run of ISO18192-1 [1] wear simulation against its tolerances (shaded grey)..... | 166 |
| Figure 4.12 Sample of load cells' axial loading readings during pilot run of ISO18192-1 [1] wear simulation against its tolerances (shaded grey) | 167 |
| Figure 4.13 Cumulative uncorrected mass loss of all UHMWPE convex parts during ISO18192-1 [1] wear simulation..... | 168 |
| Figure 4.14 Cumulative net mass loss of sliding UHMWPE convex parts during ISO18192-1 [1] wear simulation after being offset by soak control..... | 168 |
| Figure 4.15 Average (\pm standard deviation) wear rate of sliding UHMWPE convex parts during ISO18192-1 [1] wear simulation based on linear regression..... | 169 |
| Figure 4.16 Three-dimensional motion path for thirteen discrete points on the surface of UHMWPE convex part during ISO18192-1 [1] wear simulation..... | 171 |
| Figure 4.17 Two-dimensional projection of motion path for thirteen discrete points during ISO18192-1 wear simulation..... | 172 |
| Figure 4.18 An illustration of the location of 100 stitched scanned images at 20 \times magnification for course visual assessment | 173 |
| Figure 4.19 Bearing surface of UHMWPE Part 012 at 0.6 MC of ISO18192-1 [1] wear simulation..... | 174 |

| | |
|---|-----|
| Figure 4.20 Bearing surface of UHMWPE Part 014 at 4.5 MC of ISO18192-1 [1] wear simulation..... | 174 |
| Figure 4.21 Bearing surface of UHMWPE Part 016 at 0.6 MC of ISO18192-1 [1] wear simulation..... | 175 |
| Figure 4.22 Bearing surface of UHMWPE Part 018 (soak control) at 5.0 MC of ISO18192-1 [1] wear simulation | 175 |
| Figure 4.23 Location of qualitative visual assessment of the polar region of UHMWPE convex part at 10× magnification relative to the scanned area | 176 |
| Figure 4.24 Average surface roughness of bearing surface on UHMWPE convex parts during ISO18192-1 [1] wear simulation | 178 |
| Figure 4.25 Location of 1 mm ² sampled bearing surface on UHMWPE convex parts for S _a measurement during ISO18192-1 [1] wear simulation..... | 178 |
| Figure 4.26 Average surface roughness of 1 mm ² sampled bearing surface on UHMWPE convex parts during ISO18192-1 [1] wear simulation..... | 179 |
| Figure 4.27 Percentage of incremental mass change of UHMWPE convex parts over 24 hours during soaking protocol prior to ADL Flexion/Extension wear simulation..... | 180 |
| Figure 4.28 Sample of load cells' angular displacement readings during pilot run of ADL Flexion/Extension wear simulation against its own tolerances (shaded grey) | 181 |
| Figure 4.29 Sample of load cells' readings during pilot run of ADL Flexion/Extension wear simulation against its own tolerances (shaded grey). Solid lines (top three curves) represent the axial loadings whereas the dashed lines (bottom three curves) represent the anteroposterior loadings for all three stations. | 182 |
| Figure 4.30 Cumulative uncorrected mass loss of individual UHMWPE convex parts during ADL Flexion/Extension wear simulation..... | 183 |
| Figure 4.31 Cumulative net mass loss of individual UHMWPE convex parts during ADL Flexion/Extension wear simulation..... | 183 |

| | |
|---|-----|
| Figure 4.32 Average (\pm standard deviation) wear rate of UHMWPE convex parts during ADL Flexion/Extension wear simulation..... | 184 |
| Figure 4.33 Three-dimensional motion path for thirteen discrete points on the surface of UHMWPE convex part during ADL Flexion/Extension wear simulation..... | 186 |
| Figure 4.34 Two-dimensional projection of motion path for thirteen discrete points during ADL Flexion/Extension wear simulation..... | 187 |
| Figure 4.35 An illustration of the location of 100 stitched scanned images at 20 \times magnification for course visual assessment | 188 |
| Figure 4.36 Bearing surface of UHMWPE Part 011 at 4.5 MC of ADL Flexion/ Extension wear simulation..... | 189 |
| Figure 4.37 Bearing surface of UHMWPE Part 013 at 0.3 MC of ADL Flexion/ Extension wear simulation..... | 189 |
| Figure 4.38 Bearing surface of UHMWPE Part 015 at 2.0 MC of ADL Flexion/ Extension wear simulation..... | 190 |
| Figure 4.39 Bearing surface of UHMWPE Part 017 (soak control) at 5.0 MC of ADL Flexion/Extension wear simulation | 190 |
| Figure 4.40 Location of qualitative visual assessment of the polar region of UHMWPE convex part at 10 \times magnification relative to the scanned area..... | 191 |
| Figure 4.41 Average surface roughness of bearing surface on UHMWPE convex parts during ADL Flexion/Extension wear simulation..... | 193 |
| Figure 4.42 Location of 1 mm ² sampled bearing surface on UHMWPE convex parts for S _a measurement during ADL Flexion/Extension wear simulation..... | 193 |
| Figure 4.43 Average surface roughness of 1 mm ² sampled bearing surface on UHMWPE convex parts during ADL Flexion/Extension wear simulation..... | 194 |

| | |
|---|-----|
| Figure 4.44 Graph showing the differences in magnitude and phasing of angular displacement between the two sets of wear simulations carried out..... | 195 |
| Figure 4.45 Graph showing the differences in magnitude and phasing of joint loadings between the two sets of wear simulations carried out.. | 196 |
| Figure 4.46 Comparison of wear rates between ISO18192-1 [1] (blue) and ADL Flexion/Extension (red) wear profiles..... | 200 |
| Figure 4.47 Comparison of wear rates between ISO18192-1 [1] (blue) and ADL Flexion/Extension (red) wear profiles without outliers | 201 |
| Figure 4.48 Comparison of flexion/extension angle and axial loading parameters between ISO18192-1 [1] (grey) and ADL Flexion/Extension (coloured) wear profiles | 203 |
| Figure 4.49 The comparison of integration between axial load and distance traversed curves at the pole (Point 1) between ISO18192-1 [1] (blue, 545 N mm) and ADL Flexion/Extension (red, 430 N mm) after one profile cycle..... | 205 |
| Figure 4.50 Two-dimensional projection of motion path for thirteen discrete points during ISO18192-1 [1] and ADL Flexion/Extension wear simulations | 206 |
| Figure 4.51 Comparison of calculation of motion path's aspect ratio on the eleventh point between ISO18192-1 [1] (blue, left) and ADL Flexion/Extension (red, right) | 207 |
| Figure 4.52 Comparison of two-dimensional projection of motion path for thirteen discrete points between ADL Flexion/Extension (red) and ADL Looking at Traffic (purple) wear profiles..... | 208 |
| Figure 5.1 Joint contact forces calculated by Snijders <i>et al.</i> [157] during flexion/extension. Solid curve line labelled FK represents loading at C2-C3 level. The magnitude can be seen to be dipped lower than 50 N between (-)30° and (-)60° head extension..... | 220 |

List of Tables

| | |
|---|----|
| Table 2.1 Treatment algorithm for degenerative cervical spine disease (adapted from [24]) | 10 |
| Table 2.2 Summary of FDA approved intervertebral disc devices properties to date [5, 64, 75, 83] | 21 |
| Table 2.3 Surface topography methods used in implant bearings | 35 |
| Table 2.4 Parameter values, including its tolerance, prescribed by the ISO18192-1 for cervical intervertebral disc prostheses wear testing (adapted from [1]) | 42 |
| Table 2.5 Mean (and standard deviation) of cervical intervertebral discs RoM. | 47 |
| Table 2.6 List of common ADL tasks found in literature [163, 210-213]...... | 64 |
| Table 3.1 List of prompts given to the participants of the focus group discussion | 75 |
| Table 3.2 Gender, age, height, weight, and BMI of participants for the study | 76 |
| Table 3.3 Anatomical location for conventional full body marker set..... | 77 |
| Table 3.4 Output matrix for simulation analysis for one ADL task captured..... | 84 |
| Table 3.5 Tasks selected for the current study as representative of ADL involving cervical spine | 88 |
| Table 3.6 Description of situation for ADL tasks simulation | 88 |
| Table 3.7 Summary of outcome from kinematics (Kin) and inverse dynamic (Inv Dyn) simulations for all recorded trials from all subjects for all ADL task | 93 |
| Table 3.8 Mean cervical joint ranges for all ADL tasks in all directions (bolded magnitude indicates the main direction of the motion; underlined value indicates when the RoM is more than 50% of the range in the main direction of motion)..... | 94 |

| | |
|--|-----|
| Table 3.9 Cervical intervertebral joint angle (°) and joint range (°) for all of subjects for MOB, WAT, TRA, and LUL trials in flexion/extension (FE) , lateral bending (LB) , and axial rotation (AR) directions | 95 |
| Table 3.10 Cervical intervertebral joint angle (°) and joint range (°) for all of subjects for REV, BND, StS, and SiS trials in flexion/extension (FE) , lateral bending (LB) , and axial rotation (AR) directions | 96 |
| Table 3.11 Minimum (Min) and maximum (Max) cervical (superoinferior) axial loading (Newtons) for all subjects for all ADL trials (+ in direction of gravity) | 103 |
| Table 3.12 Minimum (Min) and maximum (Max) cervical mediolateral loading (Newtons) for all subjects for all ADL trials (+ in right direction) | 104 |
| Table 3.13 Minimum (Min) and maximum (Max) cervical anteroposterior loading (Newtons) for all subjects for all ADL trials (+ in anterior direction) | 105 |
| Table 3.14 Comparison of average angle (°) between the head and thorax during five ADL tasks in the current study against Cobian <i>et al.</i> [163]..... | 121 |
| Table 3.15 Comparison of individual cervical joint C5-C6 angle range between this study and Cobian <i>et al.</i> [15]. | 122 |
| Table 3.16 Comparison between ADL tasks RoM and full RoM of individual cervical vertebral joint level in pure flexion/extension movement of the head. | 123 |
| Table 3.17 Comparison between ADL tasks RoM and full RoM of individual cervical vertebral joint level in pure axial rotation movement of the head. | 123 |
| Table 3.18 Main differences in biomechanical multibody modelling between this study and Anderst <i>et al.</i> [158]. | 138 |
| Table 3.19 Coefficient of linear relationship between overall lumbar motion and motion of individual lumbar vertebrae [242] | 140 |

| | |
|---|-----|
| Table 4.1 Summary of orientation of kinematics and loading parameters for both ISO18192-1 [1] and ADL Flexion/Extension wear simulations..... | 154 |
| Table 4.2 The estimation on sliding distance of thirteen discrete points during ISO18192-1 [1] wear simulation..... | 172 |
| Table 4.3 Sequential bearing surface image of UHMWPE convex parts during the last 1.5 MC of ISO18192-1 [1] wear simulation at 10× magnification..... | 177 |
| Table 4.4 The estimation on sliding distance of thirteen discrete points during ADL Flexion/Extension wear simulation..... | 187 |
| Table 4.5 Sequential bearing surface image of UHMWPE convex parts during the last 1.5 MC of ADL Flexion/Extension wear simulation..... | 192 |
| Table 4.6 Summary of input differences between the two sets of wear simulation carried out in this study..... | 195 |
| Table 4.7 Comparison of wear rates under ISO18192-1 [1] between commercially available articulating cervical disc implants and replicas in the current study..... | 199 |
| Table 4.8 Table of comparison on sliding distance of thirteen discrete points between ISO18192-1 [1] and ADL Flexion/Extension wear profiles..... | 204 |
| Table 4.9 Table of comparison on aspect ratio of the 13 discrete, tracking points between ISO18192-1 and ADL Flexion/Extension wear profiles..... | 207 |
| Table 4.10 Table of comparison on change of surface roughness on UHMWPE convex part between current study and Hyde [256]..... | 210 |
| Table 5.1 Comparison of mean (and standard deviation) cervical intervertebral joint angles from C3 to C7 levels between studies..... | 218 |
| Table 5.2 Comparison of axial loading estimation based from several studies at C2-C3 and C1-C2 cervical intervertebral levels during head flexion/extension and axial rotation as well as ISO18192-1 [1] wear test parameters (\approx indicates approximation value obtained from published graph with ± 25 N uncertainty error)..... | 221 |

| | |
|---|-----|
| Table 5.3 The estimation for mass loss of UHMWPE from cervical disc implant after ten years of device implantation based on outcomes from both simulations..... | 225 |
|---|-----|

List of Equations

| | |
|--|-----|
| Equation 2.1 Archard's Volumetric Wear Equation | 24 |
| Equation 2.2 Lambda ratio | 30 |
| Equation 2.3 Centre-line average, R_a | 36 |
| Equation 2.4 Root-mean-square, R_q | 36 |
| Equation 2.5 Forward dynamics | 57 |
| Equation 2.6 Inverse dynamics | 58 |
| Equation 3.1 [242] Linear function motion for each individual lumbar vertebra from total movement of the lumbar region | 140 |
| Equation 4.1 Spherical cap area, S | 150 |
| Equation 4.2 Net mass loss for UHMWPE part | 159 |
| Equation 4.3 Linear fit for overall wear rate, α_G , from wear simulation | 159 |
| Equation 4.4 [249] 3D coordinate conversion matrix for incremental motion | 161 |
| Equation 4.5 [250] Sliding distance | 162 |
| Equation 4.6 [250] Zenithal equidistant projection | 163 |
| Equation 4.7 Wear coefficient | 204 |

Abbreviations

| | |
|--------|---|
| ACDF | anterior cervical discectomy and fusion |
| ADL | activities of daily living |
| AMMR | AnyBody Musculoskeletal Modeling Repository |
| ASTM | ASTM International |
| CoCrMo | cobalt-chromium-molybdenum alloy |
| CTDR | cervical total disc replacement |
| DoF | degree of freedom |
| EMG | electromyography / electromyogram |
| FDA | U.S. Food and Drug Administration |
| FSU | functional spinal unit |
| ISB | International Society of Biomechanics |
| ISO | International Organization of Standardization |
| LLJ | LifeLongJoints |
| MC | million cycles |
| MoCap | motion capture |
| MoM | metal-on-metal |
| MoP | metal-on-polymer |
| PCSA | physiological cross-sectional area |
| PEEK | polyetheretherketone |
| PoP | polymer-on-polymer |
| RoM | range of motion |
| SSED | Summary of Safety and Effectiveness Data |
| UHMWPE | ultra-high molecular weight polyethylene |

Standards

- ISO18192-1 [1] ISO18192-1 Implants for surgery — Wear of total intervertebral spinal disc prostheses — Part 1: Loading and displacement parameters for wear testing and corresponding environmental conditions for test [1]
- ISO14242-1 [2] ISO14242-1 Implants for surgery — Wear of total hip-joint prostheses — Part 1: Loading and displacement parameters or wear-testing machines and corresponding environmental conditions for test [2]
- ISO14242-2 [3] ISO14242-2 Implants for surgery — Wear of total hip-joint prostheses — Part 2: Methods of measurement [3]
- ASTM F2423-11 [4] F2423-11 Standard Guide for Functional, Kinematic, and Wear Assessment of Total Disc Prostheses

Chapter 1

Introduction

1.1 Background and Motivations

Modern prostheses for lumbar total disc replacement were first approved by the U.S. Food and Drug Administration (FDA) for clinical use in 2004; three years earlier than its cervical counterpart [5, 6]. Although the initial utilisation was higher than the articulating cervical disc implant in the United States, there has been a steady decline of lumbar disc implantation since its inception with 82% decrease between 2005 and 2017 (Figure 1.1) [7].

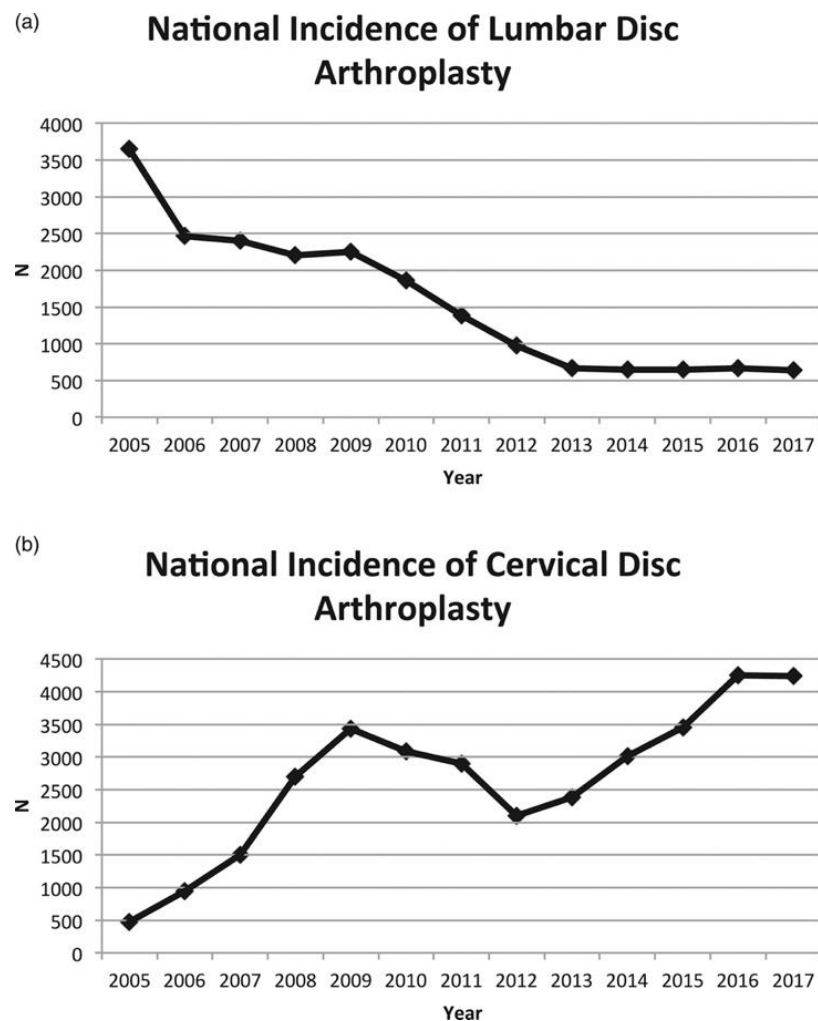


Figure 1.1 The national incidence of (a) lumbar and (b) cervical total disc replacements in the United States between 2005 to 2017 [7]

Unlike the lumbar prostheses, cervical disc arthroplasty is undergoing the opposite trend where the popularity is growing non-linearly across the United States, from about 500 procedures being carried out in 2005 to more than 4000 operations in 2017 [7-9]. It is thought that the increase in number of procedures performed is down to its consistent positive clinical outcomes as well as the expansion of clinical indications for the articulating cervical disc device beyond the initial criteria set in FDA's Investigational Device Exemption [7]. Apart from degenerative disc disease, articulating cervical disc implantation has also recently been shown to provide a similar clinical outcome for patients with traumatic cervical disc herniation when compared to fusion surgery [10]. Cervical disc replacement has been commonly performed on younger patients too (45.4 ± 0.32 years old) compared to traditional mainstream fusion surgery (51.2 ± 0.11 years old) [8, 9, 11]. Increasingly, these circumstances create a demand for the implants to last longer as the patient demographic is becoming wider and relatively young who will live longer with potentially a more active lifestyle. Despite its continuous success, the long-term outcome of articulating cervical disc prostheses is yet to be scrutinised given the innovation only being accepted into clinical practice at the start of the 21st century. To date, only limited data from retrieval studies on explanted disc implant is available, which logs devices removed due to clinical complications from the procedure rather than device-related failure, with period of *in vivo* implantation ranging between four to 49 months [12, 13].

An adequate but robust pre-clinical wear testing protocol is important on grounds of it is one of the non-clinical laboratory assessments for approval by regulatory bodies prior to clinical trials and market authorisation. Latest evidence by Lunn *et al.* [14] have also shown that the prescribed cyclic motion in ISO14242-1 [2] by the International Organization of Standardization (ISO) for hip implant poorly represents a real-world loading of the joint, with high variability amongst the subjects recruited. This is further supported by the discrepancies found in numerical wear simulation between the prescribed parameters in ISO14242-1 [2] and loading experience during actual locomotor and non-locomotor activities [15].

It is believed that a similar insufficiency exists for ISO18192-1 [1] where the prescribed testing protocols for cervical disc implant by the ISO are lacking in a

strong clinical basis or explant analysis justifications [16]. Further investigative work is needed to assess the adequacy of this wear testing standard, where it can be compared against the motions and loadings during activities of daily living in the cervical spine, which this research project is determined to accomplish.

1.2 Research Aims

The aims for this research are:-

- a) to quantify the cervical spine loads and motions during activities of daily living using motion capture technique and multibody modelling, and
- b) to undertake a mechanical wear simulation of cervical disc prostheses using the standard parameters as well as the loads and motions derived within the spectrum of activities of daily living, outlined in objective (a).

1.3 Research Hypotheses

Three hypotheses have been outlined for this research project. These hypotheses are framed based on the analysis of the available literature in the following Chapter 2.

Hypothesis I: Cervical joint angle during activities of daily living is **smaller** than prescribed cervical joint angle in ISO18192-1 [1] in all movement directions (flexion/extension, lateral bending, and axial rotation).

Hypothesis II: Cervical joint axial loading during activities of daily living is **higher** than prescribed cervical joint axial loading in ISO18192-1 [1].

Hypothesis III: the wear rate of cervical disc implant under loads and motions that represent activity of daily living is **higher** than the wear rate of the implant under loads and motions prescribed in ISO18192-1 [1].

1.4 Research Scope

The ISO18192-1 [1] document was drafted to provide a standard set of wear testing protocols for both cervical and lumbar intervertebral disc implants. For each of the implant types (cervical and lumbar), ISO18192-1 [1] also has outlined an alternative wear test condition with an alternative loading and motion, on top of the standard parameters. The work within this research project is focussing on analysing the standard wear test for the articulating cervical disc implant only.

1.5 Thesis Outline

Chapter 1 – Introduction: This introductory chapter briefly outlines the context, motivation, as well as the aims and hypotheses for the research project. Scope for each chapter that contains within this thesis is summarised here too.

Chapter 2 – Literature Review: In this chapter, readers are briefly introduced to the structure and functions of the human neck including its pathologies that requiring implantation of the cervical spinal disc devices. Then, readers are presented with a critical analysis of tribology of cervical disc implants and wear testing protocols in ISO18192-1 [1] as well as a review of the latest academic research on cervical biomechanics. Hypotheses are framed, based on this review, which steer the direction of the overall research. The aims and objectives for this research project are also outlined at the end of this review.

Chapter 3 – Study of Cervical Spine Biomechanics During Activities of Daily Living: Phase I of the research focuses on the generation of subject-specific data using motion capture techniques and musculoskeletal multibody modelling to quantify the loads and motions in the cervical spine during various tasks that are routinely performed every day. The experimental methods, results, and the associated discussion from this study, including its limitations, are presented to the readers in this chapter.

Chapter 4 – Study of Mechanical Wear Simulation on Articulating Cervical Disc Implants: Phase II of the project utilises the real-world, generated data

obtained during Phase I to inform the wear simulation study on the articulating cervical disc prostheses using a multi-station joint simulator. The wear analysis involves protocol based on functional loads and motions that are routinely experienced by the disc implant as well as the standard parameters used within the cervical disc implant industry. Readers will find the experimental protocols, results, discussion, as well as any limitations related to this study are examined in this chapter.

Chapter 5 – Overall Discussion and Conclusion: In this final chapter, the objectives as well as the hypotheses outlined in Chapter 2 are reviewed. Readers are also offered the overall discussion which ties in the outcomes from both Phases I and II through the analysis of the achievement of the research project. The conclusions that have been drawn, study limitations and the future direction of research relating to cervical biomechanics and wear tribology of cervical disc implant from this point forwards are also described here in this closing chapter.

Chapter 2

Literature Review

2.1 Cervical Spinal Disc Implant in Clinical Context

2.1.1 Description of Structure and Function of the Spine

Human vertebral column generally consists of 33 vertebral bones with the lowest nine fused together to become two separate bony units, located inferior to the remainder of the column. These two fused bones are known as the sacrum and coccyx, which are recognised as two of the five spinal anatomical regions (Figure 2.1). Lumbar, thoracic, and cervical are the other three spinal regions, located superior to sacrum and coccyx, in an ascending order. The top most region, the cervical spine, comprises of seven individual vertebrae, identified as C1 to C7 according to the level it descended from the skull.

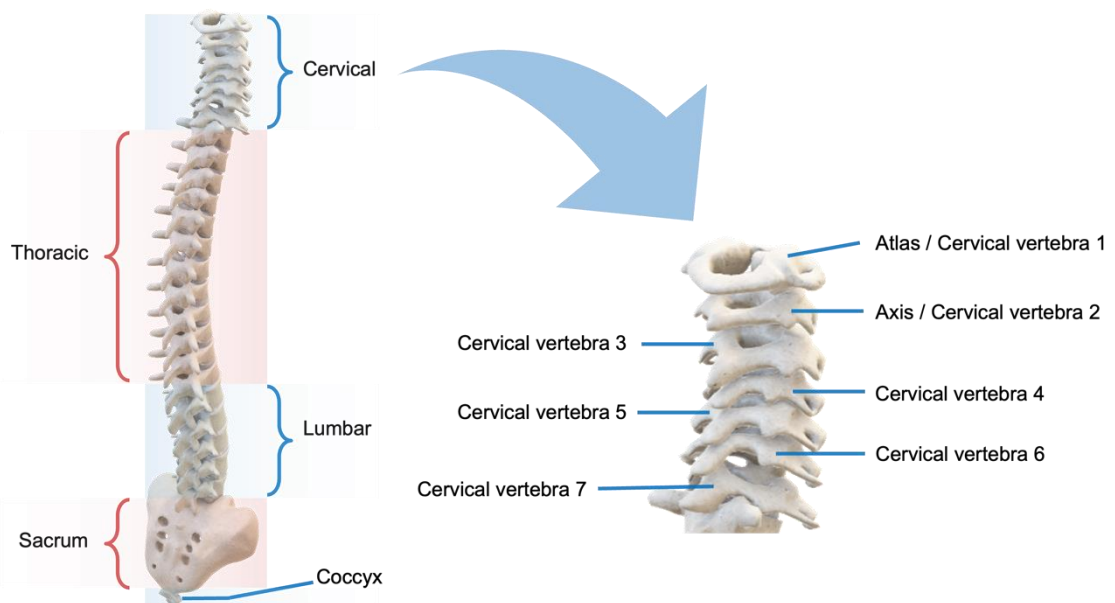


Figure 2.1 Regions of vertebral column in human

A typical vertebra is structurally split into anterior and posterior segments. The anterior segment primarily consists of a cylindrical bony mass named the vertebral body. In between those 24 individual vertebral bodies are intervertebral

discs, each comprising an outer annulus fibrosus, an inner nucleus pulposus, and two cartilaginous end plates which separate the disc from vertebral bodies above and below. The disc and both the adjacent vertebral bodies form an articulating structure called the intervertebral joint.

Many of the structural components of the vertebra form a neural arch posteriorly, which is present throughout the spinal regions. The arch, which makes up a considerable part of posterior segment, is a horizontal semi-circular structure that is attached to the posterior part of the vertebral body (Figure 2.2). The anterior segment is linked to the arch via two pedicles, which give out a lateral protuberance called transverse process on either side, before joining back together centrally via two laminae that ultimately shape the posterior component into a round foramen of the vertebra. The fusion of the laminae resulted in the formation of another protuberance called the spinous process. Apart from the arch, the morphology of the posterior segment is highly varied between the regions of the spine. It has been argued that the morphological variation is linked to the difference in range of motion afforded by each of the spinal regions. In the cervical region, however, this correlation has been found to be weak [17]. Another feature that is unique to cervical region is the presence of a transverse foramen on each side of the transverse process. These foramina form a tunnel for blood vessels that run parallel to cervical spine on either side to supply the head and brain from the heart.

There are another two bony tubercles, above and below the pedicle on each side, termed articular processes, which are not part of the arch. The superior articular process will meet the inferior articular process from the vertebra above to form a zygapophyseal joint, also known as the facet joint (Figure 2.3). The shape and orientation of the two facet joints on every level are also varied regionally and they function as a movement limiter for the respective vertebra [18]. Together with the intervertebral joint, the two facet joints (of the same vertebral level) are the three articulations that is present between two vertebrae, which forms the basic unit required for a movement in the spine, known as functional spinal unit (FSU) [19]. At each level, the FSU allows a small degree of motion, depending on the region and the level it is situated. The cumulative effect of the motion from all units of the entire column, however, results in the immense flexibility of the

human torso. The movement of the head or the cervical spine are normally described with respect to the plane of motion it occurs. Flexion/extension, lateral bending, and axial rotation, are the descriptions used when the head or the spine moves in sagittal plane, coronal plane, and transverse plane, respectively. These movements are illustrated in Figure 2.4.

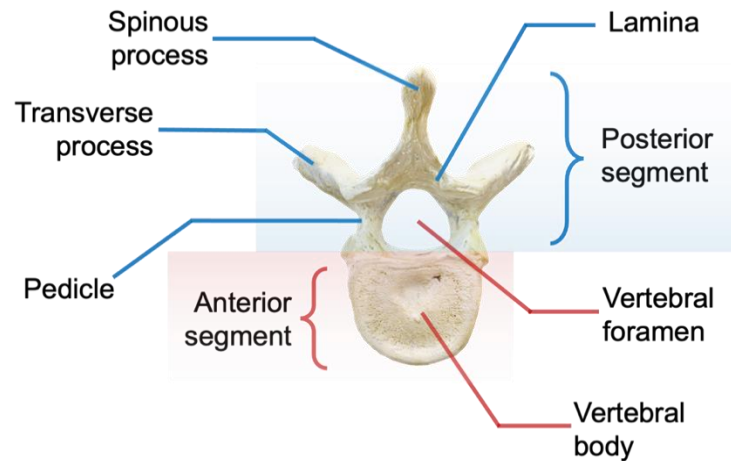


Figure 2.2 Superior view of lumbar vertebra depicting typical feature of neural arch

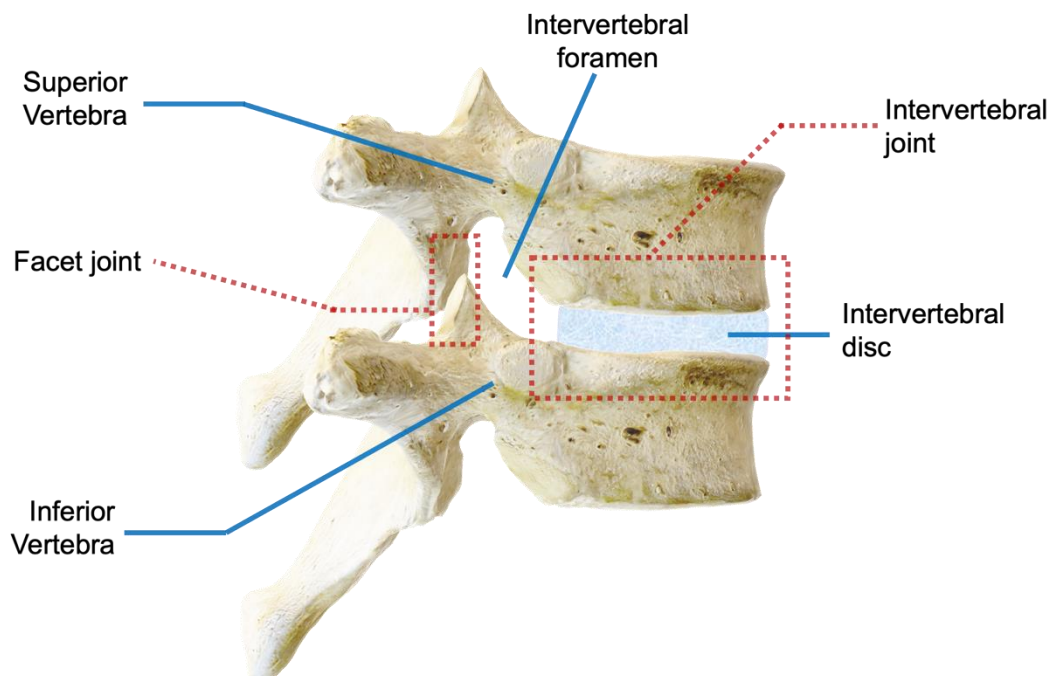


Figure 2.3 Example of a functional spinal unit from thoracic region

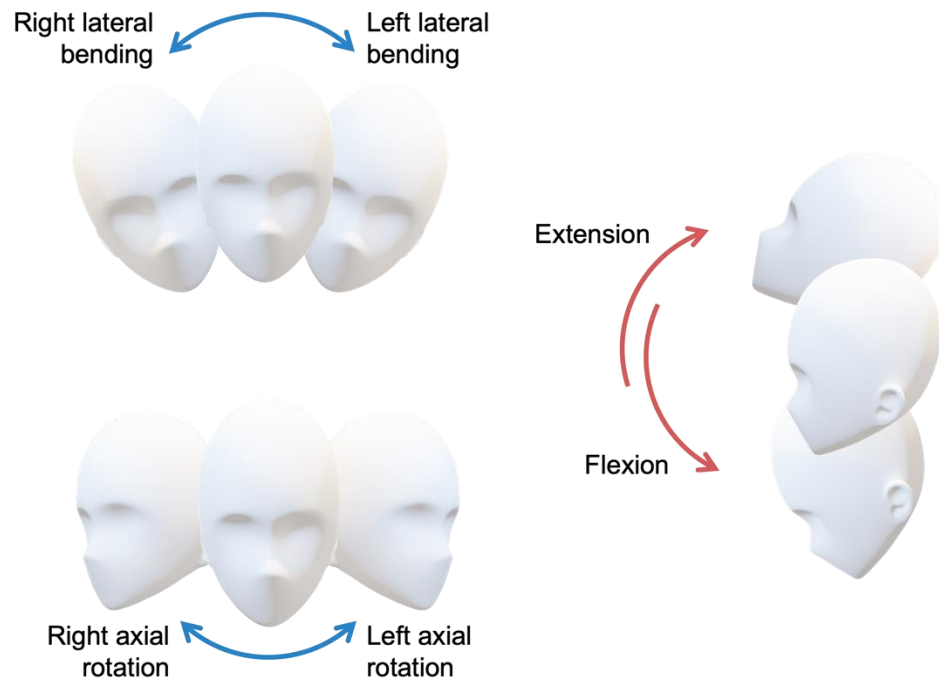


Figure 2.4 Rotational motion of the head in three main axes

Being part of the musculoskeletal system, one of the functions of the spine is to protect the tissues and organs underneath [20]. Running alongside the vertebral column posteriorly is the spinal/neural canal; formed by an aggregation of all the neural arches as well as the posterior surfaces of vertebral bodies, reinforced by spinal muscles and ligaments. This vertical tunnel houses the spinal cord – an important organ from the central nervous system that acts as a conduit for nerve fibres, connecting the brain to the rest of the human body. The nerve fibres will leave the spinal canal at every vertebral level, known as the spinal nerve, to innervate their respective body parts and organs. The exit route for each spinal nerve, called intervertebral foramen, is in close proximity to their respective vertebral body, the intervertebral disc and the vertebral body below it. The significance of these anatomical locations is further explained in Section 2.1.2 which addresses how the normal function of these structures can be affected by degenerative disease of the spine.

2.1.2 Cervical Spine and its Pathologies

It is estimated that 266 million people are suffering from degenerative spinal disease globally [21]. And this is an upward trend as seen by the rates of spine

surgery performed in the United States from 1979 to 1990, with an increase of more than 40% for cervical region and more than 33% in lumbar, throughout that period [22]. The spinal degenerative disease, called spondylosis, is essentially an osteoarthritis of the intervertebral joint. Due to its close proximity, as described in Section 2.1.1, the disease could also implicate the nearby structures such as the spinal cord or the spinal nerves. The irritation gives rise to the problem of cervical myelopathy or radiculopathy, respectively, when it occurs in the cervical region [23]. The main symptom of cervical myelopathy is the loss of function in the upper limb whereas the main symptom for cervical radiculopathy is pain that radiates down the arm [24]. A variety of treatments are available in managing the cervical spondylotic radiculopathy as shown in Table 2.1. According to the management guideline produced by the British Medical Journal Best Practice, patients who do not respond well to the more conservative treatment can be escalated to the next recommended approach, until the last stage which is a surgical intervention by decompressing the nerve [25]. A similar recommended approach is also advocated by the AOSpine North America and Cervical Spine Research Society for cervical spondylotic myelopathy, given the quality of evidence shown in clinical trials [26]. In United States alone, there has been a 211% increase in operation conducted between 2003 and 2013 in the for cervical spondylotic myelopathy, specifically [27].

| Diagnoses | Cervical Spondylotic Radiculopathy | Cervical Spondylotic Myelopathy |
|--------------------------------|---|---|
| 1 st line treatment | <ul style="list-style-type: none"> Analgesic Physiotherapy and traction (<i>adjunct</i>) Oral corticosteroids (<i>adjunct</i>) | <p>(<i>mild symptoms OR poor surgical candidate</i>)</p> <ul style="list-style-type: none"> Conservative treatment with immobilisation <p>(<i>moderate to severe symptoms OR good surgical candidate</i>)</p> <ul style="list-style-type: none"> Surgical decompression |
| 2 nd line treatment | <ul style="list-style-type: none"> Epidural anaesthesia OR cervical nerve root block | - |
| 3 rd line treatment | <ul style="list-style-type: none"> Surgical nerve decompression | - |

Table 2.1 Treatment algorithm for degenerative cervical spine disease (adapted from [25])

One method for surgical nerve decompression is a procedure called *anterior cervical discectomy and fusion* (ACDF) where the pathological disc is removed, and the vertebral bodies between the diseased tissue are fused together. The fusion of the vertebral bodies is done by placing bone grafts in the intervening joint space, that encourages bone growth and the eventual union, with the help of titanium end-plates as a stabiliser for the grafted tissue [28].

The ACDF procedure, also known as arthrodesis, has been routinely performed for decades and remains the 'gold-standard' treatment for patients with cervical myelopathy and radiculopathy [29]. The operation has an outstanding track record with a low rate of complications or re-operation [28]. Nonetheless, the procedure is not without its shortcomings. Patients who had undergone this surgery have been found to develop degenerative problems, over time, on the intervertebral joints adjacent to the level of the treated disc [30]. The seminal article by Hilibrand *et al.* [31] has shown that the annual incidence of disc degeneration at the adjacent level amongst post-ACDF patients is around 3% per year and 25.6% after ten years. It was postulated, through mathematical modelling, that excessive biomechanical stresses are exerted on the adjacent intervertebral joints to the operated disc level, in order to compensate the loss of joint mobility [32]. The overworked adjacent joints were thought to degenerate quicker than it is naturally anticipated in the non-operated cervical spine [33]. This phenomenon is called adjacent segment degeneration and can be evidently seen in radiographic investigations despite the patient being asymptomatic. This disease process is not isolated to the cervical but can also be seen in the lumbar region too [34]. The condition is defined as adjacent segment disease once the patient with segment degeneration has manifested its clinical symptoms [35]. Patients occasionally will require to undergo a subsequent operation, at the adjacent levels, to address this unwanted complication of ACDF.

The motion-preserving spinal implant was then devised in the late 20th century in the hope that it would overcome the issues of adjacent segment degeneration following the ACDF surgery. The concept of total disc replacement, using articulating spinal disc implant, was conceived amidst the hip and knee joint replacement revolution with lumbar disc arthroplasty preceding the cervical procedure [36]. Being an offshoot from the widely accepted total hip and knee

replacement, the implant for disc replacement has benefitted a lot from the technological innovations and discoveries, such as the biomaterials used and wear analysis. In spite of this, there are also areas where the total disc replacement is notably different from the total joint replacement, particularly the hip, as listed by Golish and Anderson [37]:-

- a) conformity – the bearing surfaces in hip arthroplasty have a larger diameter with deeper concavity whereas the disc implant is designed to have a relatively small and shallow articulation,
- b) loading magnitude – the cervical disc implant will have to endure the load from head and neck compared to hip which must withstand the weight of the upper body, and
- c) natural encapsulation – the hip is a true synovial joint as opposed to spinal disc joint which has no encapsulation.

Given that disc devices have adopted much of the technology from more established joint replacement technology, these differences, particularly (a) and (c), could potentially be a failure risk as pointed out by Hall *et al.* [38]. The shallow articulation is a risk for implant dislocation, although currently the rate of incidence is relatively low at 0.7% [39]. With respect to encapsulation, Golish and Anderson [37] argued that the lack of joint encasing could be both an advantage and disadvantage for disc arthroplasty. The encasing of the joint could cause accumulation of wear debris and intensification of its biological consequences within the implantation site; whereas the absence of encapsulation could cause a broader wear debris exposure area, thus a wider problem coverage, particularly when major organs are in proximity such as the spinal cord [37].

2.1.3 Cervical Total Disc Replacement

The first decade of 21st century has seen a number of spinal disc arthroplasty devices being approved by the FDA to be used in lumbar as well as in cervical intervertebral joints, following Investigational Device Exemption clinical trials [37]. The cervical disc devices are indicated specifically for patients with intractable

myelopathy and/or radiculopathy due to degenerative disc disease in one or two intervertebral disc levels [40].

As a surgical procedure, the *cervical total disc replacement* (CTDR) has been shown to have improved patients' quality of life. The patients perceived an average improvement between 2.9 to 6.4 (out of 10) in pain alleviation, based on Visual Analogue Scale, after the procedure when compared to the pain before their surgery [41-43]. When assessing patients' disability in the neck, using Neck Disability Index, average improvements of 58-63% were reported after the CTDR [41, 43].

No implant subsidence or migration was observed in any of the longitudinal studies nor was any revised surgery carried out onto those implants within the period of the studies [41-43]. All these studies were looking at patients' clinical and radiological outcomes before and after the CTDR surgery, operated by the same surgical teams. These studies, with follow-up review up to 9.4 years post-operation, found out that movement was preserved at the surgical index level with mean range of motion were between 6.4° to 9.9° [41-43].

The CTDR also has been proved to be a comparable procedure to ACDF for treatment of intractable cervical myelopathy and/or radiculopathy. A meta-analysis involving 785 patients from four randomised controlled trials who were treated with either CTDR or ACDF has found that patients in the CTDR group rated a lower pain score in the neck, with a larger range of movement at the surgical index level, as well as fewer further surgical interventions performed, when compared to ACDF post-operatively [44]. The meta-analysis also has found that there was no significant difference between the procedures in reference to the disability index scored by the patients after underwent their surgeries. A similar outcome was also seen in another meta-analysis that compares the two procedures when specifically carried out for patients with multiple diseased disc levels [45].

Additionally, the CTDR has shown to have a better peri-operative outcome too. Upadhyayula *et al.* [28] in a matched cohort comparison study has found that

CTDR had taken less operation time and a shorter hospital stay compared to ACDF surgery. This observation, however, is contradicting to the result found by Li *et al.* [45] where there was a longer operating time for CTDR when compared to ACDF. Furthermore, the study also found no statistical difference in patients' length of hospital stay between the two operations.

2.1.4 Unwanted Complications

More importantly, the ability of the CTDR in averting the problem that occurs in the adjacent vertebral level has to be evaluated as it was the foundation of the motion-preserving concept. In one of the earlier studies, Jawahar *et al.* [46] found that there is no statistically significant difference of adjacent segment degeneration involvement after CTDR or ACDF procedures. This finding was later disputed by two meta-analyses which showed the CTDR to be more advantageous over ACDF based on adjacent segment degeneration incidence [29, 33].

Although the problem is not fully obliterated, Shriver *et al.* [47] concluded that the CTDR has limited the progression of the disease from just radiological findings (adjacent segment degeneration) to symptomatic presentation (adjacent segment disease) amongst patients. The reduction of the rate of re-operation found by Ning *et al.* [44] and Li *et al.* [45] amongst CTDR patients also has been echoed by these meta-analyses when compared to the subsequent adjacent procedures carried out post-ACDF [29, 33].

As well as adjacent segment degeneration, heterotopic ossification is another well-known adverse effect from CTDR which also occurs commonly in ACDF. Heterotopic ossification is described as an abnormal bone growth within soft tissues where the presence of bone is unusual [48]. This abnormal growth of bone around the articulating disc implant may eventually cause spontaneous fusion between the vertebrae, which has been reported in both cervical and lumbar total disc replacements [49, 50]. In one of few long-term prospective studies conducted on CTDR, it has been observed that the heterotopic ossification effect only appears in much later follow-ups, with zero incidences within the first 24 months

of device implantation [41]. The finding was also confirmed in a similar study that compares the presence of heterotopic ossification in patients implanted with three other cervical intervertebral disc device brands [51]. Another interesting finding is that the presence of heterotopic ossification was found to be significantly more frequent in a constrained cervical implant than a semi-constrained device [52]. However, it has been found that the spontaneous fusion due to heterotopic ossification within the cervical region is more commonly found in semi-constrained implants [53]. In summary, like adjacent segment degeneration, heterotopic ossification is an unavoidable long-term effect of the procedure and has to be managed appropriately. It has been suggested that the use of non-steroidal anti-inflammatory drugs peri-operatively might be able to limit the heterotopic ossification development in long-term period [41].

2.1.5 Financial Incentives

There are some conflicting views, nonetheless, on the cost-effectiveness of CTDR, with regards to patients' quality of life achieved post-surgery, when compared with ACDF. A five-year Markov analysis carried out by Overley *et al.* [54] has reported that the CTDR has no advantage over ACDF in a monetary sense. However, several other studies, with a longer time period, have shown that the CTDR is more financially beneficial over ACDF in the long run [55-58]. Apart from having a better clinical outcome, it also has been found that patients undergoing CTDR have been returning to work much sooner than patients who had ACDF surgery [59]. However, no significant difference was seen concerning the return to employment between CTDR and ACDF, six months post-operation [59]. Looking at a broader scale, currently, there is no comprehensive data that reflects the true incidence of cervical myelopathy or radiculopathy, other than an extrapolation from population-based studies [60, 61]. Without an actual incidence rate, the calculation for CTDR market size in any given population for financial analysis purposes will remain inaccurate and elusive.

2.1.6 Short Summary

There are a number of articulating cervical disc implants available commercially as an alternative surgical treatment to cervical spondylosis, which has a comparable outcome to the current 'gold-standard' ACDF approach. The orthopaedic implant communities, however, are still divided and very reserved towards the CTDR despite the generally positive short- and medium-term clinical outcomes published in the scientific literature [62]. Regardless, the introduction of this innovation has given clinicians some additional leeway to treat the underlying problem as they are approaching the end of the repertoire of clinical interventions available in treating this debilitating condition.

2.2 Innovation in Spinal Intervertebral Disc Implants

2.2.1 Evolution of the Technology

The spinal intervertebral disc replacement procedures have been carried out as early as the 1960s. One of the first intervertebral disc substitutes used was the Fernström's stainless steel ball-bearing, which is considered as the earliest form of motion-preserving implant for the spine [63]. Despite its novel and innovative nature, the acceptance was low and eventually abandoned due to the subsidence of the implant into the inferior vertebral body, as well as device migration [36]. A much later clinical case series by Siemionow *et al.* [64] has shown that the implant's rudimentary design, which simply a metallic sphere as a substitution for viscoelastic disc, resulted to a high failure rate. It was postulated that the failure of the spherical implant can be attributed to the discrepancies between the ball's and the disc's stiffness properties, ability to distribute the load, and location of instantaneous axis of rotation [64]. Nonetheless, this novel concept marks the beginning of motion-preserving, spinal implant innovation.

The modern spinal disc prostheses can be broadly grouped into articulating and non-articulating/elastomeric implants [38, 65]. The articulating disc implants usually take a form of two spine-anchoring end plates sandwiching the implant hemispheric core (Figure 2.5, top). The anchoring end plates are placed at the

superior and inferior vertebral bodies at the level where the pathological intervertebral disc is being replaced [63]. Design for the implant core is the key element of the prostheses that made the motion preservation possible. The implant core could have either a uni- or bi-articular convex bearing surfaces which will slide onto an impression located on its opposing end-plates (Figure 2.5, top and middle) [38]. For a single-convex bearing implant, the core could be designed to be part of the end plate and made of the same material too (Figure 2.5, bottom). Unlike the unyielding core of an articulating device, elastomeric/non-articulating implant has a more compliant core which allows uneven compression that could cause reduction in implant's height during movement [65].

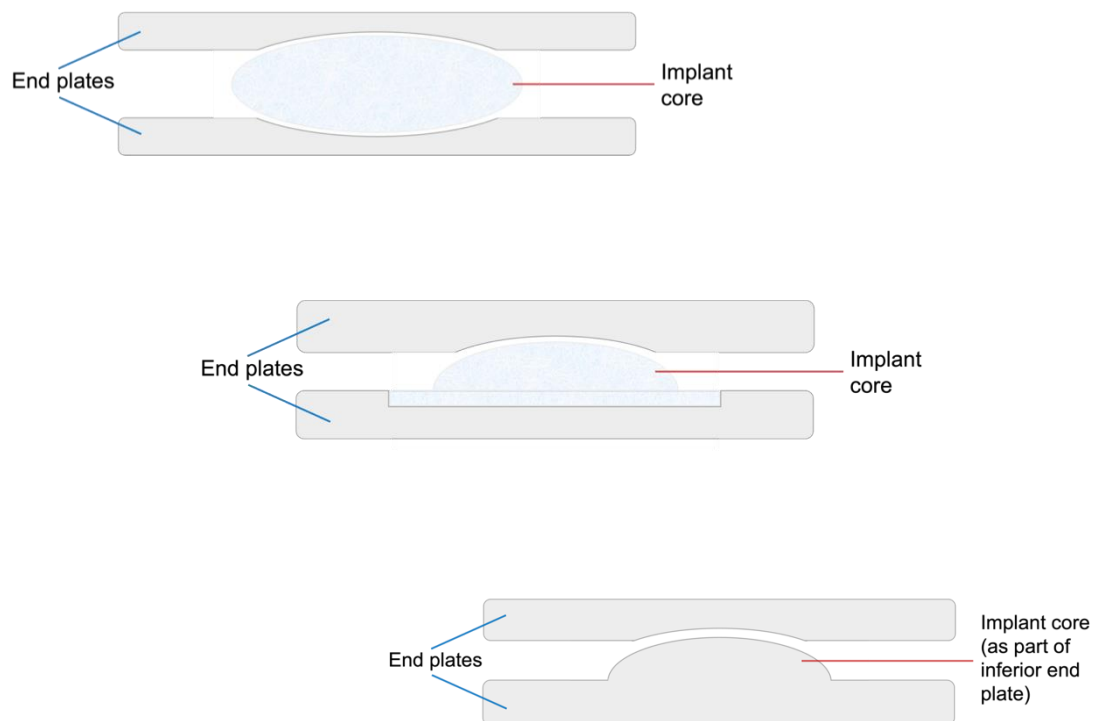


Figure 2.5 Different permutations of articulating disc prostheses

The articulating disc prostheses are normally classified into ‘unconstrained’, ‘semi-constrained’, and ‘constrained’ depending on the kinematic properties of the device (Figure 2.6) [66-68]. Patwardhan and Havey [65], however, argue that classification of the implants according to its strict degrees of freedom (DoF) allowance, based on a formulated calculation, is more beneficial in assessing its biomechanics properties than the subjective designation of its constraining ability. It is thought that the ability of an implant to constrain the joint’s DoF will indirectly affect the success rate of the disc replacement procedure. The constraint can

reduce the room for error in implant's precise vertebral positioning on the spine [38]. Although a non-constrained implant design does not require a perfect centring upon fixation on the vertebrae, there is a possibility for it to exert an additional stress to the nearby facet joints due to the lack of shear stability from the device [67]. The same cannot be certain for a constrained implant whether there is an increased or decreased in the load on the facet joints. Sandhu *et al.* [49] have presented both sides of the arguments where it is theorised that the constrained implant could either absorb or exerting an additional load onto the posterior structures due to impingement. The constraining feature of an implant certainly creates an additional burden for the spinal surgeon to have the device implanted at a precise location which ultimately contribute towards the chances for the procedure to be a success.

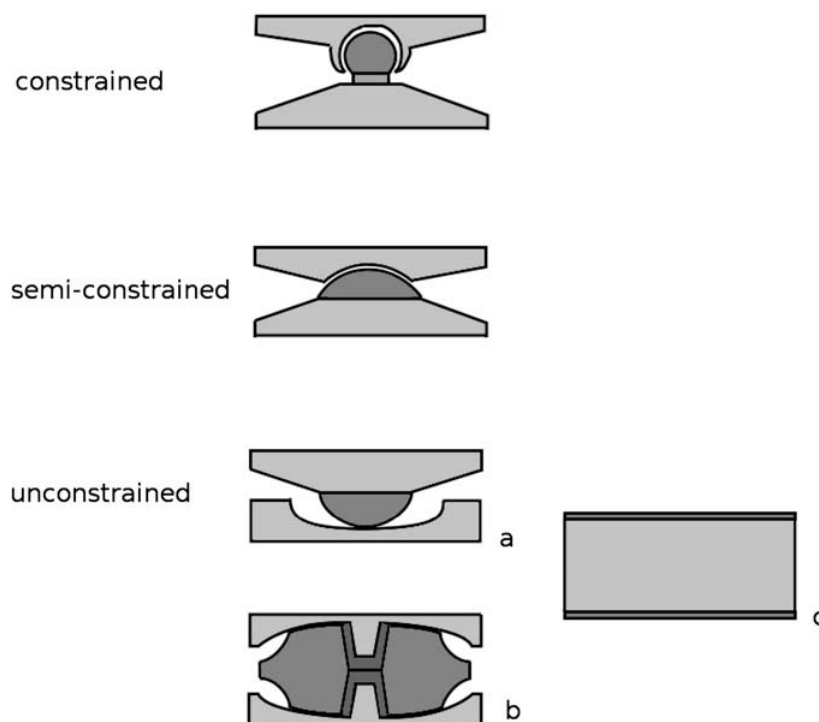


Figure 2.6 Constraining classification for cervical disc implants; unconstrained device can be further split into (a) non-conformal gliding surfaces, (b) different articulating couplings, and (c) deformable core [68]

2.2.2 Biomaterials for Spinal Intervertebral Disc Implants

Another important design aspect for any articulating implant is the bearing surfaces and the frictional couple. The materials traditionally used for bearing surfaces in artificial joints can be categorised into three main groups [67]: -

- a) metals; such as stainless steel, titanium, and cobalt-chromium (CoCrMo) alloys,
- b) polymers; such as ultra-high-molecular-weight polyethylene (UHMWPE), polyetheretherketone (PEEK), and polyurethane, and
- c) ceramics; such as zirconia-toughened alumina – the only material that has ever been used in FDA's list of approved disc implant as the principal material for the component to date [69].

Polymeric materials have been incorporated as an orthopaedic bearing surface since the early design of the hip joint prostheses. The progression began since Charnley hip implant with the use of polytetrafluoroethylene as acetabular lining before shortly being replaced with UHMWPE [70]. The UHMWPE remains extensively used as the bearing surface and has been undergoing several iterations of improvement such as cross-linking, heat and pressure treatments, the type of sterilisation process used, and doping [37].

Metal-on-polymer (MoP) bearing combination is the longest surface bearing couple ever employed in any joint replacement [67]. It has been suggested that the MoP should be the standard of reference for any new bearing materials to be compared with as it remains one of the most studied friction couple in biomaterials [37]. In contrast to a typical MoP hip implant where the 'ball' is made of metal and the 'cup' is made of polymer, the core for MoP intervertebral disc implant is made of polymer (Figure 2.5, pale blue colour) which is articulating with a metal impression on the endplate (Figure 2.5, grey colour). Paradoxically, one study

has found that the frictional torque in the metal socket/polymer ball permutation is higher than polymer socket/metal ball arrangement in majority of directions of head movement direction [71]. Two other frictional couples also have been studied for its suitability as material pair for the articulating disc implant: (a) metal-on-metal (MoM), which already have been used in marketed devices, and (b) polymer-on-polymer (PoP), which remains an investigational tribological pair [72, 73]. Ceramic, on the other hand, has only been scarcely used as biomaterial, mostly for aiding fixation of the articulating implant, until recently where zirconia-toughened alumina has been approved by FDA as a main material for the core that is articulating with a PEEK polymer [69, 74]. None of these combinations, however, are immune from the mechanical consequences of wear, which is a major biotribological concern, elaborated further in Section 0 [75].

2.2.3 Contemporary Cervical Disc Prostheses

Although there are five distinct regions of the human spine, only two have been routinely implanted with intervertebral disc prostheses, the lumbar and cervical regions, which coincidentally have the same forward lordotic curvature and where spinal spondylosis commonly presented [36, 49]. Within the cervical spine, the two uppermost vertebrae are morphologically distinct from the rest and are unsuitable for implantation of spinal disc prosthesis. Apart from the size, the prosthetic design for the cervical and lumbar spine are very similar. Nevertheless, the clinical indications for the device implantation are different [76].

Up until 2016, there were six articulating disc implants that have been approved by the FDA for clinical use in cervical disc replacement [40]. Since then, only Simplify® Cervical Disc has been approved for the same indication in 2020 [69]. These devices are indicated only for implantation at intervertebral levels between C3 to C7 due to its anatomical morphology. These devices are listed in Table 2.2 and illustrated in Figure 2.7.

| Cervical Disc Prostheses | Pre-market Approval Notification Date | # of Principal Components / Tribological Pair / # of Articulations | Materials ¢ core, € endplate | Fixation |
|--|--|--|--|--|
| ProDisc™-C Total Disc Replacement | 17 th December 2007 [77] | <ul style="list-style-type: none"> • two-piece • Metal-on-polymer • Uni-articular surfaces | <ul style="list-style-type: none"> • CoCrMo alloy[€] • UHMWPE[¢] | <ul style="list-style-type: none"> • Titanium plasma spray • Slotted keels • Porous surface |
| Bryan® Cervical Disc | 12 th May 2009 [78] | <ul style="list-style-type: none"> • three-piece • Metal-on-polymer • Bi-articular surfaces | <ul style="list-style-type: none"> • Titanium alloy[€] • Polyurethane[¢] | <ul style="list-style-type: none"> • Porous titanium surface |
| Secure®-C Cervical Artificial Disc | 28 th September 2012 [79] | <ul style="list-style-type: none"> • three-piece • Metal-on-polymer • Uni-articular surfaces | <ul style="list-style-type: none"> • CoCrMo alloy[€] • UHMWPE[¢] | <ul style="list-style-type: none"> • Porous surface • Serrated keels |
| PCM® Cervical Disc | 26 th October 2012 [80] | <ul style="list-style-type: none"> • three-piece • Metal-on-polymer • Bi-articular surfaces | <ul style="list-style-type: none"> • CoCrMo alloy[€] • UHMWPE[¢] | <ul style="list-style-type: none"> • Titanium calcium phosphate |
| Mobi-C® Cervical Disc Prosthesis | 7 th August 2013 [81] | <ul style="list-style-type: none"> • three-piece • Metal-on-polymer • Bi-articular surfaces | <ul style="list-style-type: none"> • CoCrMo alloy[€] • UHMWPE[¢] | <ul style="list-style-type: none"> • Lined of teeth • Titanium plasma spray • Hydroxyapatite |
| Prestige® LP & ST Cervical Disc System | 16 th July 2007 (ST model) [72] 24 th July 2014 (LP model) [82] | <ul style="list-style-type: none"> • two-piece • Metal-on-metal • Uni-articular surfaces | <ul style="list-style-type: none"> • Stainless steel (ST model) • Titanium alloy (LP model) | <ul style="list-style-type: none"> • Screw (ST model) • Rail (LP model) • Titanium plasma spray |
| Simplify® Cervical Artificial Disc | 18 th September 2020 [69] | <ul style="list-style-type: none"> • three-piece • Ceramic-on-polymer • Bi-articular surfaces | <ul style="list-style-type: none"> • Polyetheretherketone[€] • Zirconia-toughened alumina[¢] | <ul style="list-style-type: none"> • Keels • Titanium plasma spray |

Table 2.2 Summary of FDA approved intervertebral disc devices properties to date [6, 65, 76, 83]



Figure 2.7 Commercially available cervical disc implants [67, 84]

2.2.4 Short Summary

Throughout the developmental progression of the articulating intervertebral disc implant, there is one constant unifying aspect since the early days of Fernström's ball bearing: to restore and preserve the motion within the intervertebral joints. As the CTDR has only been introduced into clinical practice relatively recent, it is still early to categorically describe the innovation as safe when the long-term effects of the technology are yet to be scrutinised, which perhaps contributing towards the reservation and cautiousness amongst the clinicians [62]. For the time being, wear simulation of the implant has been the window to the future in predicting the tribological performance of these devices and it is one of pre-clinical assessments that must be submitted for approval by regulatory bodies prior to its market authorisation. Section 0 and 2.4 will discuss some of the tribological aspects related to articulating cervical disc implants as well as its wear testing protocols in which tribologists and implant testing engineers need to consider and address in order to improve the robustness of this innovation for it to have a better acceptance amongst the clinicians.

2.3 Tribological Performance of the Articulating Spinal Disc Devices

The study of rubbing, or *tribology*, is a branch of science that concerns the topic of wear, lubrication, and friction. Williams [85] broadly defined tribology as “*the science and technology of interacting surfaces in relative motion and of related subjects and practices*”, which also encompassing tribological system found in orthopaedic implants.

2.3.1 Wear Testing on Cervical Spinal Disc Implants

As noted earlier, much of the progress in the modern spinal disc implants stems from the joint replacement revolution, specifically the hip and knee joints [38]. Thus, the concern over the long-term adverse effect of implants' wear debris seen in joint replacement procedures has inevitably been inherited by the spinal disc replacement community.

Wear, one of the trinity in tribology, is a system response to a process of damage that results in loss of materials triggered by relative motion between opposing contact surfaces as well as the force exerted in between them [86]. Quantifying the wear durability of biomaterials used in orthopaedic implants as a function of time through a standard wear testing is one of non-clinical laboratory study requirements for manufacturers to submit to medical device regulators prior to being approved.

Archard's Volumetric Wear Equation, illustrated by Equation 2.1, is typically use to parameterise the variables involve during a wear process, which can be applied to both abrasive and adhesive wear mechanisms [87]. In his seminal paper on wear, Archard [88] concludes that the wear rate is proportional to the load applied, W , which, in the case of orthopaedic implants, would be the loading experienced within the joint. Angular excursion of the articulating joint where the implant being inserted is represented by the sliding distance, L , and the property of the biomaterial used is denoted by the material's hardness, H_v . In short, the

volumetric wear equation is a function of load, sliding distance, and surface hardness of the material.

$$V = K \times \frac{W \times L}{H_V}$$

Equation 2.1

| | |
|-----------------------------|---|
| <i>V</i> | Archard's volumetric wear (m ³) |
| <i>K</i> | Archard's wear coefficient of the system |
| <i>W</i> | normal load applied (N) |
| <i>L</i> | sliding distance (m) |
| <i>H_V</i> | hardness of the material (Pa) |

In their *Summary of Safety and Effectiveness Data* (SSED) documents submitted to FDA, ProDisc™-C and Mobi-C® were shown to produce a gravimetric wear rate of 2.59 ± 0.36 mg/million cycles and 1.546 ± 0.075 mg/million cycles, respectively, on their UHMWPE cores [77, 81]. The protocol for the former is similar to the protocol used to test the latter, which later became the standard testing protocol in '*18192-1 Implants for surgery — Wear of total intervertebral spinal disc prostheses — Part 1: Loading and displacement parameters for wear testing and corresponding environmental conditions for test*' (ISO18192-1 [1]) published by the ISO [1]. The difference between these two simulations is the application of the constant compressive load of 150 N applied throughout the wear test for ProDisc™-C whilst the test for Mobi-C® employed a dynamic compressive loading between 50 – 150 N within one test cycle. This accounts for the wear rate discrepancy between the two wear tests. It is worth noting that the ISO18192-1 [1] was first published in 2008 (and later revised in 2011), a year

after SSED for ProDisc™-C was accepted by the FDA in 2007. In a later study by Nechtow *et al.* [89] that employed 50 – 150 N dynamic compressive loading has shown a reduction in wear rate of ProDisc™-C to 1.99 ± 0.15 mg/million cycles, a value that is closer to wear rate of Mobi-C than previously reported.

More recently, titanium alloy has been studied as an alternative for the metal component within the MoP pairing. In a series of studies, Wang *et al.* [90, 91] have recorded a lower wear rate of UHMWPE as well as cross-linked UHMWPE when paired against titanium alloy, at 0.81 ± 0.26 mg/million cycles and 0.15 ± 0.08 mg/million cycles, respectively, when compared with CoCrMo alloy seen in Mobi-C® when tested under ISO18192-1 [1] conditions. A similar observation was also noted one year earlier by Wu *et al.* [92] for the same bearing surfaces with a wear rate of 0.53 ± 0.13 mg/million cycles.

Indeed, titanium alloy has been employed as a biomaterial for bearing surface against polyurethane and was approved by the FDA for Bryan® Cervical Disc implant in 2009 but no data was published related to the wear rate of the polymer from this device in their SSED [78]. Recently, MOVE-C, a research investigational disc device that utilises titanium-polyurethane bearing combination has been shown to have an equivalent gravimetric wear rate with other MoP pairings: 1.54 ± 3.6 mg/million cycles, when tested with protocols from ISO18192-1[1] [93].

The SSED for Prestige® ST Cervical Disc System, a stainless-steel MoM device, was also accepted by the FDA in 2007 with its highest volumetric wear rate of 0.733 ± 0.252 mm³/million cycles after five million cycles during coupled lateral bending/axial rotation motions and 0.067 ± 0.015 mm³/million cycles after ten million cycles during flexion/extension motion [72]. The test protocol used for Prestige® is based on document *F2423-11 Standard Guide for Functional, Kinematic, and Wear Assessment of Total Disc Prostheses* (ASTM F2423-11 [4]) issued by the ASTM International (ASTM). Testing parameters outlined in ASTM F2423-11 [4] are considerably different from testing conducted for ProDisc™-C and Mobi-C® in many aspects including the angular motions, compressive loading, and frequency. This is further discussed in Section 2.4.1. The ASTM F2324-11 [4] document also provides standard parameters for testing the lumbar

disc implant. Maveric[®] AMAV, a MoM lumbar disc device made from CoCrMo alloy, was tested using protocol set by ASTM F2324-11 [4] for lumbar with a wear rate outcome of 0.43 ± 0.06 mm³/million cycles during coupled lateral bending/axial rotation motions and 0.33 ± 0.12 mm³/million cycles during flexion/extension motion [94]. In a stark contrast, another wear study on MoM CoCrMo lumbar disc implant has shown a much higher wear rate, by an order of magnitude, between 6.2 mm³/million cycles to 12.4 mm³/million cycles, depending on carbon content in the alloy when subject to ASTM F2324-11 [4] testing parameters [95]. Meanwhile, Moghadas *et al.* [96], in a more recent study, have found that the wear rate of CoCrMo alloy for MoM bearing surface on lumbar disc implant to be 0.76 ± 0.02 mm³/million cycles when tested with parameters from ISO18192-1 [1], which is comparable with the outcome from the wear study by Paré *et al.* [94] that utilised different parameters from ASTM F2324-11 [4] for the same biomaterial interface.

Unlike ISO18192-1 [1], protocols from ASTM F2423-11 [4] requires output from the wear analysis to be converted in volumetric wear instead of gravimetric wear, as reflected in the unit for wear rate reported in the SSEDs submitted to FDA when standard from ASTM is employed for its wear testing.

Apart from MoP and MoM, a PoP also has been proposed by Grupp *et al.* [73] as an alternative tribological pairing for disc implant using PEEK as well as its derivatives. In the study, wear rates of disc implants made of conventional PEEK, carbon-reinforced PEEK, and polyaryletherone under the load and motions from ISO18192-1 [1] were compared. Carbon-reinforced PEEK demonstrated its superiority amongst other polymers in terms of wear rate, at 0.02 ± 0.02 mg/million cycles, thus making it potentially a good candidate for alternative bearing material for a disc implant [73]. The study also made a direct comparison against UHMWPE-CoCrMo bearing couple from activC[®] disc implant which has a wear rate of 1.0 ± 0.1 mg/million cycles [73] although the comparison between soft-on-soft (PoP) and hard-on-soft (MoP) tribological pairing in this instance is debatable.

Although both ISO and ASTM have outlined the simulation protocols for wear testing, neither has explicitly set the limit for the wear rate to be acceptable. Generally, it is the regulatory bodies that will determine whether the outcome from the wear simulation submitted by the device manufacturers is satisfactory or otherwise. One of FDA's medical device approval pathways, known as Premarket Notification 510(k), which is less stringent than Premarket Approval pathway, only requires manufacturers to demonstrate that "*the device is as safe and effective, that is, substantially equivalent, to a legally marketed device*" [97]. Under this premise, it is assumed that implant manufacturers would demonstrate the wear rate of the new disc prosthesis is comparable, or better, to the previously marketed ones, as evidenced from the series of SSEDs being accepted by the FDA. Nonetheless, a study has shown that devices cleared through Premarket Notification 510(k) are more likely to be recalled than devices approved via Premarket Approval pathway [98].

Mechanical wear testing as a method to elucidate the wear rate of the disc implant can be time-consuming and costly. Numerical simulation framework for wear of an implant, which is quicker and cheaper, has been devised and currently in its third iteration where it takes into account the shape of sliding wear path, on top of pressure applied and distance of the path [99]. This algorithm then can be incorporated into finite element analysis where the wear rate can be estimated *in silico*. de Jongh *et al.* [100] in 2008 presented a model that predicts the wear of a cervical disc implant which can be tailored to wear testing parameters either from ISO18192-1 [1] or ASTM F2324-11 [4], as well as loadings and kinematics data from biomechanical model of human cervical spine originated from radiographic scans. Incorporating anatomical structure into the finite element analysis for wear rate prediction has its own advantages over wear simulation with disc implant alone. Bhattacharya *et al.* [101] have shown that by incorporating the associated anatomical spinal structures into their analysis, the wear pattern is different and localised to a certain area with total volumetric wear lower than simulation without the associated structures, such as ligaments, included. They also have identified an instance where microseparation occurs between bearing interfaces during the simulation [101]. On top of that, the *in silico* simulation method also has provided an opportunity for implant designer to assess the performance of their latest innovation as demonstrated by Wo *et al.*

[102] where they calculate the range of motion (RoM), as well as the stresses, for the new cervical subtotal disc replacement prosthesis upon implantation. Numerical simulation also has been used to gauge the lumbar disc implant performance as well [103, 104]. Proper exploitation of numerical wear simulation, in summary, is needed and would be a great new tool for implant manufacturers for bench testing their innovation prior to market authorisation.

2.3.2 Lubrication Regime within the Spinal Disc Implants

The spinal intervertebral joint is a fibrocartilaginous joint which, unlike the hip, does not bathe in synovial fluid that acts as a lubricant. The lack of specific lubricant for the spinal articulation other than the interstitial fluid is a predicament for disc implant since lubrication, being the second trinity in tribology, plays a consequential role in wear performance of a sliding surfaces.

In a lubricated environment, one of three possible types of lubrication regime can be present between two sliding surfaces. They are derived from the distinctive Stribeck diagram (Figure 2.8), which shows the relationship between coefficient of friction and Sommerfeld number [105]. The Sommerfeld number is a function of rotational sliding speed (ω), bearing pressure (p) *i.e.* load/area, and lubricant viscosity (η), in which those lubrication regimes can be defined [106, 107]. A modified Stribeck curve (Figure 2.9) was later devised, by replacing Sommerfeld number with lambda ratio, λ [107]. This dimensionless ratio is essentially describing how well the lubricant is separating the bearing interfaces from touching each other at molecular scale level. The formula for calculating lambda ratio, λ , is illustrated by Equation 2.2. The effectiveness of the lubricant in performing its function within the system is calculated using a formula in Appendix F, which reflects the thickness of the lubricating film at its bare minimum, h_{min} . However, the minimum film thickness is calculated with the assumption that the bearing interfaces are smooth, without any asperities. Thus, surface roughness, R_q , has incorporated into the equation because it is thought to be closely associated with lubrication regime [107]. The parameter for surface roughness will be further discussed in Section 2.3.5. Similarly, the transition between the three lubrication regimes is also neatly shown within the modified Stribeck curve.

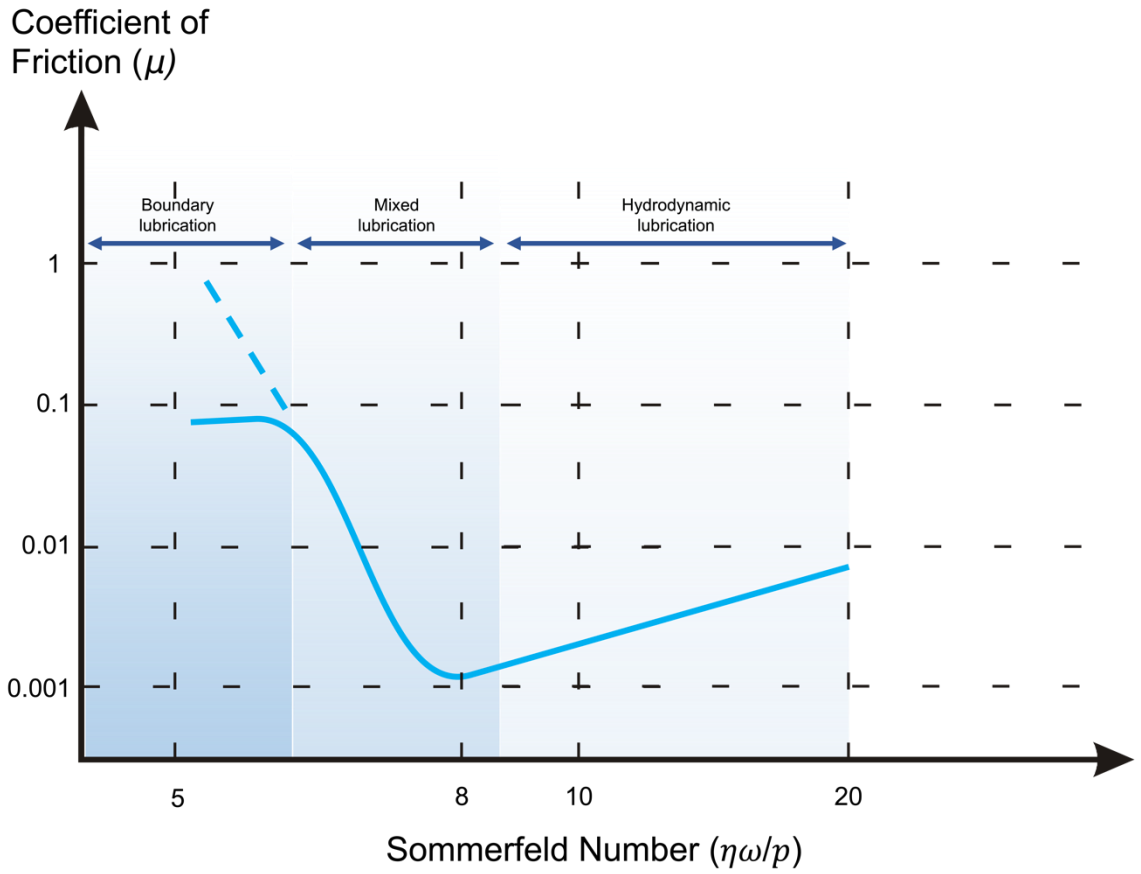


Figure 2.8 Stribeck Diagram (reproduced from [105])

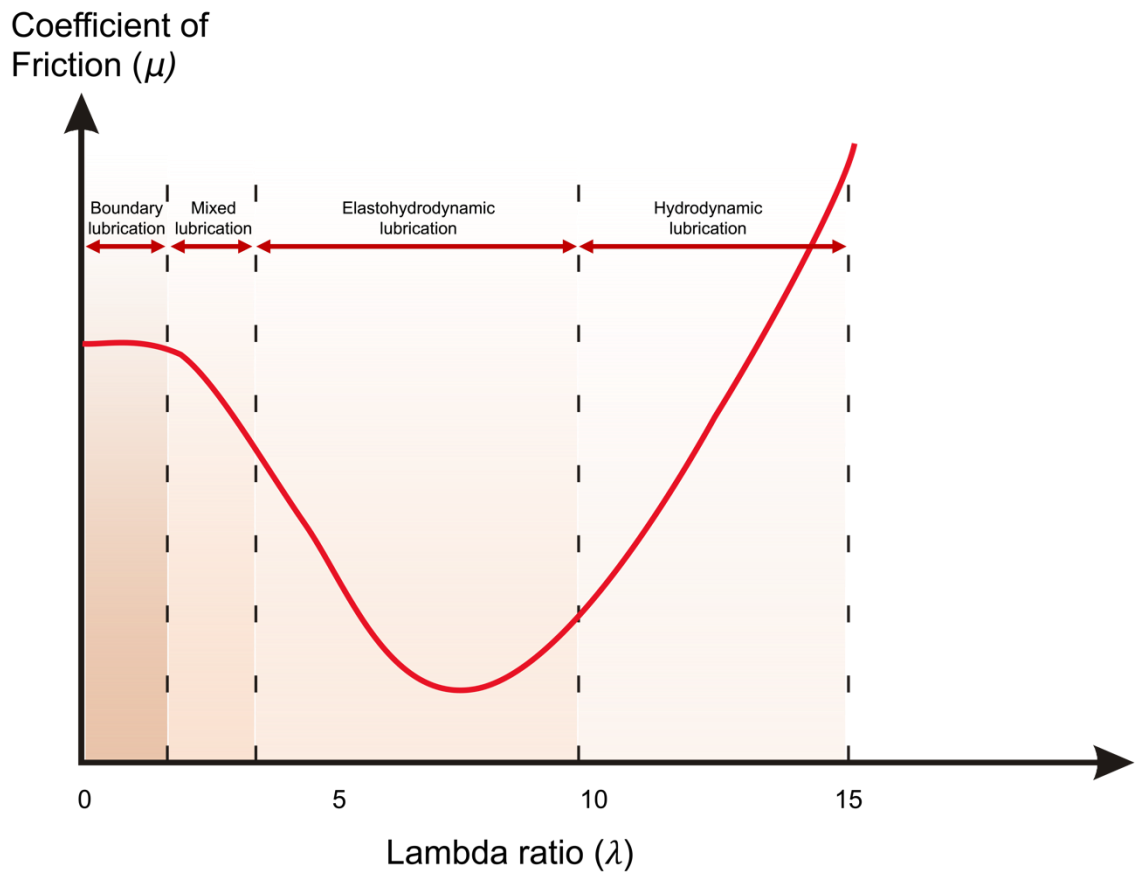


Figure 2.9 Modified Stribeck Curve (reproduced from [108])

$$\text{lambda ratio, } \lambda = \frac{\text{minimum film thickness, } h_{min}}{\text{composite surface roughness, } \sqrt{R_{q1}^2 + R_{q2}^2}}$$

Equation 2.2

h_{min} minimum film thickness of the lubricant

R_{qx} surface roughness measurement for bearing surface x

When the bearing interfaces are completely separated by the lubricant and the fluid is able to uphold the load between the surfaces, this is known as ‘*fluid-film*’ or ‘*hydrodynamic*’ lubrication regime, where $\lambda > 3$ [106]. Meanwhile, the system is said to have a ‘*boundary*’ lubrication regime with $\lambda < 1$, when, due to “breakdown of effective lubrication”, the asperities from both articular surfaces are in contact with each other thus supporting the load; wear is expected as the asperities are grazing with each other due to the sliding motion [105]. In this condition, density and viscosity of the lubricant is inconsequential [105, 108]. It is said that ‘*mixed*’ lubrication regimes are presence when the lambda ratio value is $1 < \lambda < 3$. Elastohydrodynamic is another regime that falls within the spectral shift of mixed and hydrodynamic lubrications in which the asperity contacts are more concentrated and lubricant’s physical properties are still influential but the film is thinner [108].

It has been demonstrated that MoP (UHMWPE-CoCrMo) pairing has the thickest minimum film thickness, h_{min} , when compared to MoM (CoCrMo-CrCoMo) and ceramic-on-ceramic (alumina-alumina) for lumbar disc implant [109]. However, the highest λ is found in alumina-alumina bearing surfaces for lumbar disc implant, for a constant radius and load applied, with lubrication regime occurring within the MoM and MoP bearing pairs remain below the unity value, *i.e.* $\lambda < 1$, up until 1.8 radians/s angular velocity [109]. Nevertheless, Clewlow *et al.* [110] have theorised that the lubrication regime could be improved to fluid-film lubrication in cervical disc implant, and mixed lubrication regime in lumbar disc

implant, if the concave part in MoM bearing pair is lined with a 2-mm soft layer material with Young's modulus of 10 MPa.

Shaheen and Shepherd [109], in their seminal papers on lubrication regime in lumbar disc implant, also have found that the λ is higher when the implant's hemispheric core radius is bigger and radial clearance is smaller, *ceteris paribus*. However, due to the natural size of the vertebral body where the spinal disc implant can be implanted, there is a limited range of radii that can be employed for the convex ball part of the device.

Although it has been shown that increasing the viscosity of the lubricants will improve the λ value through increasing its magnitude ratio, the lubrication of spinal intervertebral joint is only limited to interstitial fluid, which has a viscosity of 1.24 mPa s, that is eight times less viscous than synovial fluid [109, 111]. Nonetheless, 20 ± 2 g/L protein concentration of bovine calf serum, which is the prescribed lubricant for wear testing simulation in ISO18192-1 [1], has a viscosity of 1.0 mPa s that sufficiently matched with the interstitial fluid during testing [111].

Meanwhile, Xin *et al.* [112], in one of few articles that examine the lubrication regime in cervical disc prostheses, have calculated the λ for an all-polymer disc implant made of PEEK to be 0.052 at the optimum value when subjected to ISO18192-1 [1] loading condition with 0.05 mm radial clearance.

2.3.3 Frictional Torque Subjected to Spinal Disc Implants

Friction, the final trinity of tribology, is the opposing force encountered by a moving body when in contact with another body or surface [113]. In the case of cervical ball-on-socket disc implant, frictional torque is the main interest given the articulation moves principally in angular motions (flexion/extension, lateral bending, axial rotation).

Through some of the state-of-the-art joint wear simulators for wear testing, it is possible to measure frictional torque directly, in real time, during a wear test using a load cell equipped with moment-capable transducers [114]. However, the

sensor readings would have to be adjusted by transforming the origin of the transducer coordinate system to the centre of rotation of the implant's articulation as demonstrated by Sonntag *et al.* [115] as the location of the load cell can vary, either at the top or bottom of the test cell, depending on the simulator setup [114, 116, 117]. Review on the basic function of wear simulator for joint implant as well as protocols for conducting the wear test are further discussed in Section 2.4.

In a MoM lumbar disc implant, frictional torque has been shown to have a positive correlation, when a constant axial load applied, for all angular motions (flexion/extension, lateral bending, and axial rotation) as well as for all radii of the convex dome tested [118]. The study also recorded the highest frictional torque value of 9.5 N m when simulated at 0.25 Hz under 2000 N using 16 mm radius convex CoCrMo ball [118]. Both correlations are further supported by another study on tribological assessment of cervical disc implant in which the highest mean frictional torque recorded for PoP disc implant is 3.71 ± 0.22 N m when tested at 0.25 Hz under a constant axial load of 150 N using 6.3 mm radius convex PEEK implant [114].

Through direct measurement of frictional torque from load cells, lubrication regime of the tested implant can also be derived by plotting the Stribeck curves through formulated calculation of friction factor and Sommerfeld number based on work presented by Scholes and Unsworth [119]. Through this derivation, it was found that both lumbar CoCrMo MoM and cervical PEEK PoP disc implants are likely to operate under either boundary or mixed lubrication [114, 118].

2.3.4 Mechanisms of Wear in Spinal Disc Implants

There are four principal types of wear mechanism – abrasive, adhesive, flow, and fatigue; that are instigated by physical processes [106]. Kato [87], nonetheless, also considers other types, such as corrosive, melt, and diffusive, which are caused by thermal and chemical processes, as part of mechanism of wear too. In a review article by Kurtz *et al.* [120], they described how abrasion and adhesion are the most dominant wear modes reported in the published retrieval studies of the disc implants as well as from their own explanted prostheses repository.

The abrasive wear mechanism occurs when the impurities or asperities with a higher surface hardness are 'scratching' the softer opposing surface [86]. This wear mode is typically seen in MoP tribological pairing due to the discrepancy of hardness between the surfaces [121-123]. The same abrasive wear mechanism also has been seen in MoM spinal disc implants [13].

Adhesion wear mechanism, on the other hand, occurs when the asperities of the softer surface are 'plucked off' and stick to a different surface area. The mechanism has been seen to appear in MoM frictional couples; but can only be detected under scanning electron microscope [120]. This mechanism is, however, typically seen in polymeric surfaces [73, 121-123].

The debris adherence generated from adhesion wear mechanism on a MoP implant has been quantitatively recorded. An *in vitro* study by Prokopovich *et al.* [124] on lumbar disc device has shown that the surface roughness of the polyethylene core's dome is decreasing in the first half of the experiment but is increasing during the second half as more wear debris are being generated and started to accumulate within the dome area of the sliding contact. This polyethylene debris re-embedment also has been reported even in studies with milder testing regime (such as low cross-shear and pure curvilinear motions) [121, 125, 126]. Terminology related to wear testing, such as cross shear, will be further discussed in Section 2.4.2.

Occasionally, fatigue wear mode as well as plastic deformation/creep are also found in retrieved devices which caused a permanent geometry change rendering the implant to be non-functional [120].

2.3.5 Surface Analysis Methodology

Analysis of the implant's bearing surfaces allows researchers to identify the wear mechanism that occurs as well as to quantify the roughness of the articulating surfaces, which later can be used for calculating lambda ratio and establishing the lubrication regime of the said implant, as illustrated in Section 2.3.2.

Assessment of a surface topography can be broadly categorised in two ways, determined by the probe or modality employed: contacting and non-contacting methods. Contact measurement normally involves a sharpened-tip stylus, attached to a cantilever, being drawn across the surface at a constant speed whilst a transducer generates an electrical signal corresponding to the displacement of the tip which is then recorded [127]. This ultimately will produce a two-dimensional 'profile' line that represents the topography of the surface in sagittal or coronal aspect of the surface; and thus is called profilometry. A set of these profile traces, either in parallel or radially, could produce its three-dimensional areal topography across the examined surfaces [128]. Contact profilometer has several disadvantages where it may leave scratches on the analysed surface that are made of softer materials than the tip as well as is time-consuming, in which might be impractical for sequential surface roughness measurement such as in implant wear simulation [129]. Contact profilometry also known to suffer some inconsistency in measurement due to stylus tracking error [130].

Non-contacting, as the name suggests, employs a modality that does not require physical contact with the examined surfaces and usually provide a three-dimensional perspective of the assessed area instead of just a line profile. There are generally four main grouping of methods for non-contacting analysis: microscopy, interferometry, diffraction, and scattering modelling [129]. Scanning electron microscope, transmission electron microscope, and atomic force microscope are some examples that have been used to analyse surface roughness. Despite its high accuracy advantage, microscopy method is limited to samples that are small enough to fit into the machine and require preparatory work done on the examined surface [129]. Interferometry, a measurement that is based on wave interference phenomenon, provides a speedy, sub-nanometer resolution measurement with high accuracy [129]. There are several commercially available instruments set up for characterising surface topography have exploited this technique through vertical scanning interferometry and white light interferometry. The normally distributed scattering pattern from a diffracted laser beam after being shone upon a surface is how its roughness is determined from diffraction method in topographical analysis [129]. The advantage of diffraction method is that it can be used on variety of materials such as metals, ceramics, and soft plastics [129]. Scattering method from optical instrument for

surface topography examination generally provides only qualitative assessment, but quantitative analysis is possible from various modelling method based on the calculation of scattering intensity due to the asperities [129].

Some of the instruments and methods for analysing the surface roughness discussed are listed in Table 2.3 as demonstrated in some of the published studies, each with its own advantages.

| Techniques | Scanning Electron Microscopy [131] | Contact Stylus Profilometry [131, 132] | White Light Interferometry [131] | Non-contact Optical Profilometry [133] |
|---------------------|---------------------------------------|--|-------------------------------------|---|
| Vertical resolution | 3 nm | 0.07 nm | 0.05 nm | 10 nm |
| Lateral resolution | | 1 nm | 0.3 μm | 5 μm |
| Probe/modality | Electron | Sharped-tip cantilever | White light | Confocal light |
| Type of information | Visual area topography (qualitative) | Profile/Areal surface roughness/topography | Areal surface roughness/topography | Areal surface roughness/topography |
| Note | Surface-altering | Surface-altering | Non-damaging | Non-damaging |

Table 2.3 Surface topography methods used in implant bearings

The topography of a surface generally described by two main components: roughness and waviness; and they are split arbitrarily by its wavelength where the former is shorter and the latter is longer, as illustrated by Figure 2.10 [127]. Much of engineering tribology revolves around surface roughness parameters than surface waviness, as evidenced in the earlier sections. There are hundreds of surface roughness parameters and Deltombe *et al.* [134] has identified 56 three dimensional surface roughness descriptions defined by the ISO and classified them into six main categories for areal topography: amplitude, spatial, hybrid, functional, feature, and other parameters. The simplest, and most commonly used, surface roughness parameter is called centre-line average, R_a (for profile measurement) or S_a (for areal measurement), which falls under the amplitude group. It is an arithmetic average of surface roughness which is calculated using formula in Equation 2.3 where L is the measurement length and z is the asperity height from mean surface level line [127]. This is the line in which the area between the asperity surface above it (shaded blue) equals to area between the

void below it (shaded red) as shown by Figure 2.11. Classified in the same amplitude group is root-mean-square, R_q (for profile measurement) or S_q (for areal measurement), which is a square root for the arithmetic mean of the squares of the surface roughness measured. This is calculated using formula in Equation 2.4. This root-mean-square parameter is used for lambda ratio calculation, shown in Equation 2.1 earlier.

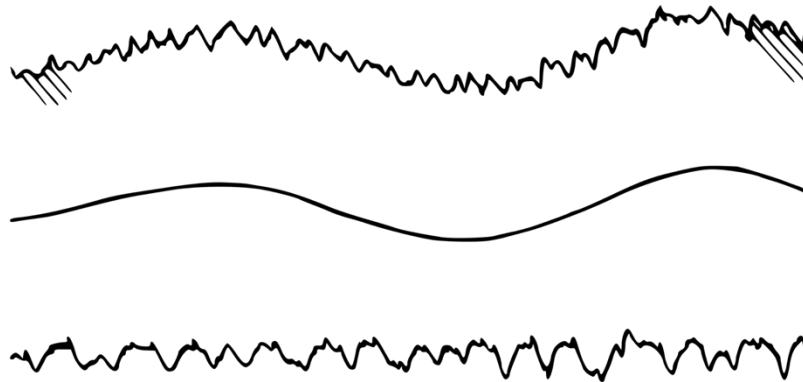


Figure 2.10 An example of profile surface topography (top line) when filtered through according to its wavelength to reveal surface waviness (middle line, after low-pass filter) and surface roughness (bottom line, after high-pass filter) (reproduced from [127])

$$R_a = \frac{1}{L} \int_0^L |z| dx$$

Equation 2.3

$$R_q = \sqrt{\frac{1}{L} \int_0^L z^2 dx}$$

Equation 2.4

L measurement length

z height of the surface asperity from mean surface level

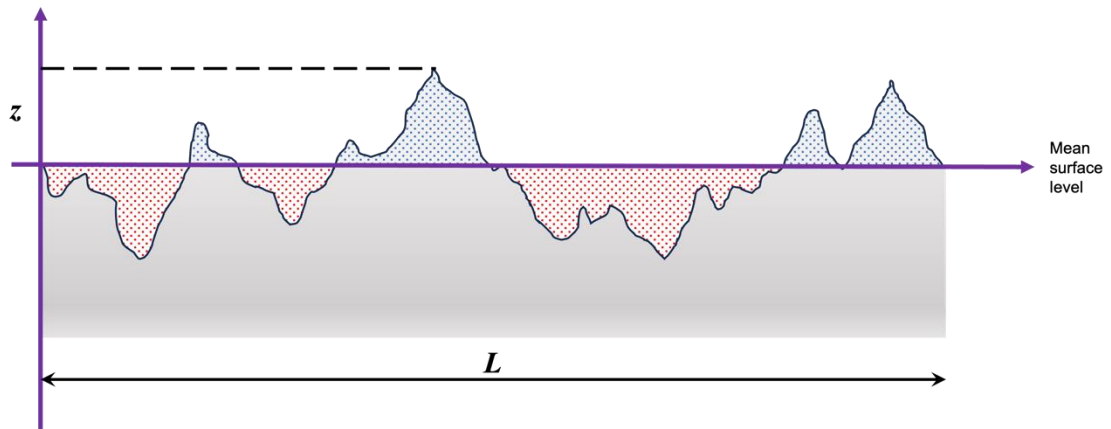


Figure 2.11 Representation of centre line average, R_a , calculation over L measurement length where the area shaded blue is equal to the area shaded red (reproduced from [127])

The most basic methods advocated by Kurtz *et al.* [120] for spinal disc implants, based on their experience in implant retrieval programme, are the optical stereomicroscopy and scanning electron microscopy which have the ability up to 40 times and 5000 times magnifications, respectively. The surface damage observed on retrieved lumbar total disc replacement is also comparable to that reported in total hip and knee replacements [135].

Kurtz *et al.* [13], in a comparison study between in vivo and simulator-tested of cervical disc implants, have used white light interferometry to analyse the stainless steel bearing surface on the MoM implants and have found the morphological appearance of the bearing surface is qualitatively similar when visualised under optical microscopy. In an earlier study, Wennerberg *et al.* [136] have already recommended using an optical profilometry when examining a relatively softer metallic biomaterial, such as titanium oxide, whilst stylus profilometry is more suitable for harder, polished steel for surface roughness measurement. This is in contrast to an even earlier study where stylus profilometry is preferred for titanium biomaterial, although the optical modalities used as a comparison in this study are standard reflected light microscopy and interference contrast microscopy [137].

As for UHMWPE polymer, Hyde *et al.* [126] have demonstrated the use of scanning electron microscopy as well as stylus profilometry in his wear simulation

on lumbar articulating disc implants when subjected to modified test conditions. Due to its surface-altering nature, these measurements are limited to the beginning and at the end of the simulation for each testing parameter studied as the wear rates are calculated gravimetrically (and some material would be inevitably removed during scanning process). Whereas, Prokopovich *et al.* [124] have showed that it is not impossible to use a stylus profilometer to measure surface roughness of a convex polymer at every million cycles of wear simulation. Through a series of the two-dimensional surface profile that gives a three-dimensional area topography, the study demonstrates the evolution of surface contour throughout the wear simulation and concludes that adhesive is the main wear mechanism occurring on a lumbar articulating disc implant [124].

Meanwhile, Green *et al.* [138] have used white light interferometry, not only to examine surface roughness of ceramic alumina used for articulating cervical disc implant, but for calculating the wear volume down to 0.0001 mm^3 , an equivalent of 0.0001 mg alumina, which is difficult to discern when employing a gravimetric measurement method for ceramic biomaterial.

2.3.6 Consequences from Wear of Spinal Disc Implants and Biological Responses

Wear debris are by-products of wear phenomenon and, as found by a review on studies of spinal implants, can be in the form of particles or ions [139]. The wear debris generated from lumbar disc implant has been shown to have cause similar physiological responses as seen in other total joint replacements, such as osteolysis, which could lead to implant failure [140, 141].

A review on lumbar disc replacement for the treatment of lower back pain concludes that particulates produced from UHMWPE core in MoP bearing pair tend to be spherical in shape, ranging between $0.1 \text{ }\mu\text{m}$ to $100 \text{ }\mu\text{m}$ in diameter [139, 142]. Moreover, the amount of polymeric wear debris from biarticular lumbar disc implants is found to be higher than uniarticular ones, although the particles are rounder in shape [143]. These characteristics, such as size, shape, and volume of the particles, can influence body response towards polyethylene wear

debris from the implants [120, 142]. Depending on the size, the particulates can trigger a diverse adverse inflammatory reaction mediated by several inflammatory markers produced when macrophages and giant cells fail to degrade the polyethylene wear debris [141]. The accumulation of the cytokinic inflammatory markers, such as interleukins and tumour necrosis factor, causes osteolysis being carried out by osteoclasts, cells that are responsible for bone resorption process, which eventually causes aseptic implant loosening and implant failure [120, 142, 144].

Metallic wear debris from MoM bearing pair gives a more troubling result compared to the polymer particles. Knowledge gathered from decades of hip arthroplasty wear analysis has shown that the MoM wear debris size is smaller but generated in a larger number, which is equally undesirable [142]. A prospective study amongst patient inserted with MoM articulating lumbar disc implant have shown a sustained increased in cobalt and chromium serum ions throughout 36 months post-operatively [145]. More worryingly, the level of serum ion concentration found in patients with MoM articulating disc implants is comparable with the ion concentration level found in well-functioning MoM hip arthroplasty patients when there is a profound size different between these devices [139, 145]. It has been found that metallic wear debris could cause cellular toxicity towards metal and also an allergic reaction [120]. This physiological response is an adaptive immune reaction, as opposed to innate immune response seen from polymeric wear debris reaction, and lymphocytic-mediated which is antigen-dependent [146]. A case review by Golish and Anderson [37] on MoM articulating disc replacement also has found reports of abnormal accumulation of soft-tissue mass called pseudotumour in four out of seven unsuccessful implantation incidents on top of cases of metal hypersensitivity. The accumulation of the metallic wear debris also renders any images from radiological modalities that relying on metallic properties, such as magnetic resonance imaging, inadequate due to artefactual signals that originate from the particles.

2.3.7 Short Summary

Despite having several biomaterials used for the cervical disc implant, none of these combinations are immune from the mechanical consequences of wear, which is a major biotribological concern [75]. Given the terrible consequences of wear debris towards the body, it is imperative that the wear performance of the articulating disc implant is assessed adequately. The analysis of tribological aspects of the device have been carried out within the industrial setting, through wear testing standards, as well as in many research domains. Nevertheless, it is believed that the main parameters prescribed in ISO18192-1 [1] for wear testing of articulating cervical disc device is lacking in physiological basis [16]. Due to the lack of accurate physiological environment reflected within the standard testing protocols, it is challenging to accurately examine long-term wear performance of the device *in vivo* or eliciting the body's immune response from the exposure towards the wear debris generated. Section 2.4 will delve into the protocols and parameters prescribed in ISO18192-1 [1] in detail and how it compares with the estimated physiological loading and motion, based on the available data in the current literature.

2.4 ISO18192-1 Wear Testing Equipment, Parameters, and Protocols

Interest in building a machine that could simulate the function of a human joint, particularly the hip, began during the second half of 20th century after the introduction of Charnley hip implant [147]. An ideal machine should be able to reproduce the motion, loadings, as well as *in vivo* environment where the replacement device will be implanted inside the joint as accurately as possible [148]. Fundamentally, the machine should be able to replicate the rotational motion of a joint within the three planes of motion as well as the loadings along the direction of the three cartesian axes, applied onto the articulating bearing surfaces of the implant by means of actuators, giving it a total of six DoF [147]. Initially, design of hip simulators were pared down and limited, typically, to only 3 DoF – rotation around the x and z axes (pitch and roll) with joint loading exerted only along the z axis (in the direction of gravity) of the tested implant [148, 149].

This limitation on the available DoF was due to cost and the precision of the technology available at the time [147]. As the technological capability improved and demands becoming more complex, controls for these actuators has evolved over time from pneumatic to hydraulic to electromechanical with more DoF and other loading directions incorporated into the simulator [116, 117]. Other joint specific simulators also have been designed and built as more implants being invented for other joint replacement procedures. Simulator for spinal implant has been developed as early as 1993 and at least four different manufacturers have developed simulator for spinal disc implant to date [150, 151]. With the advent of these simulators, it is hope that the wear performance in any of the orthopaedic implants could be elicited accordingly. The ability for the simulator to replicate the motion and loading physiologically has never been more important as concern on adverse reaction towards wear debris originated from the implant has grown, as discussed the previous sections. More often than not, these simulators are developed to meet the motion and loading demands require by wear testing standards so performance between implants under identical parameters can be compared. Nevertheless, the wear testing standard, prescribed by ISO18192-1 [1] in particular, is believed to be lacking in clinical basis [16]. Some of the aspects within this standard will be dissected in detail in the following section.

2.4.1 Spinal Disc Implant Wear Testing Protocols

As previously stated, the inevitable consequences of wear are a major concern in a motion-preserving disc implant. Protocols used by device manufacturers for wear testing of an implant prior to clinical trial and market authorisation come mainly from two major respected bodies. The commonly used protocols by the medical device companies for articulating disc implants are from ISO18192-1 [1]. The testing parameter values as well as the phasing of the curves are illustrated in Figure 2.12 and listed in Table 2.4. Prior to ISO18192-1 [1], the ASTM International has published their protocol, ASTM F2423-05 [4], in 2005 which was later revised and reapproved several times with the latest being published in 2011.

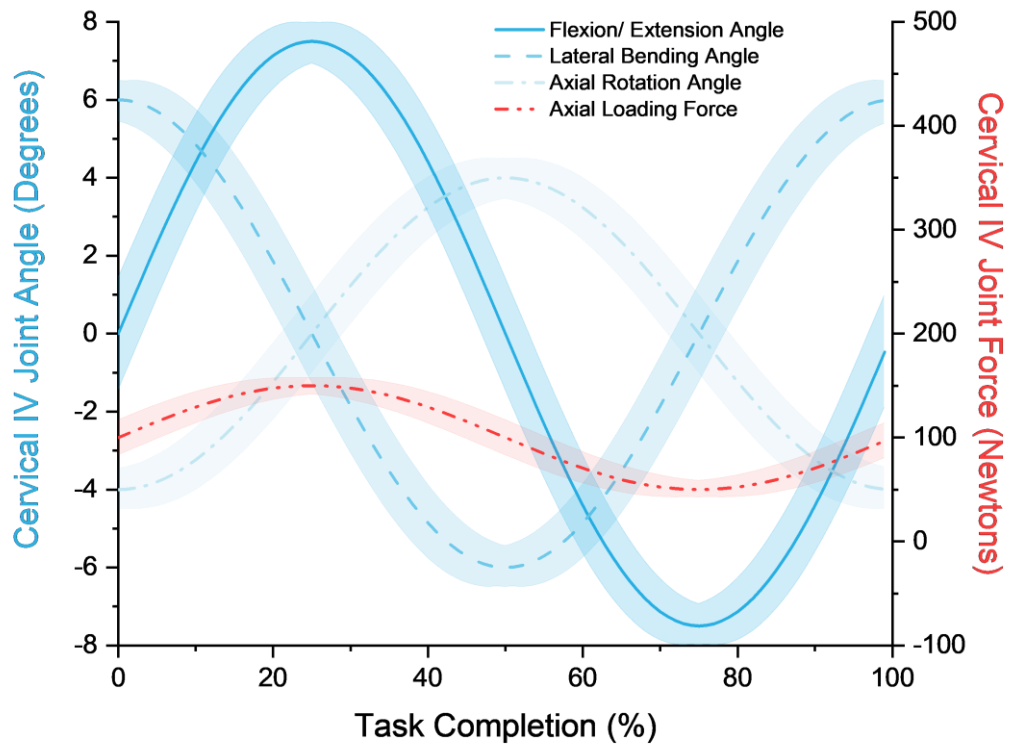


Figure 2.12 Phasing, including its tolerances (shaded region), of the load and displacement curves for cervical intervertebral disc prostheses (reproduced from ISO18192-1 [1])

| | Angular Displacements (°) | | | Load (N) |
|---------------|---------------------------|----------------|-----------------|----------------|
| | Flexion/extension | Axial rotation | Lateral bending | |
| Minimum value | -7.5 ± 0.5 | -4 ± 0.5 | -6 ± 0.5 | $+50 \pm 7.5$ |
| Maximum value | $+7.5 \pm 0.5$ | $+4 \pm 0.5$ | $+6 \pm 0.5$ | $+150 \pm 7.5$ |

Table 2.4 Parameter values, including its tolerance, prescribed by the ISO18192-1 for cervical intervertebral disc prostheses wear testing (adapted from [1])

The wear testing protocols for cervical and lumbar devices in ISO18192-1 [1] are very similar except for the magnitude of the parameters and phasing of the loading. The parameters for cervical disc implant will be individually analysed in the following sub-sections.

2.4.2 Motion Profiles and Cross Shear

The main difference between the ISO18192-1 [1] and ASTM F2423-11 [4] protocols is the motion profiles used to test the wear on the implants. The ISO18192-1 [1] protocol for intervertebral spinal disc implant adopted a composite, multidirectional angular motions for the test on the prostheses [1]. The ASTM F2423-11 [4] protocol, on the other hand, does not set the composite angular motion as an obligatory condition of the testing; rather testing the angular motions separately is still acceptable too [4]. This is in contrast to the proposition laid out by Anderson and Rouleau [76] where it mentioned the need for the cross-shear test in polyethylene bearing surface in order to accurately predict the wear rate.

The importance of cross shear in wear testing is directly linked with the molecular structure of the polymeric component of the implant. It has been shown that the more perpendicular the motion is against the direction of the long polymer chains, the higher the wear rate is [152]. Therefore, it has been postulated that if the motion is aligned with the direction of the long polymer chains (with a reduction or the absence of cross shear), fewer wear particles will be generated, thus lower wear rate.

The effect of wear from cross-shearing also has been investigated on different types of lumbar disc implant where it was found that the wear rate is significantly reduced if the cross-shear element is decreased [125, 126]. This finding is in alignment with results from a study by Grupp *et al.* [121], as well as in Nechtow *et al.* [153], that compares the two protocols from ISO18192-1 [1] and ASTM F2423-11 [4], which has shown that a composite motion profile produced a substantially higher wear rate by 20-fold, than ASTM F2423-11 [4]'s unidirectional profile (Figure 2.13). It is believed that the composite angular motion, as prescribed in ISO18192-1 [1] standard, will introduce the necessary shear forces for the implant testing. The cross-shear element also has been acknowledged and incorporated as an element for *in silico* wear simulation [99, 154].

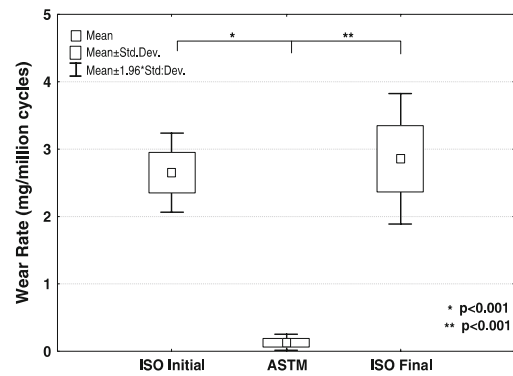


Figure 2.13 Box-and-whisker plot of statistical analysis between ISO and ASTM wear testing protocols [121]

Based on previously published implant retrieval analysis, it is also concluded that the composite motion profile, such that in ISO18192-1 [1] protocols, provides a more accurate reflection of physiological wear than a unidirectional, individual testing profile advocated by the ASTM F2423-11 [4] protocol [121]. This finding also matched with the observations recently published by Wang *et al.* [155] in a similar study which utilised titanium end-plates instead. Nevertheless, Grupp *et al.* [121], in the same experiment, found that there is no significant difference observed in the size and dimension of the wear particulates produced from the polyethylene core between the two motion profiles.

2.4.3 Axial Load Profile

The ISO18192-1 [1] standard recommends the loading for the cervical disc implant wear testing to be oscillating between 50 N to 150 N. This force is applied in a continuous sinusoidal pattern, confined by the minimum and maximum values prescribed (Figure 2.12). As specified in the protocol, these values were derived from a limited amount of knowledge available on loading in human spinal vertebrae at the time it was drafted and the test is meant only to assess the 'average' loading conditions [1].

The cervical spine is a flexible, complex body section and there are relatively fewer experiments conducted on human cervical spine compared to the lumbar segment [156]. One of the commonly employed techniques in determining the load value experienced by the spine is through a biomechanical linked-segment

modelling. The magnitude for axial loading prescribed for cervical disc implant in ISO18192-1 [1] originates from a basic link-segment model proposed by Snijders *et al.* [157] in 1991.

In a mathematical simulated model built from segmented computed tomography scans using LifeMOD software, de Jongh *et al.* [100] has illustrated that the intradiscal force experienced between the C5 and C6 cervical spine in a “typical, but arbitrarily chosen, RoM” can reach as high as 400 N. This value is more than double from the maximum advocated value in ISO18192-1 [1] standard, as shown in Figure 2.14. Please note that the x-axis of the graph in Figure 2.14 for the superimposed ISO18192-1 [1] cervical axial load is not drawn to scale. Similarly, a linked-segment model created by Anderst *et al.* [158] based on radiographic data, have found that the magnitude for axial loading during head extension could reach 200 N at the end of motion range even at cervical spine C2 level (Figure 2.15).

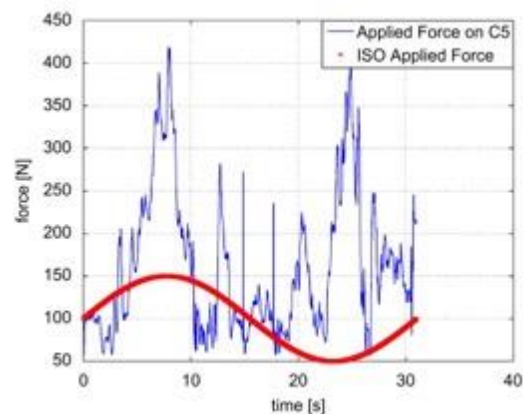


Figure 2.14 Intradiscal load at C5-C6 disc level from a kinematic simulation with superimposed ISO18192 [1] axial load input parameters in red (x-axis not to scale) [100]

Another more comprehensive multibody musculoskeletal model based on a 51 kg male cadaver, has demonstrated through its simulation that the axial force exerted on intervertebral disc could reach as high as 40% of the model's body weight (approximately 200 N) in the cervical spine during lateral bending and axial rotation, exceeding the prescribed vertical force value set by ISO18192-1 [1] [159].

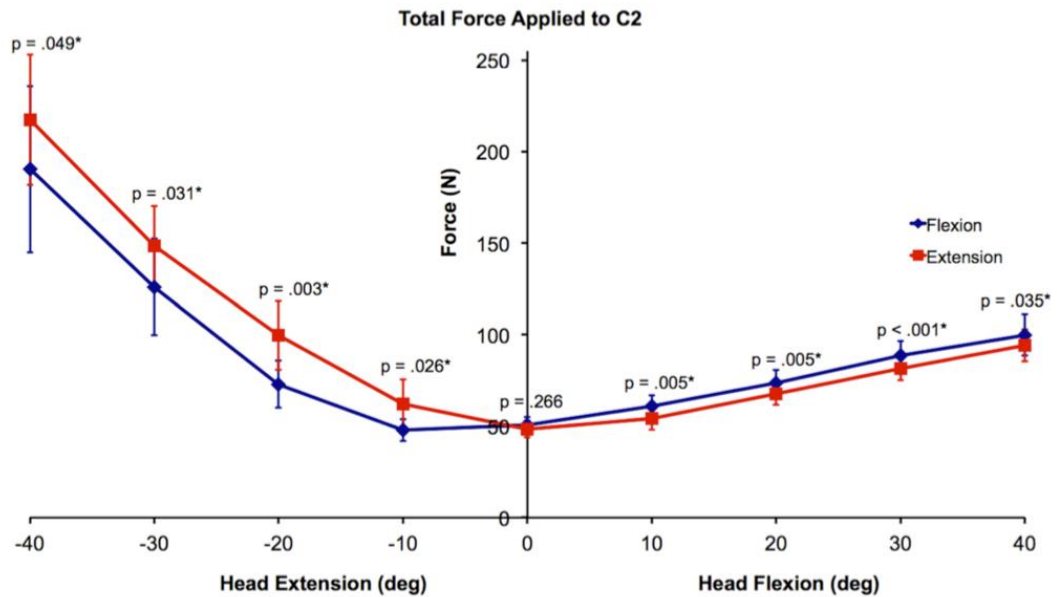


Figure 2.15 Average of total force at C2 level from 16 subjects during head movement from full flexion to full extension and vice versa [158]

These latest findings on cervical spine axial force, derived from a more sophisticated, mathematical calculations, support the need for a review on the load prescribed in the ISO18192-1 [1] protocol. As highlighted by Anderson and Rouleau [76], the wear testing also has to evaluate the effect from extreme load and motion in the cervical spine despite being infrequently occurring, which currently is not covered in the standard protocol.

A detailed review on linked-segment musculoskeletal multibody modelling is discussed in Section 2.5.

2.4.4 Angular Displacement Profiles

The same argument could not be said with regards to the angular displacement prescribed in the ISO18192-1 [1] protocol as studies on spinal kinematics have been well-established for years at the time of the publication of the standard; and some of them are cited as their source of reference [1]. Nevertheless, the reported average of the cervical intervertebral joint angle RoM in the academic literature seems to be wide ranging with no consensus.

Salem *et al.* [160] in a study that measured individual cervical intervertebral joint angle from 20 healthy individuals during a maximal passive axial rotation have established that the mean joint angles for the lower four cervical intervertebral joints (C3-C4, C4-C5, C5-C6, and C6-C7) were between $4.0 \pm 2.0^\circ$ to $5.5 \pm 1.0^\circ$ unilaterally whilst Anderst *et al.* [161] have reported a bigger range between $6.5 \pm 1.7^\circ$ to $11.8 \pm 2.1^\circ$, unilaterally, in all cervical levels (Table 2.5). Although both studies have employed the same radiographic modalities for data acquisition, subjects in the former study are moving passively, in a supine position, whilst subjects in the latter study is actively moving, in an erect posture [160, 161]. The discrepancy in RoM is even more obvious when this is compared against observations made by Panjabi *et al.* [162], from their cadaveric study of cervical spine kinematics, as well as values cited in the article by Grider-Potter *et al.* [17] relating to cervical RoM amongst primates. Table 2.5 summarises the reported RoM for cervical intervertebral joint angle for levels between C3 to C7 from these studies, where cervical articulating disc prosthesis is typically implanted.

| Intervertebral Disc Levels | Mean (\pm SD) of Unilateral Axial Rotation ($^\circ$) | | | Mean (\pm SD) of Unilateral Lateral Bending ($^\circ$) | | | Mean (\pm SD) of Flexion-Extension ($^\circ$) | | |
|----------------------------|--|----------------------|-----------------------|---|----------------------|-----------------------|--|-----------------------|-----------------------|
| | [160] | [162] | [161] | [17] | [162] | [161] | [17] | [162] | [161] |
| C3-C4 | 5.0 (± 2.0) | 2.6 (± 1.2) | 11.8 (± 2.1) | 11.0 | 4.5 (± 1.9) | 14.3 (± 2.8) | 14.0 | 7.7 (± 2.5) | 17.1 (± 3.3) |
| C4-C5 | 5.5 (± 1.0) | 3.4 (± 1.3) | 11.3 (± 1.7) | 11.0 | 4.7 (± 1.7) | 13.1 (± 3.2) | 12.0 | 10.1 (± 4.0) | 19.5 (± 3.4) |
| C5-C6 | 5.0 (± 2.0) | 2.5 (± 1.0) | 9.3 (± 1.9) | 8.0 | 3.3 (± 1.5) | 12.3 (± 3.2) | 18.0 | 9.9 (± 2.7) | 19.7 (± 3.7) |
| C6-C7 | 4.0 (± 2.0) | 1.5 (± 0.8) | 6.5 (± 1.7) | 7.0 | 2.7 (± 1.5) | 14.5 (± 3.9) | 19.0 | 7.1 (± 2.0) | 15.8 (± 4.8) |

Table 2.5 Mean (and standard deviation) of cervical intervertebral discs RoM.

Wear, as explained in Section 2.3.1, is affected by the distance of sliding motion between two opposing surfaces, which translated as joint angular displacement excursion in articulating disc implant [86]. The magnitude for angular displacements prescribed in ISO18192-1 [1] is within the cervical RoM summarised in Table 2.5. However, it can be argued that simulating the spinal disc implant with the greatest range of motion of the cervical spine might not accurately represent physiological wear *in vivo* as humans rarely utilise the extreme ends in the motion spectrum as evidenced by Cobian *et al.* [163]. As typical head motion is expected to cover merely a sizeable part of the full extent

of cervical motion range, it is unknown whether the prescribed values in ISO18192-1 [1] are an indicative of this notion *i.e.* a representative portion from full cervical RoM. An overestimation or underestimation of this value will have a heavy influence on the estimation of wear rate of the implant.

2.4.5 Duty Cycle

The ISO18192-1 [1] standard also specifies the number of cycles for the wear testing of spinal intervertebral disc prostheses has to run. The protocol outlined in the standard equates one million cycles (MC) to one year-wear *in vivo* and the prostheses are expected complete ten million cycles [1]. This is to replicate the ten-year approximation of *in vivo* implantation before the tests should be stopped unless it failed beforehand. The ISO18192-1 [1] standard, in Annex A, has cited that the association was based on the work by Nechtow *et al.* [153] and Kurtz *et al.* [164]. However, both cited articles have never drawn any conclusion nor inferred on the number of cycles equivalency in their published articles. Cobian *et al.* [16], in a study of daily motion of cervical and lumbar spine, have extrapolated the recorded neck movements and found that it is three to five times more frequent than one million cycles per year as claimed in ISO18192-1 [1]. Nonetheless, they also found that the amplitude of the movement is significantly smaller than the prescribed values in ISO18192-1 [1] which, combined with more frequent movement in the neck, equalise the total annual excursion extrapolated when compared against the total annual excursion extrapolated from the prescribed angular displacements in ISO18192-1 [1] [16].

A comparative study between the wear in simulator-tested implants with explanted Bryan[®] and Prestige[®] cervical disc prostheses from patients by Anderson *et al.* [12] pointed out that even though the association of 1 MC \equiv 1 year-wear has been generally accepted in hip joint prostheses, this might have been overestimated in cervical implants as per their observation on the retrieved devices, between five to ten folds. This view was further repeated in a review article by Kurtz *et al.* [120] where they cited another example from a conference proceeding which demonstrated similarly comparable outcomes. This was later substantiated by another comparative study where the results showed the *in vitro*

wear from 0.5 MC producing a higher result than retrieved implants of up to 4.1 years [13].

2.4.6 Degree of Freedom Coverage

The protocol outlined by ISO18192-1 [1] for disc prostheses covers all three components of rotation; flexion/extension, lateral bending, and axial rotation. Only one component of load translation that is specified in the obligatory testing protocol - the axial loading, which makes a total of four active DoFs is in the wear simulation. On top of that, the protocol also indicated that the anterior-posterior shear loading also has to be added when testing the lumbar disc prostheses by mounting the implant with 10° inclination at the line of axial load being applied [1]. This requirement is not necessary for testing the cervical implant due to the fairly horizontal nature of the cervical intervertebral disc.

As described in Section 2.2.1, the DoF within an articulating spinal intervertebral prosthesis will depend its mechanical design. The decision to test on an additional DoF, on top of the four prescribed in the ISO standard, will have to be based on the implant's DoF. Vicars *et al.* [165] has shown that the inclusion of an additional active DoF will not have a significant difference on the overall wear rate when the implant has a single bearing surface, such as ProDisc®-L lumbar disc device. Whereas the wear rate increased by almost 100% when the fifth DoF was tested on CHARITÉ™ lumbar prostheses which is a dual-bearing implant [166].

2.4.7 Frequency of Load and Motion

The ISO18192-1 [1] standard sets that each wear profile cycle should be completed within one second. There is an allowance given by the standard to increase the frequency to up to 2 Hz with proper justification [1]. An increase in the test frequency, however, will cause an increase in wear (for a constant duty cycle) as shown in a study by Kettler *et al.* [122]. Meanwhile, Kraft [167] have demonstrated that an increased in test frequency to 2 Hz generates a lower wear rate than 1 Hz. The results from this wear testing, however, need to be interpreted

cautiously as the experiment was conducted using PEEK bearing surfaces which a type of polymer that has rarely been used in CTDR except for endplates [69].

Kettler *et al.* [122] asserted that increasing the frequency will deviate from representing the real physiological wear given the high amplitude in the ISO protocols. This view is also shared by Harper *et al.* [168] where they hypothesised that increasing the frequency would cause an increased in flash temperature, which could have three consequences: (a) change in serum viscosity and losing its lubricating properties, (b) denature the protein in the lubricant, and (c) decrease in polymer's hardness and Young's modulus. All these will ultimately cause a greater wear rate in disc implants.

Whereas, lowering the wear testing frequency by half (with the same seven-day serum replacement interval) is not affecting the wear rate in MoP bearing couple in knee implants [169].

2.4.8 Cyclical Motion Conundrum

Undoubtedly, there are similarities between the spinal disc and the hip implant wear testing protocols. It can be argued that the blueprint of spinal disc protocol could have been drafted from the hip protocol at the beginning.

The hip joint is part of the lower limb in which its main function is gait and locomotion. In order to accomplish this, the two lower limbs produce predominantly a movement that is cyclical in nature and mirror-image to each other. Despite having a quintessential ball-and-socket joint, the archetypal movement of the thigh segment is not very versatile and rather prescriptive. Evolutionary adaptation of deep tissue layers surrounding the joint, as to improve joint stability, also contributing to the restrictive movement of these appendages. This is not to say that the other asynchronous or asymmetrical movements are not happening at all, only rarely and when necessary, for example during sporting activities or dancing. It would make sense, therefore, for the wear testing protocol of the hip prostheses to be designed in a repetitive, cyclical motion when it reflects the bulk of the work done by these limbs.

Nonetheless, the latest evidence by Lunn *et al.* [14] has also shown that even the prescribed cyclic motion in ISO14242-1 [2] for hip implant poorly represents a real-world loading of the joint with high variability amongst the subjects recruited. This is further supported by the discrepancies found in numerical wear simulation between the prescribed parameters in ISO14242-1 [2] and loading experience during actual locomotor and non-locomotor activities [15].

Adopting the hip wear testing protocol model in cervical disc implant is probably an appropriate initial step. However, representing the cervical intervertebral joint movement similar to hip motion profile might have simplified the versatility of cervical spine articulation radically. The extreme flexibility afforded by the cervical spine has to be acknowledged. The neck allows the head in bipedal and quadrupedal organisms to be agile and responsive to the surrounding for survival.

The motion testing profile in ISO18192-1 [1] also implies that all three cardinal movements of the head are equally common and regular, which might not reflect real-world activity. A descriptive study that aimed to quantify the frequency and magnitude of human neck motion carried out by Sterling *et al.* [170] shows the flexion/extension movement occurs twice more frequently than lateral bending or axial rotation. Another study by Cobian *et al.* [171] found that majority of the daily movements involve only a small percentage of lateral bending, based on movement recording over a five-day period, compared to flexion/extension or axial rotation. This claim was further supported by Sterling *et al.* [170] who found the median RoM in lateral bending is only 10° when compared to 13° in both flexion/extension and axial rotation.

2.4.9 Short Summary

Based on the latest evidence available in academic literature, it is believed that the main parameters prescribed in ISO18192-1 [1] for wear testing of articulating cervical disc device is lacking in physiological basis [16]. The axial load for the wear simulation is underestimated based on data from musculoskeletal modelling whilst the joint angle for sliding motion is overestimated when compared to joint RoM during typical ADL. The duty cycle required to emulate an annual joint

excursion also is found to be insufficient. All in all, the wear testing profile advocated by ISO18192-1 [1] is not reflective of a typical ADL, rather just an arbitrary, stylised sinusoidal waves.

All the arguments outlined above have highlighted the need for the cervical disc prostheses wear testing protocol to be further refined. The input parameters incorporated into the test analysis should reflect physiologically relevant load and motions, as well as real-world activities of daily living, in the neck. The following section, Section 2.5, will outline the fundamental knowledge of biomechanics and will review the cutting-edge techniques implemented within this area of research to obtain a more accurate estimation of load and motion within the cervical spine.

2.5 Cervical Spine Biomechanics

Human movement has been studied for centuries for various of reasons [172]. Human motion analysis, or kinesiology, is a study with the aim “to understand the mechanical function of musculoskeletal system during the execution of a motor task” [172]. From this analysis, joint angle as well as joint loadings can be determined for any specific joint. These variables can be used as an input for joint simulator as explained in the introductory paragraph of Section 2.4 so the machine could physiologically replicate the motion and loading of the said joint accurately. Following on to that, it also would uncover the adequacy of parameters prescribed in the wear testing protocols that were developed by the ISO or the ASTM for implant manufacturers to elicit its wear performance *in vivo* as discussed in Sections 2.4.3 and 2.4.4. As stated in Section 2.3.1, these variables also correspond to parameters in Archard’s Volumetric Wear Equation.

Joint loading is calculated through an inverse dynamic analysis which greatly relying on musculoskeletal model. In brief, it is a model that comprise of several rigid bodies (which represent bony segments in the body) linked by a number of constraining kinematic pairs (such as revolute or hinge joints, which represent skeletal joints in the body) and the interaction between them are governed by the rules of engineering mechanics (Figure 2.16). The angle between these rigid bodies represents the joint angle for which the represented body segments are

articulating. A complete human mannequin model could be built if there are enough rigid bodies to sufficiently represent the whole body. This representative model of a human body works on the assumptions that each segment has a fixed mass (located at the centre of mass) and a fixed dimension (with no distortion) and they remained constant throughout the analysis [173]. And, more importantly, the net forces are assumed to pass through these joint links via a single contact point between two segments [174]. The model can be employed to mimic a certain static posture or, with the use of trajectory equation, dynamic movement of body parts or limbs where the calculation for joint angle and loadings can be performed. Like in a typical gait analysis, the mannequin model also can be set to imitate a daily activity movement in three dimensional space using trajectory data gathered from motion capture (MoCap) system. This analysis also has been frequently supplemented by measurement from force plate to capture ground reaction force values as part of external forces acting on the model. The following section will review in detail how this could be achieved for cervical spine.

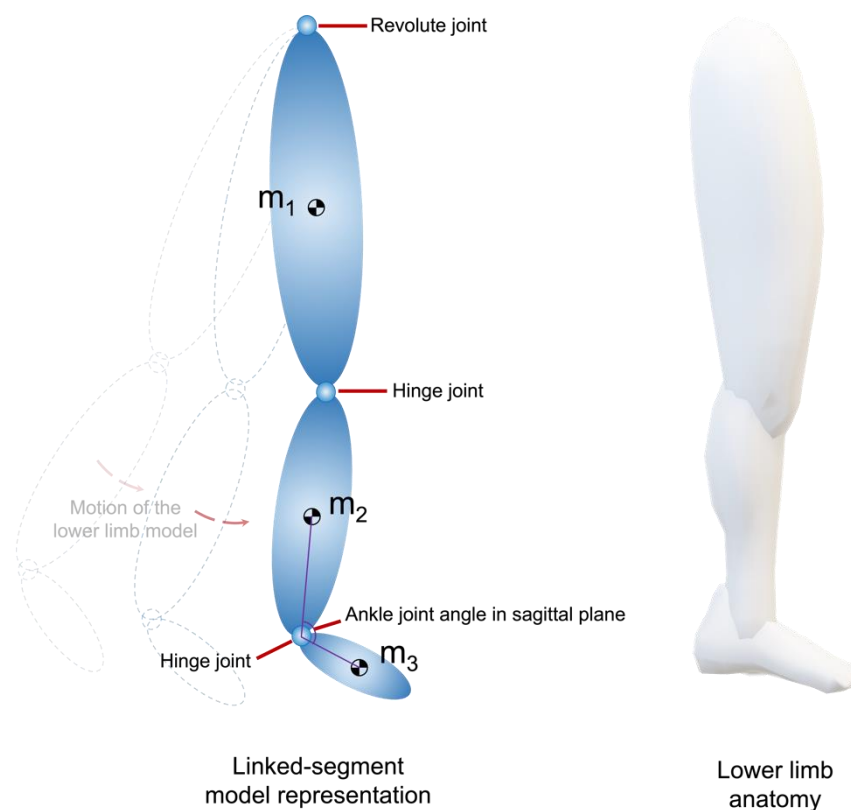


Figure 2.16 An illustration of linked-segment model as a representation for lower limb of a human (adapted and reproduced from [173])

2.5.1 Spinal Kinematics and Soft Tissue Artefacts

Using state-of-the-art technology, tracking the movement of body segment is typically done through MoCap, which employs the use of reflective markers placed on important landmarks and/or bony prominences that will reflect an infrared signal emitted at a certain frequency by an optoelectronic equipment which, at the same time, is recording it. This technique has been an established method of obtaining trajectory data in orthopaedic biomechanics, particularly in gait analysis for patients with problem with locomotion. In a typical gait biomechanics, large segments such as the thigh, shank, upper and forearm are represented and modelled as one single rigid-body which is reasonable considering it is being supported by a single long bone, with areas for marker placement in abundance. The neck, on the contrary, is a much smaller body segment that consists of multiple smaller bones which makes the tracking and placement of the markers less than ideal due to limited surface area available as well as close co-location of bony prominences.

Soft tissue artefact has been a longstanding source of error surrounding MoCap and several works have been undertaken to quantify the influence of the artefacts within the cervical spine. Although the correlation can be mapped between vertebral landmarks against its corresponding skin markers, Wang *et al.* [175] have shown that there is a high variability in skin deformation in different axes direction, even for the same movement. A contrasting outcome is seen in study by Zemp *et al.* [176] where the correlation between vertebral landmarks and corresponding skin markers is found to be low. Neither of these studies examine the effect of soft tissue artefact during axial rotation of the spine.

Suzuki *et al.* [177] has established a simple algorithm to reduce the influence of soft tissue artefact on skin marker for motion tracking in two-dimensional plane. Although the algorithm can be further developed for three-dimensional tracking, the method is only suitable for periodic movement such as gait and requires a minimum of three distinct markers for each segment. The authors also state that there is a possibility of converging failure due to larger amounts of parameters to solve in three-dimensional problem.

Effort also has been made to improve the tracking method for individual cervical vertebrae. Wu *et al.* [178] has shown the reliability in measuring individual intervertebral cervical joint angles when additional markers are placed on the bony landmarks of spinous and transverse processes of second, third, fifth, and seventh cervical vertebrae. The study is only exploring the motion in sagittal and coronal planes and reliability of marker tracking in axial rotation movement, however, was not explored.

Identifying a correct body landmark for the cervical spine, typically the spinous process for seventh cervical vertebra, is also important as it will determine the placing of the skin markers. Even with the best palpation method, and confirmed with radiographic images, only 77.1% of seventh spinous process could be correctly identified [179]. Misidentifying the only reliable body landmark for cervical spine will carry the error to the subsequent levels if additional markers to be employed. Serial radiograph remains the most reliable method of tracking individual vertebrae in motion capture with sub-millimetre accuracy [180] but this is without a trade-off, either radiation exposure for computed tomography/x-rays or long scanning time in MRI.

2.5.2 Tracking the Movement of Cervical Spinal Vertebrae

More recently, a detailed study in cervical kinematics was born from the need to analyse cervical vertebral movement during sudden accelerative events like whiplash injury and G-force experienced by jet-fighter pilots [157, 181, 182]. Despite numerous complex anatomical structures present within the neck, tracking the motion of the seven individual cervical vertebrae with high precision has been made possible through radiographic imaging. In 2010, Marin *et al.* [183] presented a new approach in which data from MoCap is combined with x-ray images of three cervical spinal positions – in full flexion, full extension, and in neutral position. This proof-of-concept of co-registration between radiograph images and MoCap is further exploited by Anderst *et al.* [184] where they use a dynamic, as opposed to a static, biplane radiograph collected at 30 images per second on 19 subjects whilst performing continuous head flexion/extension. Using the same method, Anderst *et al.* [185] then further expanded their research

to catalogue cervical spinal intervertebral kinematics from 29 participants in all axes of motion, which they then proposed an acceptable range from the aggregated curves to be considered as normal cervical kinematics.

Studies on cervical kinematics have shown that the cervical vertebrae move in a complex, and at times counter-intuitive, pattern even for simple unidirectional motion such as flexion/extension [186]. For the same head angular orientation (with respect to the torso) for any given level, the cervical intervertebral joint angle is different during head flexion motion when compared to head extension motion [184]. It has also been shown, through the radiographic-MoCap method, the presence of 'coupled motion' phenomenon within the cervical intervertebral joint during lateral bending and axial rotation of the head, where the intended motion of the cervical vertebra would also result in motion in another plane [161, 185, 187]. On top of the three cardinal angular motions, cervical intervertebral joint also has been noted to have a linear translation motion although they are mostly less than 1 mm in all directions [188, 189].

2.5.3 Other Methods of Cervical Kinematics Study

Cadaveric study also has been used as a method for obtaining kinematics of the cervical spine. This was made possible when, in early 2000, Patwardhan *et al.* [190] introduced a 'follower load' as the appropriate compressive loading technique for cervical spine, as the traditional vertical axial load that is tangential to horizontal surface applied onto the lordotic cervical spine will cause buckling of the specimen even at low force. Using the follower load on cadaveric specimens, the kinematic pattern of the individual cervical vertebrae in *in vivo* can closely replicated during *in vitro* experiment for study involving the motion of the neck [191]. For example, Colle *et al.* [192] have shown that the cervical spine with CTDR has less deviation from normal cervical kinematics than the cervical spine with ACDF when a cervical cadaveric specimen is primed with 70 N follower load.

2.5.4 Estimation of Biomechanical Forces

Study of cervical kinematics discussed in Section 2.5.2 only describes the position and movement of body segments in space or with respect to another body segment. Thus, it is natural for biomechanics researchers to want to understand the forces involved that has caused or been affected by the motion in question within the musculoskeletal system. Tremendous progress has been achieved in this area despite much of the motion source originates from the complex internal musculature, which still poses a great challenge in measuring them. Examples of device used in this field are force transducers embedded within the tendinligamentous tissues to measure the force generated by the muscle and also telemeterised device implanted in replacement of a bone, which could measure the loading exerted on the said bone by its transducer [193, 194]. Although these instruments are capable of providing a direct measurement of the loading, they are, by nature, very invasive, and the measurements are limited to only a specific body part into which it has been inserted.

2.5.5 Inverse Dynamics Study

In an ideal world where the force from a muscle that pulls a bone across a joint is known, the bone's acceleration can be calculated using Newton's Second Law of Motion by dividing the magnitude of the net force, F , with the mass of the bone, m (Equation 2.5). This is known as forward dynamics approach. The displacement of the bone also can be predicted and obtained by double integrating the acceleration of the bone.

$$a = \frac{F}{m}$$

Equation 2.5

a acceleration of bone segment in space

F net force acting on the bone

m mass of the bone, based on anthropometric data

As explained in the previous 2.5.4, it is almost impossible to know the force exerted by any single muscle in the body. Fortunately, the acceleration of the bone can be determined by the second derivative of the bone's displacement in space, based on trajectory data obtained from MoCap. Thus, the magnitude of the force exerted by the bone onto the joint can be calculated using the same Newton's Second Law of Motion in reverse (Equation 2.6). This approach is known as inverse dynamics where the internal forces are reconstructed from the resulting motion, and this concept is based on Newton-Euler mathematical method [195].

$$F = ma$$

Equation 2.6

F force exerted by the bone

m mass of the bone, based on anthropometric data

a acceleration of bone segment in space

Based on Newton's Third Law of Motion, the magnitude of force exerted by the bone onto the joint calculated earlier is the same magnitude of force experienced by the joint, but in the opposite direction, and this is known as *joint reaction force*. Similarly, the joint also transmits and exerts this force onto the adjacent bone that is articulating with it, and the process of determining the internal forces in the adjacent bone continues until the process reaches the body segment or joint of interest, within the linked-segment model, for analysis.

However, this is only half the story where it explains the bone's contribution towards the loading in the joint [173]. In reality, the bone moves due to muscle contraction, which inadvertently contributes towards the loading in the said joint as well. In fact, loading due to muscle contraction is the primary source of loading

in any joint [174]. The net loading experienced by a typical joint, or *joint contact force*, would be a combination of joint reaction force and force originating from muscle activities as an actuator of the movement [173]. Thus, joint moment calculation alone is not enough and biomechanical modelling is incomplete without muscle modelling.

2.5.6 Muscle Recruitment Algorithm

Although the movement of a bone has been established from MoCap trajectory data, discerning the muscles that are responsible for its movement is more complex due to the versatility afforded by the musculoskeletal system. The versatility, where certain motions can be accomplished by several movement strategies, is necessary as a compensating mechanism for any organism when it is affected by injury or disease [172]. This is known as theory of redundancy, where more muscles and joints are made available for the necessary intended body movement [172]. This, as a result, creating a “statically indeterminate” problem, which has been plaguing biomechanics study since the beginning where there are not enough equilibrium equations available to solve the force contributed by any given muscle [196]. Thus, attributing a bone movement to the responsible muscles requiring an optimisation technique where it will apportion the burden of pulling the bone to the crucial muscle groups according to a set criteria [174]. There are a number of optimisation algorithms that has been published and the two well-established algorithms are *polynomial criterion* and *soft saturation criterion* [197]. More recently, Rasmussen *et al.* [196] presented a new muscle recruitment algorithm called ‘*min/max*’ which is built on from the traditional polynomial criterion muscle recruitment algorithm as one of possible solutions to the muscle recruitment quandary.

2.5.7 Muscle Modelling

There are two main models that have been accepted to represent the contractility property of a muscle computationally: (a) Hill’s Muscle Model and (b) Huxley’s Sliding Filament Model [198].

Hill's Muscle Model is designed to imitate the muscle contraction phenomenon, based on experimental observation, rather than the actual mechanism of muscle's cellular physiology [174]. The model can be schematically represented with a tendon component and a muscle component arranged in series, with a pennation angle, θ , between them (Figure 2.17). The tendon component is modelled as an elastic element and operates according to a linear stress-strain curve [174]. The muscle component consists of an active contractile element and two passive elastic elements, arranged in parallel as well as in series to the contractile element; although the series-elastic element is, at times, omitted for simplicity [174]. Despite the lack of actual microscopic representation mechanism of a muscle, the Hill's muscle model is able to replicate muscle properties very well numerically with great efficiency [198].

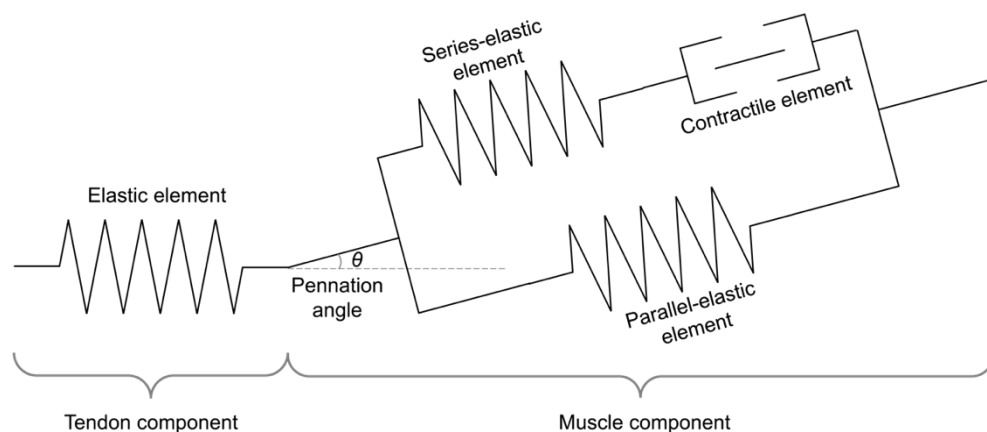


Figure 2.17 Schematic diagram that represent Hill's muscle model (reproduced from [174])

Huxley's Sliding Filament, on the other hand, is modelled according to the actual physiology of muscle cell where the pulling action originates from the cross bridge cycling phenomenon that causes the sliding of actin and myosin filaments [174]. This model however demands a high computational effort for it to be implemented [174, 198].

2.5.8 Biomechanical Modelling of the Cervical Spine

One of the earliest rigid-body modelling examples done for the head and neck was described by Snijders *et al.* [157] where they created a linked-segment model

in three different positions (full flexion, full extension, and neutral position) to predict the joint contact forces and muscle forces around the cervical spine. The model has seven individual segments including the skull. To simplify the computational work required, the vertebrae C3 to C7 was modelled as a single unit that are manoeuvred by six mid-sagittal symmetrical muscle pairs. Even with limited number of muscles, the model is still 'overdetermined', therefore an optimisation algorithm was developed to reduce it to a combination of only three muscles, at any particular time, that are responsible for generating the pulling action for the model. Despite its rudimentary nature, the model presented by Snijder *et al.* [157] has successfully computed the joint contact forces at atlanto-occipital (skull-C1), atlanto-axial (C1-C2), C2-C3, and cervicothoracic (C7-T1) joints during flexion/extension, lateral bending, and axial rotation motion, which later became the reference for the axial loading values in ISO18192-1 [1] testing parameter.

Since then, there has been a steady development and improvement of cervical spine models through discretisation and inclusion of nine basic rigid segments: the skull, seven cervical vertebrae, and first thoracic vertebra/thoracic cage [181, 182, 199, 200]. On top of the discretised cervical spine, de Jager [182] also has improved the muscle element in the model with 14 mid-sagittal symmetrical muscle pairs. The muscle also modelled to be Hill-type where it contains active contractile force, as well as passive elastic force that is attributable to muscle elongation. van der Horst [181] then further improved the muscle modelling by incorporating a more comprehensive 68 mid-sagittal Hill-type muscle pairs with a curved line of action, as opposed to a straight line of action that are employed in previous models by Snijder *et al.* [157] and de Jager [182]. van Lopik and Acar [200] also have showcased another discretised cervical spinal modelling with similar muscle properties in 2007.

2.5.9 Musculoskeletal Multibody Modelling

The emergence of discretised cervical spine also marks the beginning of transition from 'rigid-body' to multibody modelling of the cervical spine, where

other elements with different rigidities are incorporated, such as the ligaments and intervertebral discs.

de Jager [182]'s intervertebral discs are modelled to have a three-directional linear viscoelastic property whereas van der Horst [181]'s disc is modelled non-linearly. Nonetheless, both authors are in agreement when modelling their ligament as a two-dimensional, non-linear, viscoelastic object [181, 182]. The cervical biomechanical model developed by van der Horst [181] has become one of the building blocks for whole body template available in AnyBody Modeling System software, where it is also incorporated the new 'min/max' as well as polynomial criterion for muscle recruitment algorithm [197, 201].

Based on the cervical model template provided in AnyBody Modeling System, Diao *et al.* [202] have published an enhanced version of the discretised cervical spine model which includes facet joints at every level of the vertebra as well as six DoF intervertebral joints, as opposed to a ball-and-socket joint which is limited to three DoF. With the additional three DoF, the model is also able to account for the linear translation of cervical vertebrae as found by Ishii *et al.* [188, 189] in their radiographic-MoCap kinematic studies. Through the improved model, Diao *et al.* [202] have found that the intervertebral compressive force value derived from the improved model is much closer to cadaveric study measurement than the original model. This upgraded cervical spine model was later used to further assess the dynamic spinal loading during rotational motion of the neck where they have established the amount of shear forces in anterior/posterior and medial/lateral direction from the model simulation [203].

As the spine is a set of bones linked by joints, a discretised spine model can help predicting a more precise loading estimation, even in the neighbouring spinal region, which could provide a better understanding of complex loading interplay within the spine, holistically. In 2016, Ignasiak *et al.* [204] published a discretised thoracic spine model that includes individual vertebral level's articulation with ribs bilaterally, which is a departure from the conventional model of thoracic cage as a single rigid body segment. Using the discretised thoracic spine, it has been shown that there is a discernible axial loading in the upper lumbar spine from a model with a single-segment thoracic spine [205]. This is also true when

comparing the predicted maximum compressive load in the thoracic region between young and the elderly during activities of daily living. Ignasiak *et al.* [206] concluded that although the axial loading is lower in the elderly group, it does not discount the fracture risk posed to them due to a reduction in bone quality from aging process. In addition to that, it has been suggested that the motion of the upper thoracic spine plays an important part towards neck mobility and the inclusion of discretised thoracic model would be beneficial [207].

2.5.10 Other Methods for Predicting Cervical Spinal Loading

Apart from linked-segment models, a finite element approach has also been used to non-invasively predict the loading within the cervical spine, where it has the advantage of having high-fidelity anatomical structures modelled as well as being subject-specific, based on radiographic images. Using the finite element model, Goel *et al.* [208], predicted that 88% of cervical axial loading passes through anterior component of the cervical vertebrae *i.e.* intervertebral disc between C5 and C6. Following that, Kumaresan *et al.* [209] also utilised finite element modelling to predict the compression forces as well as shear forces at five specific points along the sagittal plane within the C4-C5 and C5-C6 intervertebral discs during quasi-flexion and quasi-extension motions. The downside of employing finite element analysis is the computational effort and time required in running the simulation, therefore the models used tend to be incomplete *i.e.* limited to a few cervical levels when, in real life, some of the muscles and ligaments surrounding the cervical spine stretch across several spinal levels. For example, Goel *et al.* [208] only models components for an FSU whereas Kumaresan *et al.* [209] built a three-level-vertebrae spinal model with two intervening intervertebral discs.

2.5.11 Activities of Daily Living in the Context of Cervical Spine

Studies of spinal biomechanics ordinarily will look at the spine in three pure, angular motions: flexion/extension (in sagittal plane), lateral bending (in coronal plane), and axial rotation (in transverse plane). These motions are illustrated in Figure 2.4.

Additionally, there are a number of biomechanics studies that look into the functional movement of the neck and head. These studies investigate the RoM in the neck by measuring the head tilt with respect to the torso during several activities of daily living (ADL) [163, 210-213]. Those ADLs are listed in Table 2.6.

| Activities of Daily Living | Bennett <i>et al.</i> [210] | Bible <i>et al.</i> [211] Miller <i>et al.</i> [212, 213] | Cobian <i>et al.</i> [163] |
|---|-----------------------------|--|----------------------------|
| Standing to sitting position | | ✓ | |
| Backing up a car | ✓ | ✓ | ✓ |
| Putting on socks | | ✓ | |
| Tying shoelaces | ✓ | ✓ | ✓ |
| Reading on lap | | ✓ | |
| Cutting food with knife and fork | ✓ | ✓ | |
| Rising from sitting position | ✓ | ✓ | ✓ |
| Washing hands in standing position | | ✓ | |
| Shaving facial hair/applying make-up | | ✓ | |
| Washing hair in shower | ✓ | ✓ | ✓ |
| Picking up object from floor by bending | | ✓ | ✓ |
| Picking up object from floor by squatting | | ✓ | |
| Walking | | ✓ | ✓ |
| Walking up the stairs | | ✓ | |
| Walking down the stairs | | ✓ | |
| Pick up object from one side and place on the other | | | ✓ |
| Putting on/taking off trousers | | | ✓ |
| Putting on jacket | | | ✓ |
| Clearing the table | | | ✓ |
| Reaching up to shelf/overhead | ✓ | | ✓ |
| Writing on a table | ✓ | | ✓ |
| Looking both ways to cross a street | ✓ | | ✓ |
| Talking on the phone | ✓ | | ✓ |
| Taking a drink | ✓ | | ✓ |
| Brushing teeth | | | ✓ |
| Pouring from a pitcher | ✓ | | |
| Reading a newspaper | ✓ | | |
| Opening a door | ✓ | | |

Table 2.6 List of common ADL tasks found in literature [163, 210-213].

These studies have given a further insight into the RoM of the cervical spine particularly during ADL. The study by Bennett *et al.* [210] looked at 13 different everyday tasks and found that four of them, tying shoelaces; reversing a car; washing the hair; and crossing the road; require the largest extent of the neck

motion range. Cobian *et al.* [171] later conducted a study to identify the frequency and magnitude of neck movement during the activities of daily living and found that a more intense activity will require greater cervical motion and vice versa. They later found out that the cervical motion during majority of activities of daily living only utilise 20 to 40 per cent of the maximum RoM in the neck [163]. These studies also give us an indication that activities that have an extensive neck recruitment might not necessarily be an isolated or extreme task, such as twisting the upper body whilst reversing a car which is performed by majority of adults when driving.

Conclusions drawn in these studies are based on the movement of the head with respect to the torso, as a function of cervical RoM, as opposed to individual cervical intervertebral joint angles. The joint angle of the individual FSU in those activities could be investigated and quantified using discretised cervical spine musculoskeletal model as described in Sections 2.5.8 and 2.5.9 given there is lack of study on cervical biomechanics outside the three cardinal movements described earlier in this section.

As mentioned before, it is believed that the wear testing protocol in ISO18192-1 [1] for articulating cervical disc device is lacking in physiological basis, to a point where the profile was drawn in arbitrary, stylised sinusoidal waves for all its kinematics and loading parameters [16]. These stylised curves are not only unrealistic but also not reflective of any of the relevant ADL found by these studies. All the arguments outlined above have highlighted the need for the cervical disc prostheses wear testing protocol to be further refined. The input parameters incorporated into the test analysis should reflect physiologically-relevant load and motions, as well as real-world activities of daily living, in the neck.

2.5.12 Short Summary

Capitalising on Newton's Second and Third Law of Motion, inverse dynamic analysis is a non-invasive alternative for determining joint loading in linked-segment model in kinesiology. Using anthropometric data as well as kinematics

measurement (and its derivatives) of a particular body segment, forces and loads acting on it can be derived through musculoskeletal multibody modelling, which also includes other soft tissues elements and muscle modelling. This mannequin model is used to simulate movement of a subject recorded from MoCap equipment in which the joint angle also can be computed. This method allows the analysis of biomechanics of human body during ADL, specifically in the cervical spine, where the output also can be the testing parameters for evaluating the wear performance of cervical disc implants.

2.6 Summary of Literature Review

There are several articulating cervical disc implants that are available commercially, mostly MoP or MoM, with different biomechanical properties [65]. These implants are used for CTDR where it has been indicated as an alternative surgical intervention to ACDF for cervical myelopathy and radiculopathy [44, 45]. The CTDR also has been shown to be more advantageous in terms of averting the unwanted side-effects such as adjacent segment degeneration and heterotopic ossification [29, 33, 41]. Like its predecessors in joint replacement technology, these devices are not immune to wear that is universally seen in other orthopaedic implants, with abrasion and adhesion being the most common wear mechanisms occurring in MoP [120]. The wear testing protocol intended for the spinal intervertebral disc implant published by the ISO has been widely used by many device manufacturers for pre-clinical trial assessment and market authorisation, owing to its composite, multidirectional motions, which assimilates the cross-shear effect into the simulation compared to standard issued by ASTM [121].

Nonetheless, it is believed that test parameters prescribed in ISO18192-1 [1] are lacking in a strong clinical basis or explant analysis justifications [16]. The protocols formulated its cervical axial force parameter from a limited amount of information available on loading in human cervical spine at the time it was drafted [1]. Several more recent studies have estimated a higher axial loading than the reported magnitude in ISO18192-1 [1] [100, 158, 159]. The angular displacement parameters it recommends, however, seem to cover the whole RoM for all three

planes of cervical movement when it has been shown that humans only utilise a portion of that spectrum in their daily lives [163]. In addition, the number of head movements annually is thought to be underestimated by ISO18192-1 [1] based on its 1 MC to one year wear equivalency ratio advocated in the standard [16]. The angular displacement wear profile also implies that all three cardinal motions of the head (flexion/extension, lateral bending, and axial rotation) happen in equal measure whilst studies have shown that movement in flexion/extension direction occurs more frequently than the others [16]. All in all, the ISO18192-1 [1] document comes short in representing a physiologically relevant loading and angular displacement of the cervical spine in daily life [16]. Meanwhile, the current studies on cervical biomechanics have been focussing heavily on the three cardinal motions of the head rather than the functional activities carried out every day. An investigation to ascertain the loads and angular motion of the cervical spine during activities of daily living is needed, which presently is a gap in this field of research. The outcome from this study would be a valuable input in refining the current wear testing protocols prescribed in ISO18192-1 [1] for cervical intervertebral disc prostheses and it is what motivates this research project.

2.7 Hypotheses

As summarised in Section 2.6, there are research gaps within the cervical spine biomechanical literature relating to activities of daily living, where more realistic loadings and accurate motion of individual vertebrae are being depicted. There is also a void in information on wear analysis of the cervical disc implant when it is being subjected to these parameters that are more physiologically relevant.

Based on the available evidence from the literature to date, three hypotheses are to be tested in this thesis:-

Hypothesis I: Cervical joint angle during activities of daily living is ***smaller*** than prescribed cervical joint angle in ISO18192-1 [1] in all movement directions (flexion/extension, lateral bending, and axial rotation).

Hypothesis II: Cervical joint axial loading during activities of daily living is **higher** than prescribed cervical joint axial loading in ISO18192-1 [1].

And consequently,

Hypothesis III: the wear rate of cervical disc implant under loads and motions that represent activity of daily living is **higher** than the wear rate of the implant under loads and motions prescribed in ISO18192-1 [1].

2.8 Aims and Objectives

Based on the knowledge gaps described in the summary of the literature review, a research project is, therefore, proposed to investigate the wear of cervical disc prostheses under the loads and motions that represent activities of daily living.

The aims of the research are:-

- a) to quantify the cervical spine loads and motions during activities of daily living using motion capture techniques and multibody modelling, and
- b) to undertake a mechanical wear simulation of cervical disc prostheses using the standard parameters as well as the loads and motions derived within the spectrum of activities of daily living, outlined in objective (a).

The first part of the research focuses on the generation of subject-specific data using motion capture techniques and simulation on a multibody, musculoskeletal model to quantify the loads and motions in the cervical spine during various tasks that are routinely performed every day.

The second portion of the project utilises the analysed data from the cervical biomechanical studies to be fed into an advanced, multi-station joint simulator for wear testing of cervical disc prostheses. Comparisons are made after the mechanical wear simulation on the consequences of wear parameters prescribed

by the ISO18192-1 [1] standard against loads and motions experienced during routine activities towards the disc implant.

To achieve these goals, six associated objectives are outlined below:-

- a) to determine a list of everyday tasks that are thought to have an impact on the cervical spinal disc. This objective is achieved through a focus group discussion amongst Public and Patient Involvement/Engagement (PPIE) members, who suffer from neck or cervical spine problems. The list is then compared with activities that are reported in academic literature.
- b) to establish a catalogue of cervical joint loads and motions during several activities of daily living involving the cervical spine. The catalogue will include individual cervical intervertebral joint loads between C3 to T1 disc level of healthy subjects simulated from musculoskeletal multibody dynamics modelling.
- c) to formulate new wear testing profiles based on loads and motion of cervical spine during ADL as an input for wear simulation of cervical disc implants. The input can be used for mechanical or numerical wear testing.
- d) to deploy the new wear testing profiles onto state-of-the-art electromechanical three-station Hip Joint Simulator. These simulators were developed and commissioned in 2015 by LifeLongJoints consortium, a €13-million-collaboration funded by European Commission (NMP-310477).
- e) to run mechanical wear simulations under the standard (ISO18192-1 [1]) and physiologically relevant data formulated in objective (c) on an electromechanical joint simulator for five million cycles, using replicas of disc implant bearing surfaces.
- f) to analyse and compare gravimetric mass loss, as well as surface roughness of the bearing surfaces, throughout mechanical wear testing for both wear tests conditions.

2.9 Overall Research Project Workflow

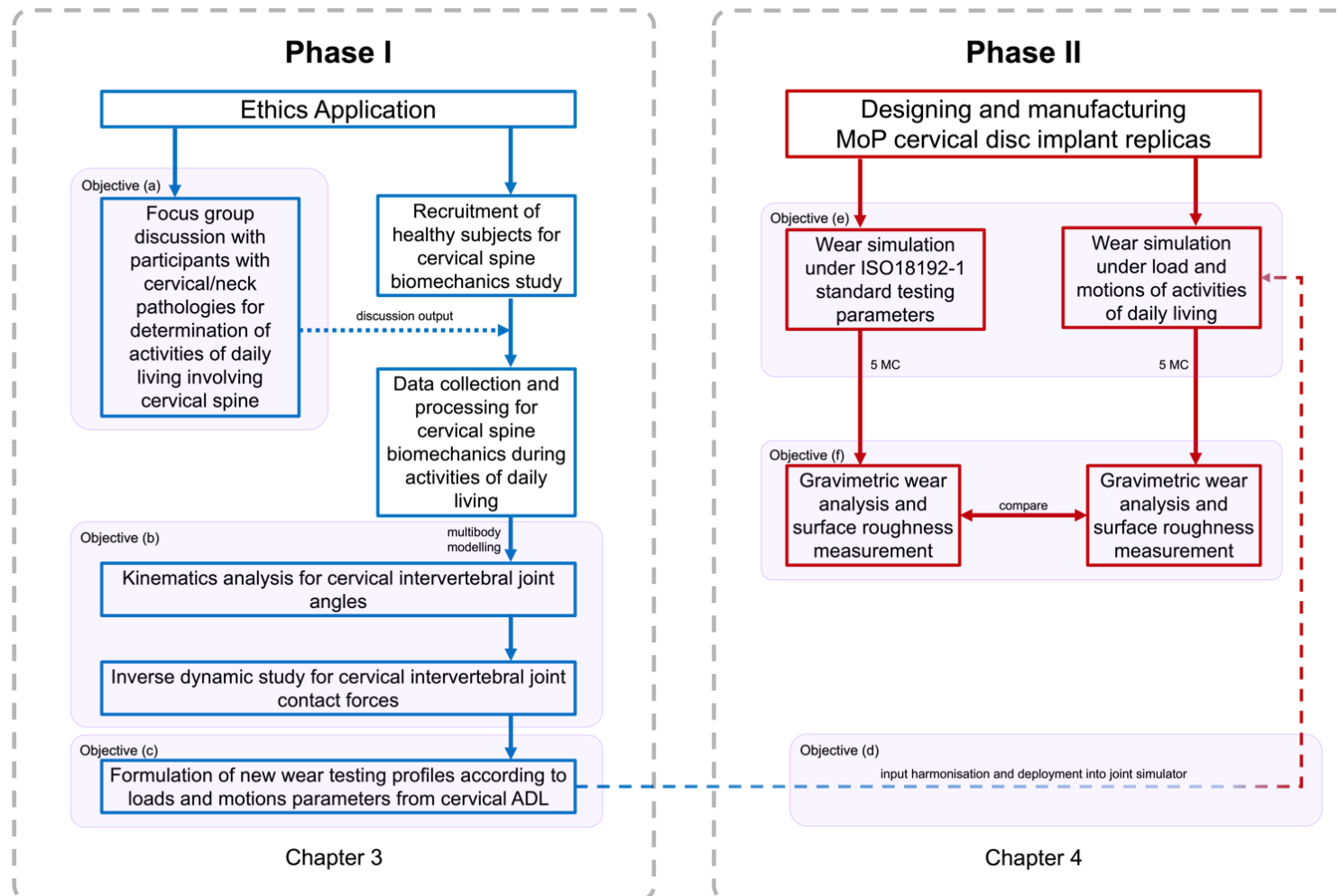


Figure 2.18 General workflow of activities involved in the current research project

Chapter 3

Study of Cervical Spine Biomechanics During Activities of Daily Living

In Chapter 2, it has been established that the parameters in ISO18192-1 [1] are not reflective of the current understanding on cervical spine biomechanics. The magnitude for axial loading prescribed for testing the implant in ISO18192-1 [1] originates from a basic link-segment model proposed by Snijders *et al.* [157] in 1991. Since then, more recent studies have estimated a higher axial loading than the reported magnitude [100, 158, 159]. The angular displacement parameters that ISO18192-1 [1] recommends seem to cover the whole RoM for all three planes of cervical movement when it has been shown that humans only utilise a portion of that spectrum movement in their daily lives [163].

Thus, the goal for Phase I of this research project is to quantify the cervical spine loads and motions during activities of daily living using motion capture techniques and multibody modelling. The study will involve a generation of cervical biomechanical data during activities of daily living from healthy adult population before being analysed through kinematics and inverse dynamic modelling. This chapter will be reporting the experimental activities carried out in fulfilling this aim. Figure 3.1 illustrates the activities involved within Phase I.

The three outlined objectives associated with Phase I in fulfilling its aim are:-

- a) to determine a list of everyday tasks that are thought to have an impact the cervical spinal disc,
- b) to establish a catalogue of cervical joint loads and motions during ADL involving the cervical spine, and
- c) to formulate new wear testing profiles based on loads and motions of cervical spine during ADL as an input for wear simulation of cervical disc implants.

Phase I

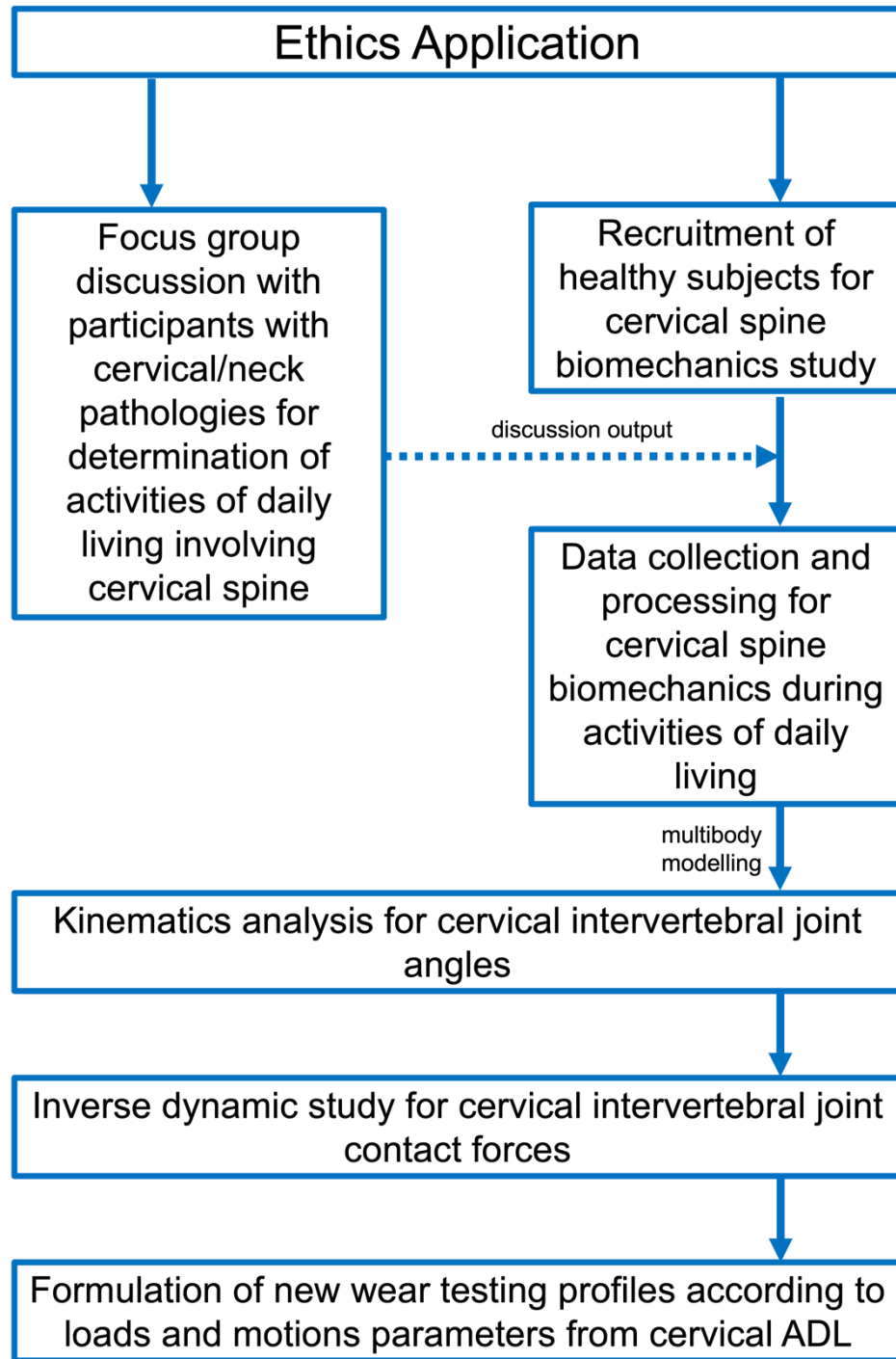


Figure 3.1 Workflow for activities involved in Phase I

3.1 Methods

3.1.1 Ethics and Covid-safety Measures

An application was submitted to Engineering and Physical Sciences Faculty Research Ethics Committee at the University of Leeds for a review on 3rd December 2019. The University-level ethical review board is responsible for evaluating any study protocol which involves healthy human participants as well as the handling of personal information data for experimental activities. The application was submitted together with Data Management Plan, Participant Information Sheet as well as all subject recruitment communications. The committee had reviewed the protocol and provided their outcome on 18th March 2020 with some minor amendments suggested. The revision to the application was made and resubmitted to the committee on 22nd April 2020 and it was favourably approved on 12th May 2020.

Subject recruitment, however, did not start until fourth quarter of 2020 due to SARS-CoV-2 global pandemic. Total population lockdown was imposed in the United Kingdom to reduce transmission rate from late March 2020 where all university's facilities were closed. Additional safety measures were put in place, from autumn 2020, for reopening of the labs as well as for research involving human participants.

Chapel Allerton Hospital, part of the Leeds Teaching Hospital NHS Trusts, where data collection took place, had required Covid-risk assessment to be carried out on all visitors to their site one day before the visit as well as ten minutes prior to their scheduled slots. Both visitors and investigator were also required to don appropriate personal protective equipment throughout the visit. The investigator would be two metres apart from the participants whenever possible and would be observing handwashing regularly throughout the session.

The university ethics committee also had requested to minimise face-to-face contact as much as possible during the period of reopening. This includes to adopt a virtual consenting process, instead of pen-and-paper based method. The virtual verbal consent script and Covid-risk assessment were added to Ethical

Review application on 22nd October 2020. All virtual consent process were done on Microsoft Teams using investigator's secured University IT account and the consent recording portions are stored in two-tier, password-protected folder in OneDrive which are located on University's owned network server.

The outcome from the ethical review is included in Appendix A.

3.1.2 Definition for Activities of Daily Living Involving Cervical Spine

Prior to cervical spine biomechanics data collection, activities of daily living that implicate the cervical spine had to be defined. The patients' perspective was decided as one of the principal sources for establishing the tasks representative of ADL involving the cervical spine movement. The patient's input is viewed as the opinion of an expert who is living with the disease condition for which an unaffected person might not appreciate.

A focus group, composed of five patients with advanced cervical pathologies and/or severe neck problems, was set up at Leeds Teaching Hospitals NHS Trust by the NIHR Leeds Biomedical Research Centre, Public & Patient Involvement/Engagement division. The session was held for 1.5 hours and was also joined by a Professor of Clinical Biomechanics (the current research project supervisor), an Outreach and Development Manager at NIHR Leeds Biomedical Research Centre who recorded the minutes, as well as the investigator for the current study who acted as the moderator. The objective of the group discussion was to establish a list of activities that they found to be challenging to execute as well as the strategies they have employed in order to complete the tasks in their daily lives. A list of prompts and questions was given to the participants in advanced for them to deliberate their views prior to the session so a meaningful discussion could take place (Table 3.1). The session was held for an hour and a short slide presentation was given at the beginning of the session to provide the participants with some background knowledge of the cervical spine anatomy, degenerative disc problem, and its treatment options.

- a. Has your neck problem prevented you from doing any of your daily activities? (not being able to do it at all)
- b. Are there any activities that you have been avoided/relied on someone else to do?
- c. Are any of your daily activities have been limited due to the cervical disc (or neck) problems? (you are still able to do but with great difficulty)
- d. To what extent your neck movement is limited to? (not able to look up, only at certain angle, etc)
- e. What are the effects that you will experience if you are doing it? (pain, discomfort, pressure and where/when)
- f. Are there any movements/postures that you think would exert a pressure on the neck?

Table 3.1 List of prompts given to the participants of the focus group discussion

The activities that were raised during this guided discussion were compiled and compared with the activities described in the academic literature, listed in Table 2.6. The ADL tasks chosen for the cervical biomechanics study were based on the frequency of the task being carried out daily, the feasibility of rendering the props involved in the lab without interrupting the data collection process, and whether it has been previously reported in the literature.

3.1.3 Recruitment of Study Participants for Cervical Biomechanics Study

For the cervical biomechanics data collection process, twelve healthy adult participants (27.2 ± 4.06 years) were recruited for the study. The main exclusion criteria were people under 18 years old and/or having any cervical spine pathologies or neck problems. All participants were given detailed information of the study and provided their written, as well as verbal, consent virtually. Summary of demographics as well as body measurements of the twelve healthy participants' for the study are shown in Table 3.2 below.

Healthy participants were recruited for cervical biomechanics data collection because there are no significant changes in cervical segmental motions, in *in*

silico and *in vitro* studies, between intact normal disc and with disc replacement in a cervical spine post-operatively [214, 215].

| Subject # | Gender | Age | Height (m) | Weight (kg) | BMI (kg/m ²) |
|--------------------|--------|------|------------|-------------|--------------------------|
| 01 | M | 23 | 1.77 | 77.8 | 24.7 |
| 02 | M | 27 | 1.78 | 61.0 | 19.2 |
| 03 | M | 30 | 1.78 | 84.6 | 26.9 |
| 04 | F | 36 | 1.60 | 63.8 | 24.8 |
| 05 | F | 25 | 1.80 | 66.9 | 20.8 |
| 06 | M | 30 | 1.92 | 93.6 | 25.5 |
| 07 | M | 30 | 1.83 | 89.7 | 26.8 |
| 08 | M | 28 | 1.91 | 112.7 | 30.9 |
| 09 | F | 23 | 1.70 | 61.2 | 21.1 |
| 10 | F | 27 | 1.76 | 65.6 | 21.3 |
| 11 | F | 26 | 1.68 | 78.5 | 28.0 |
| 12 | F | 21 | 1.61 | 67.9 | 26.1 |
| Mean | | 27.2 | 1.76 | 76.9 | 24.7 |
| Standard Deviation | | 4.1 | 0.1 | 15.9 | 3.5 |

Table 3.2 Gender, age, height, weight, and BMI of participants for the study

3.1.4 Motion Capture Method and Equipment

A conventional whole body marker set, developed by Vicon for gait analysis, was employed for data collection. This marker set, listed in Table 3.3 and illustrated in Figure 3.2, is compatible with the plug-in simulation model provided in AnyBody Musculoskeletal Modeling Repository (AMMR) that comes with AnyBody Modeling System 7.3. (AnyBody Technology, Aalborg, Denmark) employed in this study.

The motion capture process was carried out at the Gait Lab in Chapel Allerton Hospital using a ten-infrared-camera system (Vicon, Oxford Metrics, Oxford, UK) which was set at 100 frames per second and calibrated to have less than 0.2 standard deviation of the image error between each other.

A one-frame 'Static Trial' shot, where all anatomical segments were visible, was captured for anthropometric measurement for each of the participants. Then, each participant was required to perform the chosen ADL tasks (listed in Table 3.5) to be recorded. Each ADL task was repeated twice. All participants were given the chance to practice the tasks several times prior to be recorded. The ADL tasks were performed at subject-selected speed.

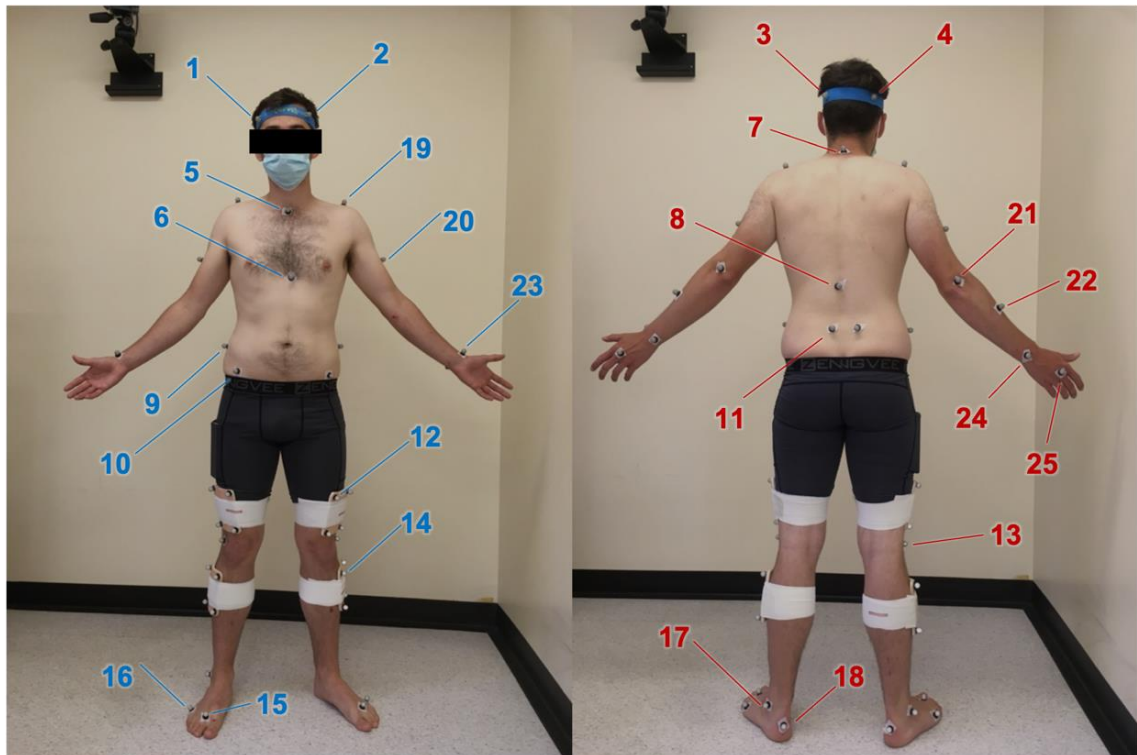


Figure 3.2 Conventional full body reflective marker set developed by Vicon

| Marker # | Segment | Anatomical Location (bony prominence) | Marker # | Segment | Anatomical Location (bony prominence) |
|----------|------------|---|----------|------------|--|
| 1 | Head | Right front skull | 14 | Lower limb | Leg (right & left) |
| 2 | Head | Left front skull | 15 | Lower limb | Toe I (right & left 2 nd metatarsal head) |
| 3 | Head | Left back skull | 16 | Lower limb | Toe II (right & left 5 th metatarsal head) |
| 4 | Head | Right back skull | 17 | Lower limb | Ankle (right & left lateral malleoli) |
| 5 | Torso | Clavicle (sternal notch) | 18 | Lower limb | Heel (right & left calcanei) |
| 6 | Torso | Sternum (xiphisternum) | 19 | Upper limb | Shoulder (right & left acromia) |
| 7 | Torso | Cervical 7 (spinous process) | 20 | Upper limb | Upper arm (right & left) |
| 8 | Torso | Thoracic 10 (spinous process) | 21 | Upper limb | Elbow (right & left lateral epicondyles) |
| 9 | Pelvis | Iliac crest (right & left) | 22 | Upper limb | Forearm (right & left) |
| 10 | Pelvis | Anterior superior iliac spine (right & left) | 23 | Upper limb | Wrist I (right & left radial heads) |
| 11 | Pelvis | Posterior superior iliac spine (right & left) | 24 | Upper limb | Wrist II (right & left ulnar heads) |
| 12 | Lower limb | Thigh (right & left) | 25 | Upper limb | Finger (right & left 3 rd metacarpal heads) |
| 13 | Lower limb | Knee (right & left lateral condyles) | | | |

Table 3.3 Anatomical location for conventional full body marker set

The marker trajectories in the recorded trials were labelled and linked in order to construct the relevant body segments using Vicon Nexus 2.10 software (Vicon, Oxford Metrics, Oxford, UK). All the trajectory gaps were filled either with 'spline fill' function, if it was fewer than ten frames, or with 'rigid-body fill' function if it was part of the same body segment (e.g. pelvis or head).

Each of the captured motions was trimmed to only include the participants' movement *i.e.* from the beginning to the end of marker trajectories of relevant body segments, where they had returned to the original position. The processed file was then exported in C3D file format for biomechanical multibody modelling simulation.

3.1.5 Kinematics and Inverse Dynamic Data Processing

AnyBody Modeling System 7.3 (AnyBody Technology, Aalborg, Denmark) software was employed to analyse the kinematics as well as to perform inverse dynamic studies of the motion capture data. The software operates on object-oriented programming language called AnyScript. The analysis was carried out using a customised musculoskeletal multibody model of a human mannequin duplicated from AnyBody Musculoskeletal Model Repository (AMMR) [216].

3.1.5.1 Folder Setup

A folder structure recommended by AnyBody Modeling System for multiple motion capture subjects and trials was adopted for this research project [217]. The folder structure template was copied and modified to match the current research project needs. The adopted folder class structure is essential to ensure that the settings and parameters are defined and remain constant for mannequin throughout the simulation without duplication. The overall folder tree structure is illustrated in Figure 3.3.

For each subject, an individual class folder, 'Subject_XX', was created where all their individual ADL task simulation files and their body anthropometric data are stored separately (Figure 3.3, number [1]). 'XX' denotes subject's study

designated number as shown in Table 3.2. The folder path for simulation output files was re-programmed (Appendix C(a)) in 'libdef.any' (Figure 3.3, number



Figure 3.3 AnyBody programming class structure for data processing

[2]) to ensure that every subject's ADL task simulation output was accurately saved into their individual 'Output' folder where data can be retrieved for analysis after the simulation completed (Figure 3.3, number [3]).

The simulation C3D input folder path was also re-programmed (Appendix C(b)) in 'LabSpecificData.any', (Figure 3.3, number [4]), so each simulation will be correctly referring to the specific subject's C3D trial file from 'Input' folder, numbered [5] in the folder tree, as an input data for the simulation.

3.1.5.2 Model Configuration

A generic body model template provided in AMMR was used as the baseline for this project and then reconfigured to meet the needs of this research study.

On top of the head and upper body, the model was also set up to incorporate the 'Arms' segments as some ADL tasks require the use of hands. The legs were set to have the Twente lower extremity model version 2 or 'TLEM2'. Both sets of arms and legs were configured to have three-element, Hill-type muscle model 'MUSCLE_3E_HILL' with a strength index of 1.0. The trunk of the model was also set to include all the associated ligaments, a non-linear disc stiffness, as well as cervical and lumbar musculatures with strength index of 1.0 in its configuration. This configuration is adopted according to models setup by de Jager and van der Horsts [181, 182].

The model was also scaled to the subject's body size based on 'LENGTHMASSFAT' setting. This scaling law setting will take into account subject's height, weight, as well as percentage of their body fat based on their BMI [218]. The lines of code for the body model configuration described above, (Appendix C(c)) were inserted in 'BodyModelConfig.any' class, numbered [6] in the folder tree.

Weak mannequin drivers for the whole model were also switched on, which is coded in 'ExtraDrivers.any' file, numbered [7] in the folder tree, so to

prevent any gimbal lock from happening on any single-marker joints, such as the shoulders and elbows in the current study. The lines of code is given in Appendix C(d).

The muscle strength parameter, F_0 , for 'LumpedHyoidT1C0', which is a class of muscle in cervical spine musculature modelled in AMMR, was set to zero for both left and right sides. This parameter setting was programmed under 'MuscleParametersCervicalSpineSimpleRight' and 'MuscleParametersCervicalSpineSimpleLeft' classes (Appendix C(e)). The strength was set to zero because the AMMR has modelled all hyoid-associated muscles as one muscle fibre and this amalgamation contributes towards unrealistic force experience in cervical spine. This is further discussed in Section 3.3.6.1.

3.1.5.3 Environment and Lab Setup

Apart from the participants' body, the environment of where the mannequin was being simulated also was re-configured according to the Gait Lab parameters.

Gravity in this musculoskeletal rigid-body modelling simulation was programmed to be in negative z-axis direction so as to align with the optoelectronic equipment setting in the Gait Lab. The line of codes for gravity direction, set in 'LabSpecificData.any' file, numbered [4] in folder tree structure, are as shown in Appendix C(f).

Force plate setup for the simulation was set to be Type 2 according to the force plates that are present in the Gait Lab where the participants performed all the ADL tasks. The lines of codes for force plate (Appendix C(g)) inserted in `ForcePlate.any` file, numbered [8] in folder tree structure.

Marker labelling protocols, programmed in 'MarkerProtocol.any', numbered [9] in folder tree structure, were made consistent throughout the process by adopting the same names from exported C3D file in Vicon system into AnyBody Modeling Software so to prevent any labelling or programming error.

3.1.5.4 Subject Setup

Each individual participants' height and weight was also updated in their respective 'SubjectSpecificData.any' class, numbered [10] in folder tree structure, as illustrated Appendix C(h), where 'Y' and 'Z' are corresponding to subjects' height (in metre) and weight (in kilogram) respectively. This information enables the software to scale the model according each subject's body measurement following the scaling law that was defined earlier in Section 3.1.5.2.

3.1.5.5 Trial Setup

As ADL task performed by different subjects are different from each other, parameters for each recorded ADL task were declared individually in every ADL class for every subject. This is done in 'TrialSpecificData.any' class, numbered [11] in folder tree structure, where it needs to refer to the individual subject's anthropometric data as well as the specific recorded ADL tasks performed by that subject.

The C3D input file containing marker trajectories of the ADL task to be analysed was also declared in the 'TrialSpecificData.any' class file where the start and end frame for the analysis to take place stated here. The lines of codes for these instructions are shown in Appendix C(i) where 'ST' is the Static Trial output file name and 'DT' is the C3D file name of the captured ADL task to be analysed. The individual subject's 'Static Trial' capture described in Section 3.1.4 was used as anthropometric data reference file, elaborated further in Section 3.1.5.6.

3.1.5.6 Simulation Studies and Output

On top the 'LENGTHMASSFAT' scaling law described in Section 3.1.5.2, the body model was further optimised to the subject's anthropometric measurements according to distances between markers attached. This is done by lines of code, shown in Appendix C(j), programmed in 'LabSpecificData.any' file, numbered [4] in folder tree structure.

The 'Main.any' file within the 'Static Trial' folder of a particular subject, numbered [12] in folder tree structure, was opened and 'RunParameterIdentification' simulation study was performed for that subject. The objective of 'RunParameterIdentification' simulation is to gather the anthropometric data of the subject as well as their body segment lengths before the model can be scaled according to each individual characteristics based on 'LENGTHMASSFAT' setting declared earlier. Throughout 'RunParameterIdentification' simulation study, 'MarkerFilterIndex' variable declared in 'C3DSettings.any' class, numbered [13] in folder tree structure, was set as -1 value because the file only contain a single frame shot and filtration of signal is not necessary. This is shown in Appendix C(k).

The 'RunParameterIdentification' simulation study for each subject was run and the output was saved in the subject's output folder before any kinematics or inverse dynamic study was carried out for that particular subject. This is because the output from 'RunParameterIdentification' simulation, where subject's body model was scaled and integrated with body measurements from anthropometric data, then become the reference for all ADL task simulation studies from this point forwards.

The 'Main.any' file within the analysed ADL task folder, e.g. 'Drinking Water_01' of a particular subject, numbered [14] in folder tree structure, was opened and 'RunAnalysis' simulation study was performed for that subject. During the 'RunAnalysis' simulation, kinematics analysis was first carried out to determine the joint angles before inverse dynamic studies was done where joint contact forces were calculated.

Once the 'RunAnalysis' simulation completed, outputs for cervical intervertebral joint angles and contact forces from C3 to T1 with respect to all three directional axes were extracted from the 'Output' class folder, numbered [3] in folder tree structure.

The 'RunAnalysis' simulation study was repeatedly carried out for all trials in all ADL tasks for all subjects.

3.1.6 Simulation Output Data Extraction

From the ‘Output’ class folder, cervical intervertebral joint angles and contact forces for all the trials from each task captured, performed by all subjects, were extracted from the simulation output files. The matrix of extracted simulation output data for every task is illustrated in Table 3.4.

| Cervical Spinal Joint Level | Cervical Intervertebral Joint Angles (Kinematics) | | | Cervical Intervertebral Joint Contact Forces (Inverse dynamic) | | |
|-----------------------------|--|--|--|--|------------------|---------------|
| | Flexion/extension | Lateral Bending | Axial Rotation | Superoinferior (axial loading) | Antero-posterior | Medio-lateral |
| C3-C4 | ✓ | ✓ | ✓ | ✓ | ✓ | ✓ |
| C4-C5 | (joint angle output is the same for all levels between C3 to T1 due to kinematic rhythm) | (joint angle output is the same for all levels between C3 to T1 due to kinematic rhythm) | (joint angle output is the same for all levels between C3 to T1 due to kinematic rhythm) | ✓ | ✓ | ✓ |
| C5-C6 | ✓ | ✓ | ✓ | ✓ | ✓ | ✓ |
| C6-C7 | ✓ | ✓ | ✓ | ✓ | ✓ | ✓ |
| C7-T1 | ✓ | ✓ | ✓ | ✓ | ✓ | ✓ |

Table 3.4 Output matrix for simulation analysis for one ADL task captured

The cervical intervertebral joints between C3 to C7 in AMMR are programmed as a spherical joint or ball-and-socket joint, which has only three degrees of freedom and all translation motions are constrained. Thus, the simulation output gives out 0 values for all linear displacement. Although the joint can be re-programmed using Force-Dependent Kinematics function from the software to account for any soft-tissue deformation in translation motion as shown by Diao *et al.* [202, 203], it was decided to not utilise it as linear/shear forces is favoured over linear displacement as an input parameter in most joint simulation.

The spine model within AMMR also utilises an algorithm called ‘kinematic rhythm’ which essentially is a method of apportioning the angle between the head and the torso equally to all cervical intervertebral joints from C3 to T1. Hence, the cervical intervertebral joint angle outputs are the same for C3-C4, C4-C5, C5-C6, C6-C7, and C7-T1 as described in Table 3.4.

3.1.7 Cervical Biomechanics Data Analysis

OriginPro 9.9 (OriginLab, Massachusetts, US) was used to analyse the extracted outputs from cervical intervertebral joint angles and contact forces for all the trials from each ADL task captured.

For every ADL task analysed, the outputs from both trials from all subjects were plotted against percentage of task completion, where the time taken for each trial was normalised from 0 to 100. Within the normalised plots for superoinferior axial loading of C5-C6 graph, the points for major peaks and/or troughs of individual trial curves were identified using *Batch Peak Analysis* tool. The percentage of task completion (*i.e.* x-value) for all the points for these major peaks and/or troughs were averaged. These averaged points were set to be the alignment points for all the peaks and troughs of that particular ADL task for all cervical levels.

In a new plot, all the superoinferior axial loading curves from all subjects were realigned at the established alignment points by interpolating the curves to 1000 data points based on individual curve's major peaks and troughs. All the aligned curves were averaged to provide a single representative curve for that particular ADL task. The same curve realignment process was carried out for anteroposterior, mediolateral, as well as kinematic graphs using the same established alignment points of the same ADL task. The whole process was repeated for other ADL tasks captured.

As elaborated in the Section 2.4.8, the head movement is lacking in a defined repetitive cyclical motion, unlike gait where there are several established 'events' and well-demarcated heel-strike-toe-off temporal parameters for any gait cycle data to be anchored to. Therefore, for cervical spine biomechanics analysis, it was decided that the highest and/or lowest axial loading events in cervical intervertebral C5-C6 level were the converging points for analysis of the kinematics as well as loading curves for all trials within the same ADL task. Axial loading was chosen as the anchoring parameter/event as the shape of the axial loading curves are more consistent across subjects than any of kinematics curves

due to high variability in spinal vertebral motion sequence for the same body movement [219, 220]. The axial loading in C5-C6 cervical intervertebral joint level was chosen as the reference point because it is the commonest implanted level for cervical disc implant as well as the commonest level for revision surgery to take place in failed prostheses [221-223].

3.1.8 Formulation of New Wear Test Profile

The cervical kinematics and loading data generated from this Phase I would later be transferred to Phase II of the research project where it would be used to simulate a more physiologically relevant wear test. Therefore, the axes and direction of motions from these data, defined according to International Society of Biomechanics (ISB) local coordinate system, were transposed and harmonised to align with ISO18192-1 [1] axes definition in formulating a new wear testing profile. The definition of the local coordinate system for both ISB and ISO are simplified in Figure 3.4.

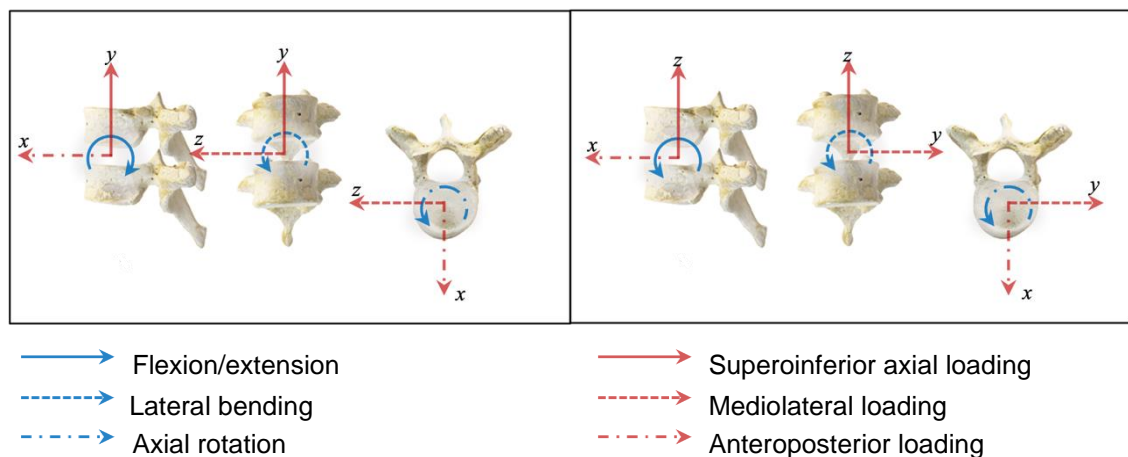


Figure 3.4 Axes definitions set by International Society of Biomechanics (left) and ISO18192-1 [1] (right). Positive direction of motion indicated by the direction of arrows [1, 224]

The y-axis was transformed from pointing superiorly to pointing laterally to the left whilst the z-axis was transformed to pointing superiorly from laterally to the right. The direction of x-axis was the same for both in ISB and ISO18192-1 [1] and require no transposition. As only the mediolateral axis direction has changed

(from left to right), therefore only mediolateral loading values signs were reversed when formulating a new wear testing profile.

The positive values for direction of motion in both local coordinate systems were not explicitly defined by either organisation. Therefore, the right-thumb rule was employed when assigning the positive values of the movement where the thumb is pointing towards the direction of the axis and the other four fingers is pointing to the positive direction of motion. This is illustrated by the light blue arrows in Figure 3.4. Consequently, the values are becoming more positive when the cervical joint is moving in extension motion of direction in ISB definition. Conversely, the values are becoming more positive as the cervical joint moving in flexion motion of direction for kinematics in ISO18192-1 [1]. Therefore, the sign for the values were reversed in flexion/extension when formulating the new wear testing profile. The signs remained the same for lateral bending and axial rotation.

As a wear testing profile, the end point of a curve must coincide with its starting point of the a unit cycle and they both must have the same speed and direction for a seamless cyclical repetition for the simulator. To achieve this, two complete 1000-point cycles of a selected ADL task were plotted next to each other so each curve representing two cycles of the ADL trial. The meeting point of kinematics and loading curves between the two profiles were smoothed using cubic interpolation with 5% smoothing buffer on either side of the point. Coordinates for the smoothed curves, as well as the remainder of the original curves, were combined in formulating the new ADL wear test profile.

3.2 Results

3.2.1 Selection of Activities Daily Living Involving the Cervical Spine

The panel from the focus group came up with a list of daily activities that they found challenging to perform due to their conditions. From this list, eight daily living tasks were chosen according to the criteria outlined in Section 3.1.2 to be simulated in the cervical spine biomechanics study, the majority of which have been reported in academic literature (Table 2.6). The eight ADL tasks are listed

in Table 3.5. Summary of points deliberated by the focus group, including all the daily activities discussed (highlighted in grey), is attached in Appendix B.

| Selected Tasks Reported to be Challenging to Perform by Patients | Bennett <i>et al.</i> [210] | Bible <i>et al.</i> [211], Miller <i>et al.</i> [212, 213] | Cobian <i>et al.</i> [163] |
|---|-----------------------------|--|----------------------------|
| Reading on lap | ✓ | ✓ | |
| Drinking from a bottle | ✓ | | ✓ |
| Looking for traffic before crossing | ✓ | | ✓ |
| Looking up laterally | | | |
| Reversing a car | ✓ | ✓ | ✓ |
| Bending Down | ✓ | ✓ | ✓ |
| Stand-to-sit | ✓ | ✓ | ✓ |
| Sit-to-stand | ✓ | ✓ | ✓ |

Table 3.5 Tasks selected for the current study as representative of ADL involving cervical spine

The ADL tasks listed in Table 3.5 were then adapted to suit to the current study according to the Gait Lab capacity. Each ADL task was given a study designated code and a description of the situation for the participants to follow upon performing the movement, as listed in Table 3.6. Props, such as mobile phone, water bottle, and chair, were provided to the participants.

| ADL Tasks | Study Code | Description of Situation |
|---|-------------------|--|
| Looking at mobile (adapted from reading on lap) | MOB | Rapidly checking the time on your mobile phone whilst standing and waiting for a train on platform |
| Drinking from a bottle | WAT | Drinking water from squeeze bottle to quench your thirst after a long walk |
| Looking for traffic before crossing | TRA | Checking for traffic on a busy Albion Street before crossing the road |
| Looking up laterally | LUL | Checking time on a clock hanged high on the wall on your right |
| Reversing a car | REV | Reversing a right-hand drive car without a rear-view camera |
| Bending down | BND | Picking up a bag of groceries from the floor without bending the knees |
| Stand-to-sit | StS | Sitting down on a very familiar chair |
| Sit-to-stand | SiS | Standing up from a very familiar chair |

Table 3.6 Description of situation for ADL tasks simulation

During the motion capture session, subjects were required to assume a comfortable 'neutral' head position, facing anteriorly, with forward gaze at the beginning of each ADL task. The subject would be standing up at the start

position except for 'reversing a car' (REV) and 'sit-to-stand' (SiS) tasks where the subject would be sitting down. During this neutral pose, subjects' hands would be at their sides if they were standing up or on their thighs if they were sitting down. The subjects were then required to perform the task described to them, paused for a brief moment at the intended posture, and returned to their 'neutral' position. One 'neutral-posture-neutral' motion was considered as one trial, which was saved and named as individual trial file for processing, except for 'stand-to-sit' (StS) and 'sit-to-stand' (SiS) movement captures where it was considered as 'neutral-posture' and 'posture-neutral', respectively.

The activities selected can be categorised into two main purposes: (a) 'looking', where the head is moved so the object/scene is within field of view – MOB, TRA, LUL, and REV; or (b) 'tasking', where head is moving because an action is being carried out – WAT, BND, StS, and SiS.

3.2.2 Motion Capture Data Processing

Out of 192 possible captured trials (12 subjects × 8 ADL tasks × 2 trials each), 186 of them met data quality standard needed for a successful multibody modelling simulation. The data quality standard is met when all the reflective markers are visible at the start as well as at the end of the trial capture and any 'dropped' of marker signal in between could be filled mathematically through 'spline' (for less than ten frames) or 'rigid-body' fill functions. Figure 3.6 shows an example of fully 'labelled' and 'linked' markers for 'Static Trial' capture of Subject 6. Figure 3.7 is an example how trajectory for a right finger marker (RFIN) was checked for 'completeness' and filled in if necessary, then 'trimmed' to the relevant movement for Subject 6 during 'drinking from a bottle' (WAT) task. The other seven recorded trials which failed to meet the standard were excluded from analysis. The list of the captured trials are summarised in Table 3.7.

3.2.3 Multibody Modelling Simulation

Out of 186 recorded trials that met data quality criteria, 178 were successfully solved by the multibody model. Out of eight failed simulations, five were aborted

during kinematic analysis due to motions of body segment going beyond the joint constraints set for the mannequin model employed in AMMR. The five failed trials are for 'bending down' (BND) and 'stand-to-sit' (StS) ADL tasks simulations. The other three failed simulations were due to muscle overload where the estimated joint loading calculated from inverse dynamic exceeded the maximum amount of force that can be generated from overall muscle bundle modelled for that particular joint. All of these happened when simulating 'reversing a car' (REV) task. The simulation failure also has been reported previously in other multibody modelling study with a large dataset involved [206]. Although three simulations failed during inverse dynamic analysis, its successful kinematics analysis output was not recorded due to the nature of 'RunAnalysis' function being programmed where no output file is being produced when failed, regardless of the stage of simulation it has completed [217]. Hence, all eight failed simulations were excluded from all analysis. The summary of outcome from multibody simulation is shown in Table 3.7. Figure 3.5 shows an example of a configured and scaled human body model from AMMR according to the setup outlined in Section 3.1.5.6. The figure is simulating 'drinking from a bottle' (WAT) task based on Subject 6's body measurements.

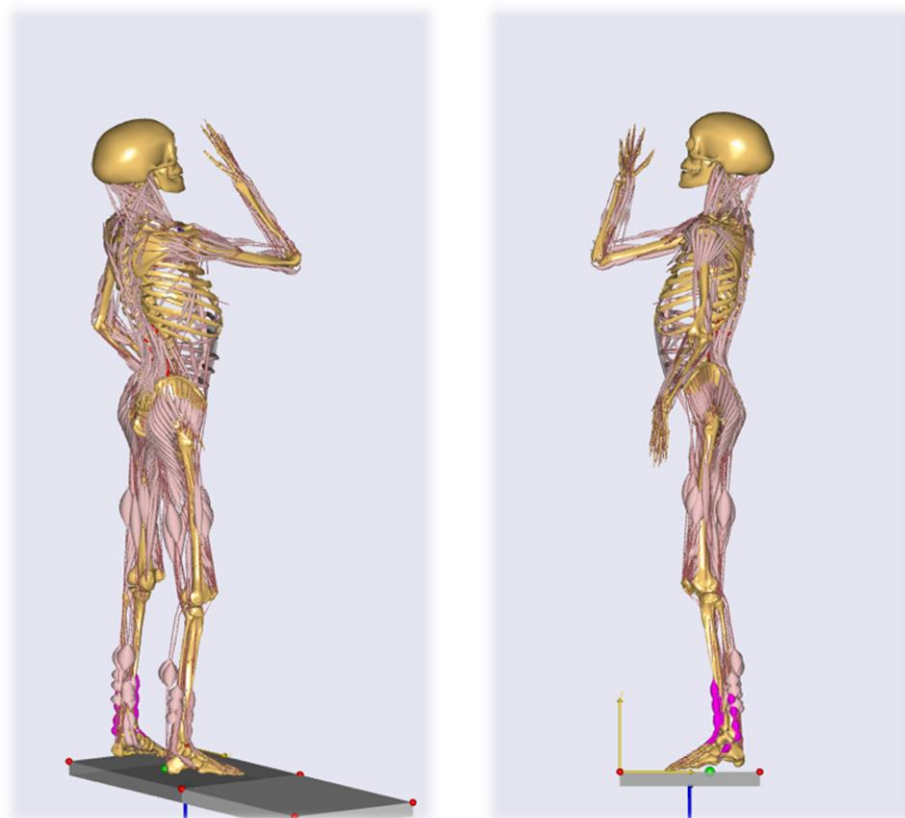


Figure 3.5 An example of a successful simulation from Subject 6's WAT trial

Linked reflective markers to form body segment

Labelled reflective markers

Body segment labels

Reflective marker labels

Gap filling function

Captured trial files

| Name | Files | Created | Modified | Description | Notes | Classification |
|--------|-------|------------------|------------------|-------------|-------|----------------|
| FL | | 20/11/2020 09:55 | 24/07/2022 23:47 | | | Good Left |
| FL 001 | | | | | | Good Left |
| FL 002 | | | | | | Good Left |
| FL 003 | | | | | | Good Left |
| FL 004 | | | | | | Good Left |
| FL 005 | | | | | | Good Left |
| FL 006 | | | | | | Good Left |

Figure 3.6 Motion capture data processing where markers were 'labelled' and 'linked' to form body segments

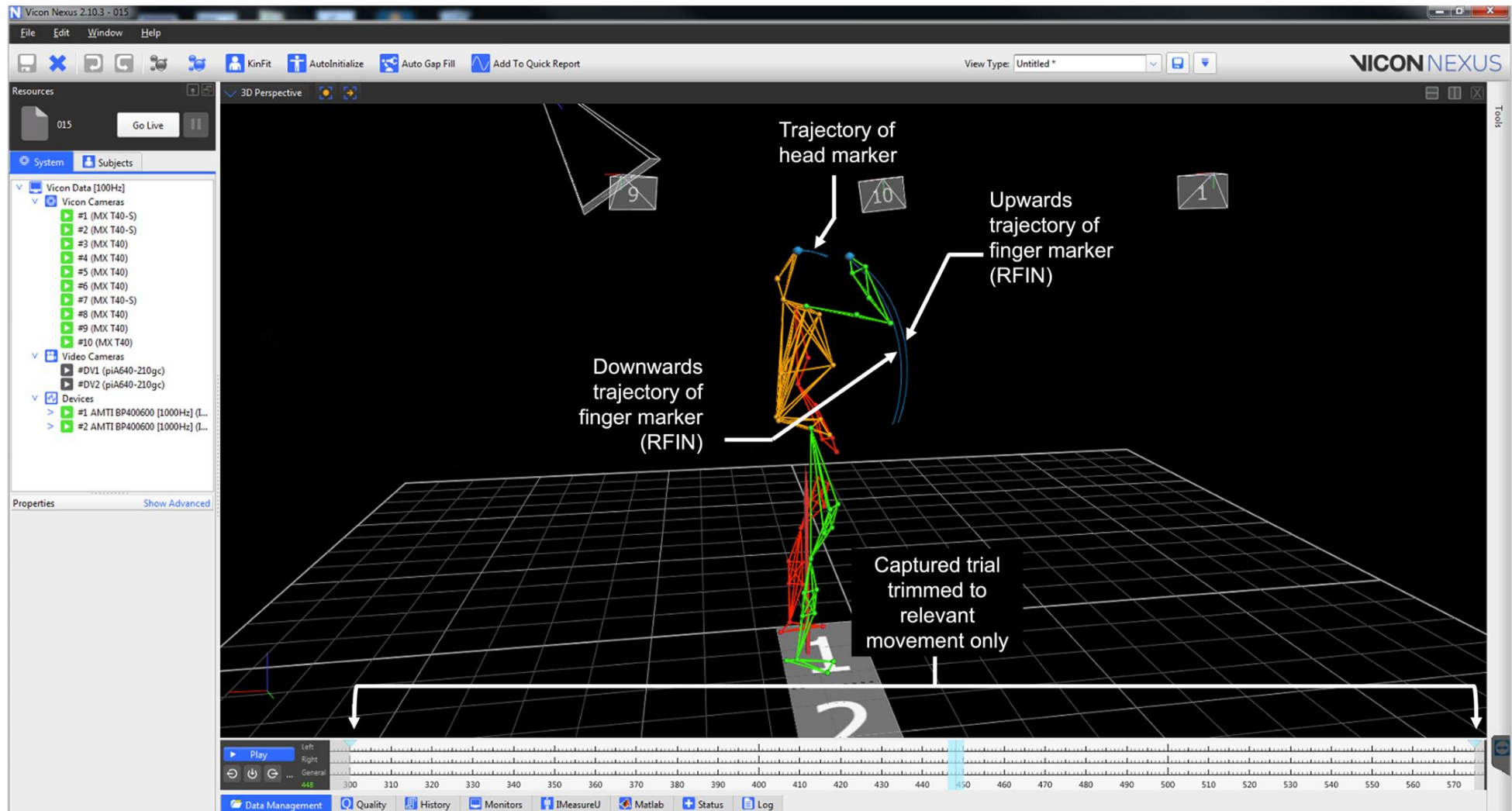


Figure 3.7 Assessment of processed motion capture data from a WAT trial where the trajectories were checked for 'completeness'

| Subject | ADL | Trial # | Subject 1 | | Subject 2 | | Subject 3 | | Subject 4 | | Subject 5 | | Subject 6 | | Subject 7 | | Subject 8 | | Subject 9 | | Subject 10 | | Subject 11 | | Subject 12 | | Total # of Trials |
|---------|-----|---------|-----------|---------|-----------|---------|-----------|---------|-----------|---------|-----------|---------|-----------|---------|-----------|---------|-----------|---------|-----------|---------|------------|---------|------------|---------|------------|---------|-------------------|
| | | | Kin | Inv Dyn | Kin | Inv Dyn | Kin | Inv Dyn | Kin | Inv Dyn | Kin | Inv Dyn | Kin | Inv Dyn | Kin | Inv Dyn | Kin | Inv Dyn | Kin | Inv Dyn | Kin | Inv Dyn | Kin | Inv Dyn | Kin | Inv Dyn | |
| MOB | 1 | ✓ | ✓ | ✓ | ✓ | ✓ | ✓ | ✓ | ✓ | ✓ | ✓ | ✓ | ✓ | ✓ | ✓ | ✓ | ✓ | ✓ | ✓ | ✓ | ✓ | ✓ | ✓ | ✓ | ✓ | ✓ | 22 |
| | 2 | ✓ | ✓ | ✓ | ✓ | ✓ | ✓ | ✓ | ✓ | ✓ | ✓ | ✓ | ✓ | ✓ | ✓ | ✓ | ✓ | ✓ | ✓ | ✓ | ✓ | ✓ | ✓ | ✓ | ✓ | ✓ | |
| WAT | 1 | ✓ | ✓ | ✓ | ✓ | ✓ | ✓ | ✓ | ✓ | ✓ | ✓ | ✓ | ✓ | ✓ | ✓ | ✓ | ✓ | ✓ | ✓ | ✓ | ✓ | ✓ | ✓ | ✓ | ✓ | ✓ | 24 |
| | 2 | ✓ | ✓ | ✓ | ✓ | ✓ | ✓ | ✓ | ✓ | ✓ | ✓ | ✓ | ✓ | ✓ | ✓ | ✓ | ✓ | ✓ | ✓ | ✓ | ✓ | ✓ | ✓ | ✓ | ✓ | ✓ | |
| TRA | 1 | ✓ | ✓ | ✓ | ✓ | ✓ | ✓ | ✓ | ✓ | ✓ | ✓ | ✓ | ✓ | ✓ | ✓ | ✓ | ✓ | ✓ | ✓ | ✓ | ✓ | ✓ | ✓ | ✓ | ✓ | ✓ | 24 |
| | 2 | ✓ | ✓ | ✓ | ✓ | ✓ | ✓ | ✓ | ✓ | ✓ | ✓ | ✓ | ✓ | ✓ | ✓ | ✓ | ✓ | ✓ | ✓ | ✓ | ✓ | ✓ | ✓ | ✓ | ✓ | ✓ | |
| LUL | 1 | ✓ | ✓ | ✓ | ✓ | ✓ | ✓ | ✓ | ✓ | ✓ | ✓ | ✓ | ✓ | ✓ | ✓ | ✓ | ✓ | ✓ | ✓ | ✓ | ✓ | ✓ | ✓ | ✓ | ✓ | ✓ | 24 |
| | 2 | ✓ | ✓ | ✓ | ✓ | ✓ | ✓ | ✓ | ✓ | ✓ | ✓ | ✓ | ✓ | ✓ | ✓ | ✓ | ✓ | ✓ | ✓ | ✓ | ✓ | ✓ | ✓ | ✓ | ✓ | ✓ | |
| REV | 1 | ✓ | ✓ | ✓ | ✓ | ✓ | ✓ | ✓ | ✓ | ✓ | ✓ | ✓ | ✓ | ✓ | ✓ | ✓ | ✓ | ✓ | F | ✓ | ✓ | ✓ | ✓ | ✓ | ✓ | ✓ | 21 |
| | 2 | ✓ | ✓ | ✓ | ✓ | ✓ | ✓ | ✓ | ✓ | ✓ | ✓ | ✓ | ✓ | ✓ | ✓ | ✓ | ✓ | ✓ | F | ✓ | ✓ | ✓ | F | ✓ | ✓ | | |
| BND | 1 | ✓ | ✓ | ✓ | ✓ | F | F | ✓ | ✓ | ✓ | ✓ | ✓ | ✓ | ✓ | ✓ | ✓ | ✓ | ✓ | ✓ | ✓ | F | F | ✓ | ✓ | ✓ | ✓ | 20 |
| | 2 | ✓ | ✓ | ✓ | ✓ | F | F | ✓ | ✓ | ✓ | ✓ | ✓ | ✓ | ✓ | ✓ | ✓ | ✓ | ✓ | ✓ | ✓ | F | F | ✓ | ✓ | ✓ | ✓ | |
| StS | 1 | ✓ | ✓ | ✓ | ✓ | ✓ | ✓ | ✓ | ✓ | ✓ | ✓ | ✓ | ✓ | ✓ | ✓ | ✓ | ✓ | ✓ | ✓ | ✓ | ✓ | ✓ | F | F | ✓ | ✓ | 22 |
| | 2 | ✓ | ✓ | ✓ | ✓ | ✓ | ✓ | ✓ | ✓ | ✓ | ✓ | ✓ | ✓ | ✓ | ✓ | ✓ | ✓ | ✓ | ✓ | ✓ | ✓ | ✓ | ✓ | ✓ | ✓ | ✓ | |
| SiS | 1 | ✓ | ✓ | ✓ | ✓ | ✓ | ✓ | ✓ | ✓ | ✓ | ✓ | ✓ | ✓ | ✓ | ✓ | ✓ | ✓ | ✓ | ✓ | ✓ | ✓ | ✓ | ✓ | ✓ | ✓ | ✓ | 22 |
| | 2 | ✓ | ✓ | ✓ | ✓ | ✓ | ✓ | ✓ | ✓ | ✓ | ✓ | ✓ | ✓ | ✓ | ✓ | ✓ | ✓ | ✓ | ✓ | ✓ | ✓ | ✓ | ✓ | ✓ | ✓ | ✓ | |



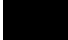

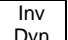
 Multibody modelling simulation solved
  Multibody modelling simulation failed
  Trial excluded due to bad data quality
  Kinematics analysis
  Inverse dynamic analysis

Table 3.7 Summary of outcome from kinematics (Kin) and inverse dynamic (Inv Dyn) simulations for all recorded trials from all subjects for all ADL task

3.2.4 Cervical Joint Kinematics

As mentioned earlier in Section 3.1.6, the multibody modelling simulation utilises a ‘kinematic rhythm’ function in determining the cervical intervertebral joint kinematics. Therefore, the cervical kinematics values presented in this section are the same for cervical intervertebral joint C3-C4, C4-C5, C5-C6, C6-C7, and C7-T1. Table 3.9 and Table 3.10 show the minimum and maximum angles of the cervical vertebral joint for all subjects in all of the ADL trials in all three directions of motion. Cervical joint range, *i.e.* the difference between the maximum (Max) and the minimum (Min) angles, is shown in bold and their mean and standard deviation are shown in right-most column. From the mean cervical joint range, the largest range in of each individual ADL task is happening in the main direction of the movement plane *e.g.* ‘looking for traffic before crossing’ (TRA) has biggest joint movement range in axial rotation direction as the head moves predominantly in transverse plane for this task. Range of motion in other directions is comparatively small with respect to the main direction of motion, except in ‘drinking from a bottle’ (WAT) and ‘reversing a car’ (REV) where lateral bending contributes, on average, more than 50% of the range in the main direction of head motion. The largest mean range is estimated during ‘bending down’ (BND) tasks for flexion/extension whereas ‘looking for traffic’ (TRA) recorded the biggest range in axial rotation direction. Summary of the cervical joint movement range for the investigated ADL tasks is in Table 3.8.

| ADL Tasks | The main plane of movement | Mean Cervical Joint Range (°) | | |
|-----------|----------------------------|-------------------------------|------------------|------------------|
| | | Flexion/extension | Lateral Bending | Axial Rotation |
| MOB | Sagittal | 3.8 ± 1.5 | 0.8 ± 0.4 | 0.5 ± 0.4 |
| WAT | Sagittal | 4.1 ± 1.6 | <u>2.2 ± 0.7</u> | 0.6 ± 0.4 |
| TRA | Transverse | 1.6 ± 0.8 | 1.1 ± 0.7 | 5.6 ± 1.1 |
| LUL | Transverse | 1.0 ± 0.8 | 0.9 ± 0.5 | 3.2 ± 1.0 |
| REV | Transverse | 1.9 ± 1.1 | <u>2.7 ± 1.6</u> | 5.0 ± 2.2 |
| BND | Sagittal | 4.3 ± 2.8 | 1.2 ± 0.8 | 0.3 ± 0.2 |
| StS | Sagittal | 4.3 ± 2.2 | 0.8 ± 0.5 | 0.3 ± 0.2 |
| SiS | Sagittal | 4.0 ± 1.8 | 0.6 ± 0.3 | 0.3 ± 0.2 |

Table 3.8 Mean cervical joint ranges for all ADL tasks in all directions (bolded magnitude indicates the main direction of the motion; underlined value indicates when the RoM is more than 50% of the range in the main direction of motion)

| ADL | Trials | Subject 1 | | Subject 2 | | Subject 3 | | Subject 4 | | Subject 5 | | Subject 6 | | Subject 7 | | Subject 8 | | Subject 9 | | Subject 10 | | Subject 11 | | Subject 12 | | Mean | Std Dev | |
|-----|--------|--------------|------------|------------|------------|------------|------------|------------|------------|------------|------------|------------|------------|------------|------------|------------|------------|------------|------------|------------|------------|------------|------------|------------|------------|------------|------------|------------|
| | | 1 | 2 | 1 | 2 | 1 | 2 | 1 | 2 | 1 | 2 | 1 | 2 | 1 | 2 | 1 | 2 | 1 | 2 | 1 | 2 | 1 | 2 | | | | | |
| MOB | FE | Min | 0.2 | -0.7 | -1.6 | -1.8 | -1.9 | -1.5 | -2.8 | -3.3 | -2.6 | -1.8 | -0.7 | -0.5 | | | -0.8 | -0.2 | -2.6 | -2.7 | -3.1 | -3.4 | -2.9 | -2.2 | -2.5 | -2.4 | | |
| | | Max | 2.1 | 2.1 | 3.0 | 3.9 | 1.5 | 2.3 | 0.7 | 1.2 | 3.2 | 3.0 | 3.1 | 2.5 | | | 4.3 | 3.4 | 1.7 | 2.1 | 0.8 | 1.3 | 2.0 | 2.3 | 1.2 | 1.4 | | |
| | | Range | 1.9 | 2.8 | 4.6 | 5.7 | 3.4 | 3.8 | 3.5 | 4.5 | 5.8 | 4.7 | 3.8 | 3.0 | -- | -- | 5.1 | 3.5 | 4.3 | 4.9 | 3.9 | 4.7 | 4.9 | 4.5 | 3.7 | 3.8 | 3.8 | 1.5 |
| | LB | Min | 0.7 | 0.0 | 0.8 | 1.1 | -0.1 | -0.3 | 0.7 | 0.5 | 0.1 | 0.8 | -0.2 | -0.2 | | | 1.0 | 1.3 | 0.2 | 0.0 | 0.1 | -0.9 | -0.9 | -0.9 | 0.3 | 0.1 | | |
| | | Max | 1.7 | 0.9 | 1.6 | 2.2 | 0.3 | 0.3 | 1.0 | 0.9 | 1.6 | 1.8 | 0.2 | 0.4 | | | 1.9 | 1.9 | 0.9 | 0.9 | 0.6 | 0.2 | 0.8 | 0.6 | 0.7 | 1.0 | | |
| | | Range | 1.0 | 1.0 | 0.9 | 1.1 | 0.4 | 0.5 | 0.3 | 0.5 | 1.5 | 1.0 | 0.4 | 0.6 | -- | -- | 0.9 | 0.7 | 0.7 | 1.0 | 0.5 | 1.1 | 1.7 | 1.4 | 0.4 | 0.9 | 0.8 | 0.4 |
| | AR | Min | -1.0 | -0.6 | -0.7 | -0.7 | -0.8 | -0.7 | -0.6 | -0.7 | -0.6 | -0.5 | -0.8 | -1.0 | | | -0.2 | -0.2 | -0.3 | -0.2 | -0.9 | -0.8 | -1.5 | -1.4 | -0.7 | -0.7 | | |
| | | Max | -0.3 | -0.3 | -0.3 | 0.0 | -0.7 | -0.6 | -0.3 | -0.2 | 0.2 | -0.2 | -0.3 | -0.5 | | | 0.8 | 0.5 | 0.0 | 0.0 | -0.2 | -0.2 | 0.4 | 0.1 | -0.1 | -0.1 | | |
| | | Range | 0.6 | 0.3 | 0.4 | 0.6 | 0.1 | 0.1 | 0.3 | 0.5 | 0.8 | 0.3 | 0.4 | 0.5 | -- | -- | 1.0 | 0.7 | 0.3 | 0.3 | 0.8 | 0.5 | 1.9 | 1.5 | 0.6 | 0.6 | 0.5 | 0.4 |
| WAT | FE | Min | 2.2 | 2.4 | 2.3 | 1.0 | 2.8 | 2.2 | 1.7 | 2.4 | 3.1 | 2.1 | 1.1 | 2.3 | 2.1 | 1.5 | 3.4 | 3.1 | 0.7 | 0.1 | 0.9 | 0.4 | 1.1 | 1.3 | 1.5 | 0.9 | | |
| | | Max | 4.9 | 4.8 | 8.6 | 8.5 | 6.7 | 7.1 | 5.8 | 5.9 | 8.0 | 7.3 | 6.1 | 6.2 | 6.3 | 6.5 | 8.4 | 7.4 | 6.1 | 4.5 | 2.1 | 2.3 | 4.5 | 7.1 | 2.9 | 3.2 | | |
| | | Range | 2.6 | 2.4 | 6.3 | 7.5 | 4.0 | 4.9 | 4.1 | 3.5 | 4.9 | 5.1 | 5.0 | 4.0 | 4.3 | 4.9 | 4.9 | 4.2 | 5.4 | 4.4 | 1.2 | 1.8 | 3.5 | 5.7 | 1.4 | 2.3 | 4.1 | 1.6 |
| | LB | Min | 0.2 | -0.6 | -2.7 | -1.0 | -0.1 | -0.4 | 0.9 | 0.9 | 0.5 | 0.1 | -0.1 | -0.4 | -0.4 | -0.3 | 0.3 | 1.0 | 0.3 | 0.9 | -0.2 | 0.3 | 0.2 | 0.7 | 0.2 | 0.0 | | |
| | | Max | 2.7 | 2.5 | 0.0 | 1.3 | 1.0 | 1.1 | 2.1 | 1.7 | 2.7 | 2.5 | 1.3 | 1.6 | 1.4 | 1.1 | 4.1 | 4.0 | 2.7 | 2.9 | 2.3 | 2.4 | 2.5 | 3.3 | 2.3 | 2.4 | | |
| | | Range | 2.5 | 3.1 | 2.8 | 2.3 | 1.2 | 1.6 | 1.2 | 0.8 | 2.3 | 2.4 | 1.4 | 2.0 | 1.8 | 1.4 | 3.8 | 3.0 | 2.5 | 2.0 | 2.5 | 2.2 | 2.2 | 2.6 | 2.1 | 2.4 | 2.2 | 0.7 |
| | AR | Min | -0.7 | -0.6 | -0.8 | -0.7 | -0.6 | -0.7 | -1.1 | -1.0 | -0.5 | -0.6 | -0.5 | -0.5 | 0.3 | 0.2 | 0.5 | 0.5 | -0.2 | -0.4 | -0.4 | -0.3 | -0.4 | -0.2 | -0.4 | -0.4 | | |
| | | Max | -0.4 | -0.3 | -0.1 | -0.2 | -0.5 | -0.5 | -0.7 | -0.6 | 0.1 | 0.1 | -0.1 | 0.2 | 0.6 | 0.5 | 1.7 | 1.6 | 1.3 | 0.9 | -0.2 | 0.0 | 0.0 | 0.6 | 0.3 | 0.3 | | |
| | | Range | 0.3 | 0.3 | 0.7 | 0.5 | 0.1 | 0.2 | 0.4 | 0.4 | 0.6 | 0.7 | 0.4 | 0.7 | 0.3 | 0.3 | 1.1 | 1.1 | 1.5 | 1.4 | 0.2 | 0.3 | 0.4 | 0.8 | 0.7 | 0.7 | 0.6 | 0.4 |
| TRA | FE | Min | 1.3 | 1.5 | 2.9 | 3.2 | 0.8 | 1.3 | 1.2 | 1.3 | 2.6 | 2.7 | 2.1 | 1.2 | 2.1 | 1.8 | 4.6 | 4.1 | 1.3 | 0.9 | 0.5 | 1.2 | 1.1 | 1.1 | 1.0 | 0.6 | | |
| | | Max | 1.7 | 2.7 | 4.1 | 3.9 | 2.7 | 3.1 | 2.6 | 3.3 | 3.8 | 5.1 | 5.1 | 3.6 | 3.5 | 3.7 | 5.0 | 5.3 | 4.0 | 3.6 | 1.2 | 1.8 | 2.3 | 4.1 | 2.4 | 2.1 | | |
| | | Range | 0.4 | 1.1 | 1.2 | 0.7 | 1.9 | 1.8 | 1.4 | 2.0 | 1.2 | 2.4 | 2.9 | 2.4 | 1.4 | 1.9 | 0.5 | 1.2 | 2.7 | 2.7 | 0.7 | 0.6 | 1.3 | 3.0 | 1.4 | 1.6 | 1.6 | 0.8 |
| | LB | Min | -0.8 | -1.0 | 0.4 | 0.7 | -0.5 | -0.4 | -0.6 | -0.6 | -0.4 | -0.2 | -2.0 | -1.7 | -1.0 | -1.1 | 0.9 | 0.5 | -0.6 | -0.6 | -0.5 | -0.6 | -0.8 | -0.9 | -1.3 | -1.5 | | |
| | | Max | 1.4 | 1.3 | 0.7 | 1.0 | 0.3 | 0.6 | 0.2 | 0.4 | 0.1 | 0.3 | -0.3 | -0.4 | 0.4 | 0.0 | 1.3 | 1.1 | 0.3 | 0.3 | 0.2 | 0.0 | 0.3 | 0.6 | 1.2 | 1.5 | | |
| | | Range | 2.1 | 2.2 | 0.4 | 0.3 | 0.8 | 1.1 | 0.8 | 1.1 | 0.5 | 0.6 | 1.7 | 1.2 | 1.4 | 1.1 | 0.4 | 0.6 | 0.9 | 0.9 | 0.7 | 0.6 | 1.1 | 1.5 | 2.5 | 3.1 | 1.1 | 0.7 |
| | AR | Min | -3.4 | -3.7 | -2.4 | -2.7 | -2.7 | -2.6 | -2.8 | -3.0 | -3.5 | -4.0 | -3.8 | -4.7 | -2.6 | -3.2 | -2.0 | -2.7 | -2.0 | -2.3 | -2.2 | -1.5 | -3.1 | -3.0 | -3.2 | -3.6 | | |
| | | Max | 2.6 | 2.9 | 2.0 | 2.5 | 1.4 | 1.6 | 3.4 | 3.3 | 2.1 | 2.1 | 2.9 | 2.6 | 3.0 | 3.4 | 2.6 | 3.3 | 1.9 | 2.3 | 2.7 | 2.5 | 3.1 | 3.2 | 3.6 | 3.6 | | |
| | | Range | 6.0 | 6.6 | 4.4 | 5.2 | 4.1 | 4.2 | 6.2 | 6.2 | 5.6 | 6.2 | 6.8 | 7.3 | 5.6 | 6.6 | 4.6 | 5.9 | 3.9 | 4.6 | 4.8 | 4.0 | 6.2 | 6.2 | 6.8 | 7.2 | 5.6 | 1.1 |
| LUL | FE | Min | 1.8 | 2.1 | 3.5 | 3.6 | 2.2 | 2.6 | 1.4 | 1.4 | 2.5 | 2.6 | 0.7 | 1.6 | 2.2 | 2.5 | 4.1 | 4.0 | 1.5 | 1.3 | 1.9 | 1.6 | 0.0 | -1.5 | 1.6 | 1.6 | | |
| | | Max | 3.6 | 3.7 | 4.0 | 3.7 | 2.6 | 3.5 | 1.9 | 1.7 | 2.8 | 2.9 | 1.4 | 2.1 | 2.6 | 2.7 | 5.9 | 5.9 | 2.3 | 3.1 | 2.8 | 2.2 | 2.5 | 1.9 | 3.0 | 2.9 | | |
| | | Range | 1.8 | 1.5 | 0.5 | 0.2 | 0.4 | 0.8 | 0.4 | 0.2 | 0.3 | 0.4 | 0.7 | 0.4 | 0.5 | 0.2 | 1.8 | 1.9 | 0.9 | 1.7 | 0.8 | 0.6 | 2.5 | 3.4 | 1.4 | 1.3 | 1.0 | 0.8 |
| | LB | Min | -0.4 | -0.3 | 0.6 | 0.6 | -1.0 | -0.8 | -0.8 | -0.5 | -1.3 | -1.0 | -0.6 | -1.4 | -0.5 | -0.9 | 0.3 | 0.5 | -1.7 | -2.0 | -1.4 | -1.9 | -0.5 | -0.8 | -1.4 | -1.7 | | |
| | | Max | 0.5 | 0.5 | 0.7 | 0.8 | -0.6 | -0.5 | 0.0 | 0.0 | -0.3 | -0.2 | 0.3 | -0.1 | -0.2 | 0.4 | 1.6 | 1.0 | -0.2 | -0.1 | -0.2 | -0.4 | -0.1 | -0.2 | -0.1 | -0.2 | | |
| | | Range | 0.9 | 0.8 | 0.2 | 0.2 | 0.4 | 0.3 | 0.8 | 0.4 | 1.0 | 0.8 | 0.9 | 1.4 | 0.3 | 1.3 | 1.3 | 0.4 | 1.5 | 1.9 | 1.2 | 1.5 | 0.4 | 0.6 | 1.3 | 1.6 | 0.9 | 0.5 |
| | AR | Min | -3.8 | -3.7 | -3.1 | -3.9 | -3.5 | -3.4 | -3.5 | -3.3 | -5.1 | -5.3 | -4.7 | -5.1 | -3.5 | -3.6 | -3.8 | -4.6 | -3.0 | -3.0 | -4.5 | -4.2 | -3.8 | -4.4 | -4.5 | -4.4 | | |
| | | Max | -0.6 | -0.4 | -1.5 | -1.8 | -2.3 | -1.3 | -0.7 | -1.2 | -0.7 | -1.4 | 0.0 | -0.3 | -0.2 | -0.1 | -0.3 | -0.3 | 0.0 | -0.7 | -1.4 | -1.2 | -0.5 | 0.5 | -1.0 | -0.3 | | |
| | | Range | 3.2 | 3.3 | 1.7 | 2.0 | 1.2 | 2.1 | 2.8 | 2.0 | 4.4 | 4.0 | 4.7 | 4.8 | 3.3 | 3.5 | 3.6 | 4.3 | 3.0 | 2.3 | 3.1 | 3.0 | 3.3 | 4.8 | 3.4 | 4.0 | 3.2 | 1.0 |

Table 3.9 Cervical intervertebral joint angle (°) and joint range (°) for all of subjects for MOB, WAT, TRA, and LUL trials in flexion/extension (FE) , lateral bending (LB) , and axial rotation (AR) directions

| ADL | Trials | Subject 1 | | Subject 2 | | Subject 3 | | Subject 4 | | Subject 5 | | Subject 6 | | Subject 7 | | Subject 8 | | Subject 9 | | Subject 10 | | Subject 11 | | Subject 12 | | Mean | Std Dev | | |
|-----|--------|-----------|------|-----------|------|-----------|------|-----------|------|-----------|------|-----------|------|-----------|------|-----------|------|-----------|------|------------|------|------------|------|------------|------|------|---------|-----|-----|
| | | 1 | 2 | 1 | 2 | 1 | 2 | 1 | 2 | 1 | 2 | 1 | 2 | 1 | 2 | 1 | 2 | 1 | 2 | 1 | 2 | 1 | 2 | 1 | 2 | | | | |
| REV | FE | Min | 2.0 | 2.2 | 1.7 | 2.0 | 3.2 | 3.2 | 2.8 | 2.4 | 2.4 | 2.7 | 3.4 | 2.9 | 2.7 | 2.4 | 3.1 | 2.9 | | 2.4 | 2.7 | 3.2 | | 4.2 | 4.2 | 1.9 | 1.1 | | |
| | | Max | 3.6 | 4.1 | 5.2 | 5.0 | 4.8 | 5.3 | 4.7 | 4.8 | 6.1 | 6.7 | 4.1 | 4.1 | 5.2 | 5.1 | 5.3 | 5.6 | | 3.4 | 3.5 | 5.1 | | 5.7 | 5.9 | | | | |
| | | Range | 1.6 | 1.9 | 3.5 | 3.0 | 1.5 | 2.1 | 1.9 | 2.4 | 3.8 | 3.9 | 0.7 | 1.2 | 2.5 | 2.7 | 2.2 | 2.7 | | F | F | 1.1 | 0.8 | 1.9 | F | | | 1.5 | 1.8 |
| | LB | Min | -3.7 | -4.3 | -3.2 | -2.6 | -2.0 | -1.8 | -1.7 | -1.7 | -2.4 | -2.7 | -3.0 | -2.8 | -3.3 | -3.7 | -2.1 | -1.9 | | -2.4 | -2.9 | -3.0 | | -3.9 | -4.3 | | | | |
| | | Max | 1.4 | 1.5 | 0.3 | -0.6 | -1.3 | -0.8 | 1.3 | 1.3 | -0.6 | 0.6 | -0.6 | -0.1 | 0.2 | 0.6 | 0.9 | 1.5 | | 0.2 | -0.6 | 0.3 | | 0.3 | 0.4 | | | | |
| | | Range | 5.1 | 5.7 | 3.6 | 2.0 | 0.7 | 1.1 | 3.0 | 2.9 | 1.8 | 3.3 | 2.4 | 2.7 | 3.5 | 4.3 | 3.0 | 3.5 | | F | F | 2.7 | 2.3 | 3.3 | F | | | 4.3 | 4.6 |
| | AR | Min | -0.6 | -0.4 | -0.2 | -0.1 | -0.4 | 0.1 | -1.6 | -1.2 | -1.0 | -0.9 | -0.5 | -0.5 | 0.0 | -7.4 | -0.6 | -0.4 | | -0.1 | -0.6 | -0.4 | | 0.0 | -0.2 | | | | |
| | | Max | 4.6 | 4.8 | 6.1 | 6.1 | 4.1 | 4.0 | 5.1 | 5.1 | 5.5 | 5.6 | 4.8 | 4.9 | 5.0 | 1.9 | 5.5 | 5.6 | | 5.6 | 5.5 | 4.7 | | 4.1 | 4.2 | | | | |
| | | Range | 5.2 | 5.2 | 6.4 | 6.2 | 4.5 | 3.9 | 6.7 | 6.2 | 6.4 | 6.5 | 5.3 | 5.4 | 5.0 | 9.2 | 6.1 | 5.9 | | F | F | 5.7 | 6.1 | 5.0 | F | | | 4.0 | 4.3 |
| BND | FE | Min | 2.3 | 1.9 | -0.1 | -1.7 | | | 0.9 | 2.4 | 2.4 | 2.9 | -0.7 | 2.2 | 1.5 | 1.7 | 1.8 | 1.1 | 0.0 | -0.3 | | | 1.6 | 1.9 | 1.1 | 1.5 | 4.3 | 2.8 | |
| | | Max | 7.2 | 7.9 | 3.6 | 5.3 | | | 2.5 | 5.9 | 7.7 | 8.7 | 4.4 | 7.4 | 8.1 | 6.5 | 4.7 | 5.2 | 9.7 | 10.3 | | | 6.4 | 6.3 | 5.0 | 4.6 | | | |
| | | Range | 4.9 | 6.0 | 3.7 | 7.0 | F | F | 1.7 | 3.5 | 5.2 | 5.8 | 5.1 | 5.1 | 6.5 | 4.8 | 2.9 | 4.1 | 9.8 | 10.6 | | | F | F | 4.8 | 4.4 | | | 3.9 |
| | LB | Min | -0.7 | -0.4 | 0.4 | 0.7 | | | -1.5 | 0.9 | -1.8 | -1.1 | -1.0 | -0.8 | -0.9 | -1.0 | 0.4 | 0.3 | -1.0 | -1.4 | | | -1.1 | -0.4 | -0.1 | -1.1 | | | |
| | | Max | 1.5 | 1.6 | 1.4 | 1.5 | | | 0.1 | 1.7 | 0.7 | 1.2 | -0.2 | -0.2 | 0.1 | -0.3 | 2.0 | 1.3 | 0.8 | 0.5 | | | 1.4 | 1.4 | 0.5 | 0.3 | | | |
| | | Range | 2.2 | 2.0 | 1.0 | 0.7 | F | F | 1.6 | 0.8 | 2.5 | 2.4 | 0.8 | 0.7 | 1.0 | 0.8 | 1.5 | 1.0 | 1.8 | 1.9 | | | F | F | 2.5 | 1.8 | | | 0.6 |
| | AR | Min | -0.6 | -0.2 | -0.3 | -0.4 | | | -0.7 | -1.0 | -0.2 | -0.5 | -0.4 | -0.4 | 0.0 | 0.2 | 0.3 | -0.1 | -0.2 | 0.1 | | | -0.6 | -0.4 | -0.1 | -0.2 | | | |
| | | Max | -0.1 | 0.1 | -0.2 | 0.0 | | | -0.5 | -0.6 | 0.0 | -0.1 | -0.2 | -0.2 | 0.5 | 0.5 | 0.9 | 0.5 | 0.3 | 0.4 | | | -0.1 | 0.0 | 0.1 | 0.1 | | | |
| | | Range | 0.5 | 0.3 | 0.1 | 0.4 | F | F | 0.1 | 0.4 | 0.2 | 0.4 | 0.2 | 0.3 | 0.5 | 0.3 | 0.6 | 0.6 | 0.5 | 0.3 | | | F | F | 0.5 | 0.4 | | | 0.2 |
| StS | FE | Min | -0.4 | 1.9 | 1.6 | 2.7 | 0.8 | 2.9 | 2.0 | 2.5 | 4.0 | | 3.8 | 1.8 | -0.5 | | 0.3 | 3.9 | 0.5 | 1.3 | 2.5 | 2.0 | | 2.9 | 2.3 | 2.6 | 4.3 | 2.2 | |
| | | Max | 3.8 | 6.5 | 5.0 | 5.2 | 5.9 | 8.0 | 6.8 | 6.5 | 9.2 | | 7.0 | 6.9 | 4.1 | | 8.3 | 7.9 | 9.2 | 8.1 | 6.2 | 6.0 | | 6.8 | 8.4 | 9.7 | | | |
| | | Range | 4.1 | 4.6 | 3.5 | 2.5 | 5.1 | 5.1 | 4.8 | 4.0 | 5.3 | -- | 3.2 | 5.1 | 4.5 | -- | 8.0 | 4.0 | 8.6 | 6.8 | 3.7 | 4.0 | | F | 3.8 | 6.1 | | | 7.0 |
| | LB | Min | -0.8 | -0.7 | 0.3 | 0.2 | -0.4 | -0.4 | 0.2 | -0.4 | 0.2 | | -0.6 | -0.3 | -1.4 | | -0.3 | -0.6 | 0.4 | 0.0 | -0.2 | -0.3 | | -0.7 | -0.1 | -0.4 | | | |
| | | Max | 0.5 | 0.2 | 1.0 | 1.0 | 0.6 | 0.3 | 0.4 | 0.7 | 1.4 | | 0.2 | -0.2 | 0.0 | | 0.8 | 1.1 | 1.4 | 1.4 | 0.0 | 0.1 | | 0.3 | 0.3 | 0.4 | | | |
| | | Range | 1.3 | 0.9 | 0.7 | 0.8 | 1.0 | 0.7 | 0.2 | 1.1 | 1.2 | -- | 0.7 | 0.2 | 1.3 | -- | 1.1 | 1.7 | 1.0 | 1.4 | 0.2 | 0.4 | | F | 1.1 | 0.3 | | | 0.8 |
| | AR | Min | -0.5 | -0.1 | -0.2 | 0.0 | -0.8 | -0.6 | -0.6 | -0.5 | -0.3 | | -0.5 | -0.3 | -0.1 | | 0.0 | 0.0 | 0.0 | -0.1 | -0.4 | -0.3 | | -0.7 | -0.2 | -0.4 | | | |
| | | Max | 0.0 | 0.2 | 0.2 | 0.5 | -0.3 | -0.3 | -0.4 | -0.1 | -0.1 | | -0.2 | -0.2 | 0.2 | | 0.4 | 0.3 | 0.4 | 0.5 | -0.3 | -0.2 | | -0.3 | 0.0 | -0.1 | | | |
| | | Range | 0.5 | 0.3 | 0.4 | 0.5 | 0.5 | 0.3 | 0.2 | 0.4 | 0.3 | -- | 0.3 | 0.1 | 0.2 | -- | 0.4 | 0.3 | 0.4 | 0.6 | 0.1 | 0.1 | | F | 0.3 | 0.2 | | | 0.3 |
| SiS | FE | Min | 2.7 | 2.9 | 5.2 | 4.5 | 5.2 | 5.2 | 3.5 | 2.2 | 4.5 | 5.1 | 3.9 | 4.3 | | | 6.5 | 7.0 | 1.4 | 1.7 | 2.2 | 2.3 | 2.4 | 1.5 | 2.5 | 3.1 | 4.0 | 1.8 | |
| | | Max | 6.4 | 7.0 | 7.9 | 8.6 | 8.3 | 7.9 | 7.5 | 7.6 | 8.6 | 9.0 | 7.5 | 7.5 | | | 10.6 | 10.2 | 9.0 | 9.8 | 6.0 | 5.9 | 6.4 | 6.7 | 8.3 | 8.5 | | | |
| | | Range | 3.7 | 4.1 | 2.6 | 4.1 | 3.0 | 2.7 | 4.0 | 5.4 | 4.1 | 3.9 | 3.6 | 3.3 | -- | -- | 4.1 | 3.3 | 7.6 | 8.1 | 3.8 | 3.6 | 4.0 | 5.2 | 5.7 | 5.4 | | | |
| | LB | Min | -0.5 | -0.5 | 0.0 | 0.2 | -0.1 | -0.1 | -0.3 | -0.1 | 0.2 | 0.0 | -0.3 | -0.3 | | | -0.7 | 0.4 | 0.4 | 0.1 | -0.6 | -0.3 | -1.1 | -1.1 | 0.0 | 0.0 | | | |
| | | Max | 0.4 | 0.2 | 0.8 | 1.0 | 0.4 | 0.2 | 0.6 | 0.7 | 1.1 | 1.0 | 0.2 | 0.2 | | | 0.7 | 1.1 | 1.4 | 1.1 | -0.1 | -0.1 | -0.3 | -0.4 | 0.5 | 0.3 | | | |
| | | Range | 0.9 | 0.7 | 0.8 | 0.8 | 0.4 | 0.3 | 0.9 | 0.8 | 0.9 | 1.0 | 0.5 | 0.5 | -- | -- | 1.4 | 0.6 | 1.0 | 1.0 | 0.4 | 0.2 | 0.8 | 0.7 | 0.5 | 0.3 | | | |
| | AR | Min | -0.1 | 0.0 | -0.2 | -0.5 | -0.7 | -0.7 | -0.1 | -0.2 | -0.4 | -0.5 | -0.3 | -0.3 | | | 0.6 | 0.1 | 0.1 | 0.1 | -0.5 | -0.3 | -0.4 | -0.2 | -0.2 | -0.2 | | | |
| | | Max | 0.1 | 0.3 | 0.1 | 0.1 | -0.4 | -0.3 | 0.0 | 0.0 | -0.1 | -0.1 | 0.0 | -0.1 | | | 1.0 | 0.6 | 0.6 | 0.5 | -0.4 | -0.2 | 0.0 | 0.4 | 0.0 | -0.1 | | | |
| | | Range | 0.1 | 0.4 | 0.4 | 0.5 | 0.3 | 0.3 | 0.1 | 0.2 | 0.3 | 0.4 | 0.3 | 0.2 | -- | -- | 0.4 | 0.5 | 0.5 | 0.4 | 0.1 | 0.1 | 0.4 | 0.7 | 0.2 | 0.2 | | | |

Table 3.10 Cervical intervertebral joint angle (°) and joint range (°) for all of subjects for REV, BND, StS, and SiS trials in flexion/extension (FE) , lateral bending (LB) , and axial rotation (AR) directions

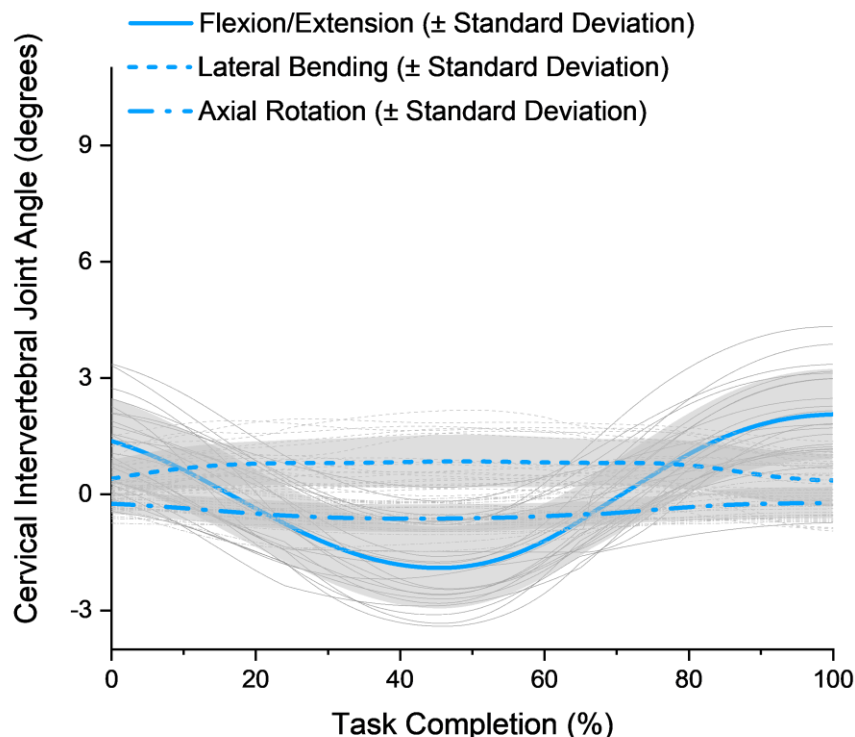
The average cervical joint angle excursion throughout the ADL task for all subjects in all activities is also illustrated in Figure 3.8 ((a) to (h), blue lines). The graphs show a time-normalised for all subjects for each ADL task. All trial curves were aligned according to peaks and troughs within superiorinferior axial loading graph.

On average, the subjects in this study tend to have a slightly extended neck posture when seated compared to standing. This phenomenon can as seen in Figure 3.8 (e) where simulation was done whilst sitting down, (g) where the simulation ended in sitting, and (h) where the simulation began with sitting.

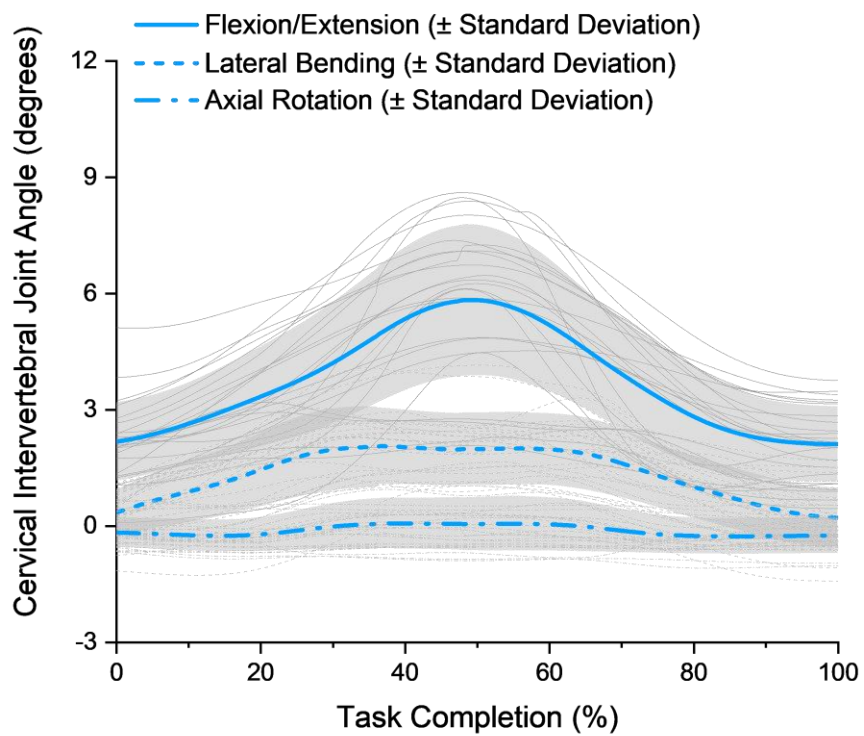
From the excursion graphs in Figure 3.8, inter-subject kinematics variations in cervical intervertebral joint at the main direction of head motion are relatively wide for all ADL tasks analysed except for 'looking for traffic before crossing' and 'looking up laterally' where the shaded band of standard deviation for axial rotation are narrow in these ADL tasks.

Figure 3.8 Normalised cervical joint excursions for all trials for all ADL tasks

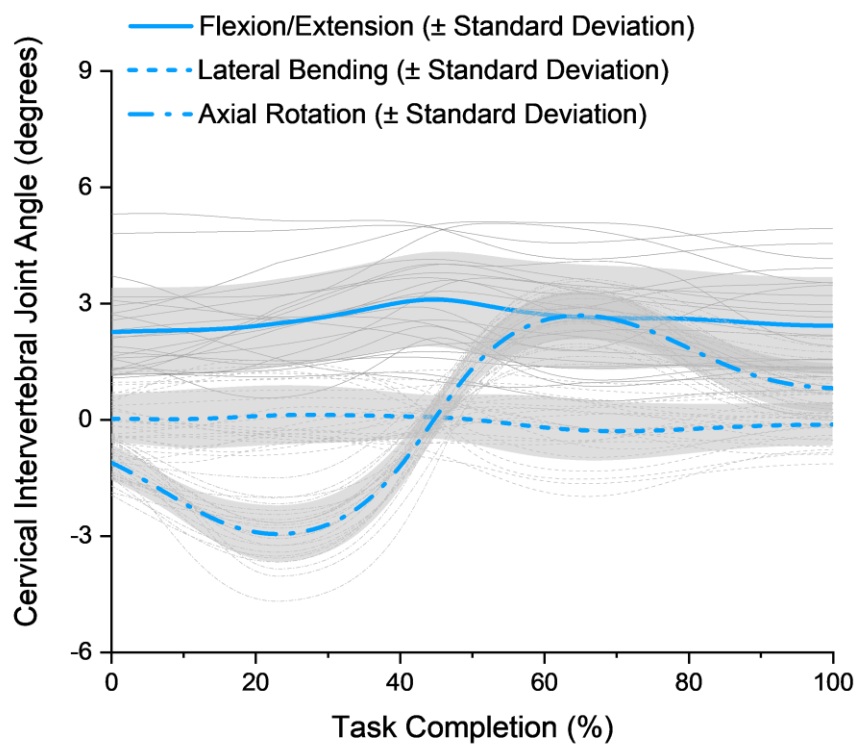
a) Looking at Mobile (MOB)



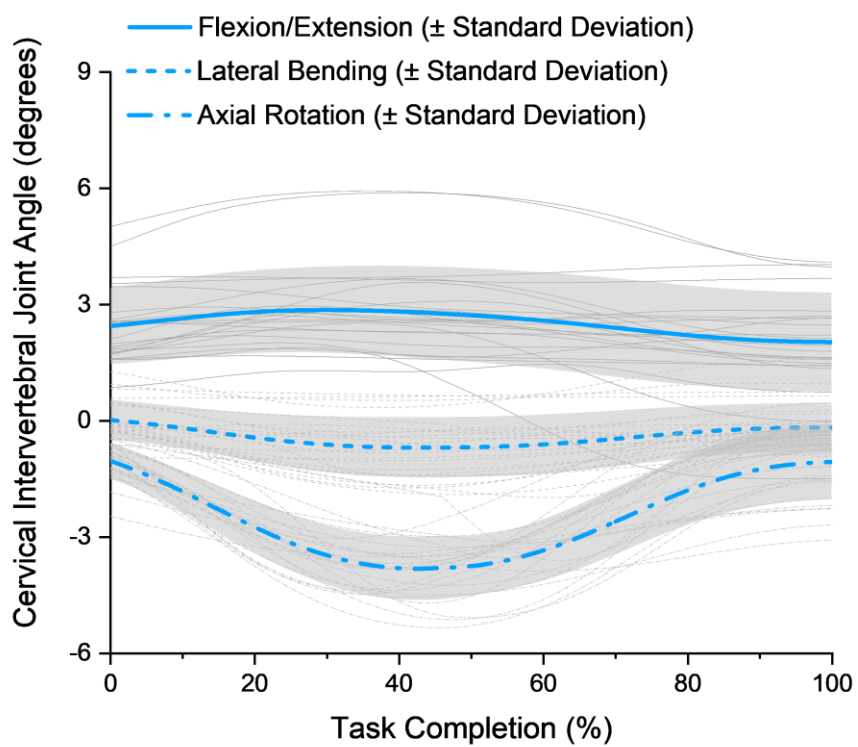
b) Drinking from a Bottle (WAT)



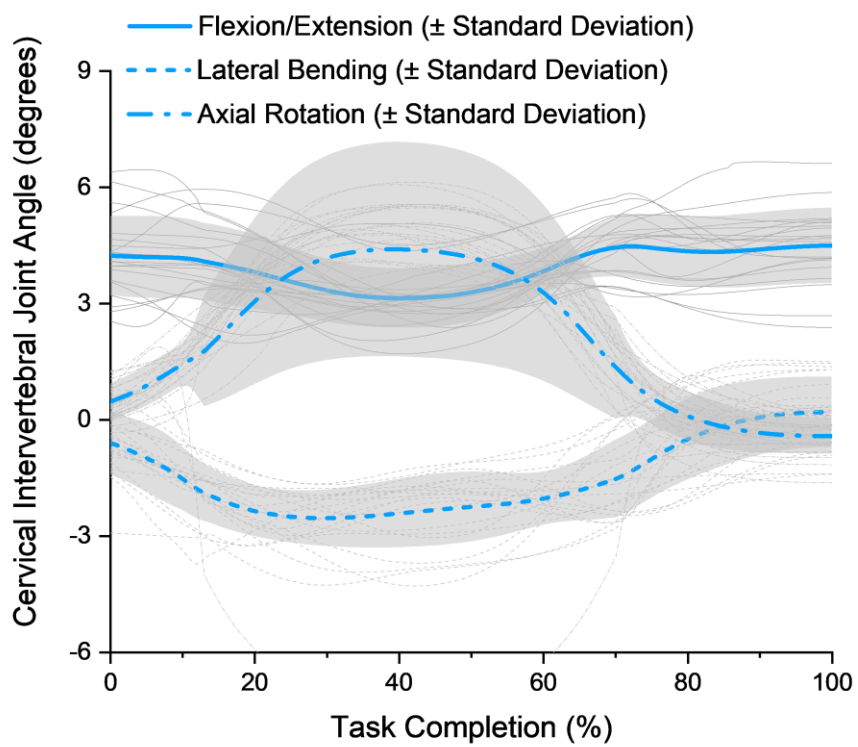
c) Looking for Traffic (TRA)



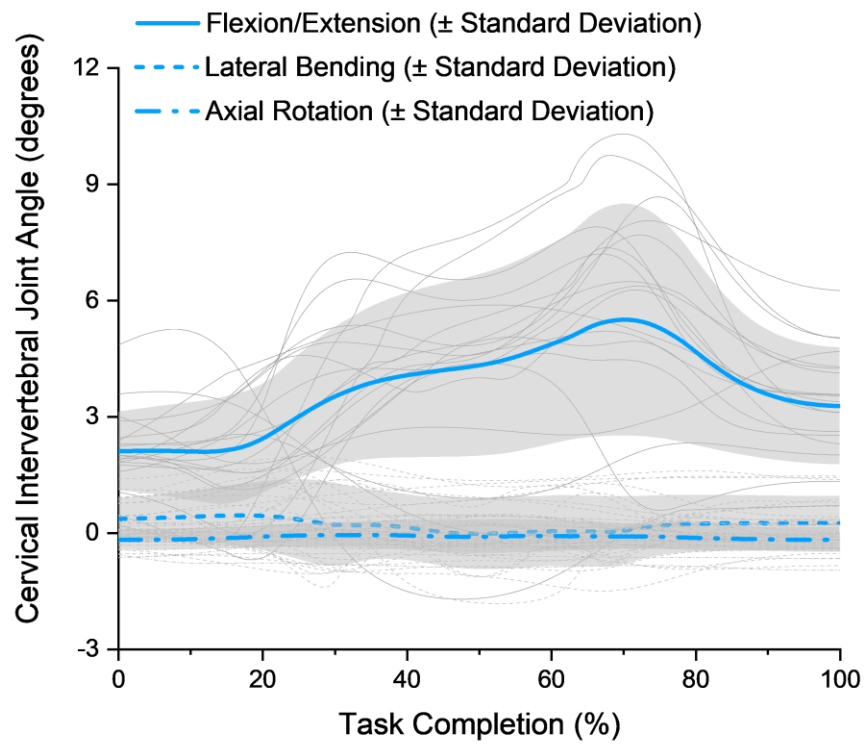
d) Looking Up Laterally (LUL)



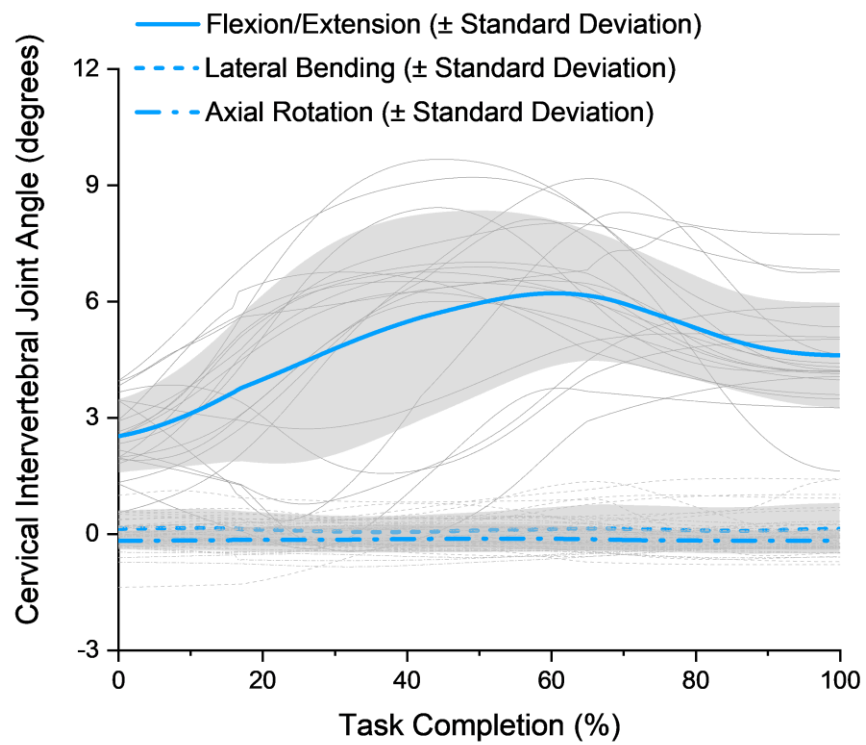
e) Reversing a Car (REV)



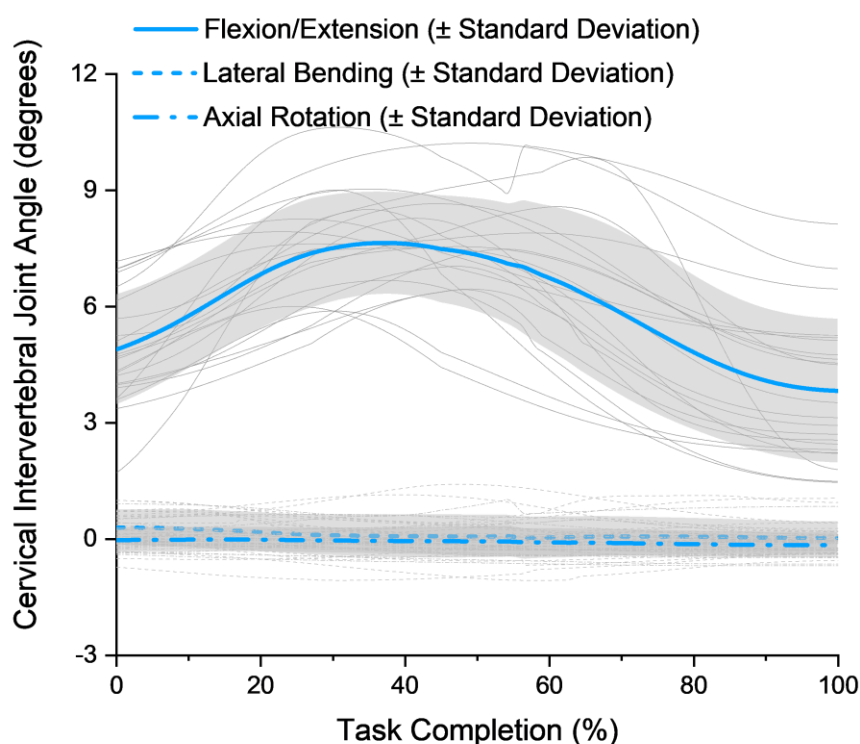
f) Bending Down (BND)



g) Stand-to-sit (StS)



h) Sit-to-stand (SiS)



3.2.5 Cervical Joint Loading

The cervical spine model in AMMR was programmed to have seven individual cervical vertebrae together with their associated muscle attachments. Therefore, the multibody simulation is capable of solving inverse dynamic analysis in each cervical intervertebral joint level. Due to immense amount of data that is available from the analysis, only joint loadings in cervical intervertebral C5-C6 are being presented and discussed in this thesis as it is the commonest implanted level for cervical disc implant and the commonest level for revision surgery to take place in failed prostheses [221-223].

Table 3.11, Table 3.12, and Table 3.13 show the minimum and maximum joint loading within the cervical spine for all subjects in all of the ADL trials in superoinferior, mediolateral, and anteroposterior direction, respectively. In general, the superoinferior direction (axial loading) has the largest force with an order of magnitude of two, followed by anteroposterior loading with an order of magnitude of one, and then mediolateral direction with an order of magnitude of almost zero. The average minimum and maximum cervical intervertebral joint

loading values and its standard deviations for all ADL tasks are shown at the bottom two rows of each table. In general, on average, the minimum axial loading during ADL tasks is estimated between 92.1 N to 186.9 N whereas the maximum axial loading is estimated between 181.3 N to 348.8 N. These values are outside the minimum and maximum magnitude prescribed in ISO18192-1 [1].

The average cervical intervertebral joint loading at C5-C6 throughout the ADL task for all subjects in all activities is also illustrates in Figure 3.9 ((a) to (h), red lines). The graphs show a time-normalised for all subjects for each ADL task. As described in Section 3.1.7, all trial curves were aligned according to peaks and troughs within superoinferior axial loading graph.

In general, the axial loading increases as the head is extended and decreases when the neck flexes the head as seen in 'looking at mobile' (MOB) and 'drinking from a bottle' (WAT) ADL tasks. This pattern of axial loading changes once the centre of gravity of the head shifted away considerably from the body's centre of gravity as seen in 'bending down' (BND), 'sitting down' (StS), and 'standing up' (SiS) as the back muscles are activated to stabilise the head, thus contributing towards the cervical intervertebral joint loadings, until the head return to its neutral position. As indicated previously, these ADL tasks are moving predominantly in sagittal plane, *i.e.* flexion/extension.

Movement that is predominantly in transverse plane, such as 'looking at traffic before crossing' (TRA) and 'looking up laterally' (LUL), however, has a less remarkable change in their axial loading pattern as the head remains relatively aligned with the body's centre of gravity and the back muscles are not fully engaged. By contrast, 'reversing a car' (REV) has one of the highest axial loading outputs registered on the cervical intervertebral joint. This task requiring the subjects to twist their bodies and then rotate their heads as well, almost to the extreme, which activates the neck and back muscles along the torso unilaterally.

Figure 3.10 ((a) to (h)) shows the combined, average joint kinematics and loadings for C5-C6 for all ADL activities investigated in this study.

| ADL | | MOB | | WAT | | TRA | | LUL | | REV | | BND | | StS | | SiS | |
|----------------|-------|-------|-------|-------|-------|-------|-------|-------|-------|-------|-------|-------|-------|-------|-------|-------|-------|
| Subject | Trial | Min | Max | Min | Max | Min | Max | Min | Max | Min | Max | Min | Max | Min | Max | Min | Max |
| 1 | 1 | 113.6 | 160.9 | 160.7 | 320.7 | 138.6 | 178.8 | 177.7 | 280.5 | 103.9 | 187.4 | 86.1 | 244.9 | 95.4 | 170.5 | 86.1 | 199.7 |
| | 2 | 98.3 | 154.8 | 160.5 | 311.1 | 166.6 | 213.1 | 167.5 | 284.4 | 106.3 | 180.5 | 85.5 | 190.1 | 84.3 | 182.9 | 91.3 | 169.2 |
| 2 | 1 | 80.5 | 147.2 | 113.9 | 369.0 | 98.3 | 167.5 | 195.0 | 233.2 | 82.5 | 195.9 | 87.5 | 176.2 | 73.3 | 197.6 | 76.6 | 223.9 |
| | 2 | 73.2 | 173.5 | 104.9 | 352.0 | 97.3 | 180.6 | 185.6 | 222.4 | 78.6 | 194.9 | 92.0 | 217.5 | 70.1 | 162.6 | 77.5 | 190.3 |
| 3 | 1 | 113.0 | 203.3 | 232.4 | 434.0 | 130.6 | 233.7 | 230.7 | 253.9 | 157.9 | 243.1 | F | F | 95.5 | 252.2 | 162.4 | 243.8 |
| | 2 | 114.0 | 220.8 | 220.1 | 450.7 | 86.6 | 243.6 | 242.5 | 269.5 | 186.5 | 247.5 | F | F | 91.3 | 248.3 | 145.4 | 248.2 |
| 4 | 1 | 79.7 | 118.5 | 153.6 | 318.8 | 83.6 | 185.2 | 174.3 | 200.1 | 111.7 | 188.0 | 82.9 | 179.7 | 74.5 | 192.3 | 79.8 | 161.8 |
| | 2 | 78.6 | 139.8 | 159.5 | 310.9 | 85.1 | 182.1 | 168.1 | 182.1 | 104.9 | 186.7 | 84.3 | 191.4 | 72.6 | 196.8 | 77.1 | 181.4 |
| 5 | 1 | 89.9 | 171.2 | 177.0 | 400.9 | 104.1 | 167.5 | 153.1 | 201.2 | 159.2 | 231.7 | 75.8 | 212.3 | 98.6 | 251.5 | 130.7 | 224.8 |
| | 2 | 89.0 | 174.3 | 170.5 | 371.3 | 92.1 | 179.7 | 177.6 | 208.0 | 164.4 | 277.1 | 77.7 | 245.6 | -- | -- | 144.8 | 210.0 |
| 6 | 1 | 125.8 | 231.9 | 157.7 | 358.9 | 119.0 | 203.7 | 154.8 | 212.9 | 180.8 | 241.3 | 111.8 | 200.3 | 114.8 | 236.1 | 117.2 | 186.2 |
| | 2 | 123.9 | 201.0 | 200.6 | 395.4 | 116.3 | 212.6 | 191.6 | 239.3 | 170.6 | 223.9 | 102.5 | 201.3 | 106.8 | 258.3 | 126.2 | 190.1 |
| 7 | 1 | -- | -- | 180.1 | 380.7 | 122.4 | 208.5 | 186.1 | 235.4 | 152.9 | 262.1 | 96.9 | 184.0 | 107.9 | 234.0 | -- | -- |
| | 2 | -- | -- | 141.0 | 362.2 | 121.8 | 240.7 | 199.1 | 227.0 | 144.0 | 257.0 | 99.1 | 249.6 | -- | -- | -- | -- |
| 8 | 1 | 156.7 | 263.4 | 219.2 | 495.4 | 232.2 | 280.9 | 268.0 | 411.8 | 220.8 | 458.4 | 140.4 | 339.8 | 128.7 | 383.2 | 148.6 | 371.5 |
| | 2 | 153.5 | 239.8 | 223.1 | 484.2 | 252.9 | 316.9 | 240.7 | 423.7 | 197.0 | 589.3 | 135.8 | 233.0 | 139.9 | 384.8 | 222.8 | 375.0 |
| 9 | 1 | 89.2 | 151.7 | 111.9 | 300.2 | 100.1 | 164.9 | 138.8 | 174.9 | F | F | 73.3 | 203.2 | 87.0 | 229.9 | 130.8 | 180.5 |
| | 2 | 85.4 | 139.2 | 117.2 | 272.0 | 89.8 | 167.6 | 148.5 | 209.9 | F | F | 69.4 | 180.8 | 86.6 | 174.8 | 89.3 | 211.2 |
| 10 | 1 | 87.3 | 157.8 | 150.8 | 203.5 | 98.8 | 191.1 | 192.8 | 211.7 | 122.0 | 588.6 | F | F | 91.5 | 143.7 | 117.4 | 165.1 |
| | 2 | 89.9 | 165.1 | 146.6 | 215.4 | 85.3 | 165.3 | 180.6 | 204.4 | 125.0 | 655.9 | F | F | 100.0 | 165.6 | 123.9 | 166.9 |
| 11 | 1 | 100.9 | 206.1 | 182.5 | 331.3 | 100.8 | 214.3 | 158.9 | 239.0 | 133.2 | 427.7 | 92.6 | 169.4 | F | F | 100.8 | 161.8 |
| | 2 | 106.7 | 200.7 | 184.9 | 410.2 | 98.4 | 210.9 | 133.8 | 214.4 | F | F | 94.5 | 184.0 | 95.2 | 157.7 | 103.4 | 149.8 |
| 12 | 1 | 88.5 | 182.0 | 188.8 | 252.9 | 144.9 | 202.3 | 221.7 | 259.3 | 170.3 | 256.9 | 76.5 | 196.1 | 122.9 | 192.6 | 140.7 | 210.5 |
| | 2 | 91.9 | 185.3 | 177.6 | 268.3 | 150.6 | 201.6 | 197.4 | 260.9 | 192.2 | 277.5 | 77.4 | 212.4 | 128.2 | 189.9 | 144.8 | 200.7 |
| Mean | | 101.3 | 181.3 | 168.1 | 348.8 | 121.5 | 204.7 | 186.9 | 244.2 | 145.9 | 303.4 | 92.1 | 210.6 | 98.3 | 219.3 | 119.9 | 210.1 |
| Std Dev | | 22.2 | 35.5 | 35.0 | 75.3 | 42.7 | 36.8 | 33.4 | 59.5 | 38.5 | 143.9 | 18.5 | 37.8 | 19.3 | 63.2 | 34.7 | 57.7 |

Table 3.11 Minimum (Min) and maximum (Max) cervical (superoinferior) axial loading (Newtons) for all subjects for all ADL trials (+ in direction of gravity)

| ADL | | MOB | | WAT | | TRA | | LUL | | REV | | BND | | StS | | SiS | |
|----------------|-------|-------|------|-------|-------|-------|------|-------|-------|----------|----------|----------|----------|----------|----------|-------|-------|
| Subject | Trial | Min | Max | Min | Max | Min | Max | Min | Max | Min | Max | Min | Max | Min | Max | Min | Max |
| 1 | 1 | -0.07 | 1.91 | 1.15 | 8.68 | -3.04 | 4.08 | -3.04 | 1.07 | -3.59 | 1.83 | -1.53 | 2.28 | -1.55 | 0.74 | -1.43 | 0.15 |
| | 2 | 0.17 | 1.65 | -1.45 | 7.63 | -4.29 | 2.00 | -2.47 | 2.08 | -3.43 | 1.33 | -0.86 | 2.36 | -1.32 | 0.00 | -1.78 | 1.11 |
| 2 | 1 | 0.49 | 2.50 | -0.16 | 6.43 | -2.71 | 3.36 | -0.76 | 2.63 | -5.99 | 2.33 | -0.17 | 3.78 | 0.46 | 1.96 | 0.26 | 1.43 |
| | 2 | -1.88 | 3.55 | -1.69 | 2.12 | -2.58 | 4.42 | -2.18 | 2.07 | -6.10 | 2.12 | 0.52 | 3.44 | 0.60 | 1.80 | 0.48 | 1.93 |
| 3 | 1 | -1.53 | 1.24 | 0.97 | 6.84 | -3.64 | 1.31 | -2.40 | -1.36 | -7.60 | -1.69 | F | F | -2.73 | 1.78 | -0.06 | 1.66 |
| | 2 | -1.35 | 1.50 | 0.84 | 7.12 | -2.68 | 1.24 | -2.24 | 0.61 | -7.89 | -3.14 | F | F | -1.58 | 0.68 | -0.02 | 0.86 |
| 4 | 1 | -0.03 | 1.57 | 0.45 | 9.01 | -3.06 | 1.68 | -2.56 | 0.15 | -3.82 | 1.85 | -5.64 | -0.30 | 0.04 | 1.20 | -0.59 | 1.90 |
| | 2 | -0.53 | 1.41 | 2.04 | 7.33 | -2.98 | 1.85 | -3.10 | -1.05 | -3.85 | 2.77 | -5.34 | -0.36 | -0.62 | 1.20 | -0.31 | 1.45 |
| 5 | 1 | -0.35 | 2.82 | 1.37 | 10.46 | -3.87 | 1.50 | -5.63 | 1.20 | -11.10 | -1.81 | -4.14 | 0.98 | 0.07 | 5.34 | 0.64 | 3.77 |
| | 2 | 1.04 | 2.93 | 0.75 | 9.86 | -4.34 | 1.60 | -5.14 | 1.62 | -11.66 | 2.24 | -3.92 | 1.90 | -- | -- | 0.33 | 2.61 |
| 6 | 1 | 0.20 | 2.75 | 1.41 | 4.59 | -4.70 | 2.91 | -7.37 | 1.46 | -9.55 | -1.10 | -4.60 | 2.00 | -1.61 | 1.31 | -0.39 | 0.66 |
| | 2 | -0.27 | 2.08 | 1.91 | 4.45 | -6.36 | 0.72 | -7.00 | 1.39 | -9.49 | 0.21 | -3.39 | 2.23 | -0.86 | 1.27 | -0.95 | 0.63 |
| 7 | 1 | -- | -- | -0.57 | 3.59 | -2.98 | 2.65 | -3.68 | 2.35 | -8.88 | 2.02 | -2.40 | 2.23 | -2.71 | 0.15 | -- | -- |
| | 2 | -- | -- | -1.50 | 2.82 | -6.14 | 3.51 | -2.75 | 2.94 | -23.90 | 0.49 | -2.69 | 0.71 | -- | -- | -- | -- |
| 8 | 1 | -1.94 | 4.44 | -4.49 | 18.45 | -1.14 | 7.14 | -3.85 | 7.74 | -9.61 | 4.97 | -1.67 | 7.02 | -1.84 | 3.46 | -4.42 | 3.28 |
| | 2 | -1.27 | 4.61 | -1.52 | 10.34 | -2.46 | 6.67 | -3.76 | 7.04 | -14.43 | 3.99 | 0.43 | 3.87 | -3.18 | 2.08 | -0.44 | 2.78 |
| 9 | 1 | -0.53 | 0.96 | -1.34 | 1.95 | -2.41 | 2.31 | -4.62 | 0.68 | F | F | -2.48 | 1.80 | -2.26 | 3.59 | -1.13 | 2.80 |
| | 2 | -0.72 | 1.54 | -0.75 | 4.15 | -3.48 | 2.92 | -4.66 | 0.32 | F | F | -2.56 | 2.50 | -1.33 | 3.21 | -1.69 | 2.99 |
| 10 | 1 | -0.89 | 1.18 | 0.84 | 6.42 | -2.09 | 5.05 | -4.21 | 1.87 | -31.21 | 1.03 | F | F | -0.58 | 1.17 | -0.51 | 2.28 |
| | 2 | -2.35 | 1.37 | 0.17 | 6.50 | -0.63 | 2.76 | -5.95 | 1.15 | -39.78 | 0.51 | F | F | -0.61 | 1.07 | -0.23 | 1.99 |
| 11 | 1 | -2.59 | 0.76 | -0.66 | 5.91 | -4.59 | 3.34 | -5.07 | -0.87 | -6.57 | 1.74 | -5.87 | 2.64 | F | F | -1.85 | -0.24 |
| | 2 | -3.80 | 1.58 | -0.75 | 8.22 | -4.55 | 3.92 | -6.77 | 0.48 | F | F | -1.17 | 3.42 | -1.92 | 0.73 | -2.20 | 0.02 |
| 12 | 1 | -1.37 | 1.55 | -0.21 | 2.91 | -5.42 | 4.69 | -3.96 | 1.19 | -7.52 | -0.12 | -0.45 | 1.60 | -0.09 | 0.53 | -0.54 | 0.95 |
| | 2 | -1.57 | 1.48 | 0.10 | 3.23 | -5.06 | 5.65 | -3.27 | 1.36 | -8.88 | 0.95 | -2.51 | 0.66 | -0.81 | 1.05 | -0.16 | 0.82 |
| Mean | | -0.96 | 2.06 | -0.13 | 6.62 | -3.55 | 3.22 | -4.02 | 1.59 | -11.18 | 1.07 | -2.52 | 2.24 | -1.16 | 1.63 | -0.77 | 1.63 |
| Std Dev | | 1.11 | 1.03 | 1.43 | 3.53 | 1.41 | 1.69 | 1.65 | 2.05 | 9.12 | 1.88 | 1.91 | 1.60 | 1.04 | 1.27 | 1.11 | 1.08 |

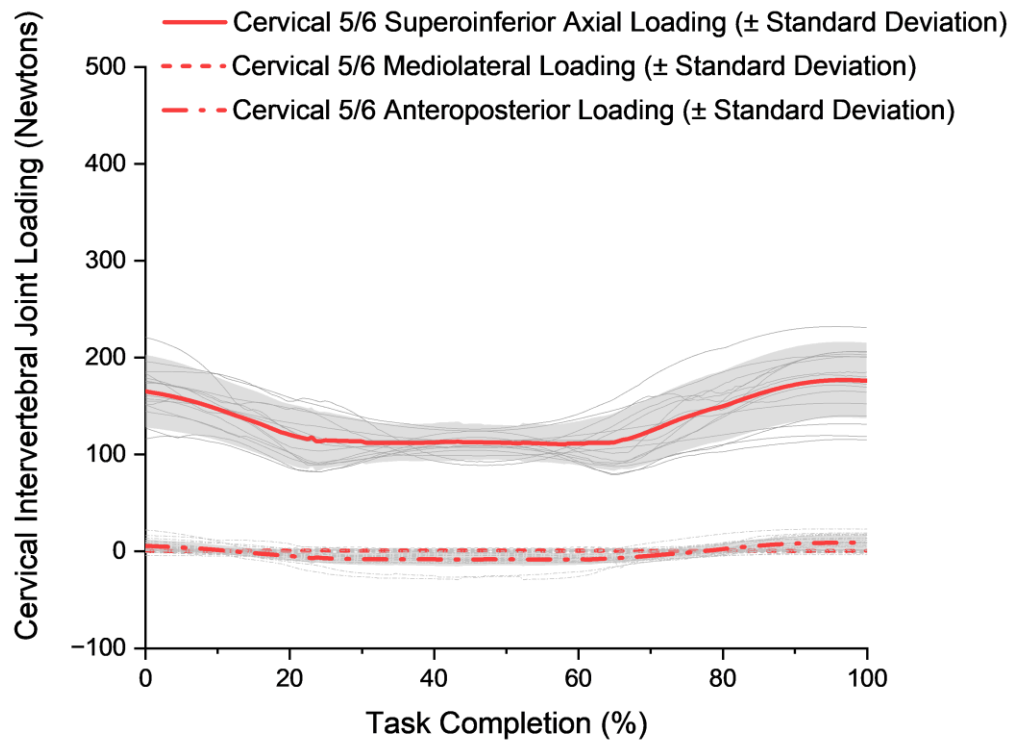
Table 3.12 Minimum (Min) and maximum (Max) cervical mediolateral loading (Newtons) for all subjects for all ADL trials (+ in right direction)

| ADL | | MOB | | WAT | | TRA | | LUL | | REV | | BND | | StS | | SiS | |
|----------------|-------|-------|------|------|------|-------|------|------|------|----------|----------|----------|----------|----------|----------|-------|------|
| Subject | Trial | Min | Max | Min | Max | Min | Max | Min | Max | Min | Max | Min | Max | Min | Max | Min | Max |
| 1 | 1 | -8.0 | 4.9 | 3.5 | 32.0 | -4.4 | 5.3 | 6.7 | 20.1 | -18.3 | -1.8 | -67.1 | 20.2 | -55.6 | -1.4 | -59.9 | 18.4 |
| | 2 | -12.5 | 5.4 | 4.2 | 30.0 | 0.1 | 13.4 | 7.1 | 20.0 | -20.6 | -2.0 | -70.8 | 7.5 | -49.4 | 8.3 | -53.6 | 10.7 |
| 2 | 1 | -16.8 | 4.6 | 1.0 | 30.2 | -19.6 | 3.6 | 4.4 | 7.4 | -23.7 | -2.4 | -34.6 | -6.0 | -37.1 | 8.3 | -40.8 | 13.6 |
| | 2 | -24.2 | 9.2 | 0.9 | 31.3 | -16.6 | 3.6 | 2.5 | 5.8 | -26.1 | -1.9 | -39.3 | -4.7 | -41.0 | -0.6 | -43.4 | 11.8 |
| 3 | 1 | -12.1 | 16.8 | 20.5 | 54.1 | -11.6 | 16.3 | 14.9 | 21.2 | -9.3 | 7.1 | F | F | -58.5 | 10.7 | -30.5 | 11.2 |
| | 2 | -11.5 | 22.2 | 16.3 | 54.9 | -6.5 | 16.9 | 14.6 | 20.7 | -2.6 | 7.6 | F | F | -71.5 | 5.8 | -32.6 | 7.1 |
| 4 | 1 | -7.6 | 1.6 | 6.8 | 32.7 | -21.3 | 11.3 | 9.7 | 13.3 | -10.4 | 2.9 | -42.6 | 13.5 | -44.9 | 9.6 | -41.3 | 11.3 |
| | 2 | -6.7 | 4.4 | 10.1 | 32.2 | -25.2 | 12.1 | 6.5 | 8.7 | -11.9 | 1.1 | -40.5 | 17.5 | -54.2 | 9.8 | -40.3 | 12.8 |
| 5 | 1 | -9.7 | 8.6 | 12.3 | 36.1 | -19.1 | 2.1 | 1.2 | 9.1 | -5.2 | 5.0 | -83.0 | 23.4 | -47.3 | 12.3 | -35.1 | 12.9 |
| | 2 | -10.8 | 9.0 | 11.8 | 36.8 | -37.0 | 9.0 | 2.3 | 9.0 | -12.7 | 8.1 | -61.9 | 16.5 | -- | -- | -28.5 | 10.9 |
| 6 | 1 | -9.7 | 23.3 | 2.7 | 46.4 | -56.8 | 12.0 | 2.9 | 11.2 | -5.5 | 11.3 | -88.0 | 6.4 | -69.1 | 12.9 | -72.2 | 5.3 |
| | 2 | -10.5 | 13.9 | 14.4 | 49.7 | -47.3 | 1.1 | 6.9 | 17.3 | -9.4 | 7.1 | -74.1 | 10.2 | -79.1 | 22.4 | -68.7 | 1.8 |
| 7 | 1 | -- | -- | 1.2 | 45.5 | -43.4 | 9.5 | 4.8 | 11.5 | -14.7 | 12.0 | -73.2 | 8.5 | -62.0 | -0.5 | -- | -- |
| | 2 | -- | -- | -5.8 | 42.7 | -40.8 | 15.6 | 5.5 | 9.8 | -16.2 | 12.1 | -75.6 | 17.2 | -- | -- | -- | -- |
| 8 | 1 | -29.2 | 10.1 | -3.5 | 40.3 | -7.7 | 5.0 | 6.2 | 21.8 | -11.9 | 22.1 | -102.7 | 37.6 | -99.9 | 26.0 | -94.7 | 25.5 |
| | 2 | -27.0 | 4.6 | -1.2 | 50.2 | -4.0 | 11.5 | 1.6 | 27.6 | -13.3 | 48.0 | -95.6 | 3.7 | -78.0 | 41.9 | -63.5 | 37.7 |
| 9 | 1 | -9.4 | 9.3 | -3.5 | 24.0 | -15.6 | 10.3 | 6.8 | 11.6 | F | F | -46.0 | 10.8 | -42.9 | 19.2 | -27.6 | 16.6 |
| | 2 | -11.3 | 6.1 | -4.8 | 20.7 | -20.8 | 11.9 | 7.8 | 15.4 | F | F | -49.3 | 16.2 | -40.3 | 15.0 | -47.5 | 18.6 |
| 10 | 1 | -6.5 | 4.8 | 4.8 | 23.2 | -10.7 | 16.8 | 8.8 | 14.0 | 1.4 | 46.1 | F | F | -31.6 | 9.2 | -17.0 | 10.5 |
| | 2 | -6.0 | 8.5 | 2.7 | 23.6 | -16.9 | 10.3 | 9.3 | 13.9 | 0.4 | 54.6 | F | F | -25.3 | 15.3 | -14.7 | 13.1 |
| 11 | 1 | -6.7 | 18.2 | 9.7 | 39.3 | -31.8 | 18.8 | 1.0 | 14.5 | -10.8 | 18.2 | -58.3 | 7.5 | F | F | -48.9 | 6.7 |
| | 2 | -4.1 | 19.1 | 9.4 | 45.8 | -36.3 | 15.5 | -3.2 | 12.2 | F | F | -59.1 | 12.9 | -55.1 | 8.0 | -45.7 | 5.3 |
| 12 | 1 | -1.4 | 14.2 | 20.7 | 26.8 | -0.1 | 19.7 | 21.9 | 25.7 | 6.2 | 14.1 | -47.6 | 23.7 | -27.9 | 24.1 | -20.9 | 27.6 |
| | 2 | -0.9 | 16.5 | 11.0 | 28.9 | 5.7 | 20.4 | 21.4 | 27.1 | 4.2 | 18.6 | -44.1 | 28.5 | -31.8 | 22.5 | -17.7 | 22.1 |
| Mean | | -11.0 | 10.7 | 6.1 | 36.6 | -20.3 | 11.3 | 7.2 | 15.4 | -10.0 | 13.7 | -62.7 | 13.5 | -52.5 | 13.3 | -43.0 | 14.2 |
| Std Dev | | 7.2 | 6.2 | 7.5 | 10.0 | 16.2 | 5.5 | 5.9 | 6.2 | 8.5 | 16.2 | 19.4 | 10.2 | 18.6 | 10.0 | 19.6 | 8.1 |

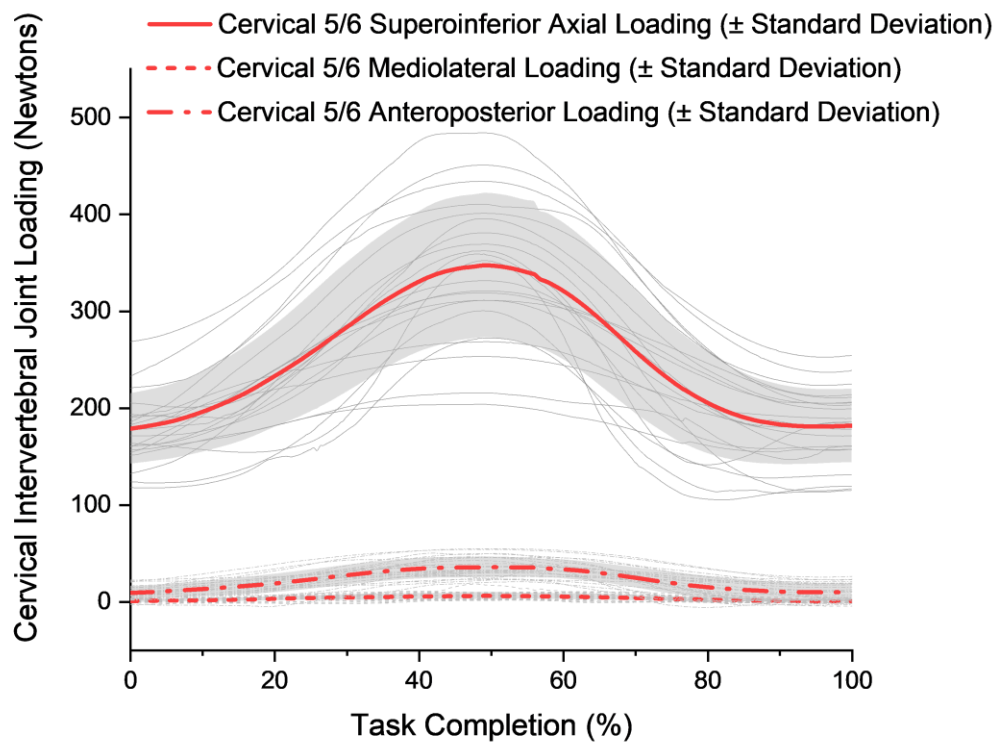
Table 3.13 Minimum (Min) and maximum (Max) cervical anteroposterior loading (Newtons) for all subjects for all ADL trials (+ in anterior direction)

Figure 3.9 Normalised cervical joint loading for all trials for all tasks

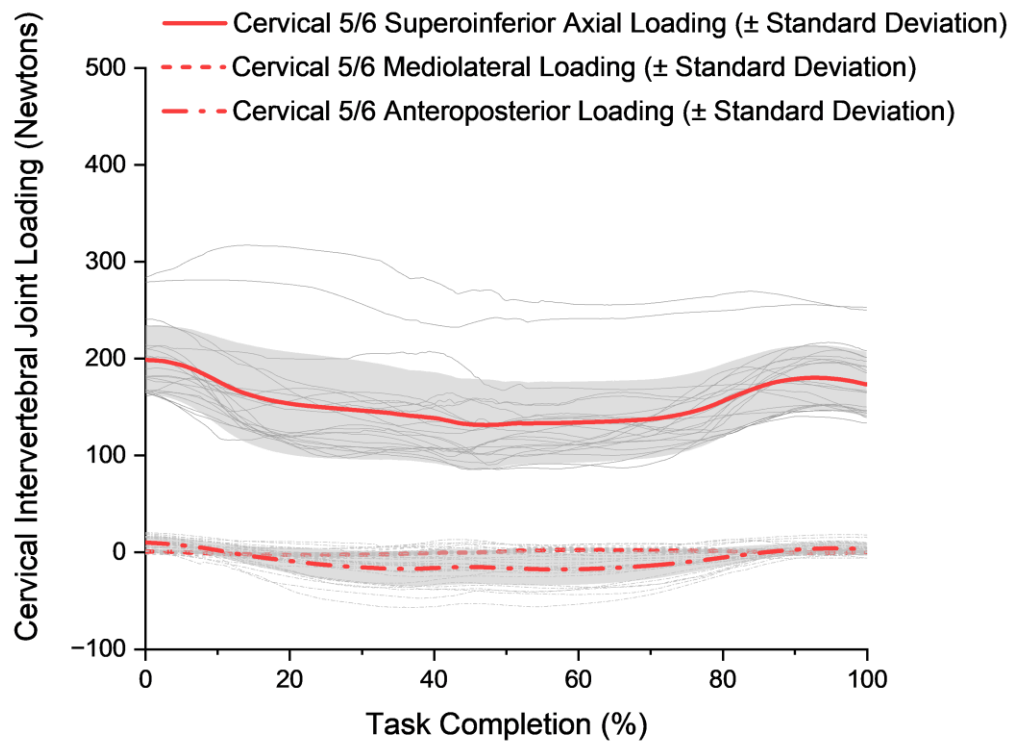
a) Looking at Mobile (MOB)



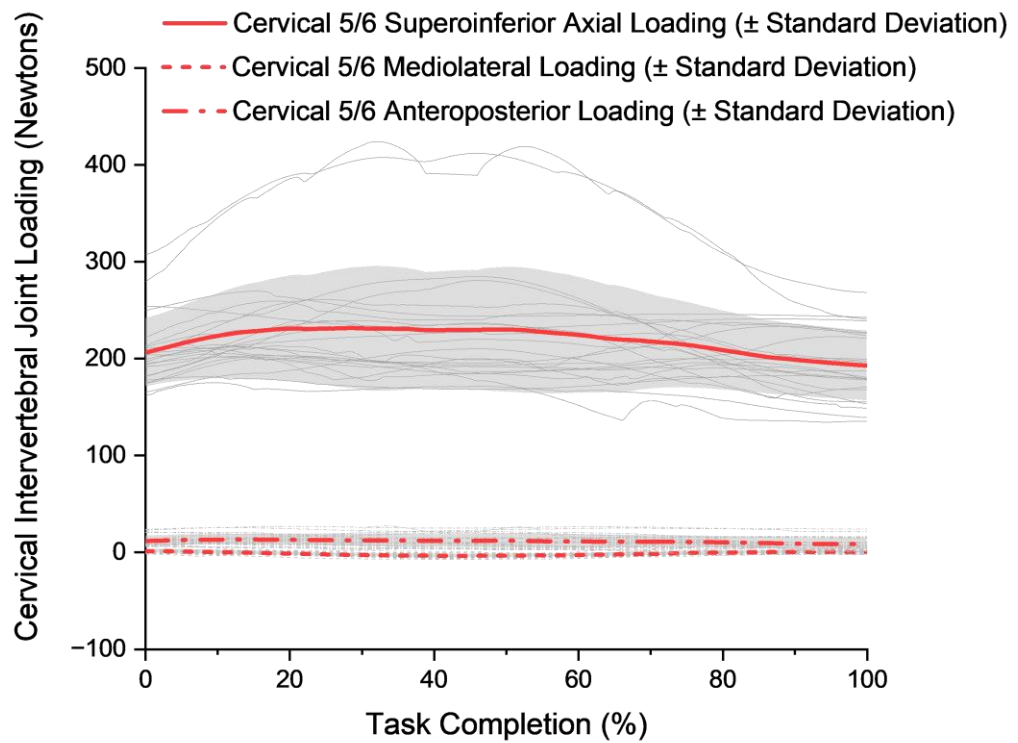
b) Drinking from a Bottle (WAT)



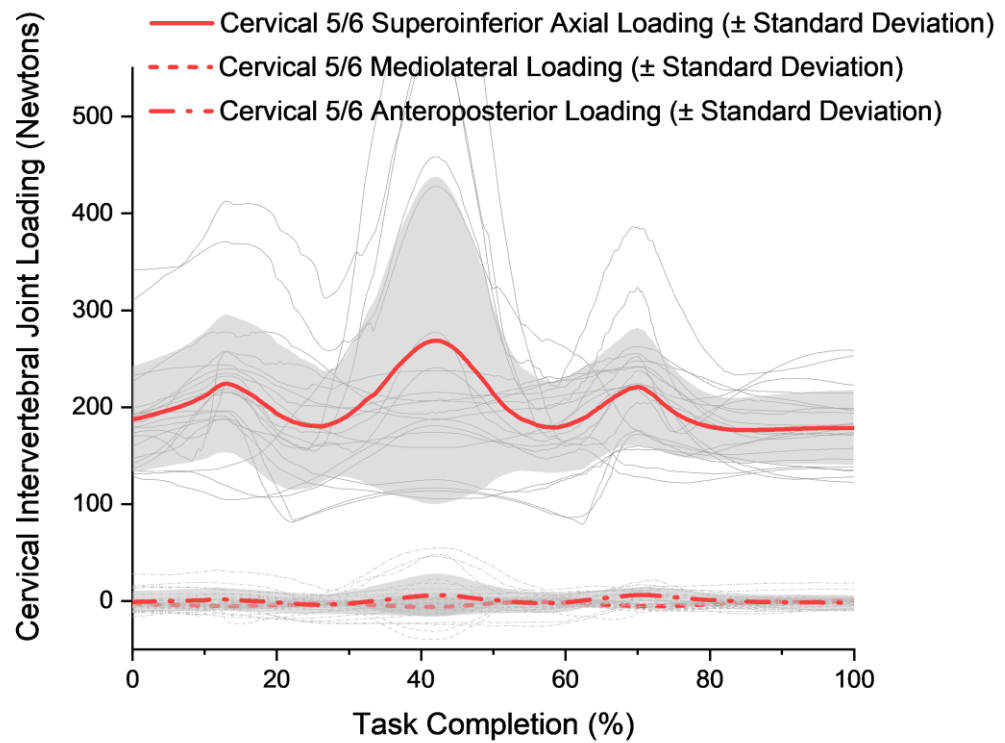
c) Looking for Traffic (TRA)



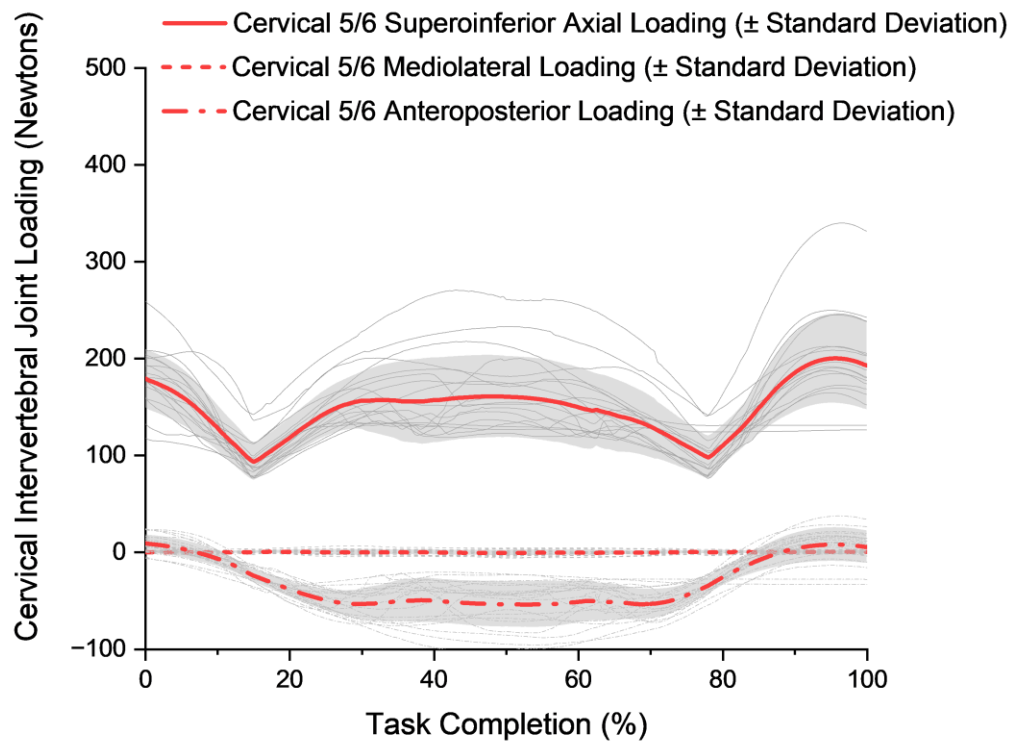
d) Looking Up Laterally (LUL)



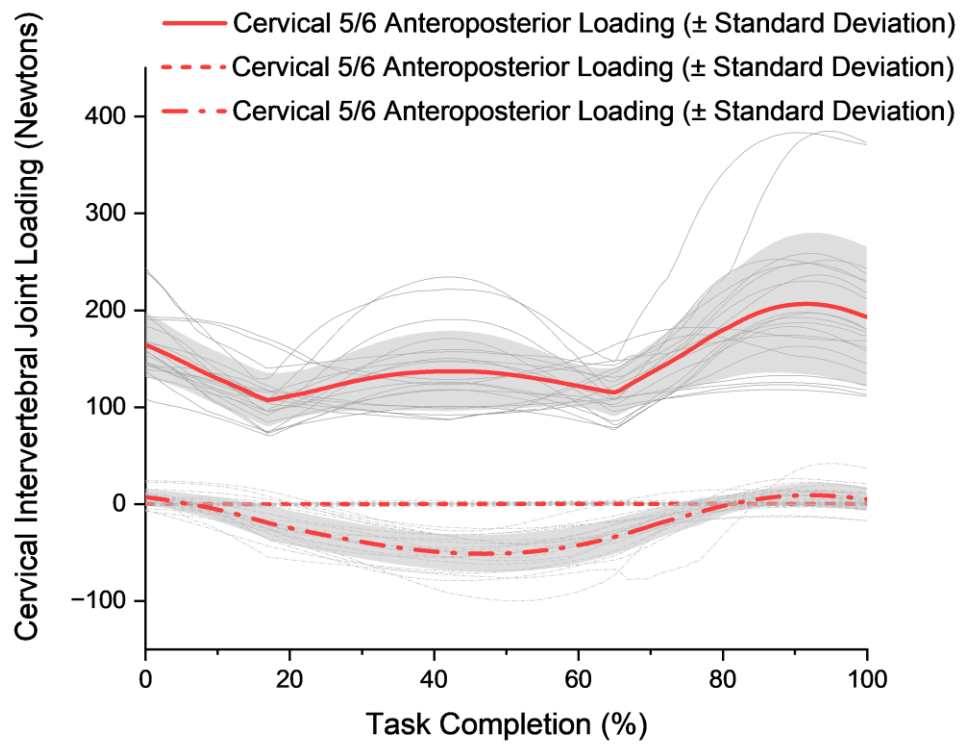
e) Reversing a Car (REV)



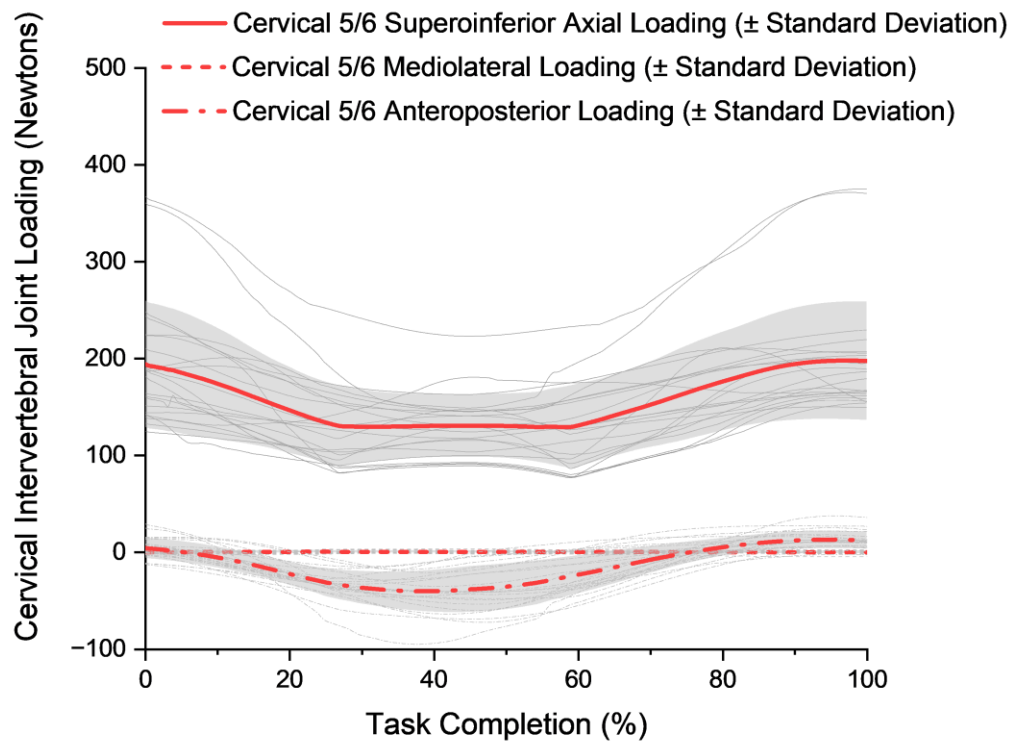
f) Bending Down (BND)



g) Stand-to-sit (StS)



h) Sit-to-stand (SiS)



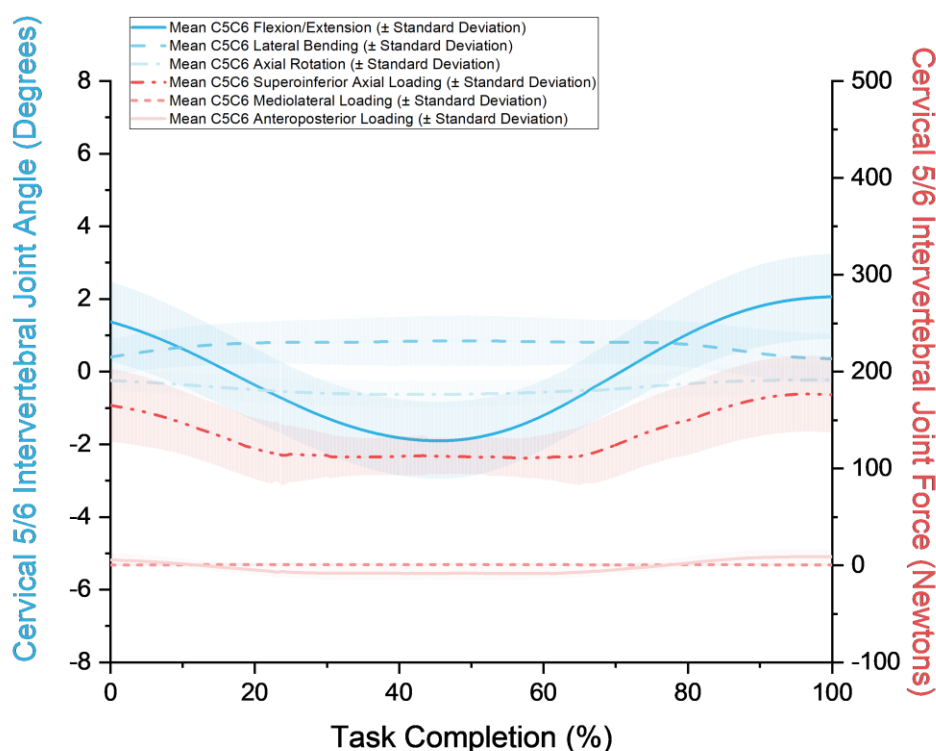
3.2.6 Combined Profile for Cervical Kinematics and Loading

The following set of graphs are a combination of average cervical joint angles (flexion/extension, lateral bending, and axial rotation) and average cervical joint loadings (superoinferior axial, mediolateral, and anteroposterior loadings) at C5-C6 intervertebral level across the cohort for individual ADL tasks studied. The shaded region represents one standard deviation on either side of the mean curve.

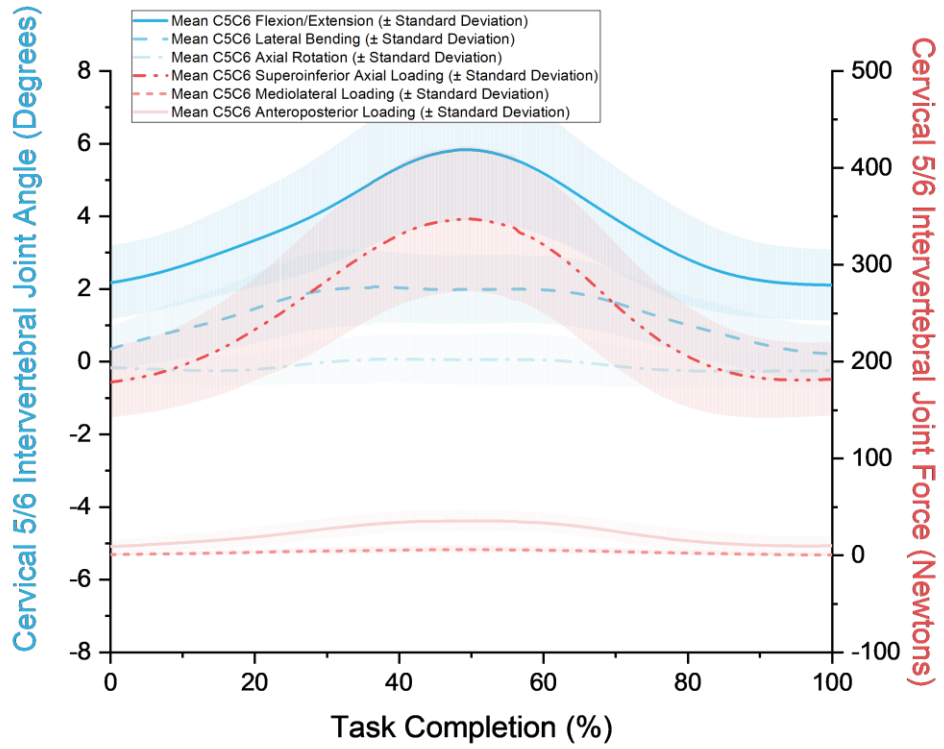
As explained in the Method, Section 3.1.6, the average value across the cohort is used as a representative curve for that particular ADL task studied. The scales for both left and right y-axes are standardised so comparison can be made between all ADL tasks investigated. These combined profiles are also the foundation for formulating new wear testing profiles for articulating cervical disc implant that reflects a more physiologically relevant loadings and motion during ADL.

Figure 3.10 Combined overall normalised cervical joint kinematics and loading

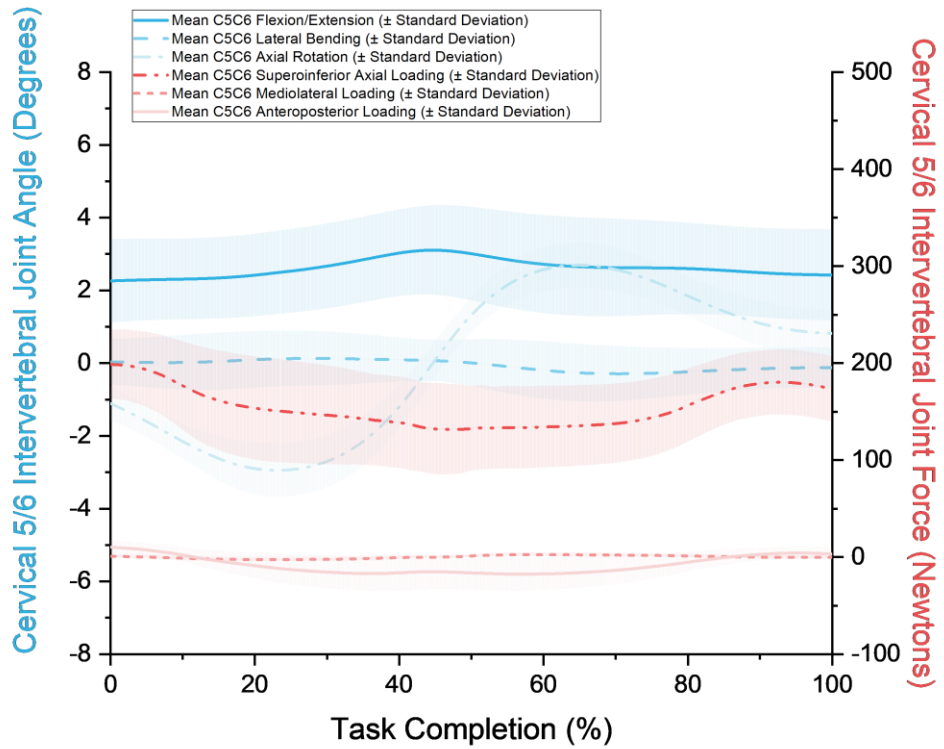
a) Looking at Mobile (MOB)



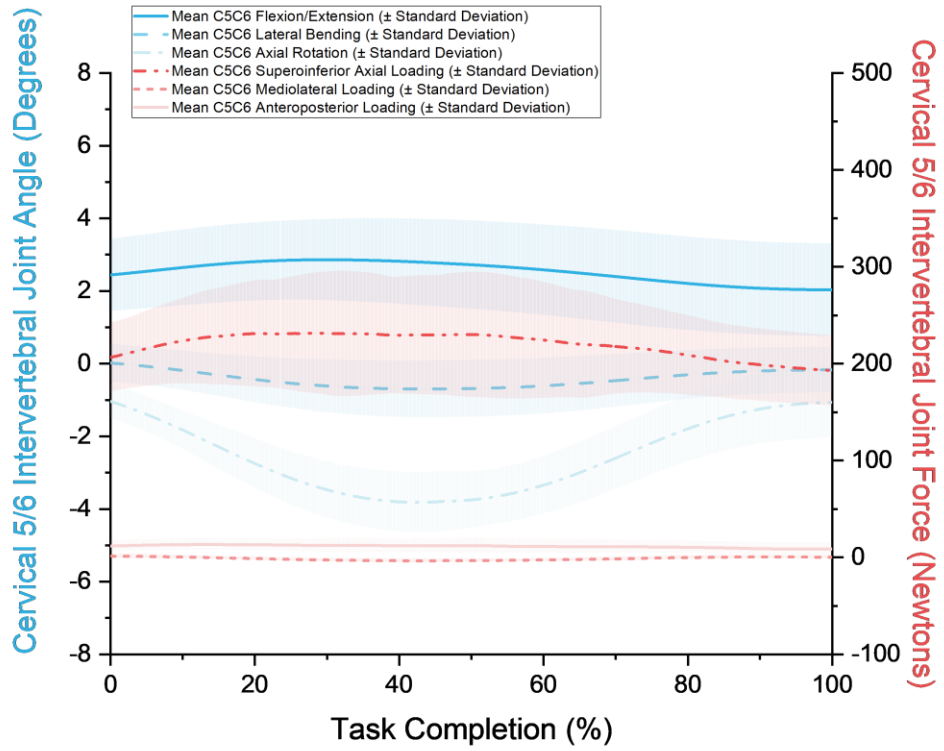
b) Drinking from a Bottle (WAT)



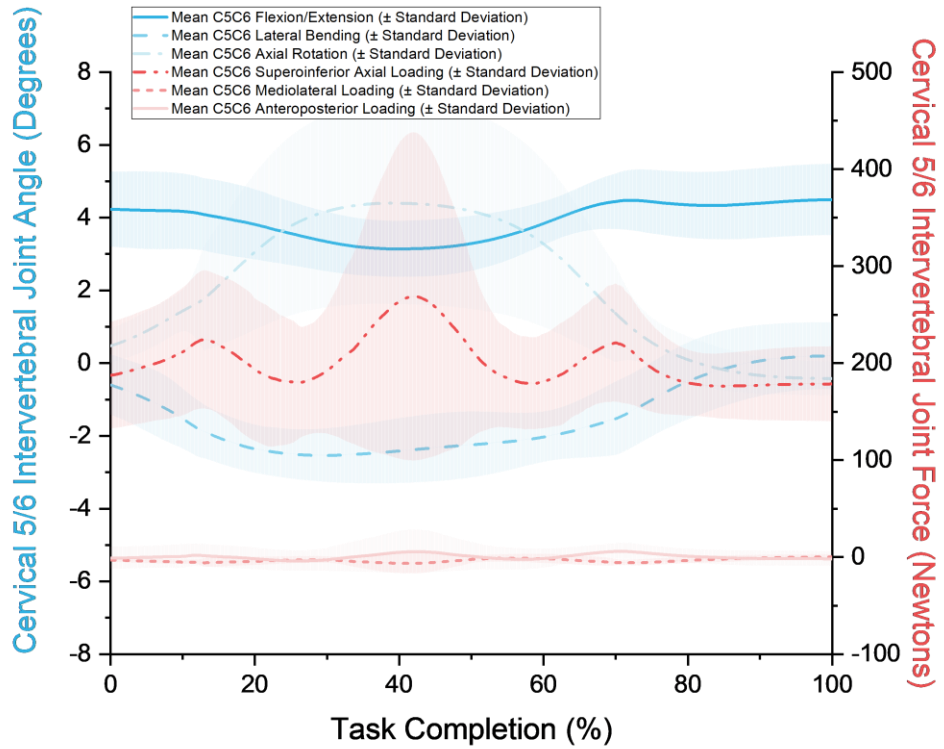
c) Looking for Traffic (TRA)



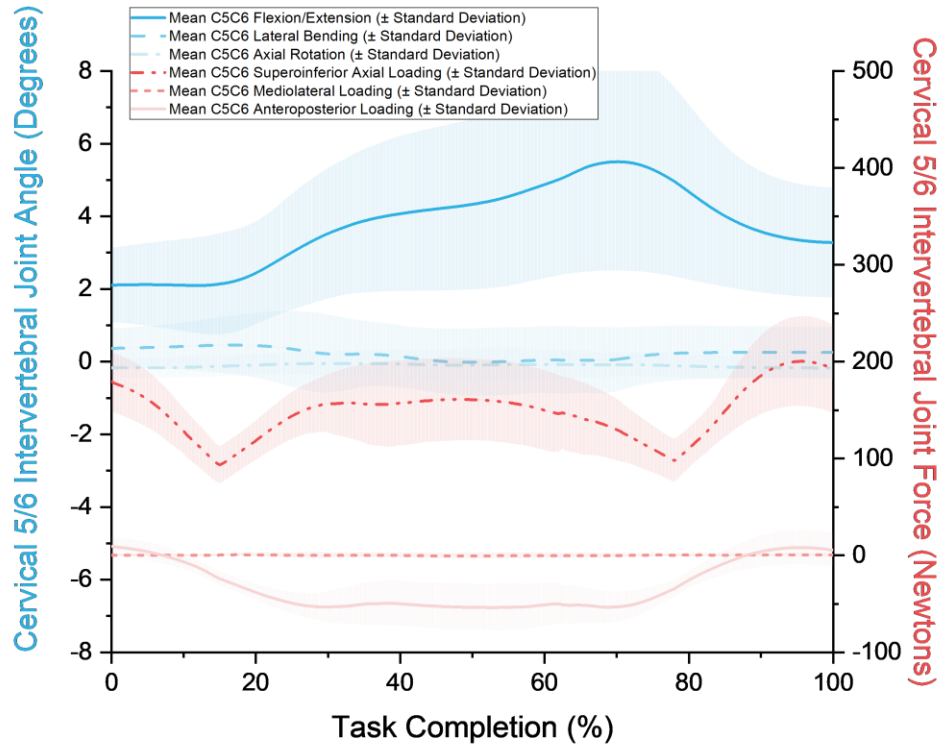
d) Looking Up Laterally (LUL)



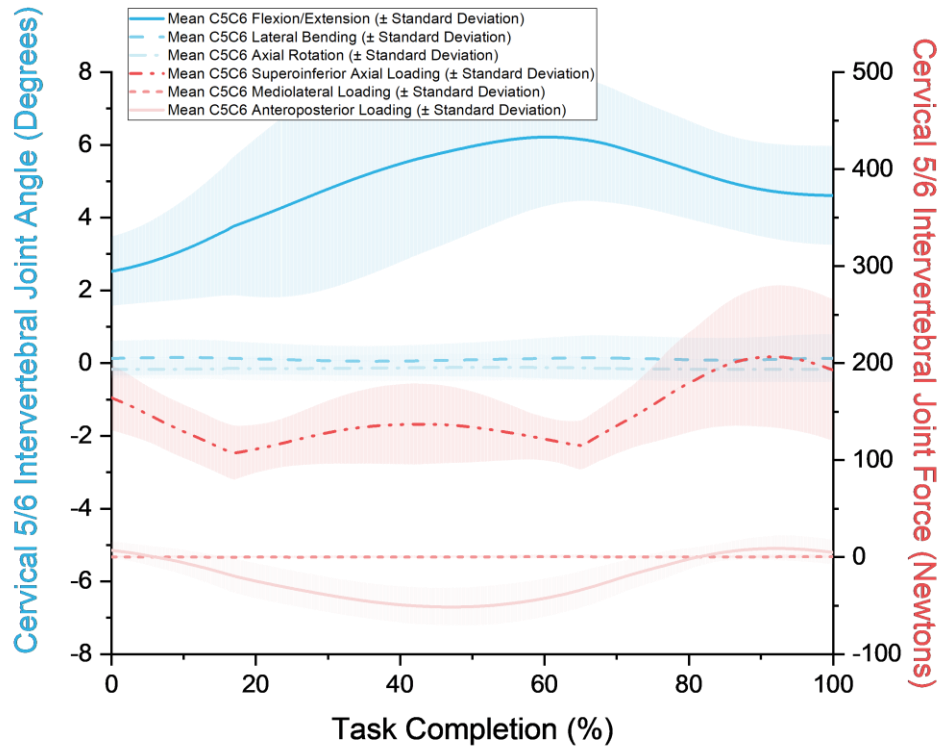
e) Reversing a Car (REV)



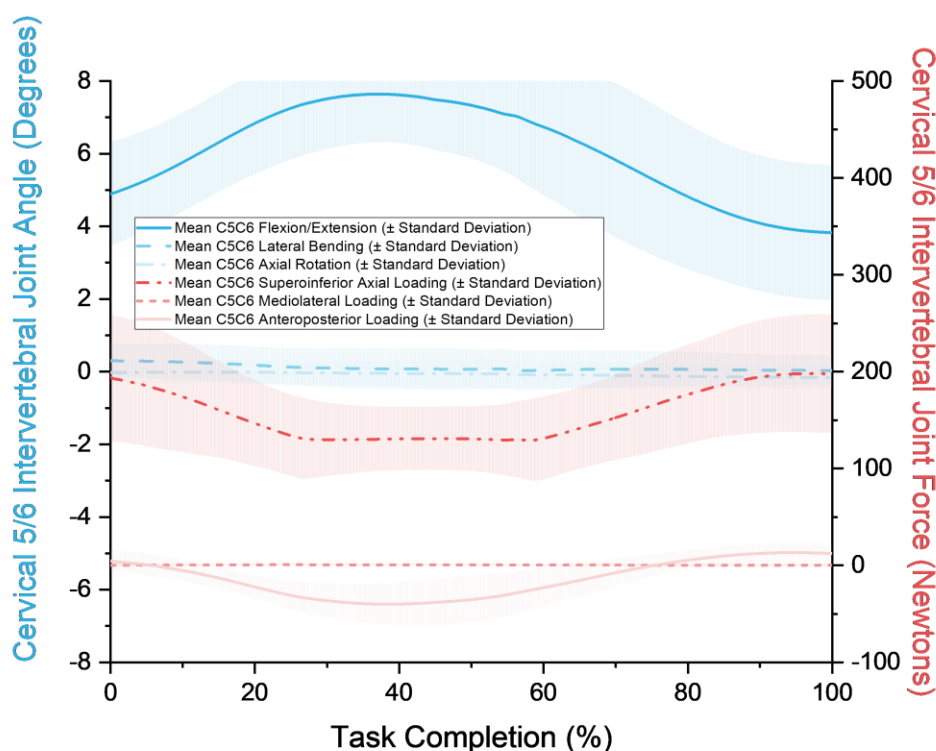
f) Bending Down (BND)



g) Stand-to-sit (StS)



h) Sit-to-stand (SiS)



3.2.7 Newly Formulated Wear Test Profiles for Cervical Disc Implant

The average joint kinematics and loading curves shown in Figure 3.10 ((a) to (h)) for all ADL activities investigated in this study can be fashioned into wear testing profiles for wear simulation of articulating cervical disc implant. Figure 3.11 and Figure 3.12 are two examples of formulated wear testing profiles derived from kinematics and loadings during 'looking for traffic before crossing' (TRA) and 'bending down' (BND) ADL tasks after their axes have been harmonised according to ISO18192-1 [1] definition with the speed and direction at the end of a cycle matched with the start of the cycle. Figure 3.11 is an example of wear testing profile that has a transverse plane-dominant or representative of 'looking' activity whilst Figure 3.12 is sagittal plane-dominant or representative of 'tasking' activity. Some of these ADL tasks are better simulated in combination than independently. An example of this would be stand-sit-stand shown in Figure 3.13, which is a combination of 'stand-to-sit' (StS) and 'sit-to-stand' (SiS) ADL tasks, as these activities routinely would be happening in pair in daily lives.

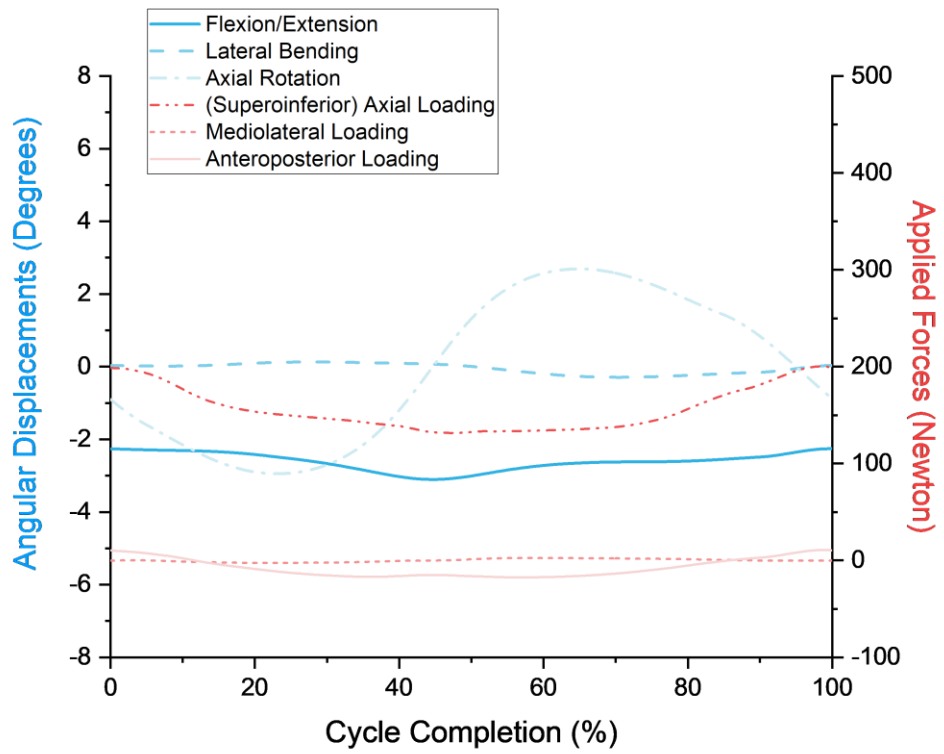


Figure 3.11 ADL Looking before Crossing (TRA) Wear Test Profile

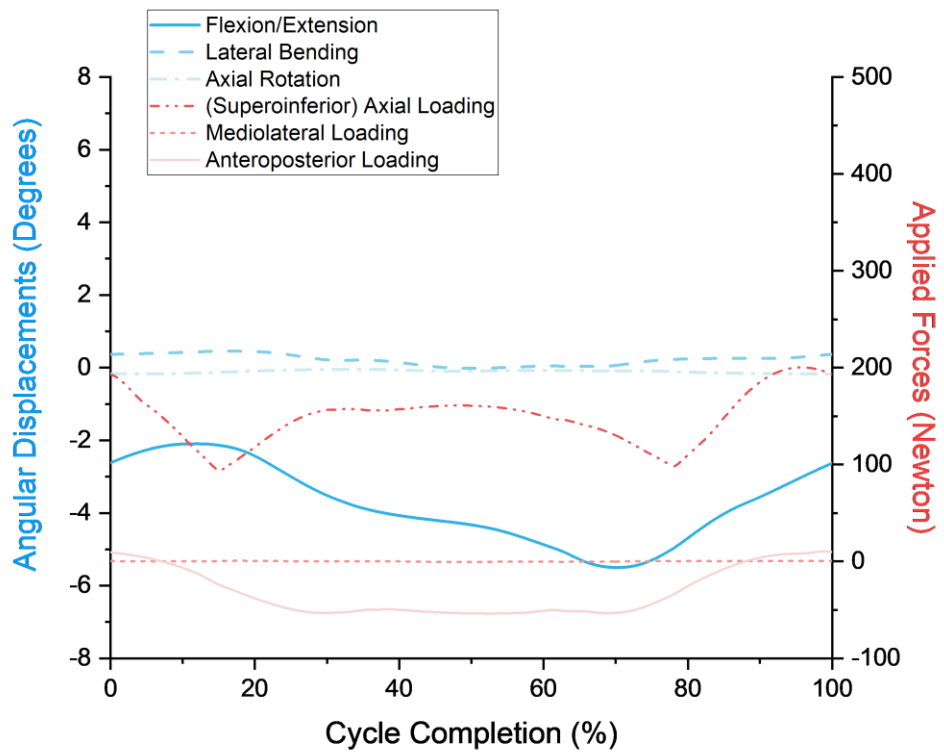


Figure 3.12 ADL Bending Down (BND) Wear Test Profile

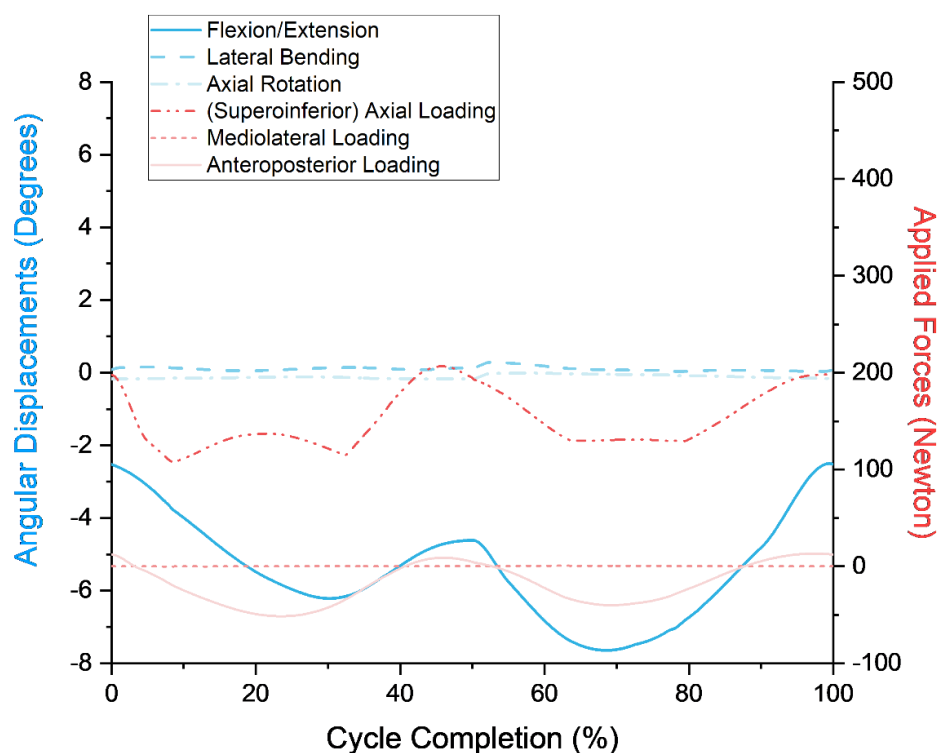


Figure 3.13 ADL Stand-sit-stand (StS+SiS) Wear Test Profile

Whereas, Figure 3.14 is a profile that represents every day flexion and extension of the head, generated by combining both ‘looking at mobile’ (MOB) and ‘drinking from a bottle’ (WAT) ADL tasks. This profile was formulated as an analogue to standard wear test profile prescribed in ISO18192-1 [1], where flexion/extension was prominently featured to have the biggest angular sliding excursion in a cycle (30°) compared to other direction of motion (24° in lateral bending and 16° in axial rotation).

Lastly, Figure 3.15 shows a testing profile formulated from an amalgamation of the largest cervical kinematics range (in all rotational directions) and the highest joint loading (from all linear directions) calculated from all ADL tasks analysed. This wear test profile is created to represent the more adverse conditions experienced in daily activities. The cervical kinematics range was taken from ‘stand-to-sit’ wear test profile for flexion/extension, ‘reversing a car’ (REV) for lateral bending, and ‘looking for traffic’ (TRA) for axial rotation. The cervical intervertebral joint loading parameters were taken from ‘drinking from a bottle’ (WAT) for superoinferior axial loading, ‘reversing a car’ (REV) for mediolateral loading, and ‘bending down’ (BND) for anteroposterior loading.

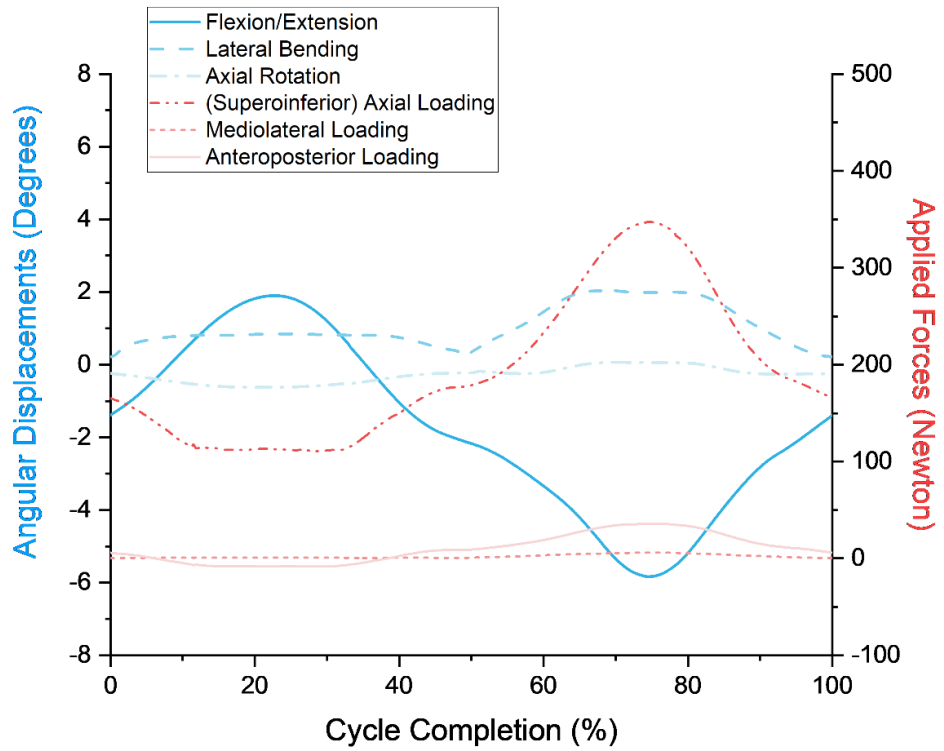


Figure 3.14 ADL Flexion/Extension (MOB+WAT) Wear Test Profile

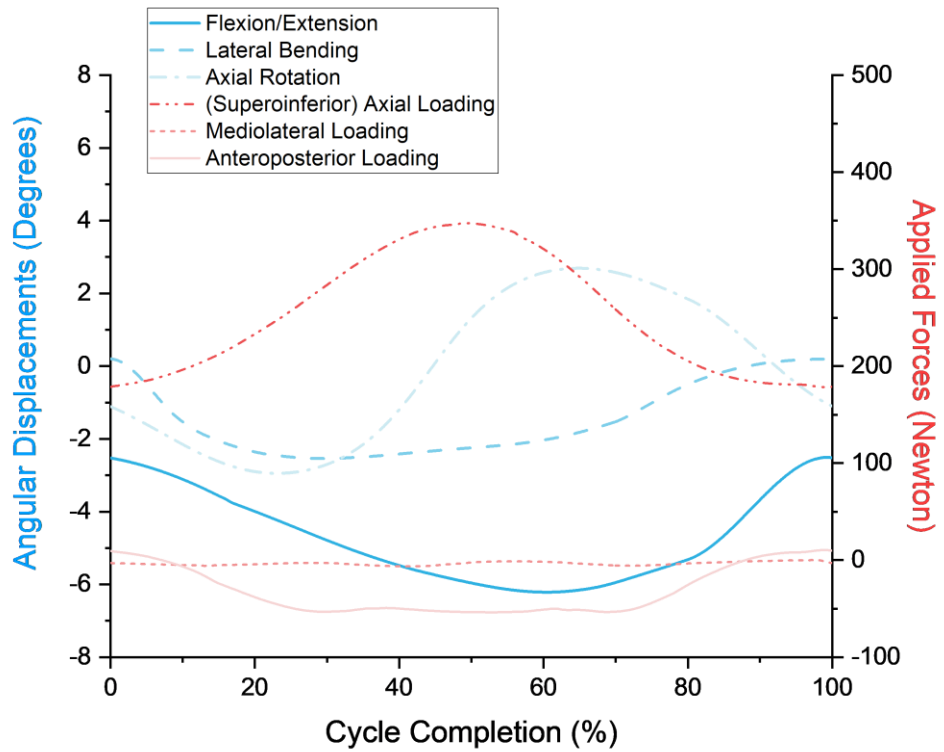


Figure 3.15 ADL Adverse Condition Wear Test Profile

3.3 Discussion

3.3.1 Selection of Activities of Daily Living Involving the Cervical Spine

The focus group discussion has established several activities of daily living involving the cervical spine or neck that are incorporated into this study. These daily activities also have been mentioned in a number of related academic articles within the physical therapy literature, which looked into similar group of patients with degenerative problem of the cervical spine (Table 2.6).

With the wide availability and usage of smartphones in this day and age, the reading activity reported in the literature has been adapted to be 'looking at mobile phone' as the head movement is very similar albeit with different objects. This activity also has been raised during focus group discussion in which the task found to be challenging to perform. They also reported this task is more frequently done daily, than reading a book on a lap, where some of them adopted a position where the phone screen is held higher to the level of their eyes as it is less painful than moving their heads. This finding is also aligned with a study by Namwongsa *et al.* [225].

Another activity that had been brought up during focus group discussion is 'looking up laterally' which is absent in academic literature. An example of this motion is when a sitting person needing to speak to another person who is standing at the side of the first person because their front is occupied by display screen equipment or a workstation. This task was incorporated as part of the ADLs involving the cervical spine as it is thought to occur frequently in many office environments. This activity involves a compound motion between neck extension and axial rotation.

3.3.2 Participants' Demographic for Cervical Biomechanics Study

The mean age of participants in this study, 27.2 ± 4.06 years, is much lower than typical mean age for patients being implanted with a disc implant. The average

age of patients undergoing cervical disc replacement reported in academic literature is between 40.0 ± 5.8 to 54.9 ± 12.6 years old [41-45, 226-228]. Nonetheless, there has been a report of implantation being carried out in patients within the 25-29 years old age bracket [8].

3.3.3 Skin Marker and Soft Tissue Artefact in Study of Cervical Spine

In this study, the conventional marker set developed by Vicon was used during the motion capture process as it is also compatible with AMMR. For the upper body, the marker set utilises four cluster markers to track the head movement, four individual markers placed around the thorax (sternal notch, xiphisternum, spinous processes of C7 and T10), and another seven markers for each arm. Of all 22 markers tracked for the upper body, only one is located on the cervical vertebra *i.e.* 7th cervical vertebra. It was decided that this is the best method in tracking the cervical spine for the current study given the substantial uncertainty of soft tissue artefact in the current state-of-the-art and the unreliability of additional markers particularly in axial rotation direction, as elaborated in Section 2.5. Like any motion capture strategies, the ever-present of soft-tissue artefacts remain the most critical contributor of error [172].

Despite having only a single marker within the cervical spine, the motion of the individual cervical vertebrae was resolved through 'kinematics rhythm', a method described in Section 3.1.6. Equally apportioning the angle between the head and thorax amongst all the cervical intervertebral joint levels might not necessarily be an accurate way of determining the cervical intervertebral joint angles but an alternative algorithm has not been made available for this problem to date. Nevertheless, the computed joint angles are still within the acceptable range as discussed in the following Section 3.3.5.1.

3.3.4 Unsuccessful Multibody Modelling Simulations

As reported in the Results Section 3.2.3, there were eight failed simulations, five during kinematics analyses and three in inverse dynamic studies. Failure from kinematic analysis is due to motions/trajectories of a certain body segment (from

MoCap) have gone beyond the joint's numerical constraints set for the mannequin model employed during the simulation. Whereas, failure during inverse dynamic analysis is due to muscle overload where the estimated joint loading exceeded the maximum amount of force that can be generated from overall muscle bundle modelled for that particular joint. In other words, the mannequin model is unable to complete the simulation without defying the numerical limits put on the joints' RoM or the force generating capabilities from the muscles responsible. Like all simulation models, the AMMR functions with a set of numerical constraints, based on an average human measurements and capabilities, translated into mathematical functions. Despite having scaled and morphed into subject-specific anthropometric dimension, the mannequin might not be able to emulate individual uniqueness of every person e.g. underdeveloped bones or hyper elastic soft tissues due to specific genetic or environmental factors. These irregularities could have assisted the person to bend or twist their bodies more than the model could have achieved through simulation. A good example of this would be the 'touch your toes' test where varying degrees of capabilities can be seen from a cohort of random people, which coincidentally a similar movement is performed during 'bending down' (BND) task. Although many of them are simple everyday activities, some of the ADL tasks investigated are also pushing the body to its limit e.g. twisting the head and torso during 'reversing a car' that even a highly-developed mathematical model might not be able to successfully simulate all the time.

3.3.5 Kinematics Analysis

Kinematics analysis was successfully simulated in 181 trials where the cervical joint angle was calculated throughout the ADL tasks captured. However, only 178 simulations output were produced and analysed in this study.

3.3.5.1 Kinematics Validation

In general, the average angle between the head and torso segments measured during current kinematics analysis in this study is larger compared to some of the data presented by Cobian *et al.* [163] for five of the comparable ADL tasks analysed.

This comparison is illustrated in Table 3.14. Both this study and Cobian *et al.* [163] have very similar mean height and weight amongst the subject cohorts. On average, the twelve people involved in this study are five years older than the ten subjects reported by Cobian *et al.* [163]. The difference in the angle between the head and torso between both studies, however, can be attributed to how the activities were simulated by the participants as head motion in ADL tasks can be quite versatile owing to the flexibility it can afford to unlike motion in gait which can be prescriptive and predictive.

| ADL Tasks (This study / Cobian <i>et al.</i> [163]) | Average angle between the head and thorax (°) | | | | | |
|---|---|----------------------------|-----------------|----------------------------|----------------|----------------------------|
| | Flexion/extension | | Lateral Bending | | Axial Rotation | |
| | This study | Cobian <i>et al.</i> [163] | This study | Cobian <i>et al.</i> [163] | This study | Cobian <i>et al.</i> [163] |
| WAT / Taking a drink | 36.4 | 20.4 | 13.4 | 3.3 | 8.1 | 7.7 |
| TRA / Looking for traffic | 13.8 | 10.5 | 7.5 | 8.6 | 80.9 | 47.1 |
| REV / Backing up car | 24.0 | 4.5 | 19.5 | 3.3 | 84.5 | 14.2 |
| BND / Pick up from floor | 45.0 | 31.8 | 9.0 | 6.5 | 5.1 | 12.3 |
| SiS / Sit to stand | 38.9 | 26.1 | 4.4 | 4.3 | 3.8 | 7.4 |

Table 3.14 Comparison of average angle (°) between the head and thorax during five ADL tasks in the current study against Cobian *et al.* [163]

At an individual cervical level, the median cervical joint angle range from all ADL tasks observed in this study is deviated from published data. Another study done by Cobian *et al.* [16] reported median C5-C6 joint angle range of 2.6°, 2.3°, and 2.2° in flexion/extension, lateral bending, and axial rotation respectively. The median values published by Cobian *et al.* [16] are only a proportional estimation of individual cervical level from overall flexion/extension motion of the head (*i.e.* cervical intervertebral joint C5-C6 contributes 18%, 17%, and 10% from total motion of the head in flexion/extension, lateral bending, and axial rotation directions, respectively). Conversely, the current study measures the angle between cervical vertebrae C5 and C6 directly, albeit using ‘kinematic rhythm’. The distinction between methods employed also accounts for the difference in median cervical joint angle ranges observed. The comparison of individual cervical intervertebral joint angle range is summarised in Table 3.15.

| Study | Statistical description | Cervical Intervertebral Joint C5-C6 Angle Range (°) | | |
|---------------------------|-------------------------|---|-----------------|----------------|
| | | Flexion/extension | Lateral Bending | Axial Rotation |
| Cobian <i>et al.</i> [16] | Median | 2.6 | 2.3 | 2.2 |
| This study | Median | 3.4 | 1.0 | 0.6 |
| This study | Mean | 3.3 | 1.4 | 2.1 |

Table 3.15 Comparison of individual cervical joint C5-C6 angle range between this study and Cobian *et al.* [16].

It has been observed that cervical joint angle range during ADL is a fraction of full cervical RoM and the joint angle range for ADL is also smaller than joint angle range prescribed in ISO18192-1 [1] [163]. This notion is evidenced when comparing some of ADL tasks in the current study with the full cervical RoM, observed and catalogued by Anderst *et al.* [161], which ranges between 42% to 86% (excluding cervicothoracic junction) for pure flexion/extension and pure axial rotation movements of the head in the primary plane of motion. The comparison is summarised in Table 3.16 for flexion/extension motion and Table 3.17 for axial rotation motion.

The comparison in pure flexion/extension movement in Table 3.16 was made from combining kinematics from 'looking at mobile' (MOB) and 'drinking from a bottle' (WAT) trials in the current study where the movement is predominantly flexion/extension of the head. 'Looking for traffic before crossing' (TRA) trials from the current study, where motion of the head is mainly axial rotation, were used for the comparisons made in Table 3.17.

Upon comparing the pure flexion/extension motion (Table 3.16), it is evidenced that the vertebral RoM during ADL in transverse plane is exceedingly higher than RoM seen in Anderst *et al.* [161]. This is because, in the MOB and WAT tasks, which were selected for the comparison, all subjects were holding a water bottle as well as their mobile phones with their right hand during the trials. These subjects had rotated their head slightly towards the objects when conducting their daily activities to economise their movement, which likely accounts for the increase of head rotation when compared to purely flexion/extension motion as carried out in Anderst *et al.* [161].

| Cervical joint levels | Sagittal Plane (primary motion) | | | Coronal Plane | | | Transverse Plane | | |
|-----------------------|---------------------------------|-----------------------------|-----------|------------------|-----------------------------|-----------|------------------|-----------------------------|------------|
| | This study (ADL) | Anderst <i>et al.</i> [161] | | This study (ADL) | Anderst <i>et al.</i> [161] | | This study (ADL) | Anderst <i>et al.</i> [161] | |
| | RoM (°) | Full RoM (°) | % | RoM (°) | RoM (°) | % | RoM (°) | RoM (°) | % |
| C1–C2 | 9.6 ± 4.1 | 15.6 ± 5.8 | 62 | NA | 2.3 ± 1.3 | - | NA | 8.6 ± 3.8 | - |
| C2–C3 | 8.2 ± 2.2 | 12.7 ± 2.6 | 65 | 1.2 ± 0.6 | 3.2 ± 1.4 | 38 | 3.0 ± 0.9 | 1.9 ± 0.7 | 160 |
| C3–C4 | 8.2 ± 2.2 | 17.1 ± 3.3 | 48 | 1.2 ± 0.6 | 2.3 ± 0.7 | 52 | 3.0 ± 0.9 | 1.9 ± 0.7 | 160 |
| C4–C5 | 8.2 ± 2.2 | 19.5 ± 3.4 | 42 | 1.2 ± 0.6 | 2.0 ± 0.7 | 60 | 3.0 ± 0.9 | 1.8 ± 0.6 | 167 |
| C5–C6 | 8.2 ± 2.2 | 19.7 ± 3.7 | 42 | 1.2 ± 0.6 | 2.1 ± 0.6 | 57 | 3.0 ± 0.9 | 1.7 ± 0.7 | 176 |
| C6–C7 | 8.2 ± 2.2 | 15.8 ± 4.8 | 52 | 1.2 ± 0.6 | 2.4 ± 1.0 | 50 | 3.0 ± 0.9 | 1.6 ± 0.7 | 186 |
| C7–T1 | 8.2 ± 2.2 | 8.3 ± 3.5 | 99 | 1.2 ± 0.6 | 2.0 ± 0.8 | 60 | 3.0 ± 0.9 | 1.4 ± 1.1 | 214 |

Table 3.16 Comparison between ADL tasks RoM and full RoM of individual cervical vertebral joint level in pure flexion/extension movement of the head.

| Cervical joint levels | Sagittal Plane | | | Coronal Plane | | | Transverse Plane (primary motion) | | |
|-----------------------|------------------|-----------------------------|-----------|------------------|-----------------------------|-----------|-----------------------------------|-----------------------------|------------|
| | This study (ADL) | Anderst <i>et al.</i> [161] | | This study (ADL) | Anderst <i>et al.</i> [161] | | This study (ADL) | Anderst <i>et al.</i> [161] | |
| | RoM (°) | RoM (°) | % | RoM (°) | RoM (°) | % | RoM (°) | Full RoM (°) | % |
| C3–C4 | 1.6 ± 0.8 | 5.1 ± 1.6 | 31 | 1.2 ± 0.7 | 13.4 ± 2.1 | 9 | 5.6 ± 1.1 | 11.8 ± 2.1 | 47 |
| C4–C5 | 1.6 ± 0.8 | 4.7 ± 2.0 | 34 | 1.2 ± 0.7 | 12.8 ± 2.8 | 9 | 5.6 ± 1.1 | 11.3 ± 1.7 | 50 |
| C5–C6 | 1.6 ± 0.8 | 4.5 ± 2.0 | 36 | 1.2 ± 0.7 | 11.7 ± 3.0 | 10 | 5.6 ± 1.1 | 9.3 ± 1.9 | 60 |
| C6–C7 | 1.6 ± 0.8 | 3.4 ± 1.2 | 47 | 1.2 ± 0.7 | 12.6 ± 3.1 | 10 | 5.6 ± 1.1 | 6.5 ± 1.7 | 86 |
| C7–T1 | 1.6 ± 0.8 | 3.5 ± 1.4 | 46 | 1.2 ± 0.7 | 4.8 ± 2.0 | 25 | 5.6 ± 1.1 | 3.8 ± 1.2 | 147 |

Table 3.17 Comparison between ADL tasks RoM and full RoM of individual cervical vertebral joint level in pure axial rotation movement of the head.

Despite being equally apportioned, all individual cervical vertebral joint excursions calculated in this study are found to be within the average band range of kinematics expected for the motion. The majority of the joint excursions from all subjects are within the prediction bands for normal cervical kinematics proposed by Anderst *et al.* [185]. Figure 3.16 and Figure 3.17 show the cervical joint excursions from all of the ‘looking at mobile’ (MOB) and ‘drinking from a bottle’ (WAT) trials when superimposed over the normal prediction band for flexion/extension motion. Similarly, Figure 3.18 shows all the joint excursions from ‘looking for traffic before crossing’ (TRA) trials against normal prediction band. Due to the differences on how the ADL trials were conducted, kinematic data from the current study was rearranged, in phases, according to the direction of motion of the head to match with data presented in Anderst *et al.* [185] for comparison purposes. The rearrangement the kinematics curves was also normalised to index vertebrae’s neutral position.

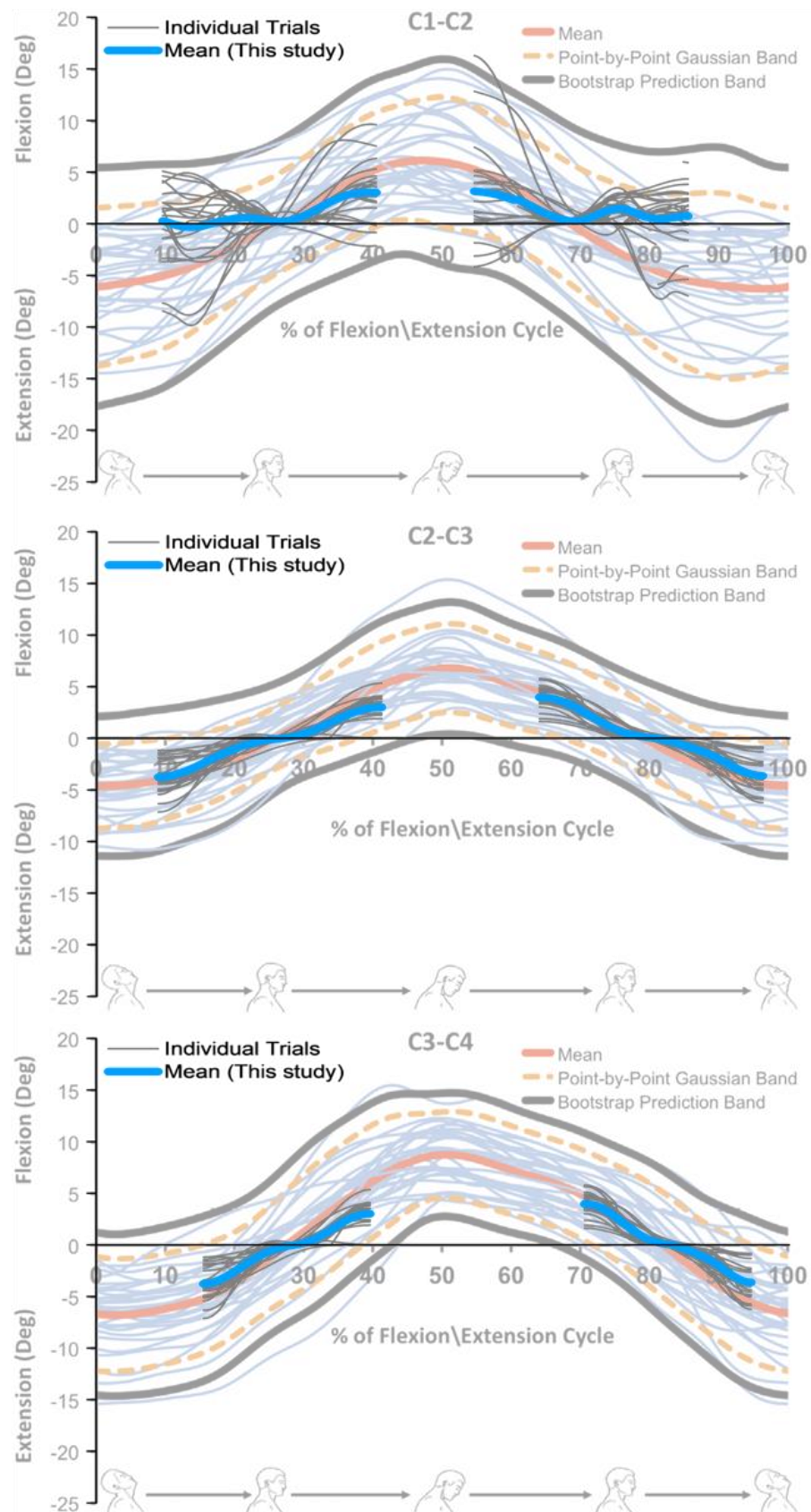


Figure 3.16 Mean cervical intervertebral joint excursion during flexion/extension compared against normal cervical kinematics prediction bands between C1 to C4 [185].

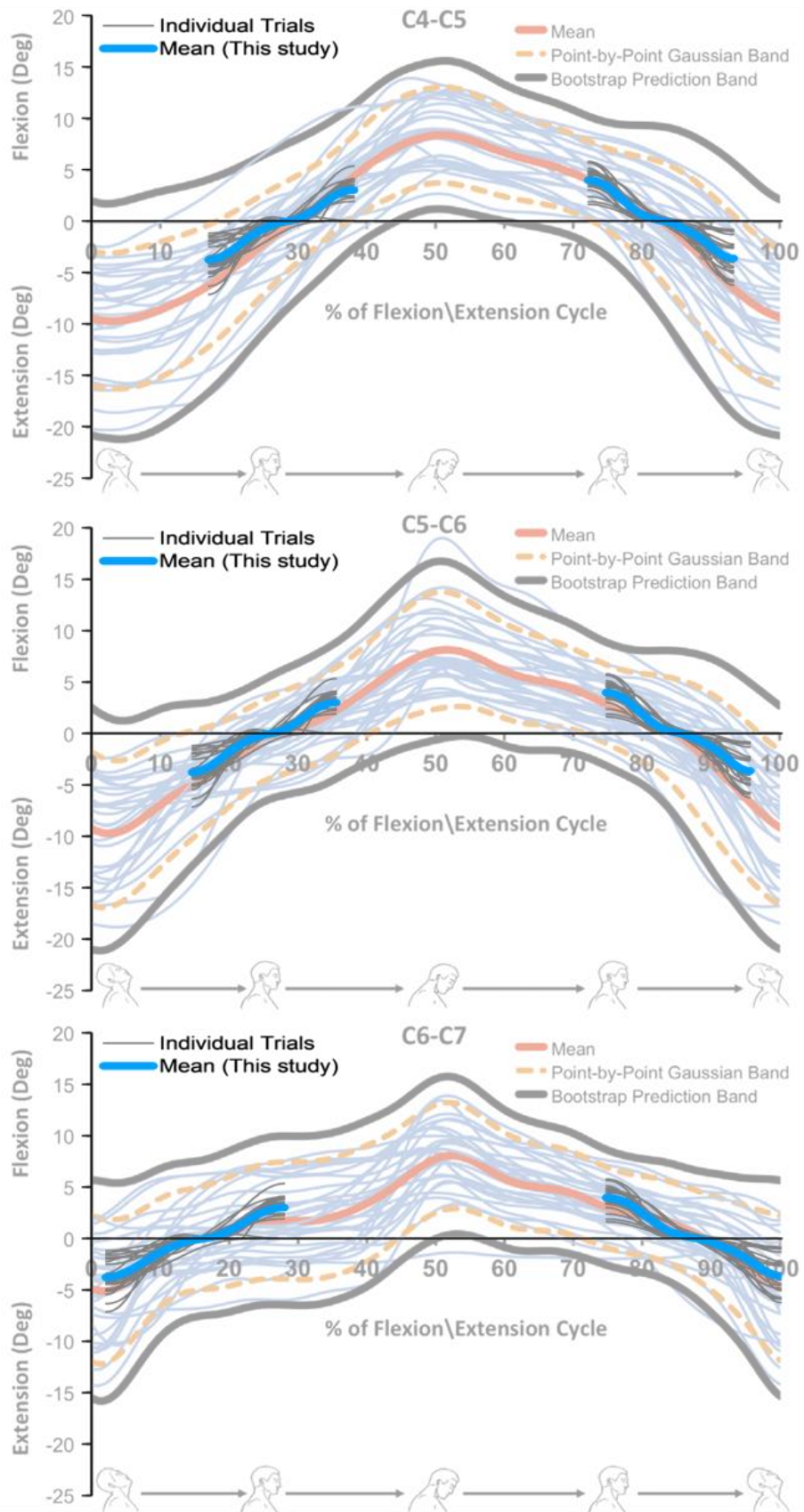


Figure 3.17 Mean cervical intervertebral joint excursion during flexion/extension compared against normal cervical kinematics prediction bands between C4 to C7 [185].

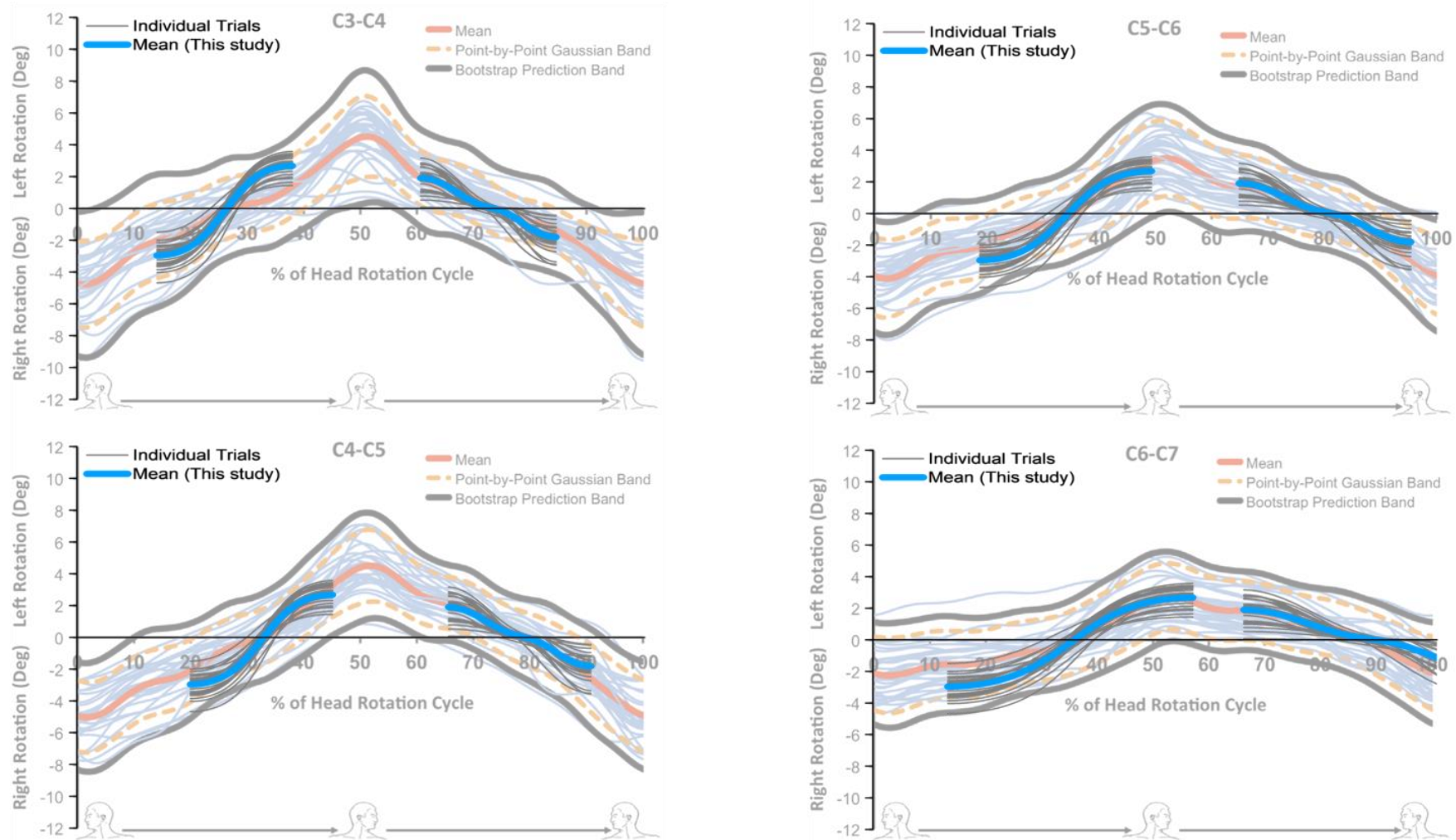


Figure 3.18 Mean cervical intervertebral joint excursion during axial rotation compared against normal cervical kinematics prediction bands between C3 to C7 [185]

3.3.5.2 Kinematics Variations

As stated in the Section 3.2.4, inter-subject kinematics variations in cervical intervertebral joint C5-C6 are wide in six out of eight ADL tasks investigated even for the main direction of head motion. A study by Beaudette *et al.* [220] has found several motor strategies in recruiting different spinal regions during flexion/extension motion even in a homogenous group of subjects. The study found no discernible pattern that can relate the employed strategies back to participants' demographics. This outcome mirrored the observation made in an earlier study by Gatton *et al.* [219] in 1998 when looking at the spinal intervertebral joints. The evidence of idiosyncratic recruitment of the spine is in parallel with the wide kinematic variance seen in cervical spine in the current study.

As more body segments are being engaged for 'tasking' category of ADL, such as 'bending down' (BND), 'stand-to-sit' (StS), and 'sit-to-stand' (SiS), the displacement in body's centre of gravity is understandably larger. Given that visual stimulus is one of inputs that influence the balance in human body and being rectified in real-time, it is important that the cervical spine is able to respond to this demand in maintaining head stability as the receptors for the stimulus are located on the head [229]. Hence, this has impacted on the variation of kinematics observed in this study.

Concession also has to be given to individual eccentricities as each subject simulated the activities according to how they perform their own daily routine despite being instructed how the ADL tasks is supposed to be performed. For example, during 'bending down' (BND) task, majority of subjects maintained their vision at the horizon and causing their neck to be extended for the early part of the motion. A small number of subjects, however, had their vision/head followed where the torso is heading and the head is not as prominently extended as the others.

3.3.6 Inverse Dynamics

Inverse dynamic analysis was successfully carried out using multibody modelling in 178 trials where the joint contact force was calculated for all the ADL tasks performed.

3.3.6.1 Verification of Cervical Muscle Modelling

On top of the seven individual cervical vertebrae, the cervical spine in AMMR for this study was also modelled with 136 individual muscle fascicles as well as their associated ligaments, including non-linear disc stiffness programmed numerically, as configured by van der Horst [181, 201]. The hyoid bone, a human analogue of a wishbone, located within the neck, however was not included in this model. Like the patella, hyoid is a floating sesamoid bone, suspended by two surrounding muscle groups with no direct articulation with other bones. The hyoid bone is suspended superiorly by the suprahyoid muscle group which consists of geniohyoid, stylohyoid, mylohyoid, and digastric muscles. Inferiorly, the bone is attached to infrahyoid group which consists of sternohyoid, sternothyroid, thyrohyoid, and omohyoid. In general, the hyoid bone is indirectly connected to the skull, mandible, tongue, sternum, and scapulae via these muscles and they are involved in respiratory, swallowing and speech processes [230]. Both the infrahyoid and suprahyoid muscle groups have been shown to be involved in cervical flexion (from neutral position) although their contribution in cervical extension (from neutral position) is unknown [231]. Several musculoskeletal multibody studies have successfully modelled hyoid-associated muscles with their attachments modified to be on vertebra C1 for suprahyoid and vertebra C3 for infrahyoid, instead of hyoid bone [158, 232]. In AMMR, a single muscle entity, named 'LumpedHyoidT1C0', was modelled as a representative to infrahyoid muscle group [181, 201]. Despite the infrahyoid muscles' various origins and insertions, this muscle representation was modelled to have its origin at the base of the skull and inserting at the top of the thorax (which is also modelled as a single rigid segment as opposed to discretised thoracic model) with no intervening rigid segment to represent the hyoid bone itself. Graphical representation of the modelling is illustrated in Figure 3.19. The

'LumpedHyoidT1C0' muscle in AMMR is modelled to have physiological cross-sectional area (PCSA), a ratio to represent the strength of a muscle, of 2.35 cm^2 and this value is the sum of all PCSA of infrahyoid components [181]. This value is higher than a detailed cadaveric study done by Borst *et al.* [233] where the total PCSA of infrahyoid group is found to be 2.178 cm^2 with various attachment sites on the thorax, hyoid bone, as well as other soft tissues for each of the component.

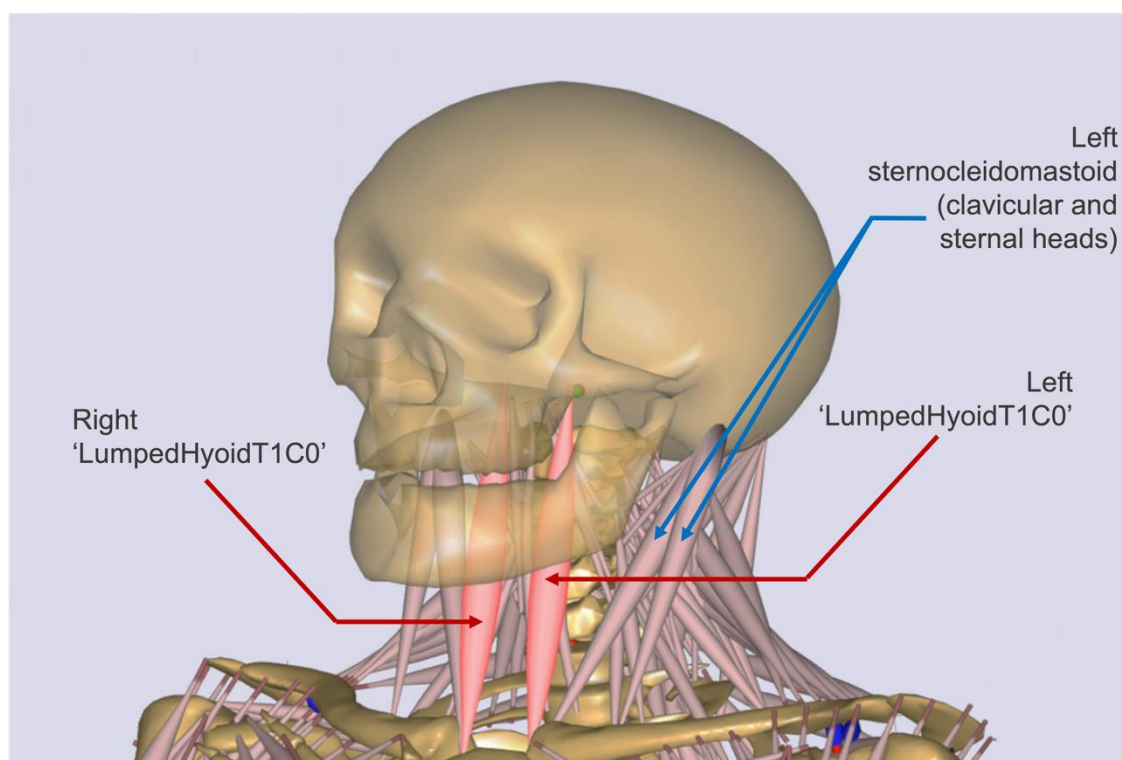


Figure 3.19 Graphical representation of left and right 'LumpedHyoidT1C0', which is highlighted in the multibody modelling, without any intervening hyoid bone.

Upon verification, the 'LumpedHyoidT1C0' is found to be contributing a higher amount of loading than necessary during head flexion/extension in 'drinking from a bottle' (WAT) ADL task, close to 100 N, shown in Figure 3.20. As the 'LumpedHyoidT1C0' is modelled with longer lever arm and larger PCSA value, it is therefore the preferred muscle to be recruited economically by the algorithm in terms of energy expenditure as set by AMMR [234].

Due to the model simplification, it was decided that ‘LumpedHyoidT1C0’ muscle would be excluded from the current study altogether due to its excessive contribution in cervical intervertebral joint loading. Although it has been numerically modelled in previous studies, programming the hyoid-associate muscle to be attached to C1 and C3 will also increase the joint loadings in the adjacent cervical intervertebral joint levels. The exclusion of the muscle was achieved by setting the muscle strength parameter, F_0 , to be zero for both left and right ‘LumpedHyoidT1C0’ muscles. Figure 3.21 shows the cervical joint loading of the same captured trial in Figure 3.20 but without the influence of ‘LumpedHyoidT1C0’ muscle.

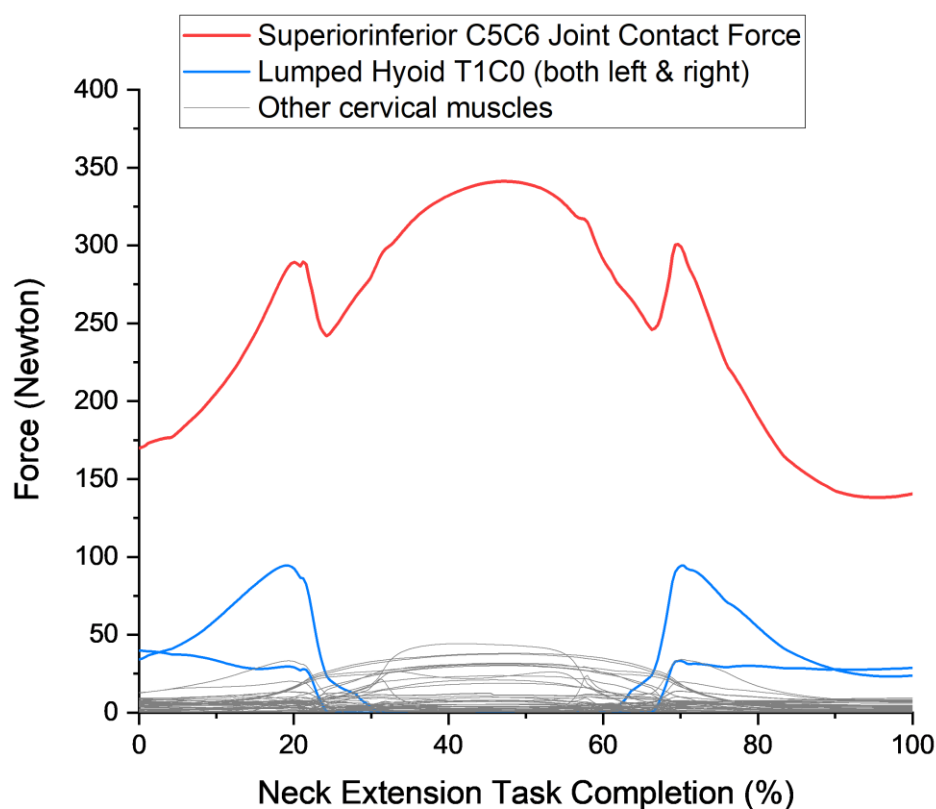


Figure 3.20 Muscle force contribution from ‘LumpedHyoidT1C0’ and cervical joint contact force at C5-C6 vertebral level during neck extension motion (WAT) in Subject 5 Trial 2

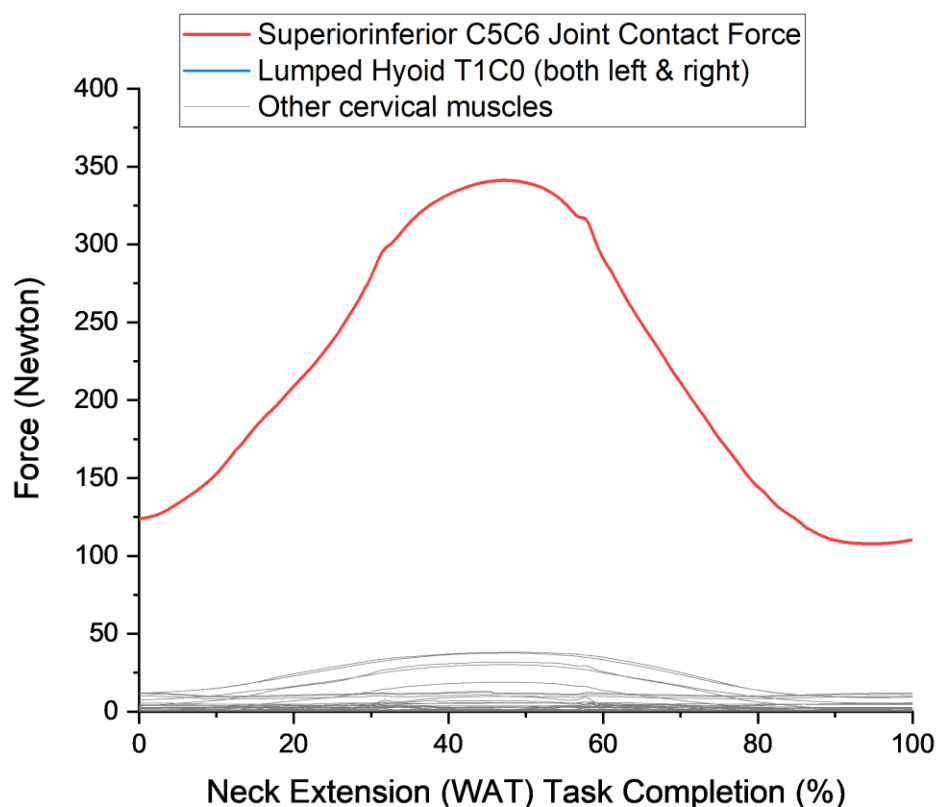


Figure 3.21 Muscle force contribution and cervical joint contact force at C5-C6 vertebral level during neck extension motion (WAT) in Subject 5 Trial 2 with the omission of 'LumpedHyoidT1C0'

3.3.6.2 Cervical Muscle Recruitment Validation

The muscle recruitment during 'looking at mobile' ADL task is used to validate the results with previously published cervical spine muscles electromyography (EMG) studies for flexion/extension of the head. In the current study, the muscles are recruited by solving the inverse dynamics according to polynomial criterion where the loading burden is apportioned according to individual muscle strength *i.e.* the higher the PCSA, the higher the polynomial, the bigger the muscle contraction, the more contribution to the loading. In the current study, the third order polynomial function (cubic) was used as the solver as this provides the most appropriate muscle synergism to be replicated physiologically [196, 234]. The muscle recruitment algorithm in AMMR also incorporates co-contraction amongst antagonistic muscles. During head flexion in the current study, flexor components such as longus capitis and longus colli (known as deep cervical muscles, located anteriorly to the vertebral column) as well as sternocleidomastoid are activated

for concentric contraction. This result is also observed in EMG studies carried out by Falla *et al.* [235] for deep cervical muscles (Figure 3.22) and by Cheng *et al.* [236] for sternocleidomastoid (Figure 3.23). In the same study, Cheng *et al.* [236] also recorded an eccentric contraction by the extensor components, namely splenius capitis and semispinalis capitis, during head flexion which are also replicated in this study too. Upon returning to neutral head posture, these extensor components are concentrically contracting whilst the sternocleidomastoid is eccentrically contracting [236] which are also seen in the current study. The deep cervical muscles are also recruited eccentrically in the simulation model but no EMG study has been published to validate this recruitment pattern.

The recruitment pattern of the cervical flexor and extensor muscles during head flexion and extension is roughly symmetrical as seen in Figure 3.21 which shows the force contribution from individual muscle. This is, however, not the case according to the EMG observation by Cheng *et al.* [236] where a co-contraction ratio (CCR), a ratio of antagonist muscles to all recruited muscles, is higher when the head is flexing (0.9) than when the head is return to neutral position (0.1) for all speed of movement (Figure 3.24). Although there is a degree of correlation between muscle activation data from EMG and force generated by the muscle in isometric contraction, the relationship is more complex during dynamic contraction where other muscle contractility factors come into play and any correlation must be interpreted cautiously [237, 238].

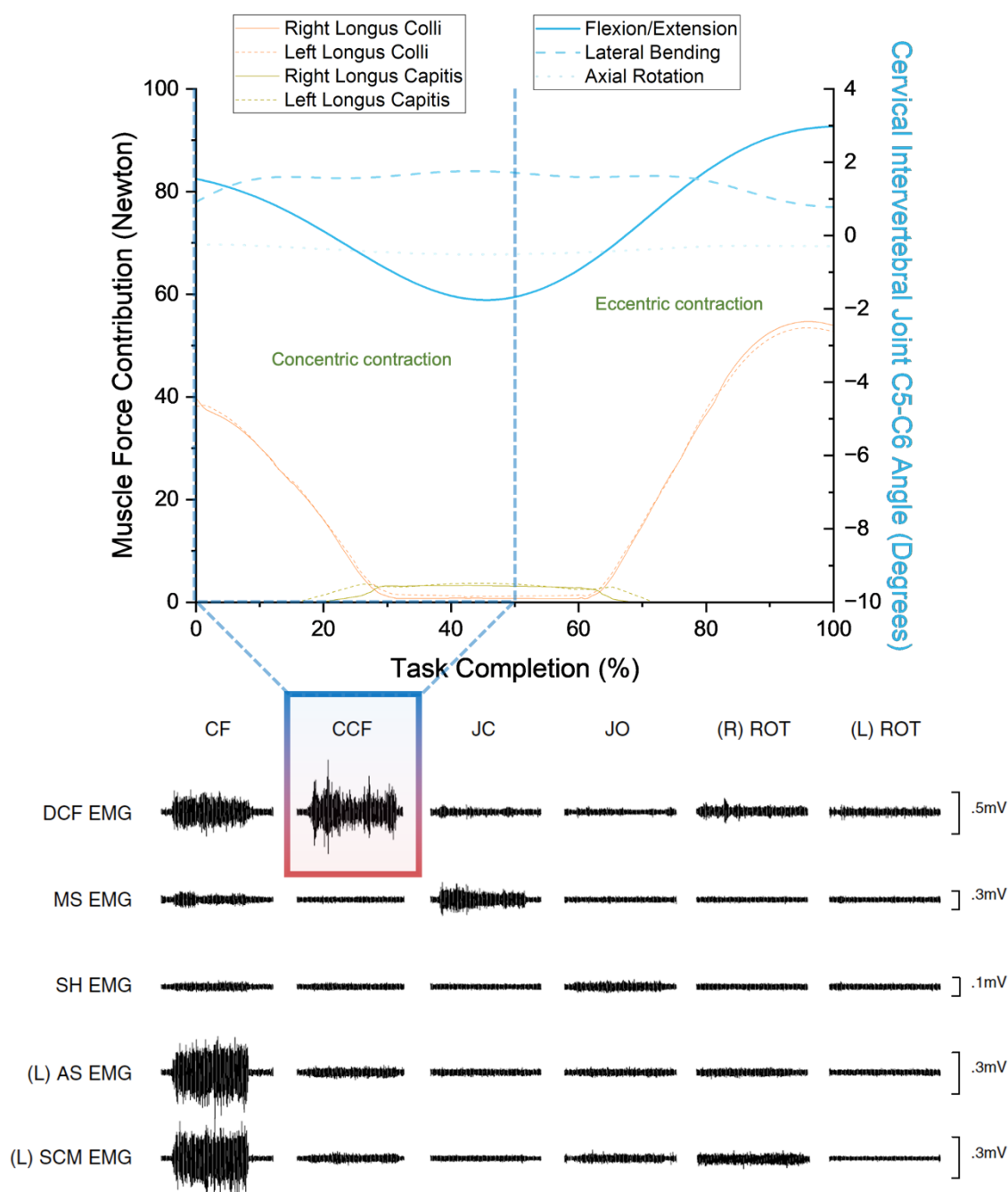


Figure 3.22 Activation of deep cervical flexor (DCF, longi colli and longi capitis) during head flexion from neutral position as seen in EMG study [235] (bottom diagram) and the corresponding muscle recruitment seen in this study (top diagram). In the EMG study by Falla *et al.* [235], data were collected whilst subject was supine. Subjects were required to lift their heads off the bed for cervical flexion (CF) and only nodding their head without lifting their heads off the bed for crano-cervical flexion (CCF). Other activities are jaw-clenching (JC), jaw-opening (JO), and head rotation to right (R-ROT) and left (L-ROT).

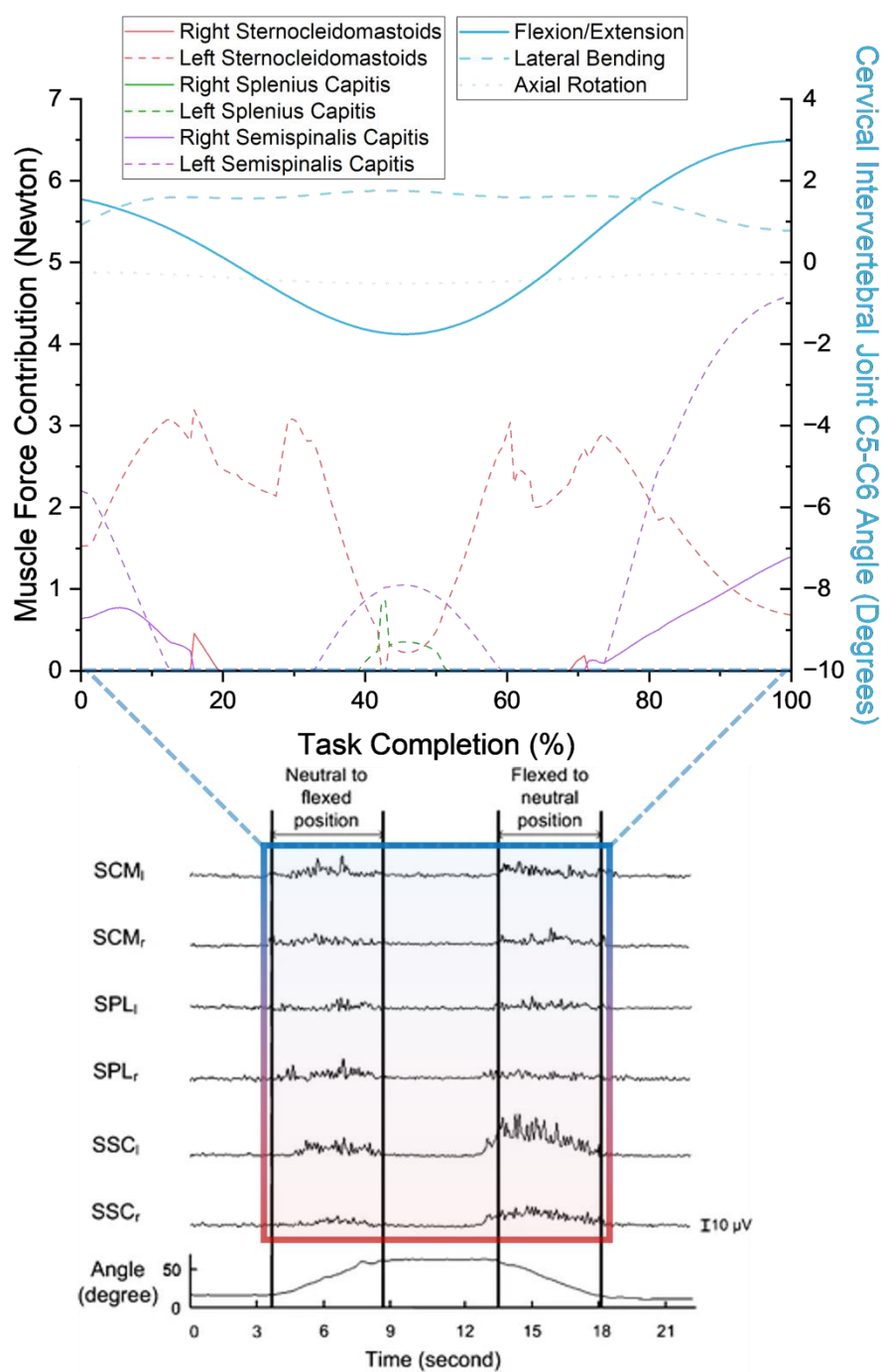


Figure 3.23 Activation of sternocleidomastoids (SCM_l & _r) during head flexion from neutral position and return as seen in EMG study [236] (bottom diagram, top two lines) and the corresponding muscle recruitment seen in this study (top diagram, red lines). Eccentric contraction by the sternocleidomastoids is also observed in both diagrams in the second half of the trial. Extensor components (splenii and semispinales capitis; SPL_l & _r, SSC_l & _r, green and purple lines) were eccentrically contracting during the first half and concentrically contracting during the second half in both studies.

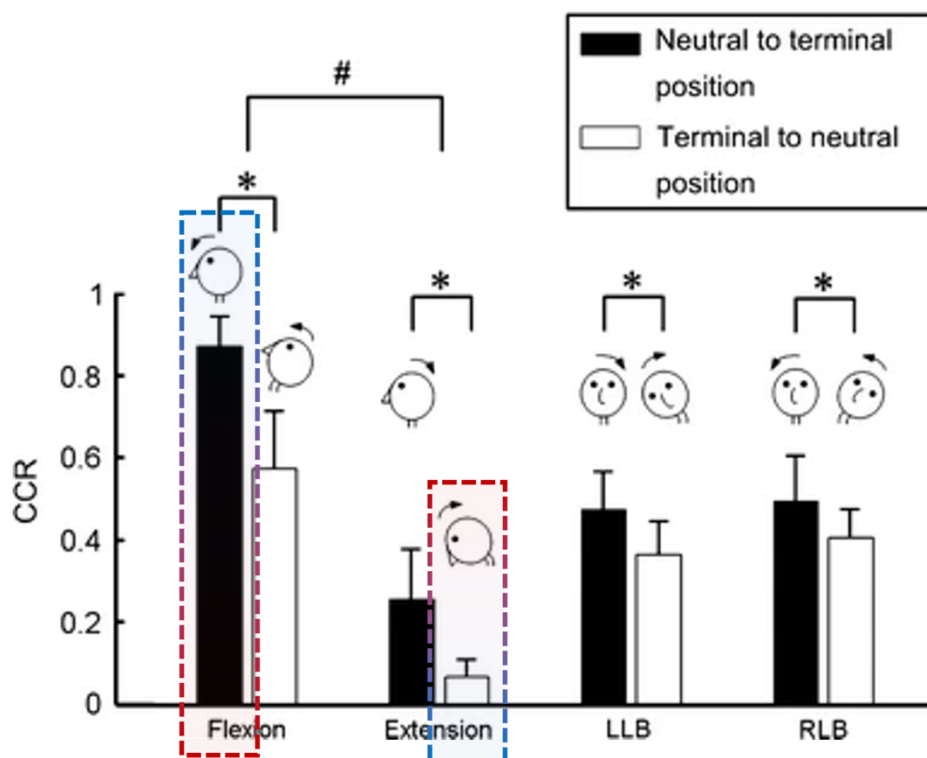


Figure 3.24 Co-contraction ratio during head flexion from neutral position (left dashed box, 0.9) compared to flexed head back to neutral position (right dashed box, 0.1) [236].

3.3.6.3 Cervical Intervertebral Joint Loading Validation

The outcome of cervical joint loading from the current study differs slightly from the published cervical joint loading during flexion/extension motion in certain phases of the movement. Upon comparing the cervical intervertebral joint axial loading at C1-C2 level, the current study's results are closer to Anderst *et al.* [158]'s data when the head moves towards the end of the motion spectrum than at the neutral position. At a neutral head position, the mean axial loading from the current study is more than 50 N higher than the magnitude reported by Anderst *et al.* [158]. This is illustrated in Figure 3.25.

There are several distinctions between multibody modelling employed in both studies that could explain the dissimilarities in the results. The biomechanical model utilised by Anderst *et al.* [158] has only three flexor and four extensor muscles and works with two main assumptions: (a) equal muscle activation in all recruited muscle, and (b) zero co-contraction between agonist and antagonist muscle groups. On the other hand, the AMMR model employed in this study has

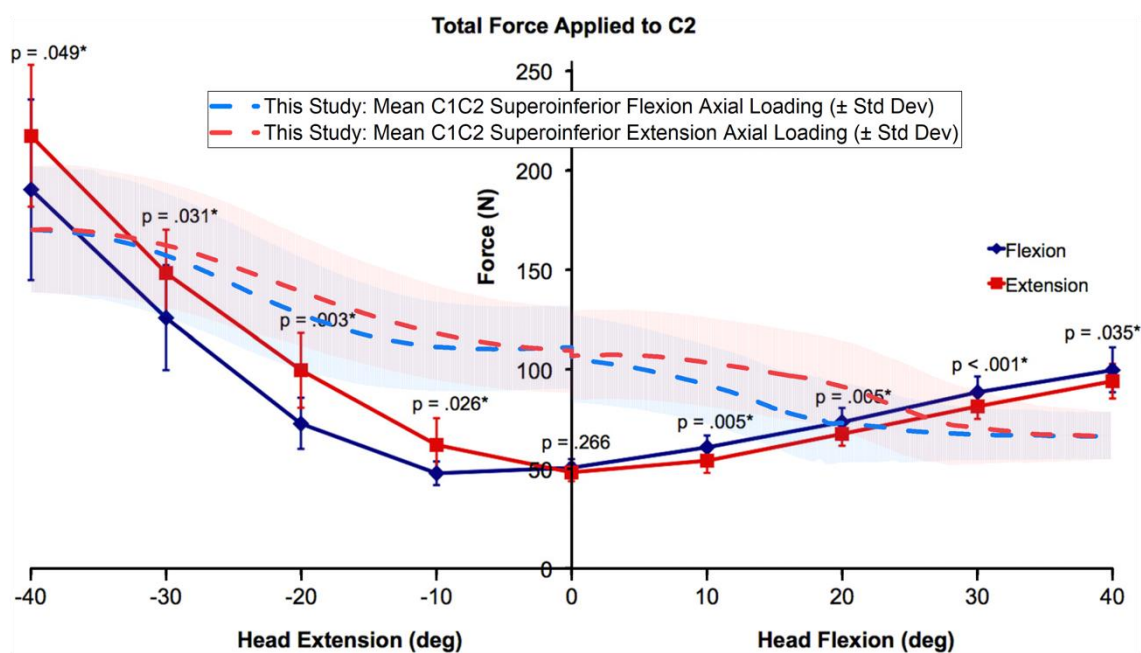


Figure 3.25 Comparison of cervical axial joint loading at C1-C2 vertebral level from this study (dash lines) superimposed over results from Anderst *et al.* [158] (solid lines).

a near-complete cervical musculature including its individual muscle fibre, apart from supra- and infrahyoid muscle which were omitted. As mentioned previously, the muscles are activated according to a cubic polynomial solver which represent the synergistic pattern seen physiologically better, as opposed to equal percentage of muscle activation regardless of muscle bulk utilised by Anderst *et al.* [197, 234] [158]. Muscle recruitment in the AMMR model also employs eccentric contraction which means co-contraction is present between antagonistic muscle groups that eventually contribute to the net joint loading, as evidenced by EMG studies [239, 240]. This is in contrast with the model used by Anderst *et al.* [158] where only pure flexor or pure extensor contraction was employed in each motion investigated. In addition, the current study has included soft tissue elements namely the disc stiffness and ligaments as part of the elastic components in the model, which are absent in biomechanical model used by Anderst *et al.* [158].

On top of the elastic body differences, there is also a difference in the rigid body components programmed between these two models. The skull mass modelled in AMMR is scaled to 5.994% of individual subject's body mass whereas the Anderst *et al.* [158] head model is consistently set at 4.2 kg and 3.4 kg for male and female respectively, which is based on work by Yoganandan *et al.* [241]. In contrast, the current study has its head mass averaging at 5.2 kg for male subjects and 4.0 for female subjects when scaled accordingly. The percentage calculation of head mass employed by AMMR is based on published work by Winter *et al.* [173]. These differences in head mass are further discussed in Chapter 5 as it has an indirect implication on wear performance of cervical disc implant.

There are also differences in kinematic aspects between these studies. The motion captured in the study by Anderst *et al.* [158] is from extreme flexion to extreme extension and *vice versa*. Meanwhile, the analysis from current study is taken from two different ADL tasks that has flexion or extension as the main movement from neutral head posture. This has an implication on the effect of inertia as more force will be used to initiate the head motion from static equilibrium position maintained by eccentric contraction of both flexor and extensor components during neutral head posture. A monophasic motion, from extreme extension to extreme flexion, seen in Anderst *et al.* [158], on the other hand, will require less force from the muscle at 0° head flexion/extension as the head segment still retain its momentum from dynamic inertia and move with fewer oppositional muscular force that maintains static head equilibrium. This could justify the lower axial loading observed in Anderst *et al.* [158] at neutral head position than average value measured in the current study. All the differences in biomechanical model employed between the current study and Anderst *et al.* [158] are summarised in Table 3.18. All in all, the musculoskeletal multibody model simulated in the current study is more comprehensive and elegant compared to biomechanical model utilised by Anderst *et al.* [158] in determining a more realistic cervical spine joint loading during ADL for the assessment of wear performance of disc implant.

| Aspects from Multibody Modelling | This study | Anderst <i>et al.</i> [158] |
|----------------------------------|--|--|
| Movement & Kinematics | <ul style="list-style-type: none"> Neutral-to-neutral Cervical intervertebral angle is calculated theoretically using kinematic rhythm RoM in ADL is only a fraction from full cervical RoM | <ul style="list-style-type: none"> Extreme-to-extreme Cervical intervertebral angle is measured from segmented individual subject's radiographic images Full cervical RoM |
| Rigid segments | <ul style="list-style-type: none"> Skull mass is scaled to 5.994% of subject's body mass (average of 5.2 kg for male and 4.0 for female) | <ul style="list-style-type: none"> Skull mass is 4.2 kg for male and 3.4 kg for female regardless of subject's body mass |
| Elastic bodies: Muscle Modelling | <ul style="list-style-type: none"> Near-complete cervical musculature; hyoid-associated muscles omitted | <ul style="list-style-type: none"> Three flexors (sternocleidomastoid, longus capitis, and infrahyoid) and four extensors (trapezius, splenius capitis, semispinalis capitis, and rectus capitis) |
| Elastic bodies: Soft tissue | <ul style="list-style-type: none"> Non-linear disc stiffness Ligamentous property included | <ul style="list-style-type: none"> None |
| Muscle Recruitment | <ul style="list-style-type: none"> Cubic polynomial solver for optimum synergy of muscle recruitment Presence of co-contraction amongst antagonistic muscles | <ul style="list-style-type: none"> Equal activation of muscles regardless of bulk size Zero co-contraction |

Table 3.18 Main differences in biomechanical multibody modelling between this study and Anderst *et al.* [158].

3.3.6.4 Variation in Cervical Joint Loading

Cervical joint loading in majority of ADL tasks analysed certainly gives a peculiar inter-subject, as well as inter-task, variation pattern that seems discontinuous. Whilst there are some steady and smooth loading pattern seen in some of the tasks, other ADL tasks have shown such a dramatic change in loading pattern, such as the ravine-like troughs in 'bending down' (BND), 'stand-to-sit' (StS), and 'sit-to-stand' (SiS). As explained in the Results, Section 3.2.5, such drastic change in joint loading pattern, particularly for superoinferior axial loading, is because of the changes in the head's centre of gravity where it moves away from the body's centre of gravity and the need to engage and activate back muscles to stabilise the head to prevent it from flopping over.

There is also a wide cervical joint axial loading variation during 'reversing a car' (REV) task amongst the subjects. This inter-subject variation is due to cubic polynomial criteria employed for muscle recruitment. The polynomial criteria is essentially an optimisation method to encourage muscle synergism through

equity in burden of pulling the loads amongst the differing sizes of muscle bulk [234]. The higher the polynomial utilised, the larger the burden taken by a bigger muscle [196]. Within polynomial criteria method, all muscles are also equipped with an upper bound limit *i.e.* the maximum amount of force any muscle fibre could contribute towards joint loading (based on its anthropometric size). As the movement in 'reversing a car' (REV) is quite extreme, more auxiliary back muscles also have to be engaged as the main muscle have reached their contracting capacity based on the algorithm. Depending on individual's kinematics and body anthropometrics, some subjects might not need to recruit the reinforcement as their bulkier muscle has not reached its limit yet. Thus, a wide variation in cervical joint loading for 'reversing a car' (REV) can be seen within the cohort in Figure 3.9 (e). The high polynomial order also has been noted to cause an abrupt activation of the subsidiary muscle when the dominant muscle bulk is approaching its limit [234]. Nonetheless, this occurrence is thought to be improbable to happen in a muscle, physiologically.

3.3.7 Phase I: Cervical Biomechanics Study Limitations

From kinematic perspective, the main limitation from the current study is the lack of more accurate tracking capability for individual cervical vertebrae. Kinematic rhythm has been employed to apportion cervical intervertebral joint angle as only a single reflective marker is used to capture the trajectory of cervical spine throughout this study. Although the apportioning cervical joint angle falls within the acceptable band proposed by Anderst *et al.* [158] for all cervical joint levels, this theoretical method limits the capability for multibody modelling from AMMR to simulate a true subject-specific kinematics.

Currently, the segmental distribution for the lumbar spine motion has been mapped out, but data for cervical spine is still scanty. Christophy *et al.* [242], for their new musculoskeletal multibody modelling of lumbar spine, have assumed the motion for each individual lumbar vertebra as a linear function from the total movement of the spinal region (Equation 3.1). The coefficient for the linear function, k , is given in Table 3.19 and it is unique for every direction of motion

and for every vertebral level. These coefficient values are derived from other studies that look into lumbar kinematics.

$$y = kx$$

Equation 3.1 [242]

y angle of vertebral motion in the specific plane (°)

k coefficient of linear function (for specific plane and lumbar level)

x total angular motion of entire lumbar spine in the specific plane (°)

For instance, the flexion/extension angle of L3 vertebra, y_{L3FE} , is given by 0.204 times the total flexion/extension angle of the whole lumbar spine, $x_{LumbarFE}$. It is unknown if there is any similar study that has mapped the proportional kinematic rhythm for cervical spine.

| Lumbar Vertebra Level | Coefficient for Proportional Kinematic Rhythm for Lumbar Spine (k) | | |
|-----------------------|--|-----------------------|----------------------|
| | Flexion/extension [243] | Lateral bending [244] | Axial Rotation [245] |
| L1 | 0.255 | 0.188 | 0.0288889 |
| L2 | 0.231 | 0.25 | 0.311111 |
| L3 | 0.204 | 0.2452 | 0.037778 |
| L4 | 0.185 | 0.1812 | 0.037778 |
| L5 | 0.125 | 0.1356 | 0.0355556 |

Table 3.19 Coefficient of linear relationship between overall lumbar motion and motion of individual lumbar vertebrae [242]

As seen from Table 3.19, the distribution of angle is not the same between all of the rotational directions (flexion/extension, lateral bending, and axial rotation) in lumbar spine and the apportionment is definitely not equal between intervertebral levels. In flexion/extension of the lumbar, the proportion of angle is smaller in lower lumbar levels than the upper lumbar levels whilst in lateral bending, the proportion is bigger in the middle lumbar region than at the top or bottom of the

lumbar spine. If a similar discrepancy is also present in the cervical spine, thus, joint excursion in any cervical vertebral level would be different from one another. This would have a significant implication on wear performance of cervical disc implant, which will be further discussed in Chapter 5.

Movement in the spine is inherently challenging to measure owing to the fact that the spinal joint has six DoF (three rotational and three translational) as described in Section 2.5.2 which resulted in coupling of movement of the vertebra. The complexity of having six DoF, as opposed to a spherical, ball-and-socket, joint is magnified when the instantaneous axis of rotation for the spinal joint is located outside the joint itself, which can also migrate in anteroposterior direction during flexion/extension movement due to translational ability of the joint [246, 247].

Another limitation in the current study is related to the transfer of net force between two rigid bodies during inverse dynamic analysis, which is through a single contact point. As described in Section 2.1.1, the spinal column's basic component for movement is the FSU – consisted of two vertebrae stacked on top of each. And within this FSU, there are three main articulations: an intervertebral joint and two facet joints. Consequently, the load transfer between these vertebrae is split three ways, with 80% of the compressive force is thought to pass through the intervertebral joint, at neutral position, whilst the remainder is via facet joints [246]. The proportion is thought to be higher in the cervical region due to its morphological feature [246]. The presence of facet joints also implicates how the shear forces are transferred and distributed within FSU too [246]. Nevertheless, it is still an imprecise estimation from the current study given the linked-segment modelled employed for inverse dynamic analysis only has a single contact point for load transfer between the cervical vertebral segments. Similarly, this would have a significant implication on wear performance assessment of the cervical disc implant, which will be further elaborated in Chapter 5. Currently, there are very limited number of studies that have incorporate facet joint, either geometrically or numerically, in their modelling [182, 202].

In the current study, the muscle recruitment algorithm used is the polynomial criteria, specifically in the third order, as explained in Sections 2.5.6 and 3.3.6.1.

Whilst this method is widely accepted as it represents muscles recruitment physiology generally, this has caused inaccurate muscle recruitment within the cervical spine model in the current study where hyoid-associated muscles are modelled as single entity. The oversimplification of the hyoid-associated muscles contributes towards the unrealistic joint loading pattern due to its inflated muscle bulk size causing it to be the preferred actuator over other muscle groups from this optimisation. This has prompted the total omission of the LumpedHyoids muscle group even though part of hyoid-associated muscles also involve in cervical flexion, as substantiated by studies cited in Section 3.3.6.3. Theoretically, it is possible to model these muscles according to its individual origin and insertion. Programming and validating a new cervical musculature is, however, time-consuming and fell beyond the scope of the current research project. Thus, the lack of hyoid-associated muscles in the musculoskeletal multibody modelling poses a limitation onto the outcome of this study.

Cubic polynomial muscle recruitment criteria also poses an issue with cervical joint loading pattern when complex ADL task is simulated. During 'reversing a car' (REV), wide variation of loading pattern can be seen across the cohort as the movement requires the body to engage a plethora of back muscle groups for this complicated motion. Depending on the subjects' anthropometric as well as their kinematics, some of the main muscles might have reached its maximum capacity and the auxiliary muscle groups had to be recruited to solve the simulation which adds into the joint loading. A high polynomial order algorithm is notoriously known to cause a sudden muscle activation as the main muscle bulk approaching its limit and this has caused the multitude of loading pattern as observed in Figure 3.9 (h) [196, 234].

Finally, the almost-symmetrical pattern of muscle recruitment during head neutral-flexion-neutral movement seems to be too perfect when it is known that there is discrepancy of co-contraction ratio between head flexion and head extension. Nonetheless, an improvement to the current muscle recruitment algorithm for a more realistic recruitment pattern is not impossible for future work.

3.3.8 ADL Wear Testing Profiles

A wear simulator for joint implant generally operates by repeating a cyclical motion for an extended period of time according to a set of biomechanical parameters such as the angular displacements and loadings. For lower limb implants (hip, knee, and ankle), one unilateral gait cycle is typically used to demarcate the repeating unit for the joint simulator to simulate the wear. This is also true when testing for other ADL involving locomotion, such as running or climbing a stair where 'heel strike-heel strike' cycle can be employed as the repeating unit.

In the cervical spine, however, there is no prescriptive, cyclical motion that can be considered 'typical' in which a spatiotemporal parameter that could be used to defined as a discrete unit or even to align the biomechanical parameters. Thus, each of ADL tasks analysed in this study can be regarded as a cycle on its own because all the parameters begin and end when the head is at a neutral position. In the current study, for each ADL task, the cervical joint loading in axial direction was used as reference frame to align all the biomechanics parameters throughout the cohort instead of kinematics data, as conventionally applied in gait analysis, due to its large variation as explained in Sections 3.1.7, 3.2.4, and 3.3.5.2. All the kinematics and loading curves are aligned to either the major peaks or troughs seen in superoinferior axial loading graph when normalised to percentage of task completion.

The cervical intervertebral joint loading at C5-C6 is also used as a reference when formulating the wear testing profile because it is the commonest implanted level for cervical disc implant as well as the commonest level for revision surgery in failed prostheses [221-223]. Due to kinematic rhythm, the intervertebral joint angle output from the current study is the same regardless of the cervical level.

The newly formulated wear testing profile is also devised to have six degrees of freedom with 1000 data points of loading cycle so it could be re-sampled to suit individual joint simulator input requirements as well as their axes harmonised according to ISO18192-1 [1] definition.

In the current cervical biomechanics study, the average curve across all the trials is chosen as the representative pattern for that particular ADL task. And this curve is also used as the input parameters within the wear testing profile. One might argue the appropriateness of having an average curve as the representative value for testing when these parameters are only covering half of the population and the rest might potentially wear out their implant earlier just because they have above average biomechanics. It is worth noting that wear simulation is one of a battery of tests that an orthopaedic implant is subjected to prior to commercialisation. More importantly, the objective of wear simulation is to evaluate the tribological performance of the device in a typical *in vivo* environment where implant manufacturers and regulators could use as a guide to estimate the debris production over time and decide whether mitigation is needed when this poses a risk to the patients. Crucially, it should not be meant to be the bare minimum requirement that the device has to achieve and certainly a broader safety margin is imperative. Conversely, an unnecessarily harsher wear testing regime might hinder innovation and delay commercialisation for the implant. An intricate balance between these competing demands should be sought with benefits towards the patient as the ultimate goal.

The ADL Flexion/Extension wear profile (Figure 3.14), formulated in Section 3.2.7, is devised to represent everyday flexion and extension of the head. It is a movement that happens twice more commonly than lateral bending or axial rotation [170]. Although they are not isolated, the wear profile prescribed in ISO18192-1 [1] also has flexion/extension as the more dominant motion in a unit cycle with the biggest excursion (30°) compared to other directions of motion. Consequently, this ADL Flexion/Extension wear profile was chosen to be implemented in Phase II of this research project where a mechanical wear simulation is being carried out. The similarity would allow comparison to be made between a standard wear testing and a profile with more physiologically relevant parameters.

3.4 Summary

In this chapter, the study to quantify cervical spinal loads and motions during activities of daily living has been presented and discussed in detail guided by the three outlined objectives.

Using motion capture technique and multibody modelling, a catalogue of cervical joint loads and motions was established for eight different daily activity tasks which was previously absent in the literature. These investigated tasks were determined by inputs received from patients with cervical spinal issues as well as peer-reviewed articles. From this biomechanics study of cervical spine:-

- a) the cervical joint angle during ADL tasks was estimated to be only a fraction of the total cervical RoM,
- b) the joint excursion is smaller than what currently being prescribed in ISO18192-1 [1] during ADL tasks, and
- c) the estimation for cervical joint loadings during ADL tasks is higher than the value proposed by the ISO18192-1 [1] for axial loading in all tasks analysed.

Using biomechanical data from this study, several wear testing profiles were formulated based on ADL tasks that are commonly performed every day. The newly formulated profiles have a more physiologically-relevant test parameter based on ADL for assessing the wear of disc implant than the currently advocated by the standards. One of these profiles is employed in Phase II of the research project where mechanical wear testing on disc implant replicas is being carried out.

Chapter 4

Study of Mechanical Wear Simulation on Articulating Cervical Disc Implants

It has been stated in Chapter 2 that the prescribed testing protocols for cervical disc implant by the ISO are lacking in a strong clinical basis or explant analysis justifications [16]. The current standard wear testing profile emphasises on the head moving in an arbitrary, stylised sinusoidal pattern rather than the functional activities carried out by the patients every day. The wear simulation profile also implies that all three cardinal motions of the head (flexion/extension, lateral bending, and axial rotation) happen in equal measure whilst studies have shown that movement in flexion/extension direction occurs more frequently than the others [16].

Therefore, Phase II of this research project aims to investigate the wear performance of cervical disc implant under loads and motions derived within the spectrum of activities of daily living. It involves the utilisation of cervical biomechanics data gathered from Phase I as testing parameters, in addition to the standard testing protocols, controlled by a bespoke, multi-station joint simulator where the implants were mounted. This study compares outcomes from simulation under the standard parameters from ISO18192-1 [1] as well as parameters that represent activities of daily living. This chapter will report the experimental study carried out in achieving this aim. Figure 4.1 illustrates the activities involved within Phase II.

The three outlined objectives associated with Phase II in fulfilling its aim are:-

- d) to deploy the new wear testing profiles onto state-of-the-art electromechanical three-station hip joint simulator,
- e) to run mechanical wear simulation under the standard (ISO18192-1 [1]) and physiologically relevant data formulated in Phase I on

electromechanical joint simulator for five million cycles, using replicas of disc implant bearing surfaces, and

- f) to analyse and compare gravimetric mass loss as well as surface roughness of the bearing surfaces throughout mechanical wear testing for both wear test conditions.

Phase II

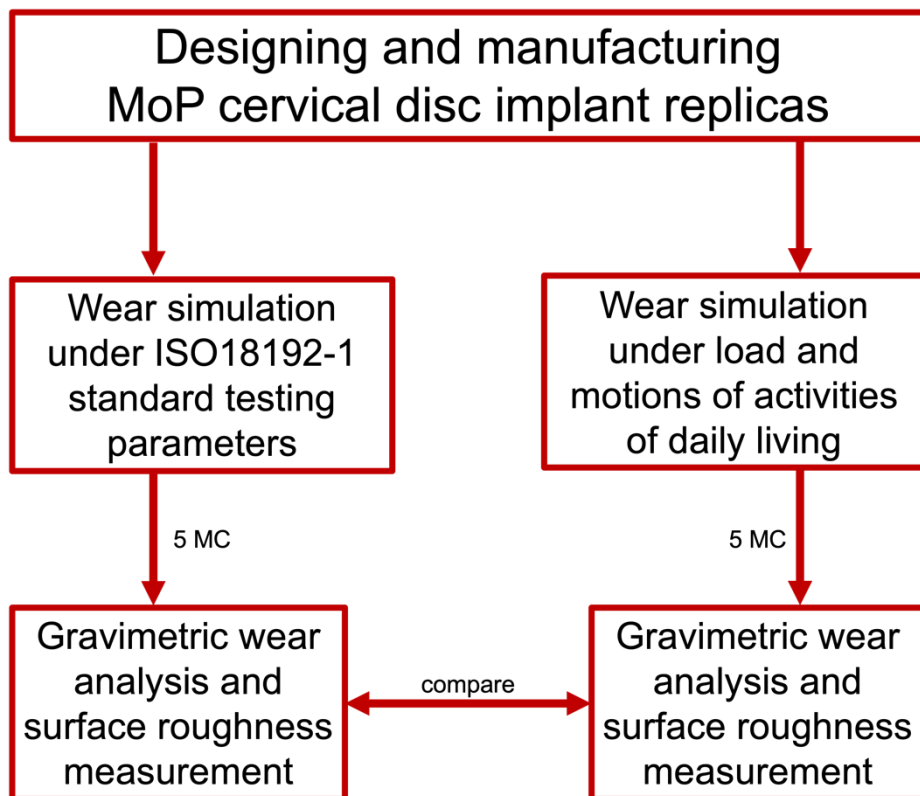


Figure 4.1 Workflow for activities involved in Phase II

4.1 Methods

4.1.1 Replica Design of Cervical Spinal Disc Implant Bearing Surfaces

For the purpose of this project, a shallow ‘ball-and-socket’ implant configuration was chosen to represent the articulation of a typical cervical disc prosthesis, as seen in Table 2.2. The replica was designed to be a single bearing joint. And it was intended to replicate only the tribological pairing, *i.e.* the bearing surfaces, of a typical cervical disc implant rather than actual geometry of the device.

4.1.1.1 Replica’s Convex Bearing Surface

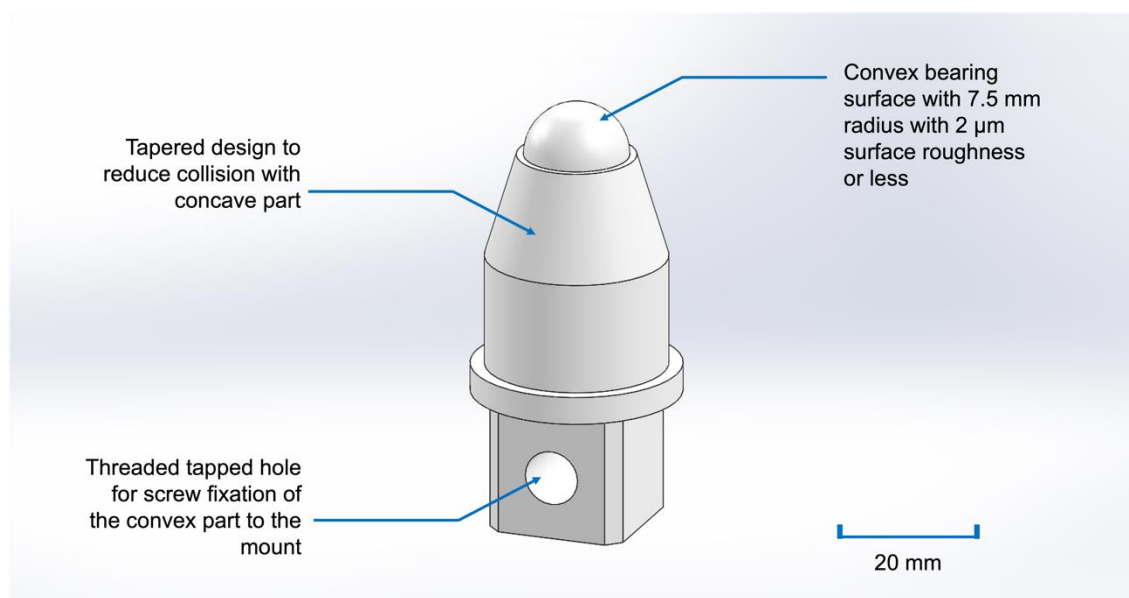


Figure 4.2 Design features of UHMWPE convex bearing part

Ultra-high molecular weight polyethylene (UHMWPE) (GUR 1050) supplied by Industrial Plastic Supplies Ltd (Leeds, UK) was selected as a material for the inlay, or the ‘ball’ part, of a typical disc prosthesis. The UHMWPE was machined within the School of Mechanical Engineering’s workshop to form a convex hemispheric bearing surface with 7.5 mm radius and a surface roughness, R_a , of 2 μm or less (Figure 4.2). The UHMWPE was chosen as it is the commonest biomaterial found for the core of a typical approved disc implant as illustrated in Table 2.2. The convex part was also designed to have a portion, underneath the hemisphere, for fixation to a mount, with a tapered geometry to ensure a collision-

free movement upon assembly (Figure 4.6). A complete geometry of the UHMWPE convex part used for this research is attached in Appendix D(b).

4.1.1.2 Replica's Concave Bearing Surface

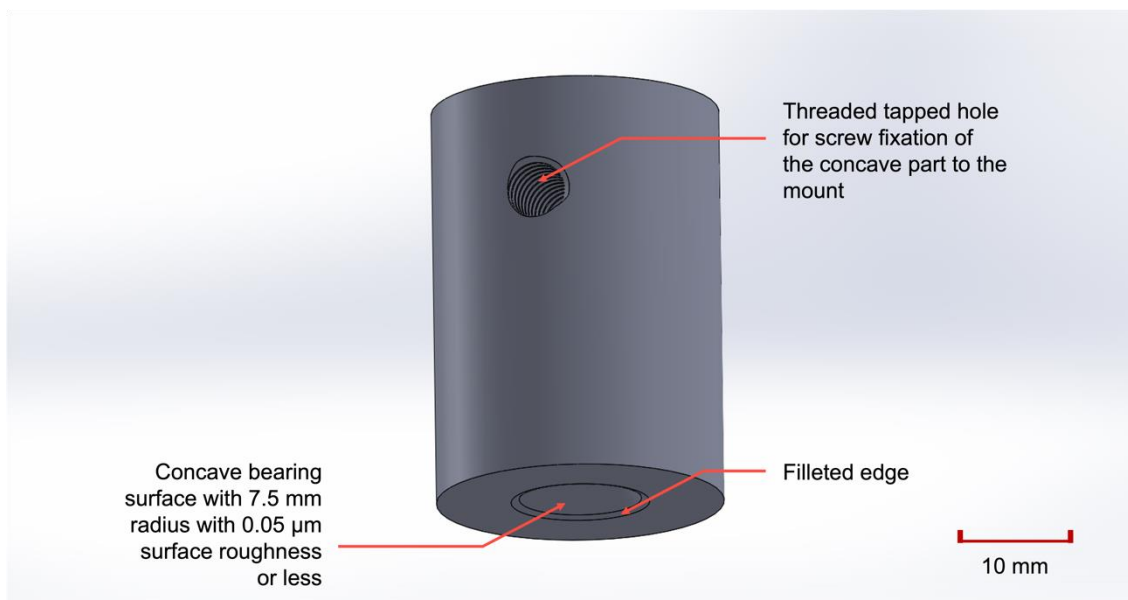


Figure 4.3 Design features of CoCrMo concave bearing part

A concave part was produced from a low-carbon cobalt-chromium-molybdenum (CoCrMo) alloy bar (ASTM F1537-20, UNS R31537) supplied by Oracle Special Metals Ltd (Bracknell, UK) and was machined at Kirkstall Precision Engineering Ltd (Leeds, UK). The radius of the hemispheric socket was designed to be 7.5 mm with a surface roughness, R_a , of 0.05 μm or less. The depth of the concave was set to be 2.5 mm from the surface of the brim. The CoCrMo material was chosen based on the commonest biomaterial used for the endplate, or the 'socket' part, in a typically approved cervical disc implant shown in Table 2.2. The CoCrMo part was designed with a filleted edge around concave brim and also a thread for a simple screw fixation (Figure 4.3). A complete geometry of the CoCrMo concave part used for this research is attached in Appendix D(a).

4.1.1.3 Radial Clearance and Nominal Contact Area

The replicas' tolerances for radius were set between -0.20 to 0.00 mm for convex bearing surface and between 0.00 to +0.20 mm for concave surface. Based on

these, the overall range for radial clearance upon assembly is between 0.00 to 0.40 mm.

As depth of the socket in the CoCrMo concave part, h , was designed to be 2.5 mm, the nominal contact area was estimated to be 37.5π mm² or 117.8 mm² based on spherical cap area, S , formula in Equation 4.1 below.

$$S = 2 \times \pi \times r \times h$$

Equation 4.1

r radius of sphere

h height of the spherical cap

4.1.2 Joint Simulator for Cervical Disc Implant Wear Testing

A three-station, electromechanical hip joint simulator (Simulation Solutions, Stockport, UK) commissioned by LifeLongJoints consortium (LLJ) was used to simulate long-term wear phenomenon on the produced articulating cervical disc implant replicas (Figure 4.4).

The machine was originally built to simulate wear of hip implants and was anatomically designed as a left hip. Each simulator bank has three kinematic stations and a control station, all are fitted with a six-axis load cell that continuously samples all the forces and displacements at 1024 Hz. The kinematic stations have five controlled axes of motions, actuated by programmable motors:

- flexion/extension ($\pm 61^\circ$),
- abduction/adduction ($+ 25^\circ/- 10^\circ$),
- inward/outward rotation ($\pm 45^\circ$),
- axial loading (up to 8000 Newtons),
- medial/lateral (0.0 – 5.0 millimetres or up to 1500 Newtons).

The medial/lateral motor can be set either to have a displacement or load control. Anterior/posterior, however, is an uncontrolled motion axis and it is free-floating from the test cell's top suspension within the simulator. Motion in medial/lateral and axial loading directions are controlled superiorly. Whereas motion in flexion/extension, abduction/adduction, inward/outward rotations are controlled inferiorly. The location of these motor controls was designed according to the physiological motion of a left femur in hip joint with respect to a static pelvic bone.



Figure 4.4 3-station, electromechanical LLJ hip joint simulator

4.1.3 Parameters for Wear Tests

Two sets of wear test on the replica of cervical disc implants were devised. The first set of tests was considered as the standard wear test, prescribed by ISO18192-1 [1]. Whereas the second set of tests was chosen from one of the newly formulated wear testing profiles, at the end of Phase I, which was based on a more physiologically relevant cervical kinematics and loadings during ADL.

4.1.3.1 Standard Wear Test and Settings for Simulator

Load and displacement parameters prescribed in Appendix B of ISO18192-1 [1], summarised in Table 2.4, were used as the standard wear test parameters for the simulation of the cervical disc implant replicas.

To avoid confusion, two of cervical spine's axes of motion were appropriated according to simulator's left femoral axes of motion terminologies as below:

- cervical spine right (+)/left (-) lateral bending \equiv hip adduction (+)/abduction (-),
- cervical spine axial rotation \equiv hip inward/outward rotation.

Direction of axis for cervical axial rotation kinematics data from ISO18192-1 [1] was also transformed to harmonise with the simulator's rotational axis definition, which was originally designed according to ISO14242-1 [2], a standard that outlined the parameters for wear-testing of a hip implant. The transformations were:

- cervical spine right axial rotation (-) \equiv left hip inward rotation (+),
- cervical spine left axial rotation (+) \equiv left hip outward rotation (-).

After the motion transformation, the 100-point parameter values provided ISO18192-1 [1] were plotted using cubic spline interpolation in OriginPro software. The plotted curves were resampled to 128 points as per joint simulator input requirement and saved as *ISO18192-1 Cervical.txt* file. The order of column for the test parameters within the file can be seen Appendix E(a).

4.1.3.2 ADL Wear Test and Settings for Simulator

There are several ADL wear profiles devised from output in Phase I. ADL Flexion/Extension wear test profile, as illustrated in Figure 3.14, was chosen as a representative for ADL wear testing in this research project.

On top of kinematics parameters (flexion/extension, lateral bending, axial rotation) and superoinferior axial loading, anteroposterior loading was also incorporated into the adverse wear test profile as an additional test parameter.

The anatomical orientation of the wear simulator was rotated 90° anti-clockwise along the superoinferior axis (in transverse plane) in order to accommodate this additional degree of freedom (of anteroposterior loading) in the ADL Flexion/Extension wear test profile. The anteroposterior loading was driven by medial/lateral actuated motor due to the lack of actuator motor in anteroposterior direction, and the motor was set as 'force control' (as opposed to displacement control). The parameter for the anteroposterior loading were filtered to only have positive values and all negative integers were set to 0; this is due to medial/lateral actuator motor can only accept an input of 0 or higher.

After 90° anti-clockwise rotation, the simulator's anatomical orientation was redefined as below:

- left hip flexion (+)/extension (-) axis \equiv cervical spine right (+)/left (-) lateral bending,
- left hip abduction (-)/adduction (+) \equiv cervical spine flexion (+)/extension (-).

Orientation in other axes remained the same. Then, the 1000-point wear test profile formulated in Phase I was resampled to 128-point for simulator input and saved as *ADL FlexExt Cervical.txt* file, which also can be seen in Appendix E(b). These anatomical orientation definitions and harmonisation are illustrated in Figure 4.5 and summarised in Table 4.1.

| LLJ Simulator Input Definition for Left Hip | Typical Left Hip Wear Test (original purpose) | Standard Cervical Wear Test | Cervical ADL Wear Test |
|---|---|----------------------------------|------------------------------|
| Test Profile | ISO14242-1 [2] | ISO18192-1 [1] (Cervical) | ADL Flexion/Extension |
| <u>Angular Motion Control</u> | | | |
| Flexion (+) | + | + | + (right lateral bending) |
| Extension (-) | - | - | - (left lateral bending) |

| | | | |
|----------------------|---|---------------------------|--------------------------|
| Adduction (+) | + | + (right lateral bending) | - (extension) |
| Abduction (-) | - | - (left lateral bending) | + (flexion) |
| Inward Rotation (-) | + | - (right axial rotation) | - (right axial rotation) |
| Outward Rotation (+) | - | + (left axial rotation) | + (left axial rotation) |

Linear Loading Control

| | | | |
|---------------------|---|---|---|
| Axial Loading (+) | + (inferiorly, in direction of gravity) | + (inferiorly, in direction of gravity) | + (inferiorly, in direction of gravity) |
| Medial Loading (+) | Not tested | Not tested | + (anteriorly, from 0N) |
| Lateral Loading (-) | Not tested | Not tested | - (posteriorly, until 0N) |

Table 4.1 Summary of orientation of kinematics and loading parameters for both ISO18192-1 [1] and ADL Flexion/Extension wear simulations

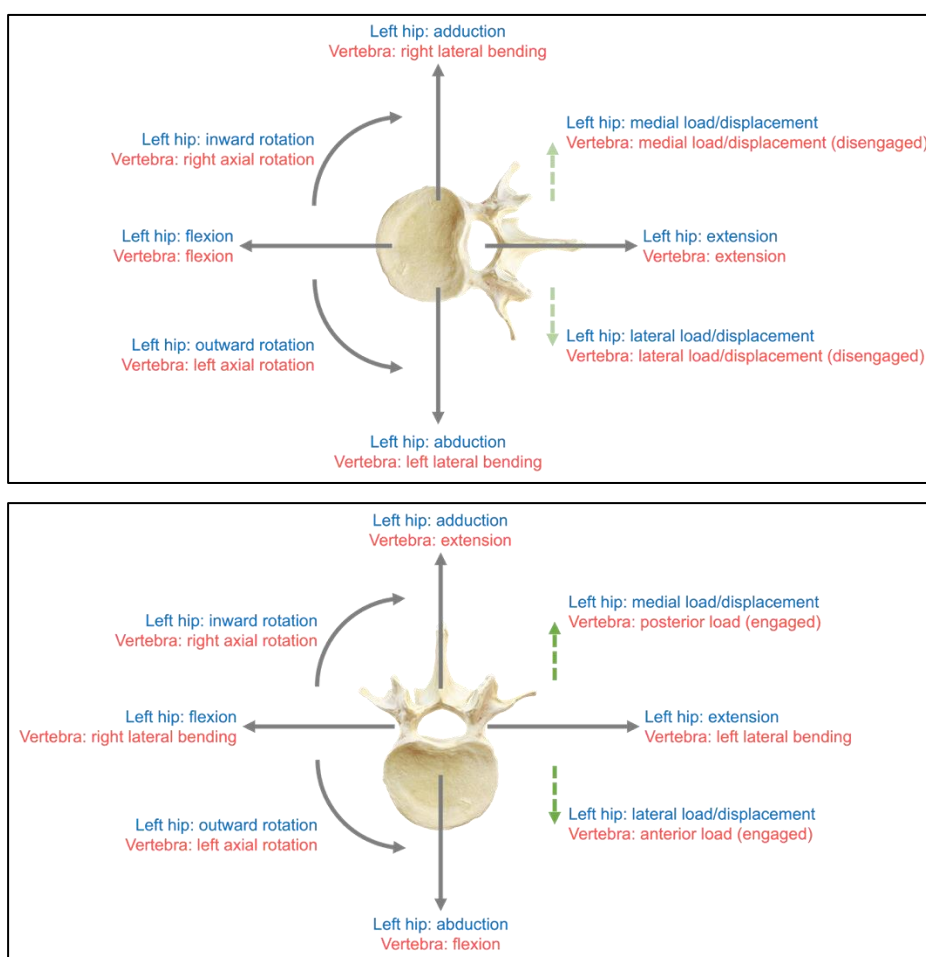


Figure 4.5 Comparison of axis orientation for kinematics and loadings between a typical left hip (blue) and cervical vertebra (red) wear simulation in ISO18192-1 [1] (top) and ADL Flexion/Extension (bottom) wear tests

4.1.4 Wear Test Protocol

Apart from the load and displacements test parameters, other experimental protocols and variables outlined in ISO18192-1 [1] such as reagents; apparatuses; and procedures were followed and set as constant variables for both sets of wear test. A reference made in ISO18192-1 [1] towards document *ISO14242-2 Implants for surgery — Wear of total hip-joint prostheses — Part 2: Methods of measurement* (ISO14242-2 [3]) was also followed for preparatory and measurement steps.

4.1.4.1 Preparations of Implant Replica's Convex and Concave Bearing Parts

Prior to commencing the wear tests, the replica's UHMWPE convex parts were soaked in deionised water for at least two weeks. The convex parts were cleaned, dried, and weighed at a 48-hour interval according to the procedures outlined in ISO14242-2 [3]. This process was repeated until the incremental mass change of UHMWPE parts over 24 hours was less than 10% of the previous cumulative mass change of the said parts [3]. The final mass, weighed after fluid absorption stabilised, was recorded and set as the mass of that convex part at the beginning of the wear test (*i.e.* mass at 0 million cycles).

Due to the fibrous nature of its constituents, UHMWPE is porous and readily absorbing fluid [248]. Its fluid uptake property can mask its loss of material due to wear and it is the principal source of error in gravimetric wear analysis measurement [168]. By pre-soaking them in excess, the UHMWPE parts are saturated with fluid and the mass are stabilised prior to the simulation to reduce the uncertainty of this error [248]. Furthermore, the gravimetric measurement during wear simulation is carried out after the UHMWPE parts being desiccated so it is "nominally dry" to minimise as much as possible the trapped residual liquid which can be the source of error. [248]. Additionally, the error from fluid absorption is mitigated by the use of 'active soak control' where UHMWPE part from the controlled test cell is subjected to the identical environment and conditions in other UHMWPE parts, such as equal lubricant submerging period,

system temperature, as well as loading force exerted, with the exception of sliding motion [248]. The measurement from the control experiment is then used to offset any change in fluid uptake from the other UHMWPE parts throughout the wear simulation because it is assumed that all of them behaves similarly [168, 248].

The replica's CoCrMo concave parts were weighed just once before commencing the test using the same protocol in ISO14242-2 [3] as CoCrMo is known to have a negligible fluid absorption potential. The mass of CoCrMo concave parts were recorded and set as the mass of that concave part at the start of the wear test (mass at 0 million cycles).

4.1.4.2 Test Cell Setup

The UHMWPE convex and CoCrMo concave parts were both screwed onto bottom and top mounts, respectively. A silicon gaiter was attached to both mounts together, which eventually enclosed the space surrounding the implant replica, and was secured with a jubilee clip on each mount. Both bottom and top mounts were designed to have an inlet and an outlet, respectively, for continuous flow of test medium that effectively bathed the implant replica's bearing surfaces. The top mount of the test cell was attached to the top suspension of the simulator in which the axial loading and medial/lateral motors were actuated. The bottom mount was fixed onto a rocker which controlled by motors for flexion/extension, abduction/adduction, and inward/outward rotation. A schematic diagram of the test cell as well as its cross-section is illustrated in Figure 4.6.

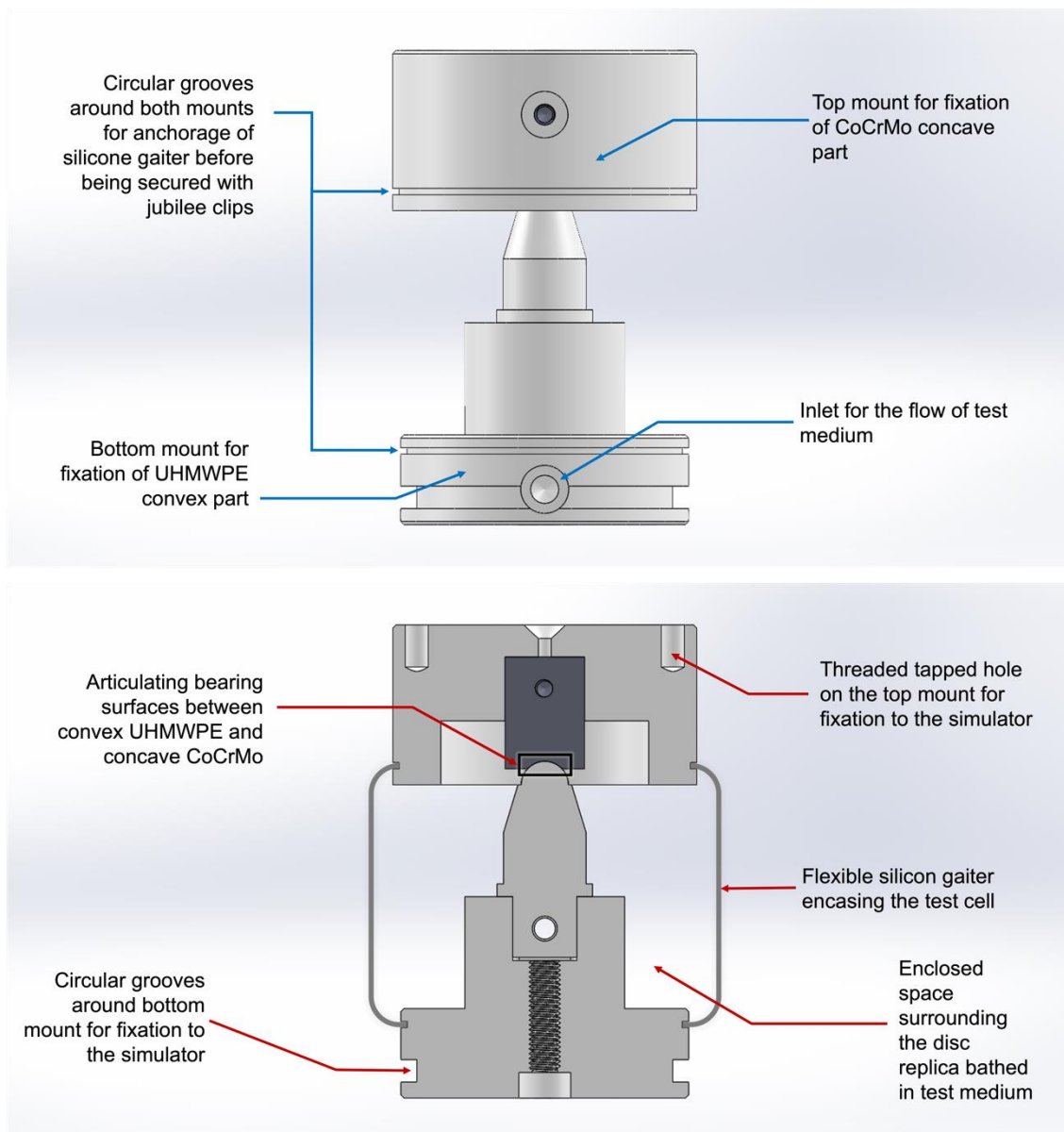


Figure 4.6 Schematic diagram of test cell assembly (top) and its cross-section (bottom)

4.1.4.3 Fluid Test Medium

HyClone™ Triple-0.1 μ -filtered bovine calf serum (Cytiva, Massachusetts, United States), which met the requirement set by ISO18192-1 [1], was selected as fluid medium for both sets of wear test. The serum was diluted with deionised water, together with 0.03% (w/v) sodium azide as an antimicrobial component, to form 20 ± 2 g/L of total protein concentration lubrication medium for the test. This protein concentration of bovine calf serum has a viscosity of 1.0 mPa s, which is similar to viscosity of the interstitial fluid (1.24 mPa s) that surrounds the spinal intervertebral disc [92, 94].

The test medium was constantly pumped into the sealed space inside the test cell and was maintained at 37 ± 2 °C throughout the test period.

4.1.4.4 Pilot Test for Simulation Output Verification

Prior to commencement of the tests, output verification was carried out where all the engaged actuated motors were tuned to be within the acceptable range of magnitude and phasing set by ISO18192-1 [1] for both wear simulations for all angular motions and loading parameters.

4.1.4.5 Wear Test Simulation

Both sets of wear test were run for 5.0 million cycles. For the first million cycles, the simulation was stopped at every $\frac{1}{3}$ million cycles for cleaning, drying, and weighing of the implant replicas as well as for a complete test medium replacement. After 1.0 million cycles, the simulation was only stopped at every $\frac{1}{2}$ million cycles for cleaning, drying, and weighing as well as for a complete test medium replacement. The same protocol outlined in ISO14242-2 [3] was used for cleaning, drying, and weighing during this intervening period of simulation.

Both sets of wear test were run at 1 Hz frequency for one wear test profile cycle.

4.1.5 Gravimetric Analysis

During the initial as well as the intervening simulation period, known as gravimetric measurement timepoints, the mass for both UHMWPE convex and CoCrMo concave parts were measured using XP205 analytical balance (Mettler Toledo, Greifensee, Switzerland) which was set to 0.00001 grams precision.

All the parts were weighed in rotation within 90 minutes after being vacuum dried until three readings, within 0.0001 grams, were achieved and these values were then averaged.

In both sets of wear test, the net mass lost due to wear for each individual part was calculated using formula given in Equation 4.2 from ISO14242-2 [3].

$$W_n = W_{an} + S_n$$

Equation 4.2

W_n net mass loss after n cycles of simulation,

W_{an} average mass loss after n cycles of simulation,

S_n average change of mass of soak replica after n cycles of simulation.

The overall wear rate, a_G , from the simulation was derived from the gradient of linear fit between average net mass loss after n cycles, W_n , and the number of simulation cycles completed, n . The linear regression formula is given in Equation 4.3.

$$W_n = (a_G \times n) + b$$

Equation 4.3

b y-intercept constant for linear fit

4.1.6 Estimation of Sliding Distance and Aspect Ratio from Wear Profiles for the Simulation

As illustrated in Equation 2.1 in Section 2.3.1, wear is a function of sliding distance. Wear also known to be influence by cross shear as discussed in Section 2.4.2. To compare between the two sets of wear test, their sliding distance was calculated and cross shear for each individual wear profile was also quantified

through the calculation of aspect ratio, a measurement of multidirectionality of the wear path. These analyses were carried out to supplement the comparison of gravimetric wear rate between the two wear test conditions.

4.1.6.1 Estimation of Sliding Distance, L

Calculation for sliding distance estimation, L , were done in two stages: (a) outlining a three-dimensional motion path of individual points on the UHMWPE bearing surface, and (b) measurement of three-dimensional distance of the outlined motion paths. Due to the shallow articulation between the convex and concave parts, only 13 discrete points (Figure 4.7) around the polar region of concave CoCrMo part were chosen for charting the motion path that traverses on the UHMWPE bearing surface.

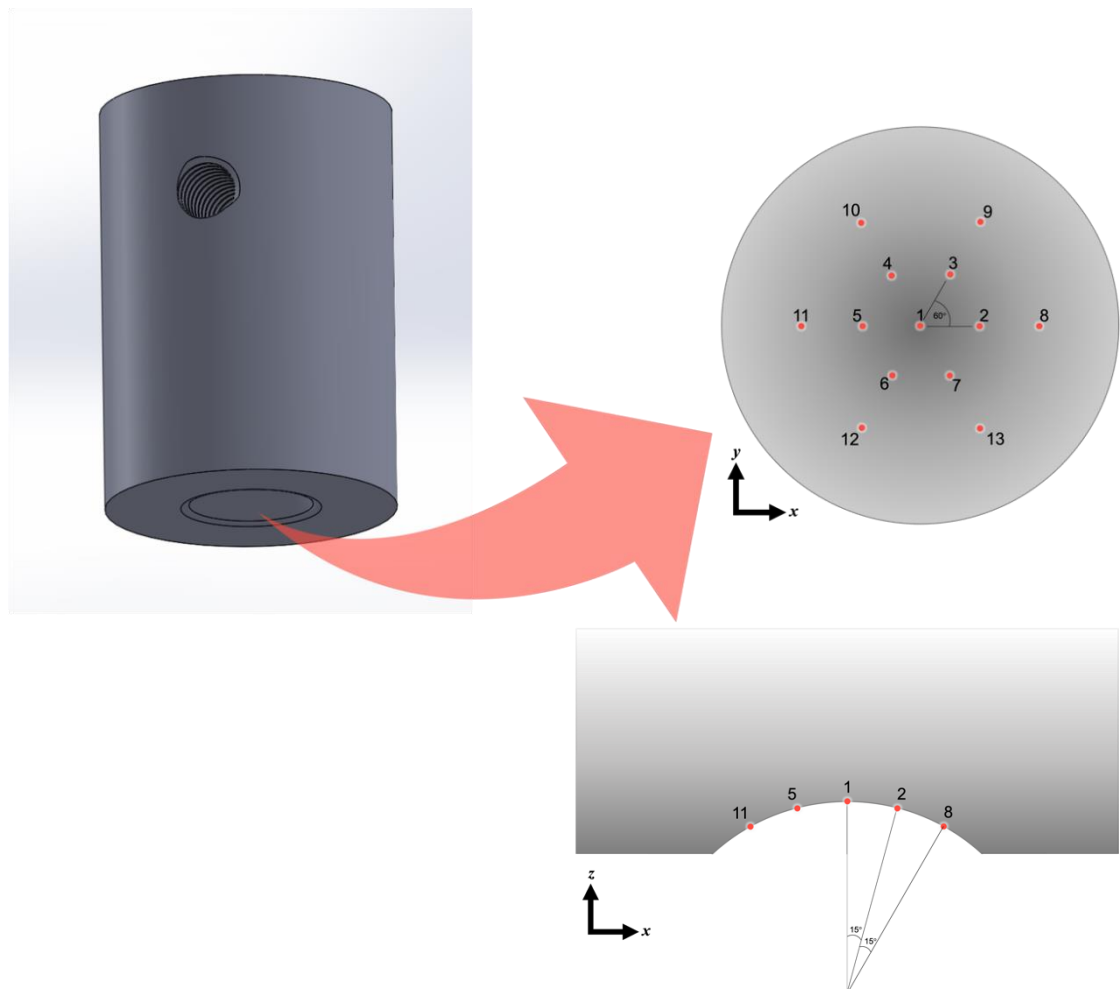


Figure 4.7 Location of thirteen discrete points on concave surface of CoCrMo part for calculation of motion path (top: inferior view, bottom: cross-section view)

Using the coordinate conversion matrix published by Budenberg *et al.* [249], the three-dimensional motion path for each point that traverses on the convex UHMWPE surface was outlined in 128 increments, based on the 128-point simulator input for both ISO18192-1 [1] and ADL Flexion/Extension wear profiles, until a full cycle path was completed. The formula for the matrix conversion is shown in Equation 4.4 and illustrated by Figure 4.8 for visualisation.

$$\begin{pmatrix} x_{i+1} \\ y_{i+1} \\ z_{i+1} \end{pmatrix} = \begin{pmatrix} \cos \beta \cos \gamma & \sin \alpha \sin \beta - \cos \alpha \cos \beta \sin \gamma & \sin \alpha \cos \beta \sin \gamma + \cos \alpha \sin \beta \\ \sin \gamma & \cos \alpha \cos \gamma & -\sin \alpha \cos \gamma \\ -\sin \beta \cos \gamma & \cos \alpha \sin \beta \sin \gamma + \sin \alpha \cos \beta & \cos \alpha \cos \beta - \sin \alpha \sin \beta \sin \gamma \end{pmatrix} \cdot \begin{pmatrix} x_i \\ y_i \\ z_i \end{pmatrix}$$

Equation 4.4 [249]

$\begin{pmatrix} x_{i+1} \\ y_{i+1} \\ z_{i+1} \end{pmatrix}$ coordinate for the next incremental point

$\begin{pmatrix} x_i \\ y_i \\ z_i \end{pmatrix}$ coordinate for the index point

α angular displacement in flexion/extension direction during next incremental point (based on 128-point simulator input)

β angular displacement in lateral bending direction during next incremental point (based on 128-point simulator input)

γ angular displacement in axial rotation direction during next incremental point (based on 128-point simulator input)

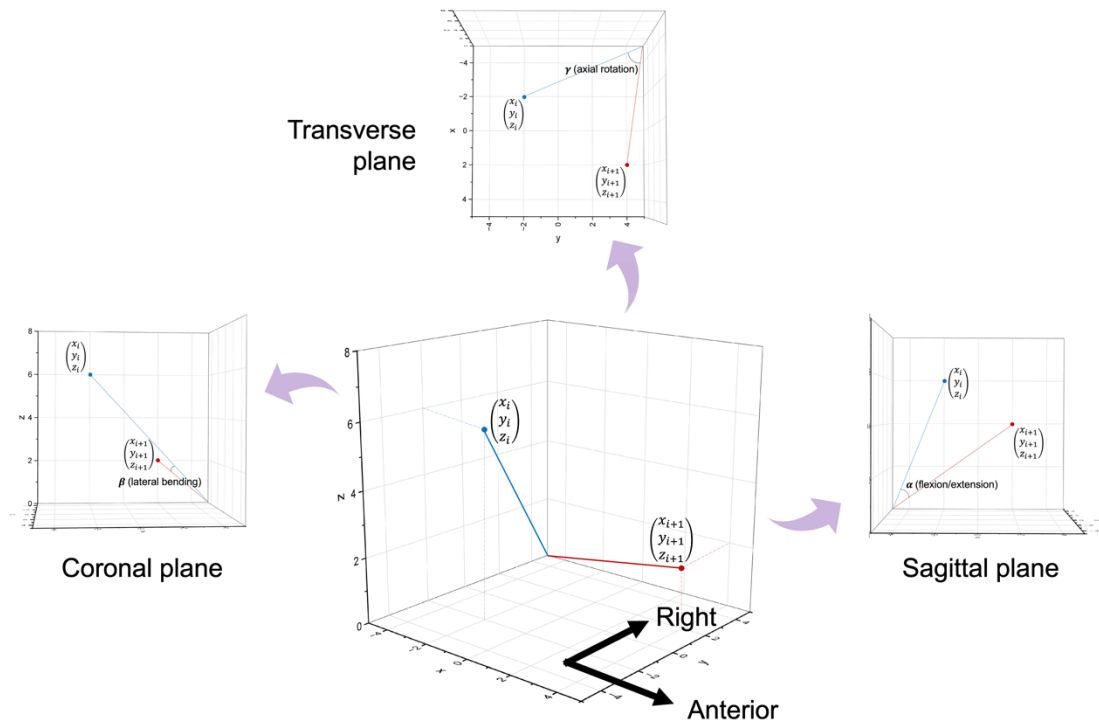


Figure 4.8 An illustration of a conversion from index coordinate point to the next incremental coordinate based on angular displacement of flexion/extension, lateral bending, axial rotation given in wear profile

Then, the three-dimensional distance of the outlined motion path for every discrete point was calculated, using the formula proposed by Bennett *et al.* [250]. For every discrete point, the distance between those 128 incremental coordinates were added together until it returned to the first coordinate. The formula for the sliding distance is shown in Equation 4.5.

$$\sum_{i=1}^{i=128} \left[\sqrt{(x_{(i+1)} - x_i)^2 + (y_{(i+1)} - y_i)^2 + (z_{(i+1)} - z_i)^2} \right]$$

Equation 4.5 [250]

4.1.6.2 Estimation of Aspect Ratio for Individual Point's Motion Path

The three-dimensional motion paths outlined in Section 4.1.6.1 can be used to estimate an aspect ratio, an indicator for its multidirectionality, for any of these individual points. This also was done in two stages: (a) projecting the three-

dimensional path onto two-dimensional plane and (b) measuring the path's dimensional geometric length within the two-dimensional plane.

The three-dimensional motion path was projected into two-dimensional locus through zenithal equidistant projection formula proposed by Bennett *et al.* [250]. The zenithal equidistant projection formula is shown in Equation 4.6.

$$\begin{pmatrix} x_{2D} \\ y_{2D} \end{pmatrix} = \begin{pmatrix} \frac{rx_i[\cos^{-1}(z_i/r)]}{\sqrt{x_i^2 + y_i^2}} \\ \frac{ry_i[\cos^{-1}(z_i/r)]}{\sqrt{x_i^2 + y_i^2}} \end{pmatrix}$$

Equation 4.6 [250]

r radius of hemisphere

Then, two measurements were taken from the projection, (a) the length of the longest distant between two points in the locus, "L", and (b) the separation length between two lines that are parallel with L that bordering the locus, "B". Then, aspect ratio of the loci was derived from the proportion of measurement "L" from measurement "B" *i.e.* L/B [250].

4.1.7 Surface Roughness Measurement

As well as cleaning and weighing of the samples, the UHMWPE convex bearing surface was also scanned using Alicona Infinite Focus (Bruker, Massachusetts, United States), a focus variation microscope, at all gravimetric measurement time points throughout the wear simulation surface roughness assessment.

The bearing surface was wipe-cleaned with isopropyl alcohol prior to be scanned. Then, the UHMWPE convex part was placed at the centre of the Alicona's scanning stage with its fixation hole facing north of the stage. The scanning light was set to confocal only. At 5× magnification lens, the focus was adjusted to have

a clear visual of the highest point of the convex dome and centred to the visual field. The process of focussing the lens was repeated using higher optical lens power until it reached 20× magnification and the pole area was set as a reference point. Once the brightness and contrast ratio had been adjusted, the scan boundaries were set to be 3 mm around the reference point. Settings of the scan were set to 2.94 μm for lateral resolution and 0.04 – 0.05 μm for vertical resolution. These settings were based on work by Holland *et al.* [251]. A three-dimensional scan was then performed on the focussed UHMWPE hemispheric bearing surface.

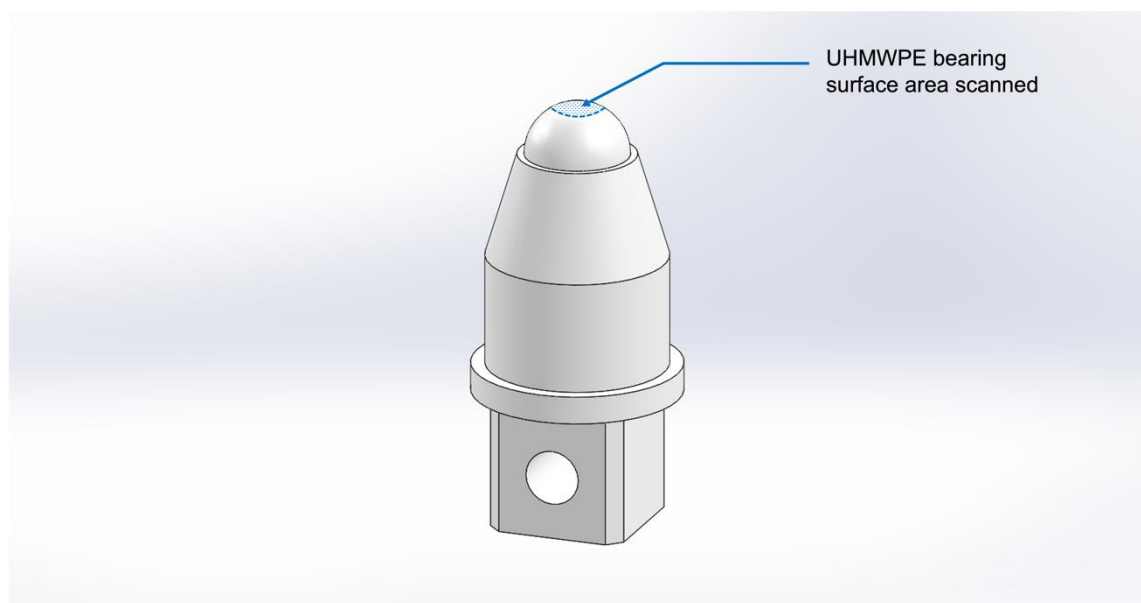


Figure 4.9 Illustration of the location of the scanned area from the UHMWPE convex bearing surface

The scanned data was processed using Vision64 Map software (Bruker, Massachusetts, United States). The ‘form’ of three-dimensional surface data was removed using high-pass Butterworth filter. Noise present in the scanned data was removed *e.g.* pixel pitting. Surface areal analysis function was performed onto the noise-freed, ‘flattened’ three-dimensional data to obtain areal topographical parameters. The calculated topographical parameters for all UHMWPE parts for all simulation time points were plotted.

4.2 Results

4.2.1 ISO18192-1 Wear Test on Cervical Disc Replicas

Three replica bearing pairs (UHMWPE-CoCrMo) were successfully tested under loads and kinematics parameters from ISO18192-1 [1] over five million cycles with another bearing pair acted as a soak control where only loading parameter was applied. The bearing pairs used in this study, labelled 012, 014, and 016, were setup on Station 1, 2, and 3, respectively, whilst 018 was used as a soak control at Station 4 of the joint simulator.

4.2.1.1 Pre-simulation UHMWPE Fluid Sorption

During the pre-simulation soaking period, all four UHMWPE convex parts were losing its mass in the last two measurement intervals prior to the start of the wear test. Nonetheless, the daily rate of fluid loss was less than 10% than the previous

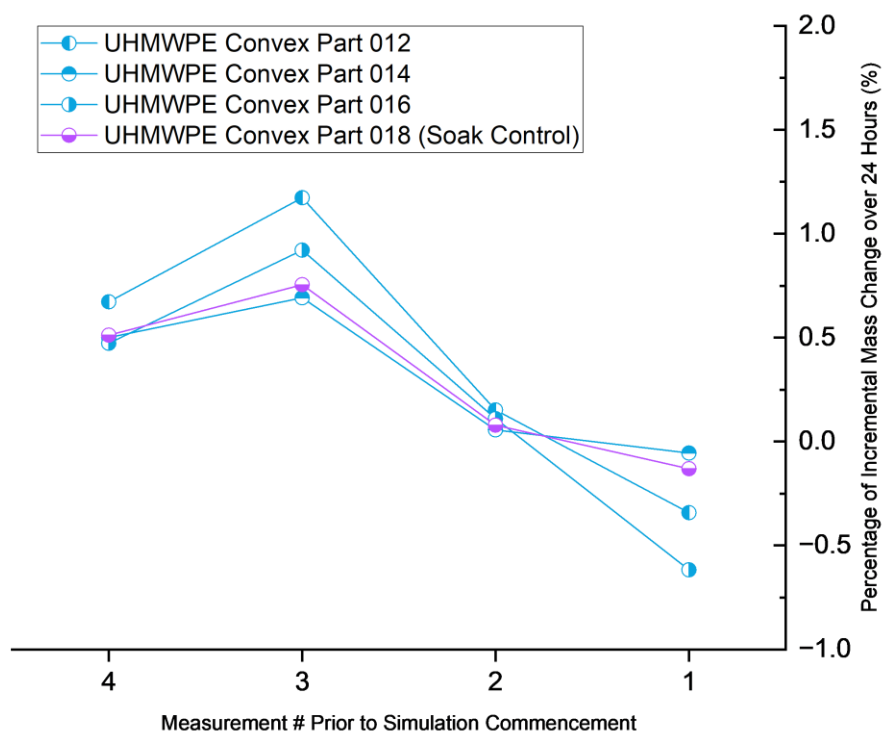


Figure 4.10 Percentage of incremental mass change of UHMWPE convex parts over 24 hours during soaking protocol prior to ISO18192-1 [1] wear simulation

cumulative mass change for each individual part in the last four measurement intervals. The final four measurements of percentage mass change of each UHMWPE part before the commencement of the simulation are shown in Figure 4.10.

4.2.1.2 ISO18192-1 Pilot Test Output Verification

All actuator motors for angular motion as well as axial force were successfully tuned to be within the magnitude and phasing tolerances set by the ISO18192-1 [1] based on the individual stations' load cell readings. A one-cycle sample of angular motion verification data taken from load cells reading during ISO18192-1 [1] pilot simulation are shown in Figure 4.11. The joint simulator was able to closely meet the input demands from ISO18192-1 [1] for all three angular motions in all the stations that all of the output lines are overlapping on each other, as seen on the graphs.

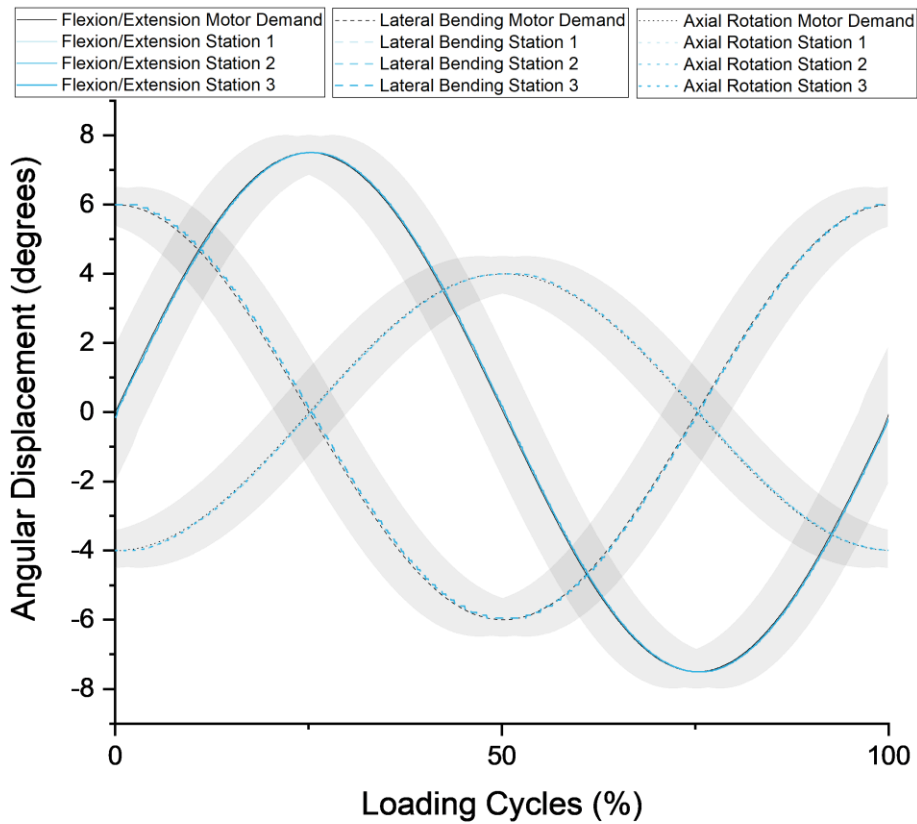


Figure 4.11 Sample of load cells' angular displacement readings during pilot run of ISO18192-1 [1] wear simulation against its tolerances (shaded grey)

The axial loading actuator motor was also successfully tuned to the magnitude and phasing tolerances set in ISO18192-1 [1] ($\pm 5\%$ of the maximum force value for the cycle, $\pm 3\%$ of the full cycle time for phasing) for the standard wear simulations. A sample of loading verification data taken during ISO18192-1 [1] pilot simulation is shown in Figure 4.12. As seen in the graphs, the electromechanical hip-joint simulator was able to meet the axial loading input demands in all three stations within the grey shaded tolerance requirements for ISO18192-1 [1] wear testing profile.

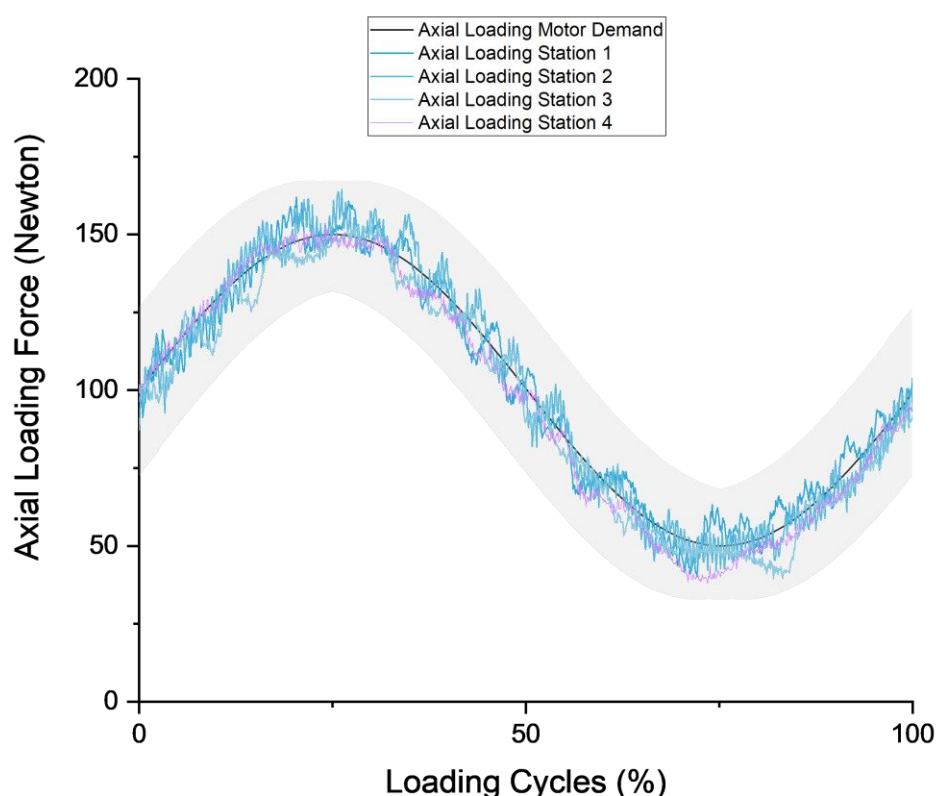


Figure 4.12 Sample of load cells' axial loading readings during pilot run of ISO18192-1 [1] wear simulation against its tolerances (shaded grey)

4.2.1.3 UHMWPE Gravimetric Wear Rate

The UHMWPE Convex Part 018 for soak control continued to lose its mass throughout the wear simulation (Figure 4.13) and the amount of mass loss at each time point was used to offset the mass loss in other sliding UHMWPE parts due to factors other than wear, at the said time point during gravimetric measurement (Figure 4.14).

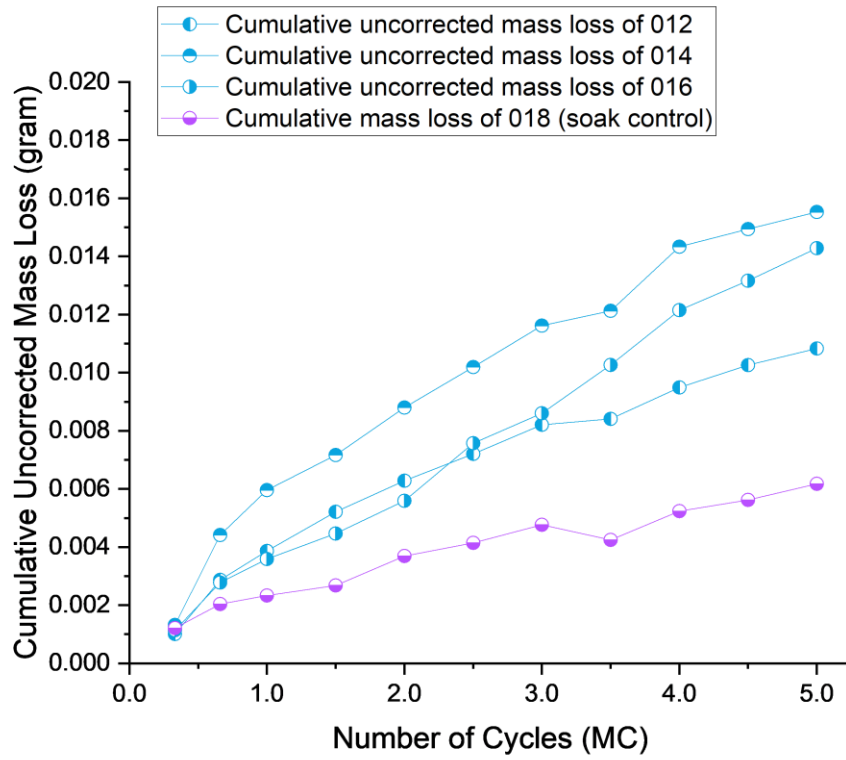


Figure 4.13 Cumulative uncorrected mass loss of all UHMWPE convex parts during ISO18192-1 [1] wear simulation

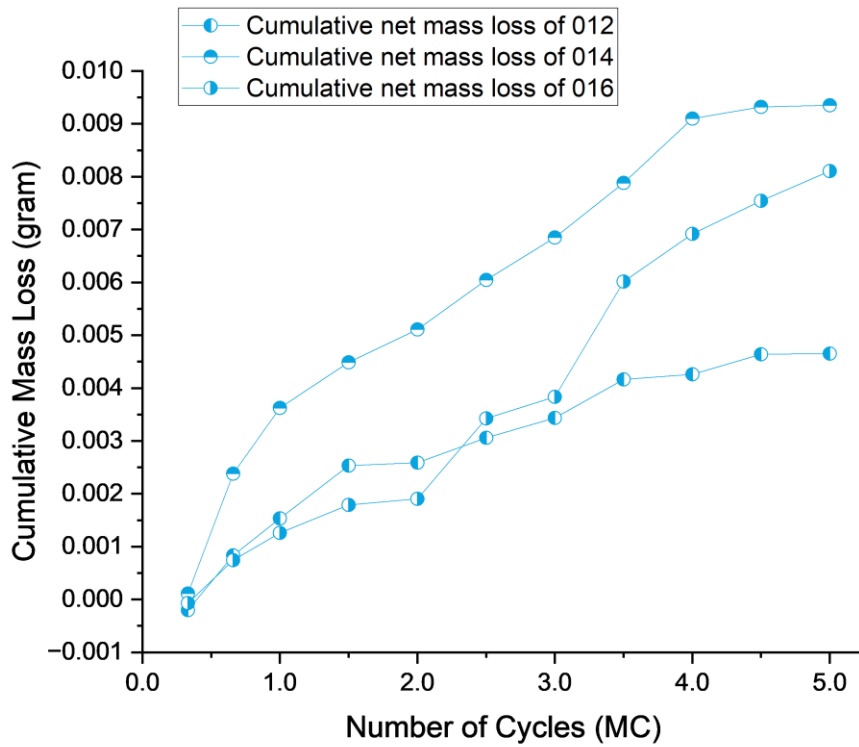


Figure 4.14 Cumulative net mass loss of sliding UHMWPE convex parts during ISO18192-1 [1] wear simulation after being offset by soak control

The plotted graph of average wear rate for ISO18192-1 [1] simulation parameters shows a distinct bedding-in period during the first million cycles of the simulation (Figure 4.15). The gravimetric wear rate during bedding-in period is 3.56 ± 0.42 mg/million cycles whereas the gravimetric wear rate during simulation's steady-state is 1.42 ± 0.071 mg/million cycles.

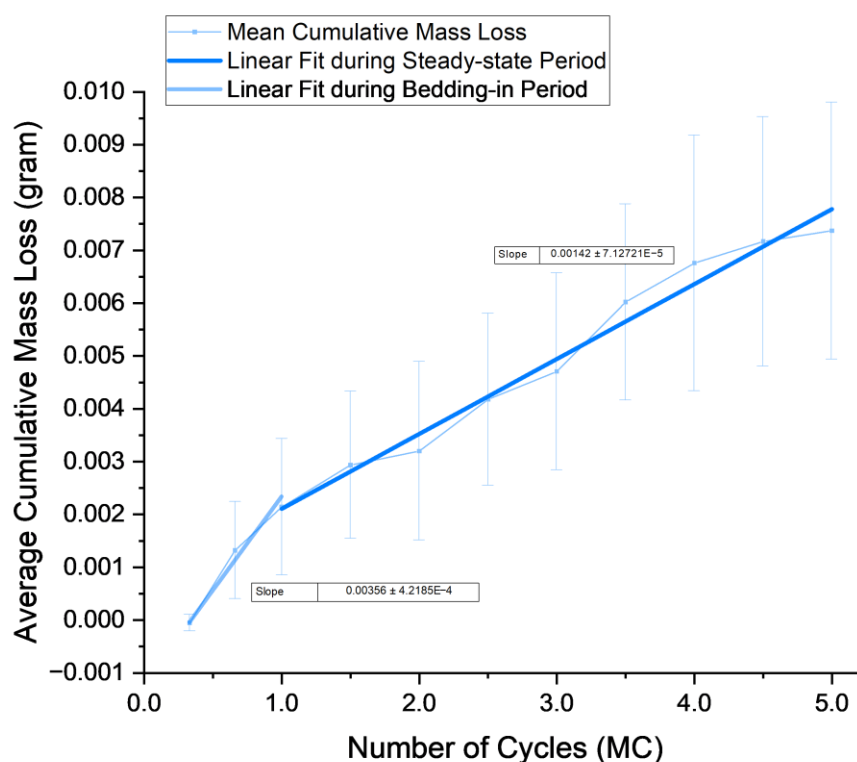


Figure 4.15 Average (\pm standard deviation) wear rate of sliding UHMWPE convex parts during ISO18192-1 [1] wear simulation based on linear regression

4.2.1.4 Analysis of Variance

Based on normality test using Shapiro-Wilk method, the net mass loss (as opposed to cumulative mass loss) from all UHMWPE Parts at every time point during steady-state wear simulation under parameters set by ISO18192-1 [1] does not indicate the observation values are distributed normally. Thus, the variance in net mass loss for each individual part as well as for each measurement time point were tested non-parametrically, using Friedman's test. This test shows that there are no significant difference within the results observed between all three UHMWPE parts ($p = 0.121$) and between all nine steady-state measurement time points ($p = 0.083$).

4.2.1.5 Motion Path, Sliding Distance, and Aspect Ratio

The motion paths of the 13 discrete points on CoCrMo that traverse on the convex UHMWPE surface for ISO18192-1 [1] wear simulation are illustrated three-dimensionally in Figure 4.16. The sliding distance as well as the aspect ratio for each motion path are given in the Table 4.8. The two-dimensional projection of all the motion paths are illustrated in Figure 4.17.

In general, all the motion paths are elliptical in shape and tend to be rounder and bigger anteriorly and more oblong and narrower posteriorly. This is also reflected in their sliding distances where the length is longer for points located anteriorly than points located posteriorly. Similarly, points located anteriorly tend to be more multidirectional with their aspect ratios closer to one than points located posteriorly with their aspect ratios tend to be higher than one.

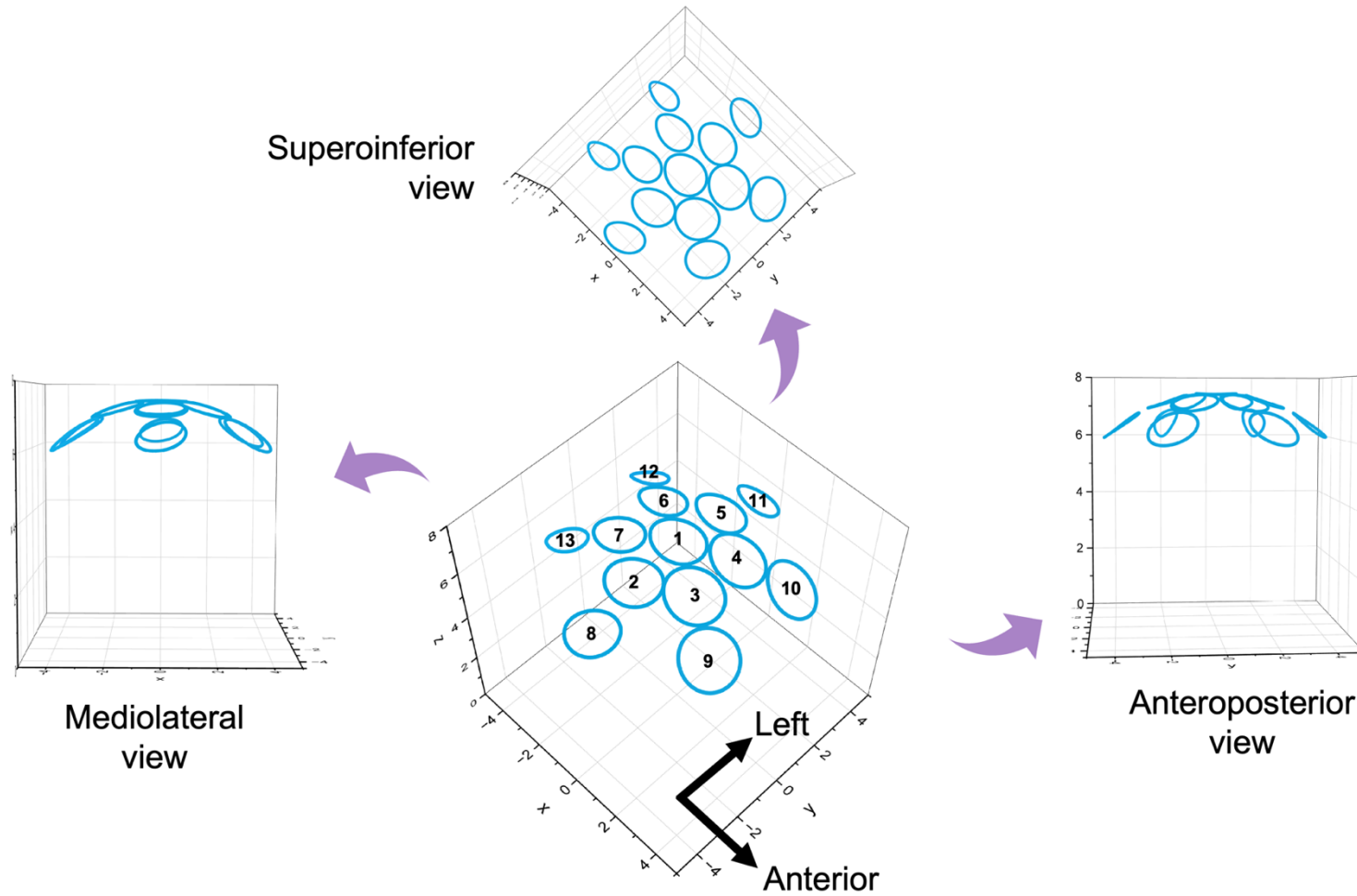


Figure 4.16 Three-dimensional motion path for thirteen discrete points on the surface of UHMWPE convex part during ISO18192-1 [1] wear simulation

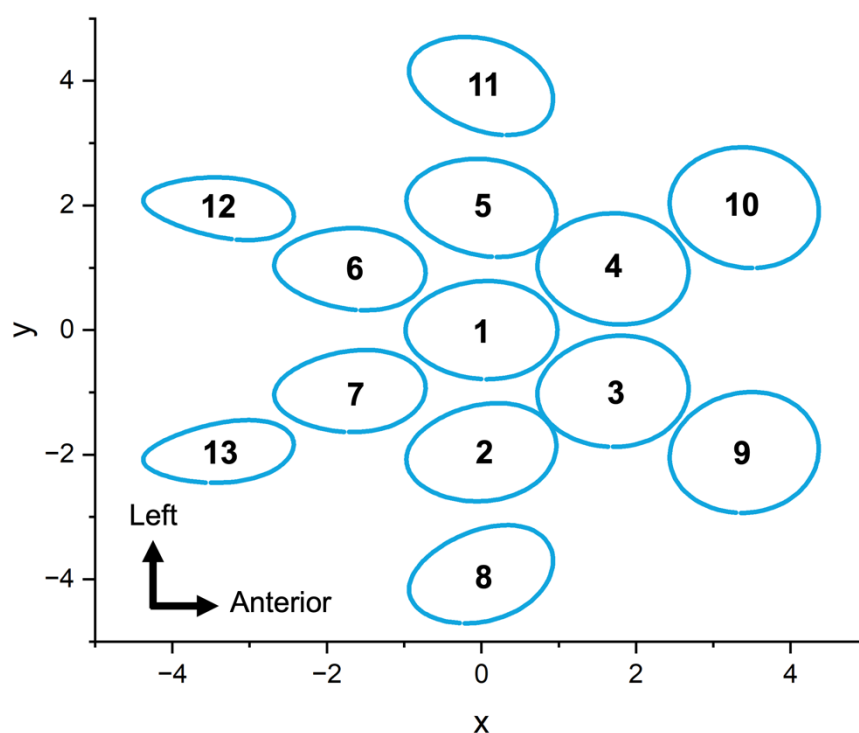


Figure 4.17 Two-dimensional projection of motion path for thirteen discrete points during ISO18192-1 wear simulation

| Point | Location of Point (viewed from top) | Sliding Distance (millimetres) | Aspect Ratio |
|---------------------------|--|--------------------------------|--------------|
| 1 | Pole | 5.56 | 1.50 |
| 2 | Inner ring – east | 5.47 | 1.57 |
| 3 | Inner ring – northeast | 5.82 | 1.38 |
| 4 | Inner ring – northwest | 5.82 | 1.38 |
| 5 | Inner ring – west | 5.47 | 1.62 |
| 6 | Inner ring – southwest | 5.15 | 1.18 |
| 7 | Inner ring – southeast | 5.15 | 1.18 |
| 8 | Outer ring – east | 5.23 | 1.65 |
| 9 | Outer ring – northeast | 5.91 | 1.27 |
| 10 | Outer ring – northwest | 5.91 | 1.27 |
| 11 | Outer ring – west | 5.23 | 1.65 |
| 12 | Outer ring – southwest | 4.66 | 1.38 |
| 13 | Outer ring – southeast | 4.66 | 1.38 |
| Mean | | 5.39 | 1.41 |
| Standard Deviation | | 0.43 | 0.17 |

Table 4.2 The estimation on sliding distance of thirteen discrete points during ISO18192-1 [1] wear simulation

4.2.1.6 UHMWPE Bearing Surface Analysis

A coarse visual assessment of the UHMWPE convex surfaces seen from 100 stitched images of 20× magnification scanned data, revealed a variable topographical pattern across all samples throughout the simulation. The location of the scanned area is illustrated in Figure 4.18. At 0.6 million cycles, UHMWPE Part 012 already showed a polishing effect throughout the bearing surface as well as a distinct elliptical wear scar seen at the polar region (Figure 4.19). Meanwhile, UHMWPE Part 014 showed several noticeable linear scarrings with polishing effects present outside the polar area. The polar region of Part 014 has retained some manufacturing machining marks even at 4.5 million cycles (Figure 4.20). At 0.6 MC, UHMWPE Part 016 exhibited a substantial elliptical wear scarring at a latitudinal band around the polar region as well as roughened polar area (Figure 4.21). In soak control, UHMWPE Part 018 has retained much of the machining marks throughout the bearing surface at the conclusion of the wear simulation (5.0 MC) with some linear scarrings (Figure 4.22).

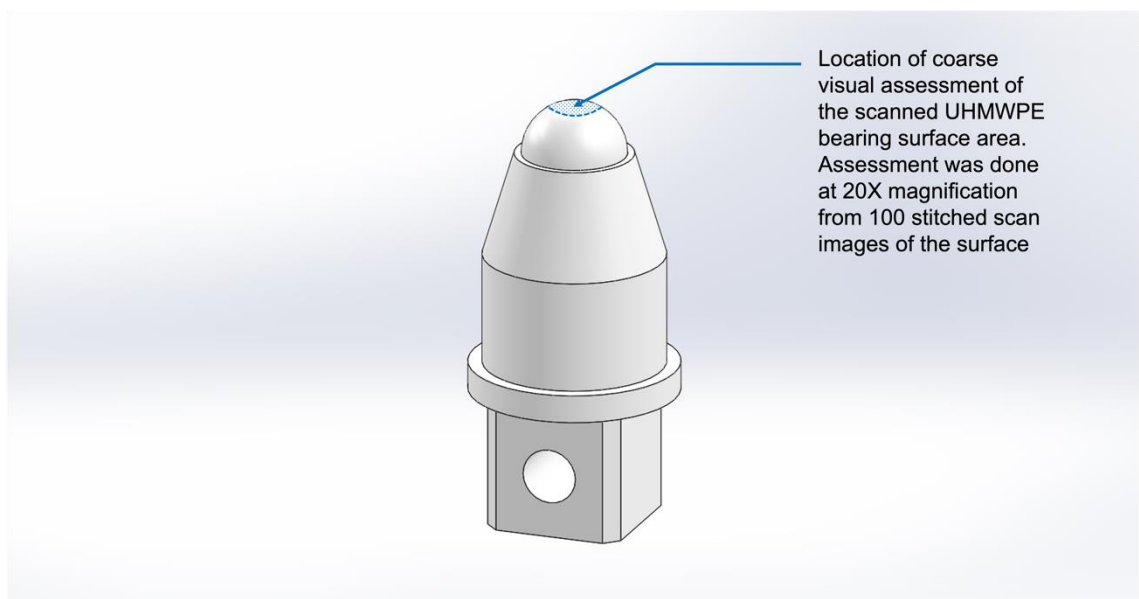


Figure 4.18 An illustration of the location of 100 stitched scanned images at 20× magnification for course visual assessment

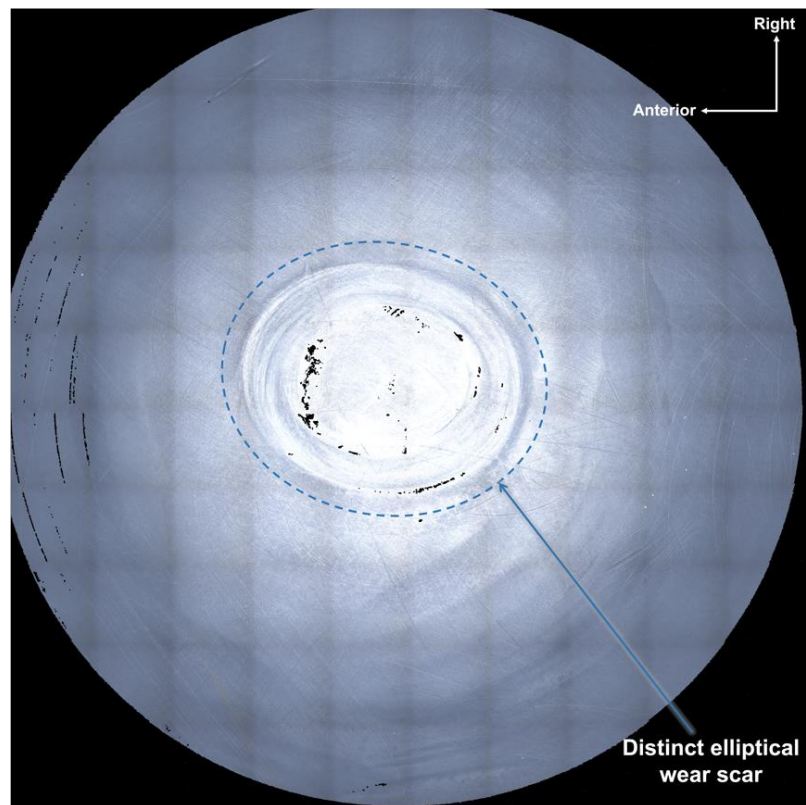


Figure 4.19 Bearing surface of UHMWPE Part 012 at 0.6 MC of ISO18192-1 [1] wear simulation

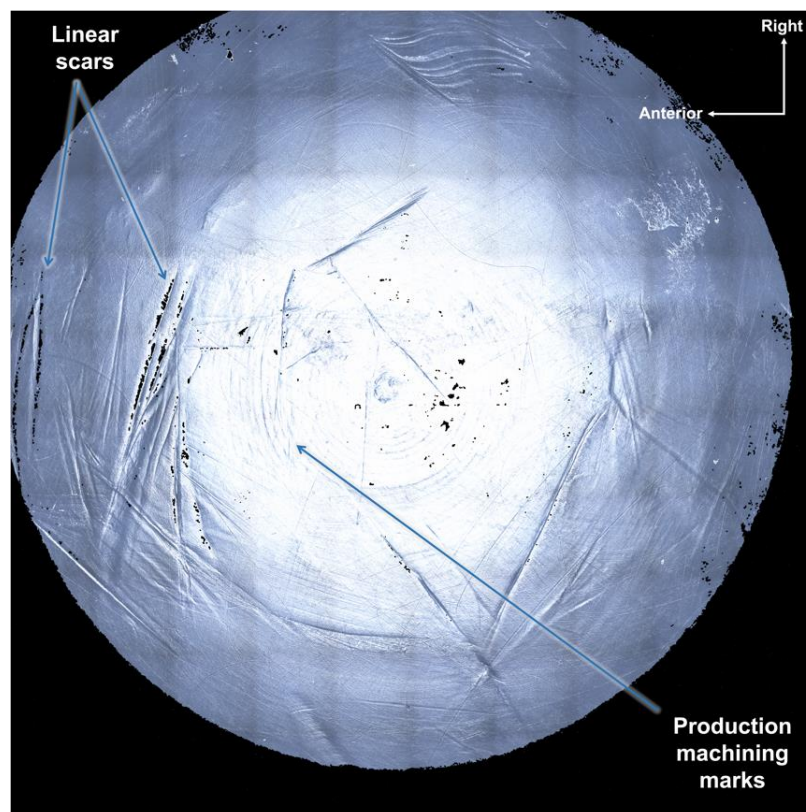


Figure 4.20 Bearing surface of UHMWPE Part 014 at 4.5 MC of ISO18192-1 [1] wear simulation

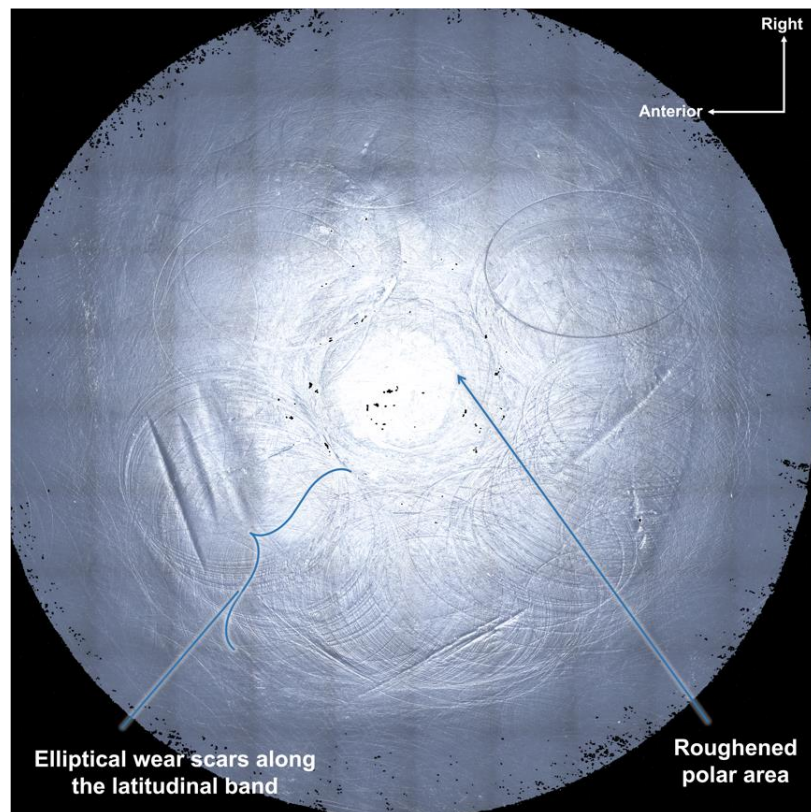


Figure 4.21 Bearing surface of UHMWPE Part 016 at 0.6 MC of ISO18192-1 [1] wear simulation

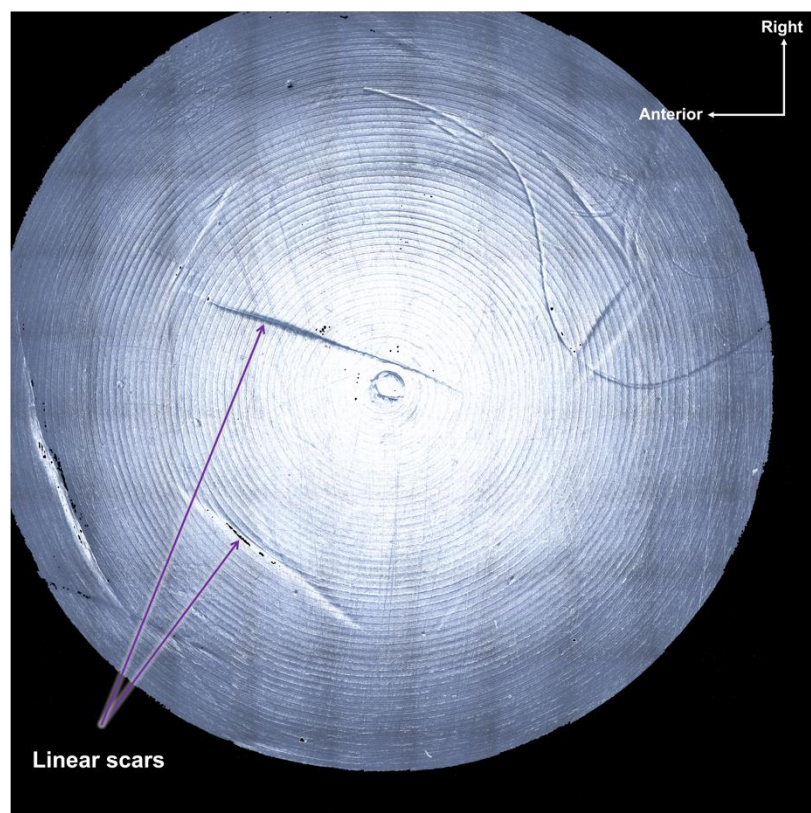


Figure 4.22 Bearing surface of UHMWPE Part 018 (soak control) at 5.0 MC of ISO18192-1 [1] wear simulation

At 10× magnification, a sequential, qualitative visual assessment of the polar region between 3.5 MC to 5.0 MC also showed mixed observation amongst the UHMWPE parts (Figure 4.23, Table 4.3). A changing direction of linear micro-scarring could be seen throughout that simulation period on UHMWPE Part 012 over a generally smooth surface background as well as a faint elliptical scar at the pole. UHMWPE Part 014 showed a minimal change during that time period with significant scarring and machining marks still visible, as noted in coarse assessment in Figure 4.20. The polar region on UHMWPE Part 016 showed an ever-changing roughened and raised pattern over the course of last 1.5 million cycles (Figure 4.21). Meanwhile, UHMWPE Part 018 has retained much of the machining marks with a linear scar appeared between 3.5 to 4.0 million cycles and remained until the end of the simulation.

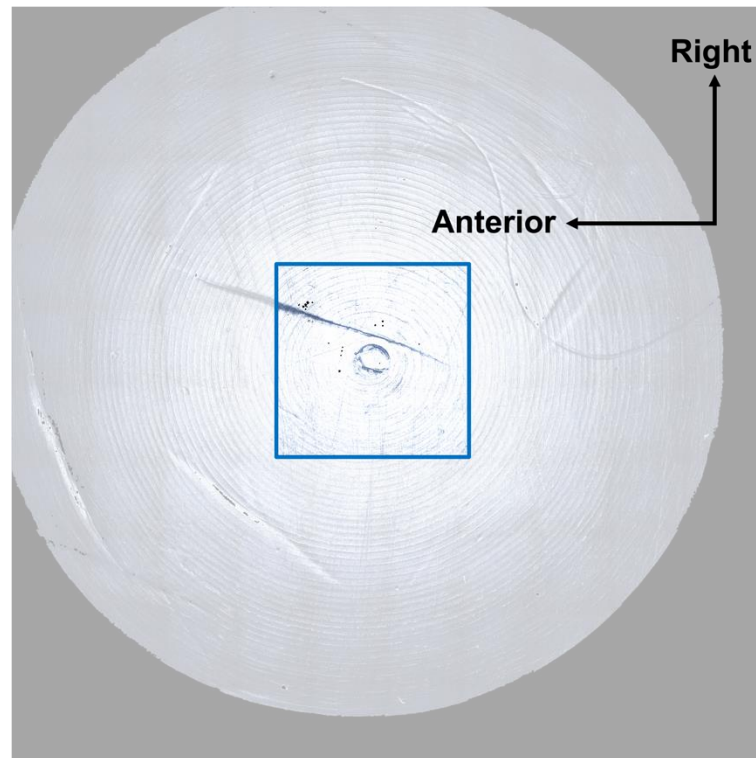


Figure 4.23 Location of qualitative visual assessment of the polar region of UHMWPE convex part at 10× magnification relative to the scanned area

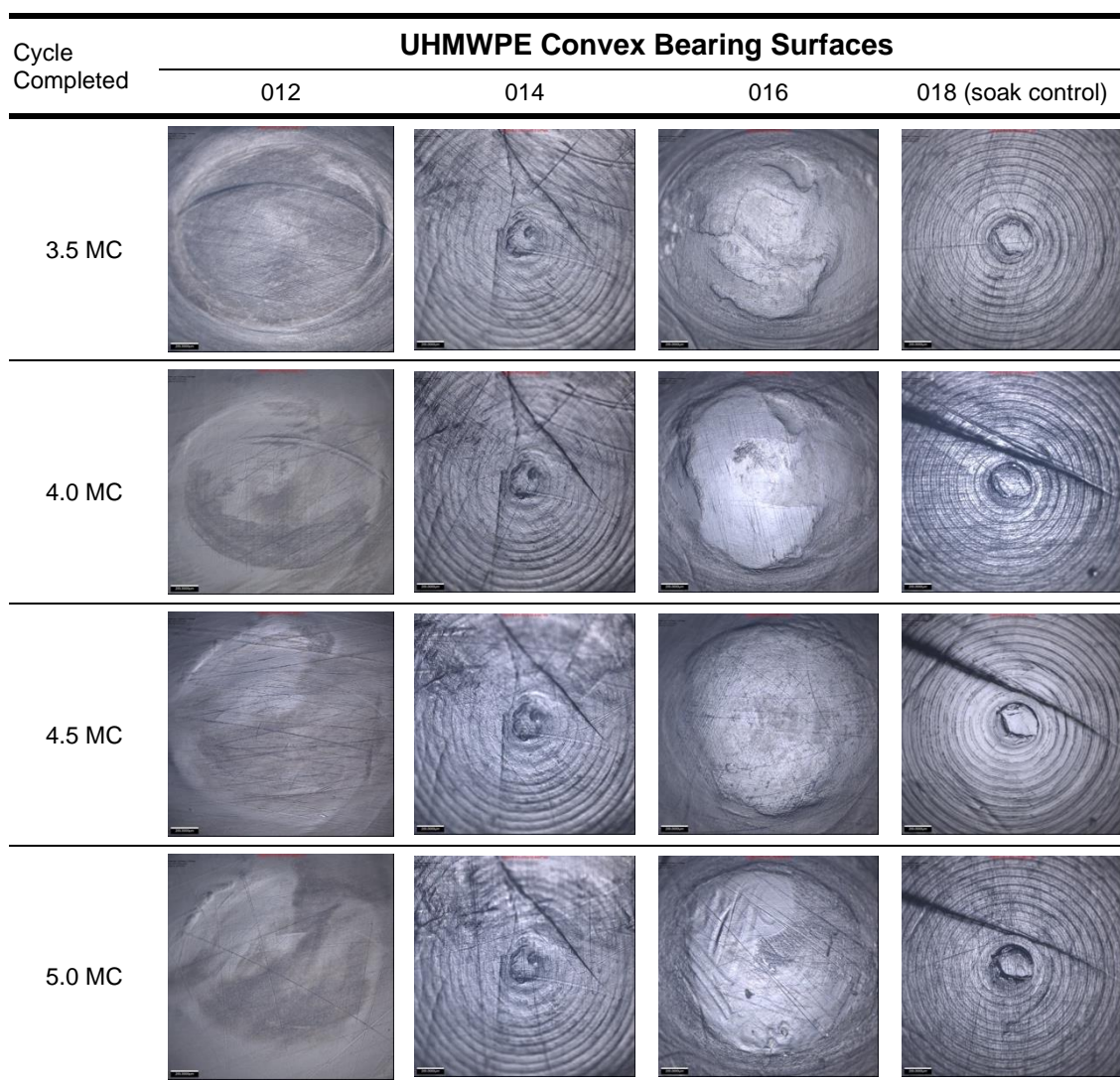


Table 4.3 Sequential bearing surface image of UHMWPE convex parts during the last 1.5 MC of ISO18192-1 [1] wear simulation at 10x magnification

A general quantitative areal surface roughness measurement, S_a , was also carried out on the scanned bearing surfaces from all UHMWPE parts. Throughout the wear simulation, the average overall surface roughness for 012, 014, and 016 was between 300 to 400 nm and it was consistently lower than Part 018 soak control, which was above 400 nm throughout 5.0 MC (Figure 4.24).

However, an average surface roughness of a 1 mm × 1 mm area, sampled consistently at the same location outside the polar region throughout the wear simulation, for all UHMWPE parts showed a more fluctuating pattern between 200 and 700 nm compared to the soak control where the S_a value hovered around 300 nm throughout the simulation (Figure 4.26). The 1 mm² sampling area was located in the southern region of the scanning area, about halfway between the

pole and the margin of the scanning area, where it was an area with the least affected by any significant linear scarring (Figure 4.25).

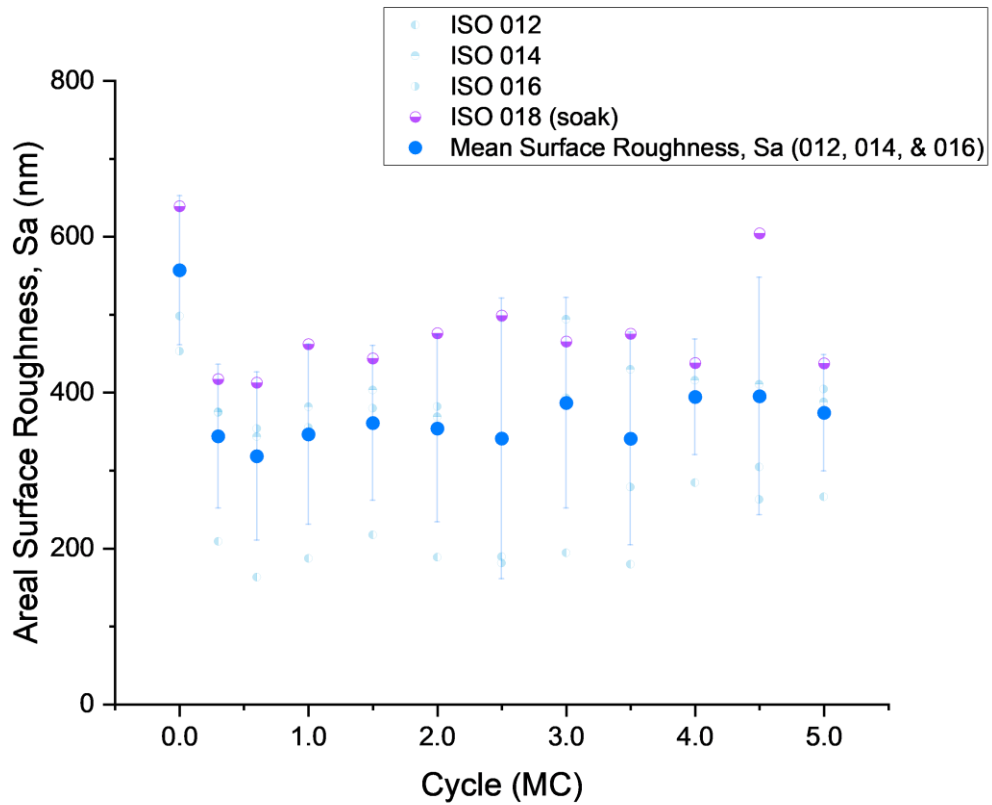


Figure 4.24 Average surface roughness of bearing surface on UHMWPE convex parts during ISO18192-1 [1] wear simulation

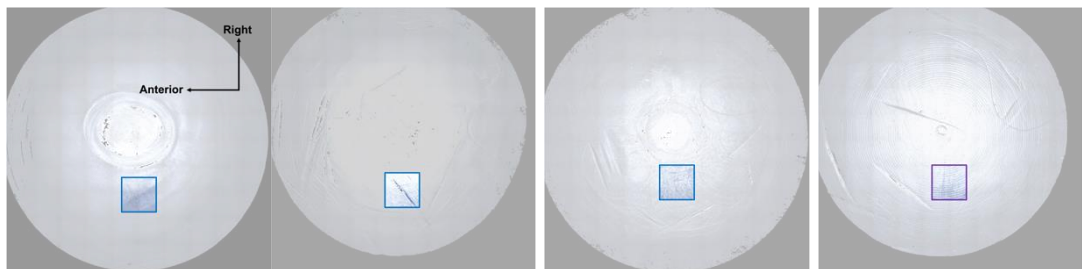


Figure 4.25 Location of 1 mm² sampled bearing surface on UHMWPE convex parts for Sa measurement during ISO18192-1 [1] wear simulation

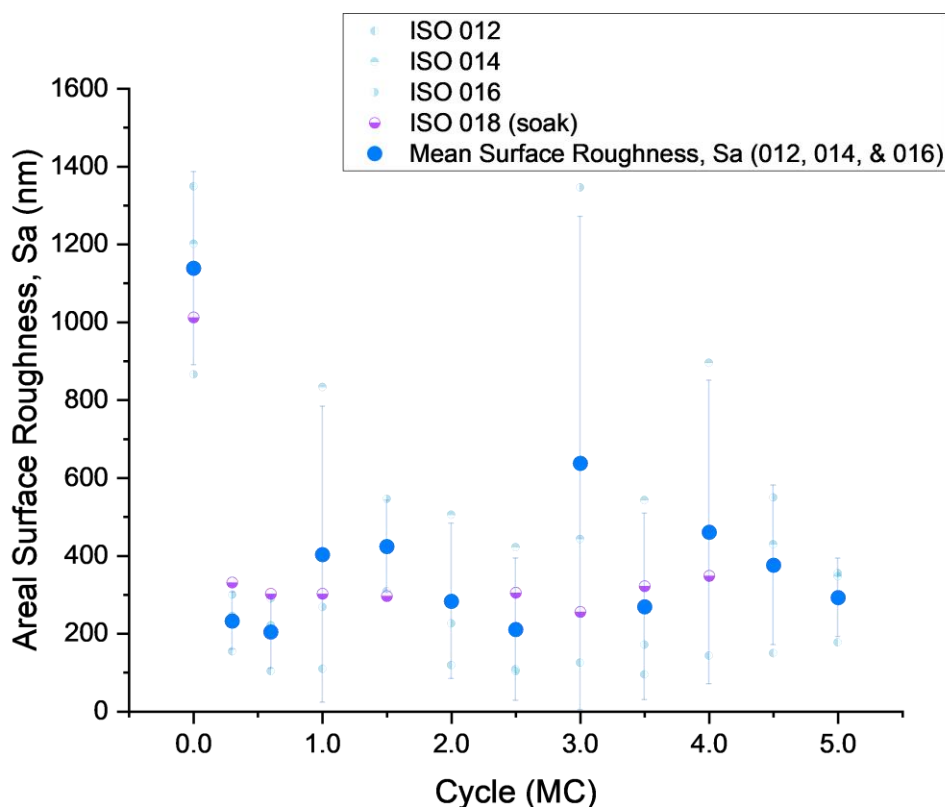


Figure 4.26 Average surface roughness of 1 mm² sampled bearing surface on UHMWPE convex parts during ISO18192-1 [1] wear simulation

4.2.2 ADL Flexion/Extension Wear Test on Cervical Disc Replicas

The five-million-cycle wear simulation using parameters from ADL Flexion/Extension wear profile was successfully completed on four UHMWPE-CoCrMo replica bearing pairs, including a soak control. The bearing pairs, labelled 011, 013, and 015, were setup on Station 1, 2, and 3, respectively, whilst 017 was used as soak control at Station 4 of the hip joint simulator.

4.2.2.1 Pre-simulation UHMWPE Fluid Sorption

After being soaked for several weeks, all four UHMWPE convex parts were gaining some mass in the second last measurement interval before three out of four UHMWPE convex parts were losing mass in the last measurement interval during pre-simulation soaking protocol period. The daily rate of fluid loss was, however, less than 10% than the previous cumulative mass change in the last four measurement intervals for each individual part, ranging between 0.0% to

2.0%. The final four measurements of percentage mass change of each UHMWPE part before the commencement of the simulation are shown in Figure 4.27.

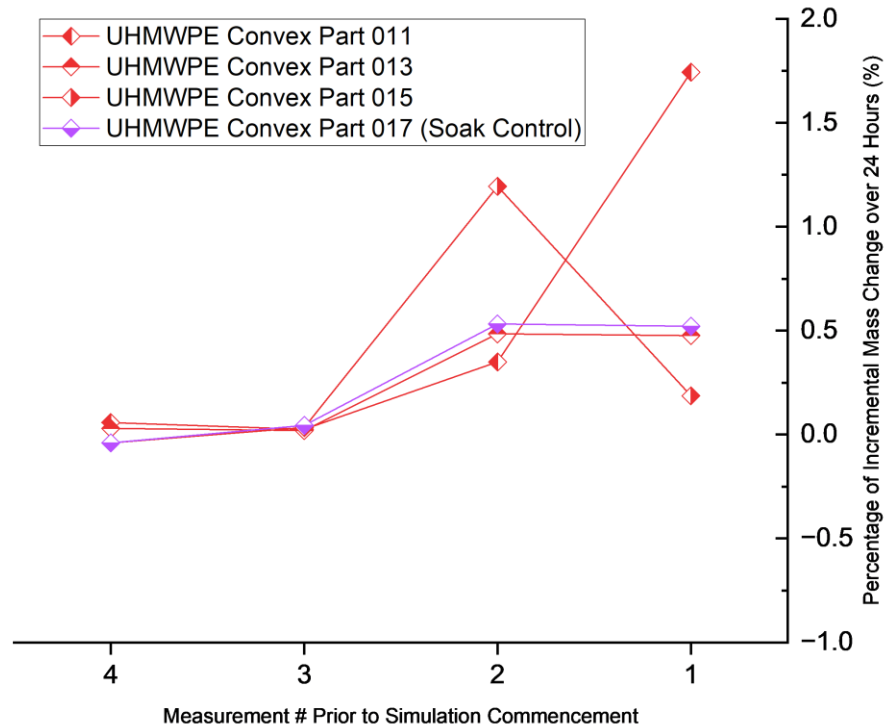


Figure 4.27 Percentage of incremental mass change of UHMWPE convex parts over 24 hours during soaking protocol prior to ADL Flexion/Extension wear simulation

4.2.2.2 ADL Flexion/Extension Pilot Test Output Verification

All actuator motors for angular motion were successfully tuned according to magnitude and phasing tolerance criteria stated in ISO18192-1 [1], which was adapted to comply with ADL Flexion/Extension wear profile. A one-cycle sample of angular motion verification data taken from load cells reading during ADL Flexion/Extension pilot simulation is shown in Figure 4.28. Once again, the hip-joint simulator was able to tightly meet the input demands from this newly formulated ADL wear profile for all three angular motions in all the sliding stations. All of the output lines are overlapping on each other, as seen on the graphs.

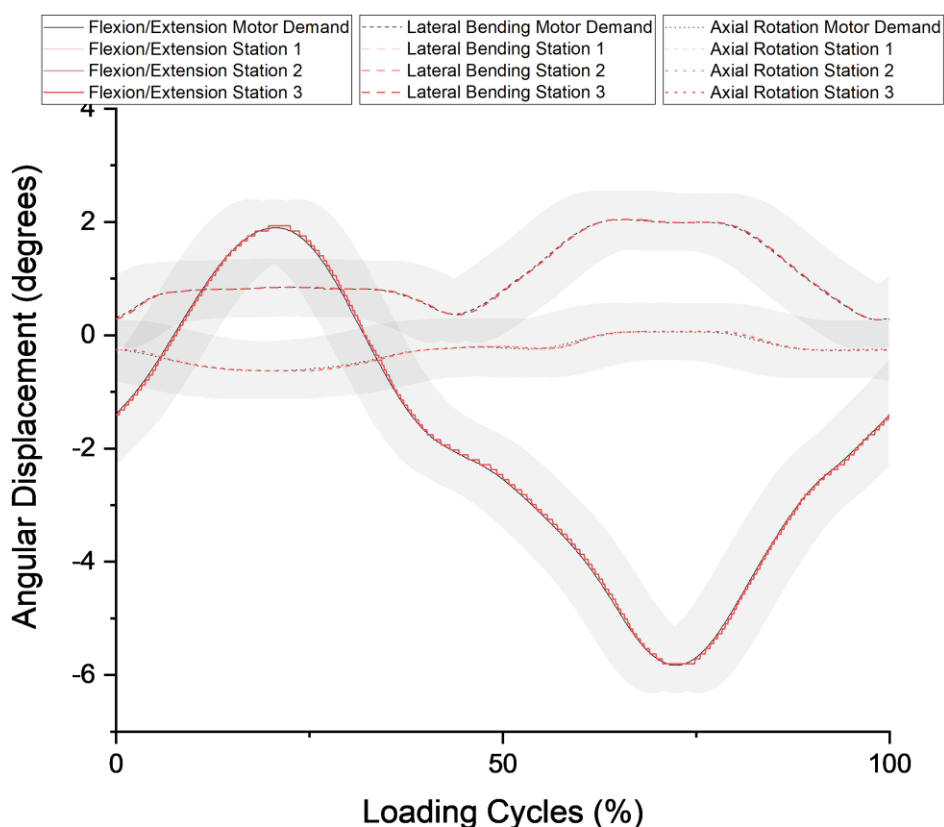


Figure 4.28 Sample of load cells' angular displacement readings during pilot run of ADL Flexion/Extension wear simulation against its own tolerances (shaded grey)

The axial loading actuator motor was also successfully tuned to be within the ISO18192-1 [1] criteria for the new ADL Flexion/Extension wear profile ($\pm 5\%$ of the maximum force value for the cycle, $\pm 3\%$ of the full cycle time for phasing). A sample of loading verification data taken during ADL Flexion/Extension pilot simulation is shown in Figure 4.29. As seen in the graphs, the electromechanical hip-joint simulator was able to meet the axial loading input demands in all three stations within the grey shaded tolerance of the ADL Flexion/Extension wear testing profile.

Additionally, the medial-lateral motor actuator was also tuned with the same tolerance criteria as this motor was also engaged, using load control, to simulate the anteroposterior loading within the cervical spine. A sample of loading verification data taken during the pilot simulation is also shown in Figure 4.29 (bottom three curves). Tuning of the medial-lateral load actuator to be within the same tolerance criteria set by ISO18192-1 [1] proved to be tricky given the load

demand in this direction is relatively low (0 N to 40 N). Based on the load cell's readings, the medial-lateral actuators are able to meet between 45-60% of the demand for all three stations at low input magnitude.

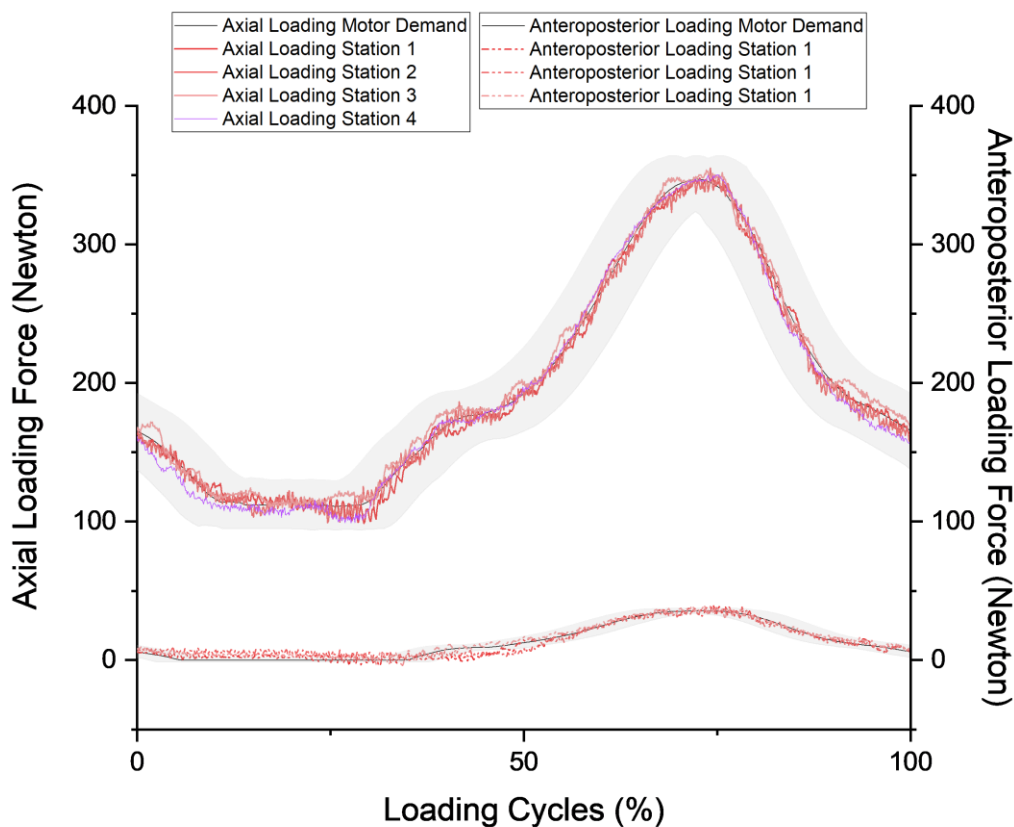


Figure 4.29 Sample of load cells' readings during pilot run of ADL Flexion/Extension wear simulation against its own tolerances (shaded grey). Solid lines (top three curves) represent the axial loadings whereas the dashed lines (bottom three curves) represent the anteroposterior loadings for all three stations.

4.2.2.3 UHMWPE Gravimetric Wear Rate

Throughout the wear simulation, the UHMWPE Convex Part 017 soak control continued to lose its mass (Figure 4.30) and this value was used to offset the mass loss in other UHMWPE sliding parts at each time point during gravimetric measurement (Figure 4.31). The gravimetric wear rate during the first million cycles is 1.78 ± 0.0062 mg/million cycles whereas the gravimetric wear rate after that is 1.26 ± 0.084 mg/million cycles (Figure 4.32).

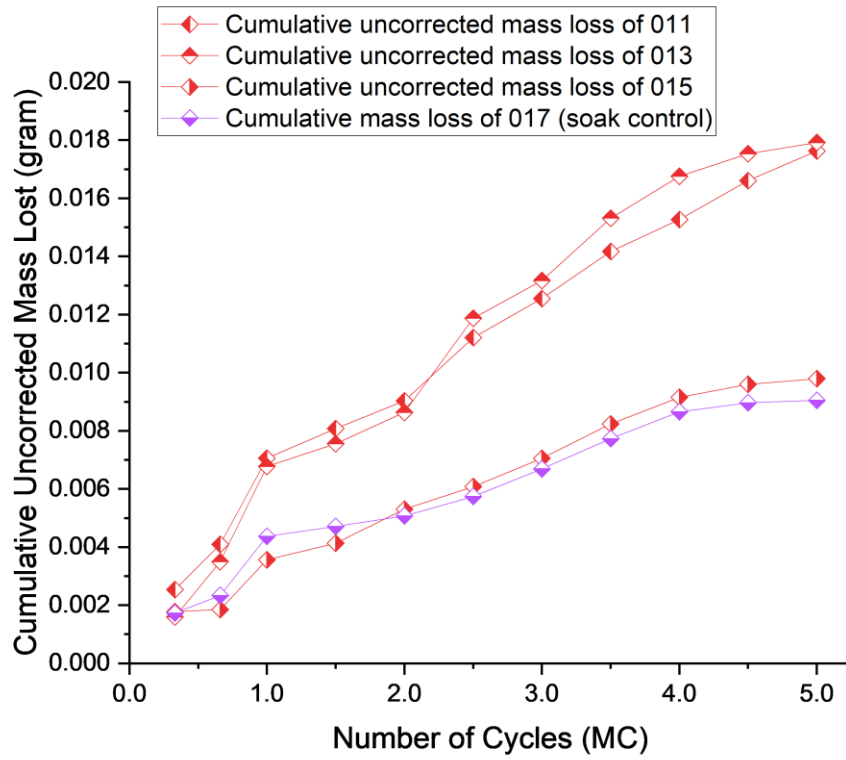


Figure 4.30 Cumulative uncorrected mass loss of individual UHMWPE convex parts during ADL Flexion/Extension wear simulation

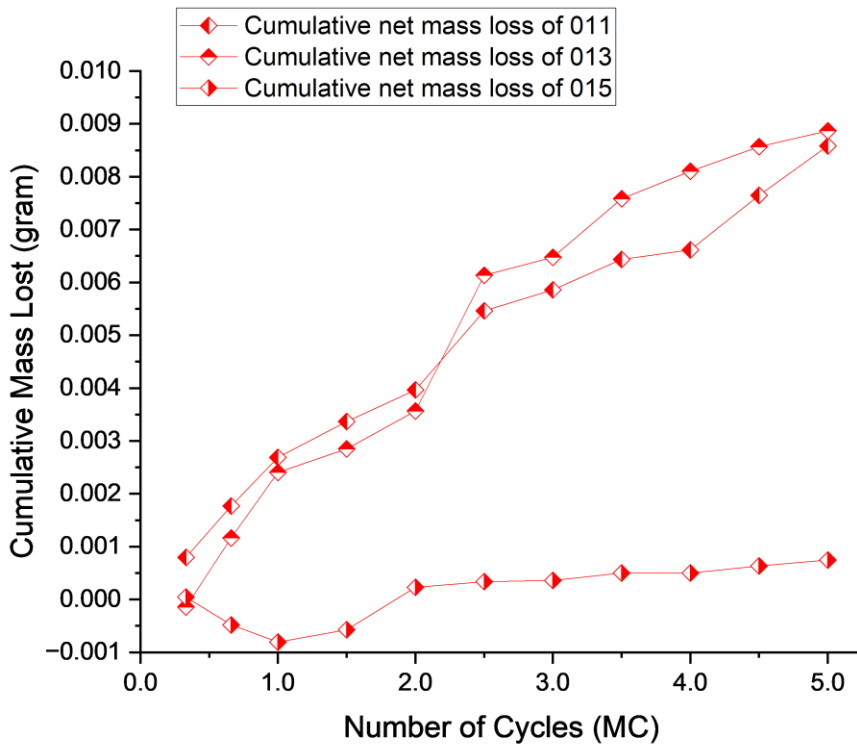


Figure 4.31 Cumulative net mass loss of individual UHMWPE convex parts during ADL Flexion/Extension wear simulation

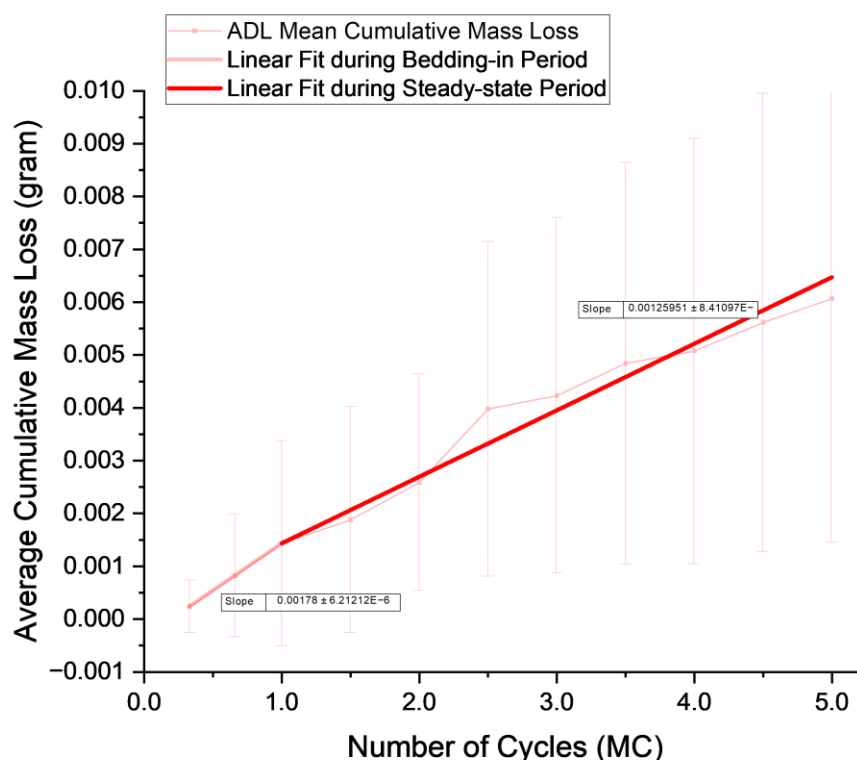


Figure 4.32 Average (\pm standard deviation) wear rate of UHMWPE convex parts during ADL Flexion/Extension wear simulation

4.2.2.4 Analysis of Variance

Similarly, the individual net mass loss from all UHMWPE Parts at every time point during steady-state ADL Flexion/Extension wear simulation does not indicate the observation values are distributed normally ($p < 0.01$), based on normality test using Shapiro-Wilk method. Thus, the variance in net mass loss for each individual UHMWPE part as well as for each measurement time point were tested non-parametrically, using Friedman's test. The test shows that there is a significant difference within the results observed between the three UHMWPE parts ($p = 0.016$). As seen in Figure 4.31, the cumulative mass loss from UHMWPE Part 015 seems to be an outlier amongst the three repeats (parts 011, 013, 015). However, there is no significant difference between net mass loss measurements taken throughout nine steady-state time points ($p = 0.367$).

4.2.2.5 Motion Path, Sliding Distance, and Aspect Ratio

The three-dimensional motion paths of the 13 points that traverse on the convex UHMWPE surface for ADL Flexion/Extension wear simulation are illustrated in Figure 4.33. The estimated sliding distance for these individual discrete points is given in the Table 4.4, including the aspect ratio for each path. The two-dimensional projection of the motion paths are illustrated in Figure 4.34.

Based on observation from the two-dimensional projection, all the plotted motion paths are curvilinear and almost identical with each other. The length of sliding distances is longer for points located along the midline of the sagittal plane, as the motion is predominantly in flexion/extension direction, and it is getting shorter as the points are located away from midline. All 13 points have shown a degree of unidirectional as seen by their aspect ratio values, calculated to be between 5.67 and 6.00.

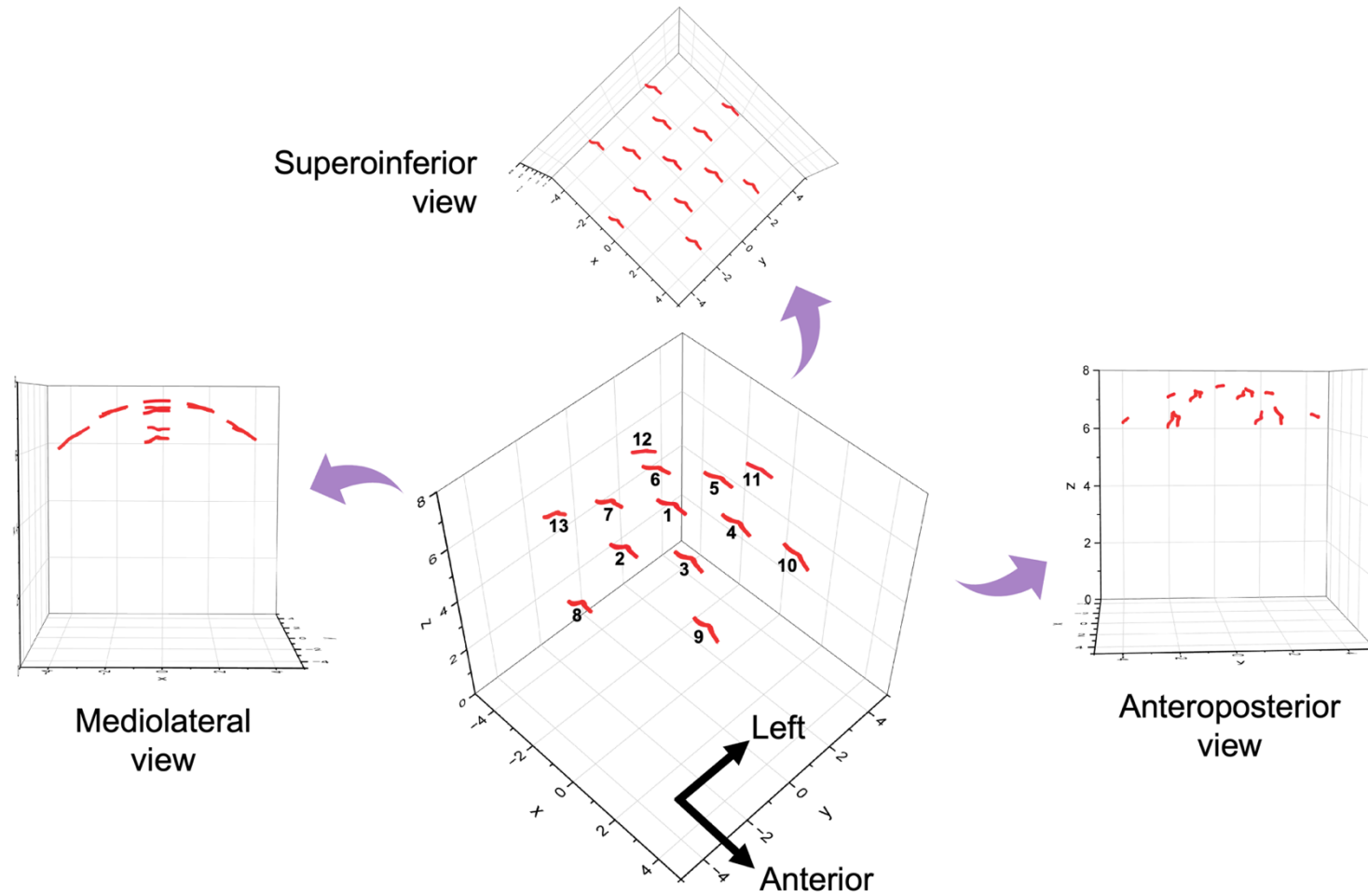


Figure 4.33 Three-dimensional motion path for thirteen discrete points on the surface of UHMWPE convex part during ADL Flexion/Extension wear simulation

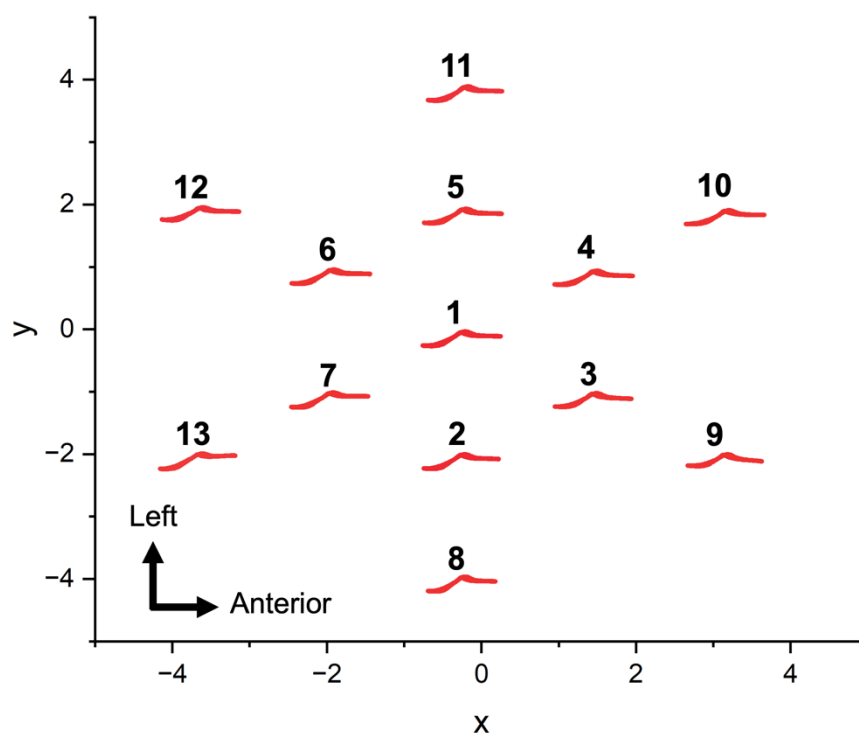


Figure 4.34 Two-dimensional projection of motion path for thirteen discrete points during ADL Flexion/Extension wear simulation

| Point | Location of Point (viewed from top) | Sliding Distance (millimetres) | Aspect Ratio |
|---------------------------|-------------------------------------|--------------------------------|--------------|
| 1 | Pole | 2.18 | 6.00 |
| 2 | Inner ring – east | 2.08 | 5.67 |
| 3 | Inner ring – northeast | 2.13 | 5.67 |
| 4 | Inner ring – northwest | 2.18 | 6.00 |
| 5 | Inner ring – west | 2.15 | 5.67 |
| 6 | Inner ring – southwest | 2.17 | 6.00 |
| 7 | Inner ring – southeast | 2.15 | 5.67 |
| 8 | Outer ring – east | 1.85 | 5.00 |
| 9 | Outer ring – northeast | 2.03 | 5.67 |
| 10 | Outer ring – northwest | 2.15 | 6.00 |
| 11 | Outer ring – west | 2.00 | 5.67 |
| 12 | Outer ring – southwest | 2.10 | 6.00 |
| 13 | Outer ring – southeast | 2.09 | 5.67 |
| Mean | | 2.10 | 5.74 |
| Standard Deviation | | 0.09 | 0.28 |

Table 4.4 The estimation on sliding distance of thirteen discrete points during ADL Flexion/Extension wear simulation

4.2.2.6 UHMWPE Bearing Surface Analysis

Coarse visual assessment on the UHMWPE convex surfaces from 100, 20× magnification, stitched scanned data, shows a similar wear effect across all three sliding samples. At the conclusion of the simulation (5.0 MC), UHMWPE Part 011 exhibited multiple wavy wear scars against a polished bearing surface throughout the scanning region with some roughened area along the latitude at the south of the scanning region (Figure 4.36). The same wavy wear scars had begun to appear on UHMWPE Part 013 surface at 0.3 MC as well as several short linear scars around the polar region with some machining marks still present (Figure 4.37). At 2.0 MC, all machining marks have been obliterated in UHMWPE Part 015 and wavy wear scars were present throughout the bearing surface area (Figure 4.38). These wavy scars seen in all of the sliding parts are consistent with the motion path pattern charted in Figure 4.33. In soak control, UHMWPE Part 017 has retained much of the machining marks throughout the bearing surface after 5.0 MC of wear simulation (Figure 4.39). Figure 4.35 shows an illustration of the location of the course visual assessment being carried out.

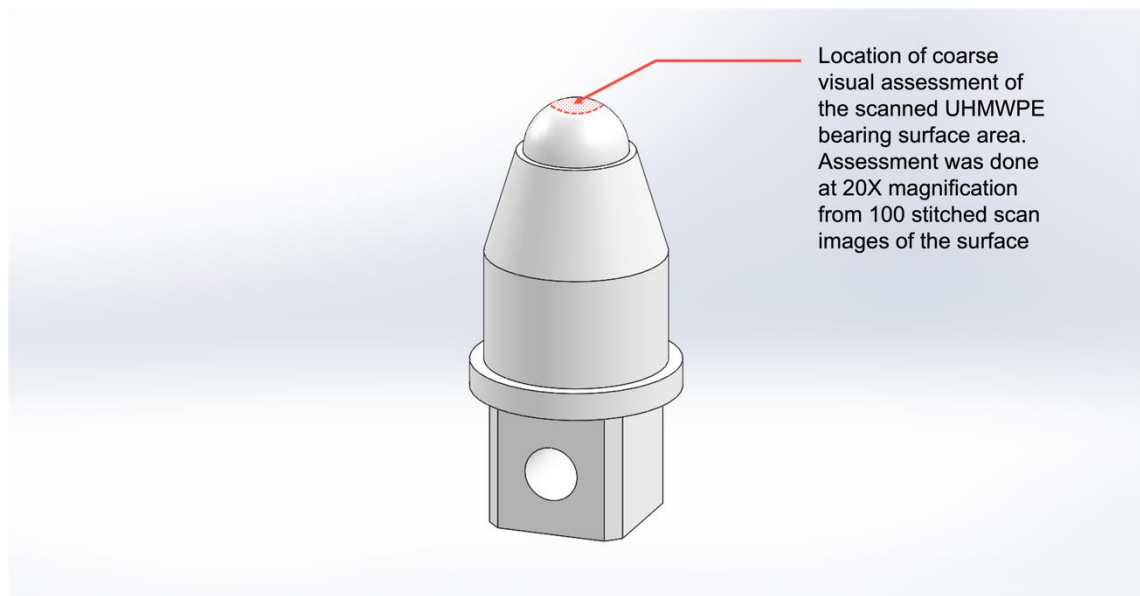


Figure 4.35 An illustration of the location of 100 stitched scanned images at 20× magnification for course visual assessment

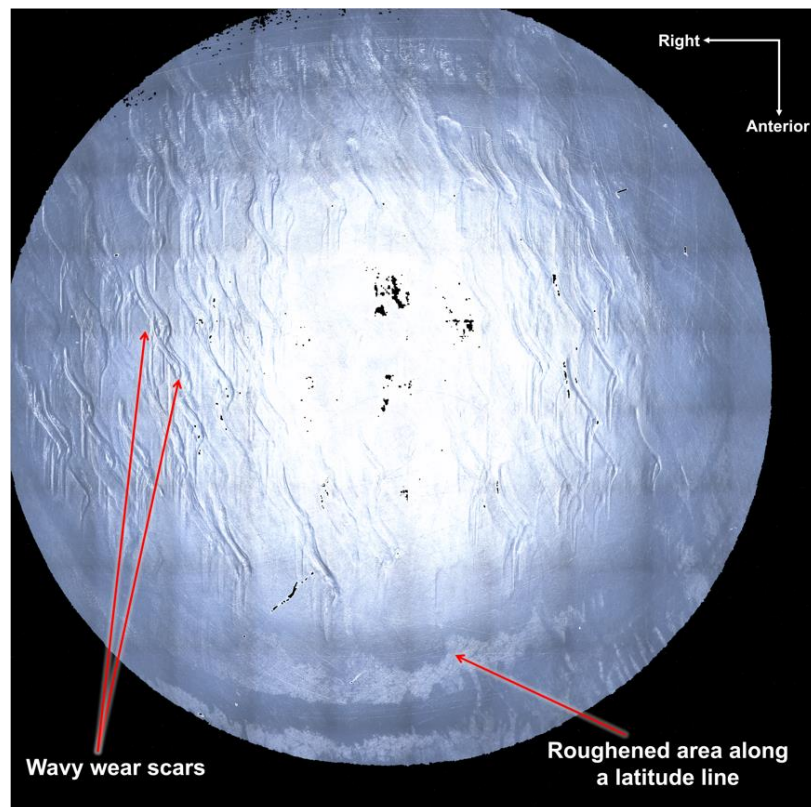


Figure 4.36 Bearing surface of UHMWPE Part 011 at 4.5 MC of ADL Flexion/Extension wear simulation

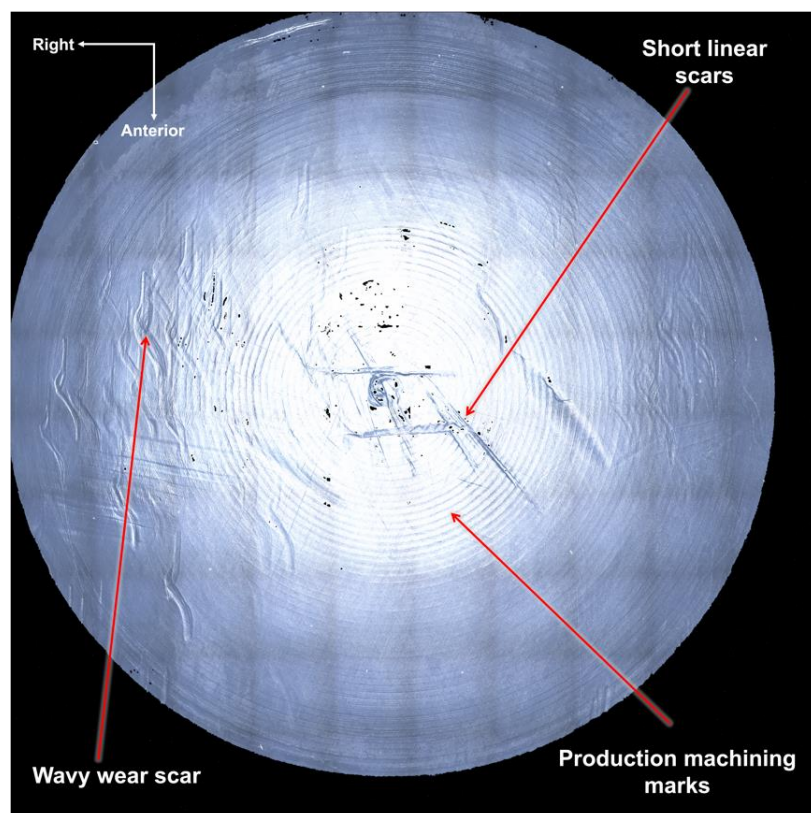


Figure 4.37 Bearing surface of UHMWPE Part 013 at 0.3 MC of ADL Flexion/Extension wear simulation

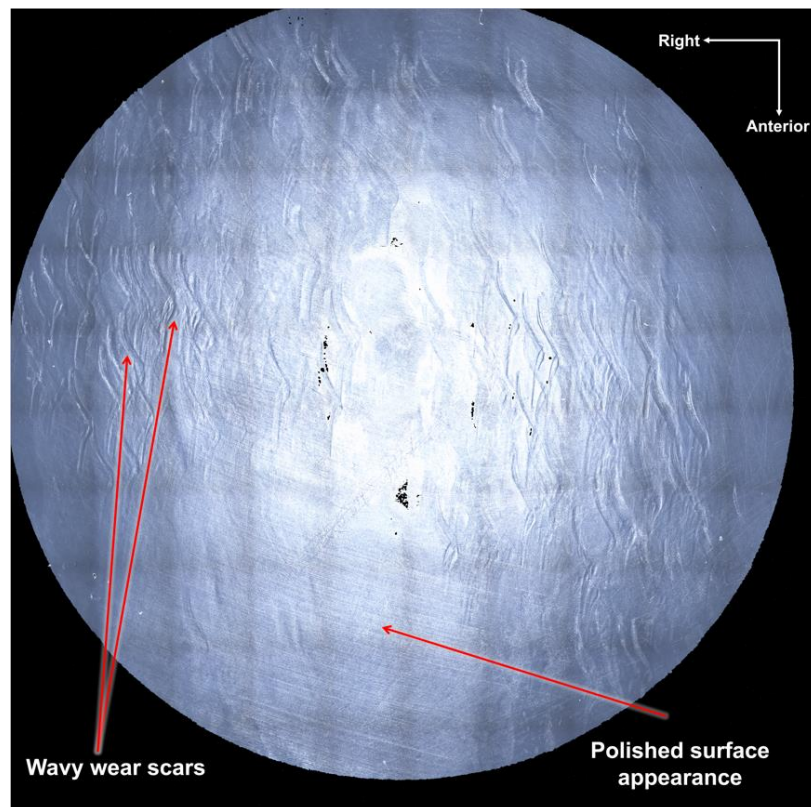


Figure 4.38 Bearing surface of UHMWPE Part 015 at 2.0 MC of ADL Flexion/Extension wear simulation

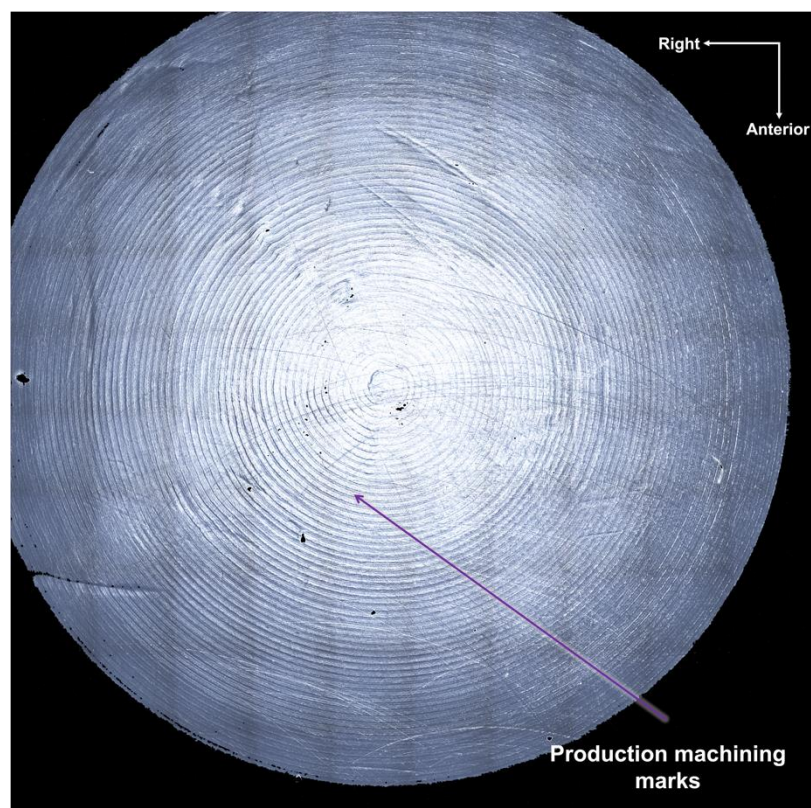


Figure 4.39 Bearing surface of UHMWPE Part 017 (soak control) at 5.0 MC of ADL Flexion/Extension wear simulation

A fine, sequential, qualitative visual assessment of the polar region between 3.5 MC to 5.0 MC at 10× magnification also shows a homogenous pattern across the UHMWPE parts that were sliding against CoCrMo parts (Table 4.5). Across the three sliding UHMWPE parts (Parts 011, 013, and 015), a roughened area could be seen emerging at different simulation cycles timepoints as well as linear micro-scars in various directions. The UHMWPE Part 017, on the other hand, has retained much of the machining marks until the end of wear simulation with some linear micro-scar appeared between 3.5 to 4.0 million cycles.

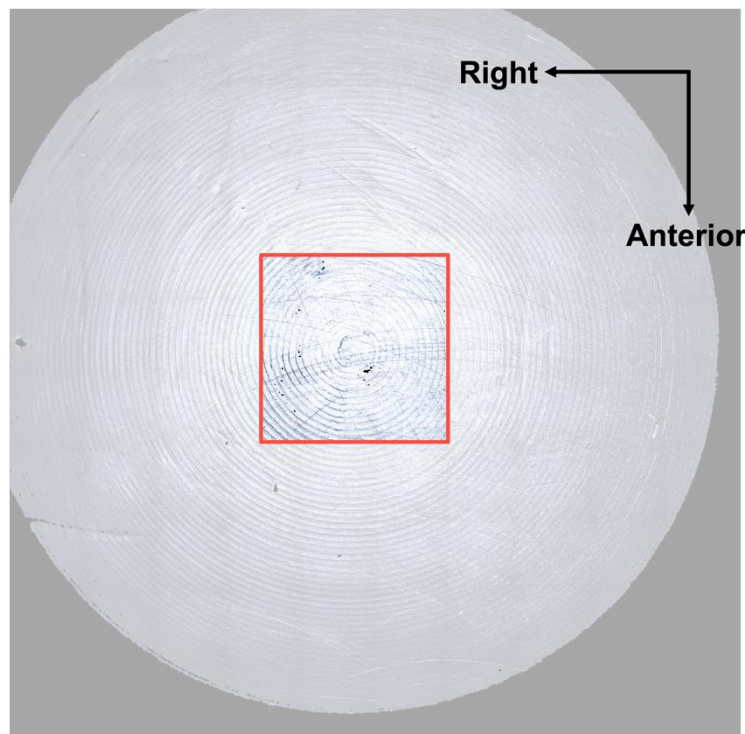


Figure 4.40 Location of qualitative visual assessment of the polar region of UHMWPE convex part at 10× magnification relative to the scanned area

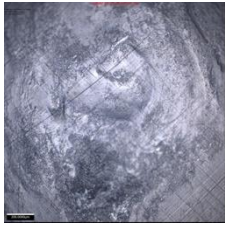
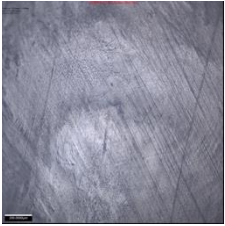
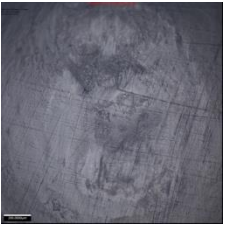
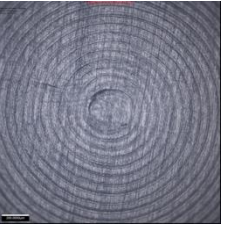
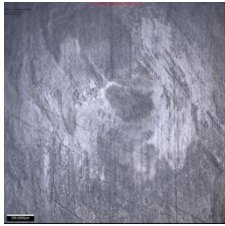

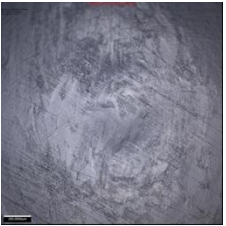
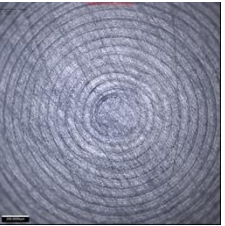
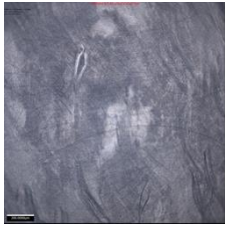
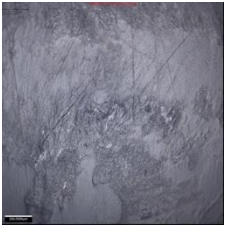
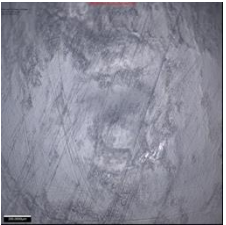
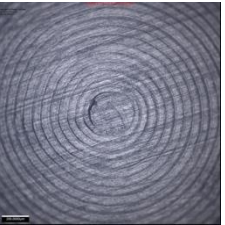
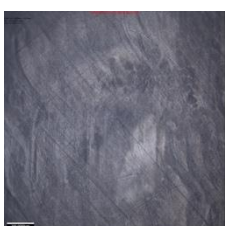
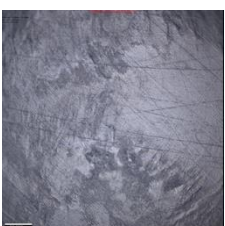
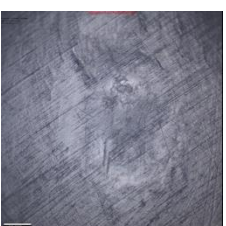
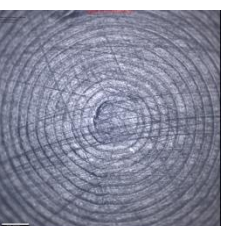
| Cycle Completed | UHMWPE Convex Bearing Surfaces | | | |
|-----------------|--|--|---|--|
| | 011 | 013 | 015 | 017 (soak control) |
| 3.5 MC |  |  |  |  |
| 4.0 MC |  |  |  |  |
| 4.5 MC |  |  |  |  |
| 5.0 MC |  |  |  |  |

Table 4.5 Sequential bearing surface image of UHMWPE convex parts during the last 1.5 MC of ADL Flexion/Extension wear simulation

A quantitative surface roughness measurement on the bearing surfaces from all UHMWPE parts throughout the wear simulation showed a generally lower mean S_a for UHMWPE Parts 011, 013, and 015 than Part 017 soak control (Figure 4.41). Throughout the wear simulation, the average overall surface roughness for 011, 013, and 015 was between 300 to 450 nm and it was consistently lower than Part 017 soak control, which was above 400 nm throughout 5.0 MC and has a general downward trend.

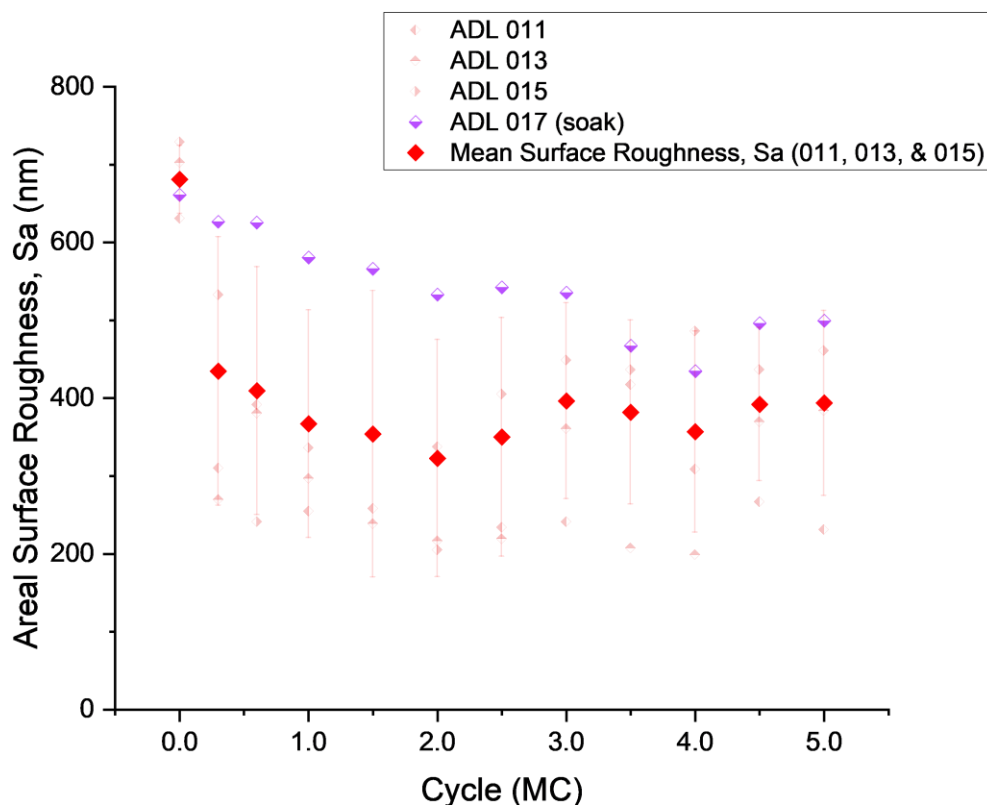


Figure 4.41 Average surface roughness of bearing surface on UHMWPE convex parts during ADL Flexion/Extension wear simulation

The average surface roughness of a $1\text{ mm} \times 1\text{ mm}$ sampled area showed a similar fluctuating S_a value throughout the wear simulation for both sliding UHMWPE parts (between 250 nm to 650 nm) as well as soak control (between 300 nm to 550 nm), (Figure 4.43). The 1 mm^2 sampling area was in the eastern side of the scanned area, about halfway between the pole and the edge of scanning region (Figure 4.42).

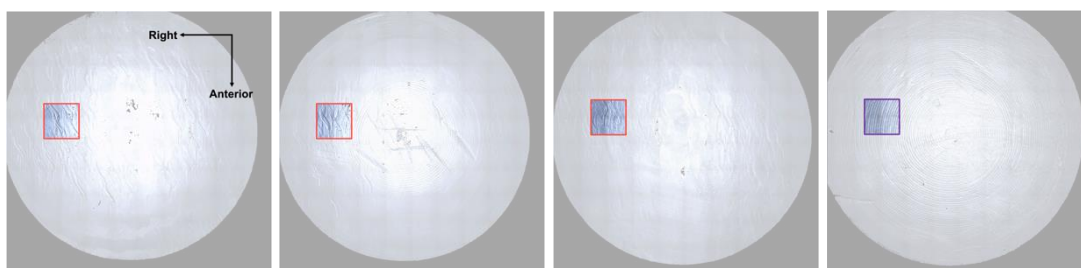


Figure 4.42 Location of 1 mm^2 sampled bearing surface on UHMWPE convex parts for S_a measurement during ADL Flexion/Extension wear simulation

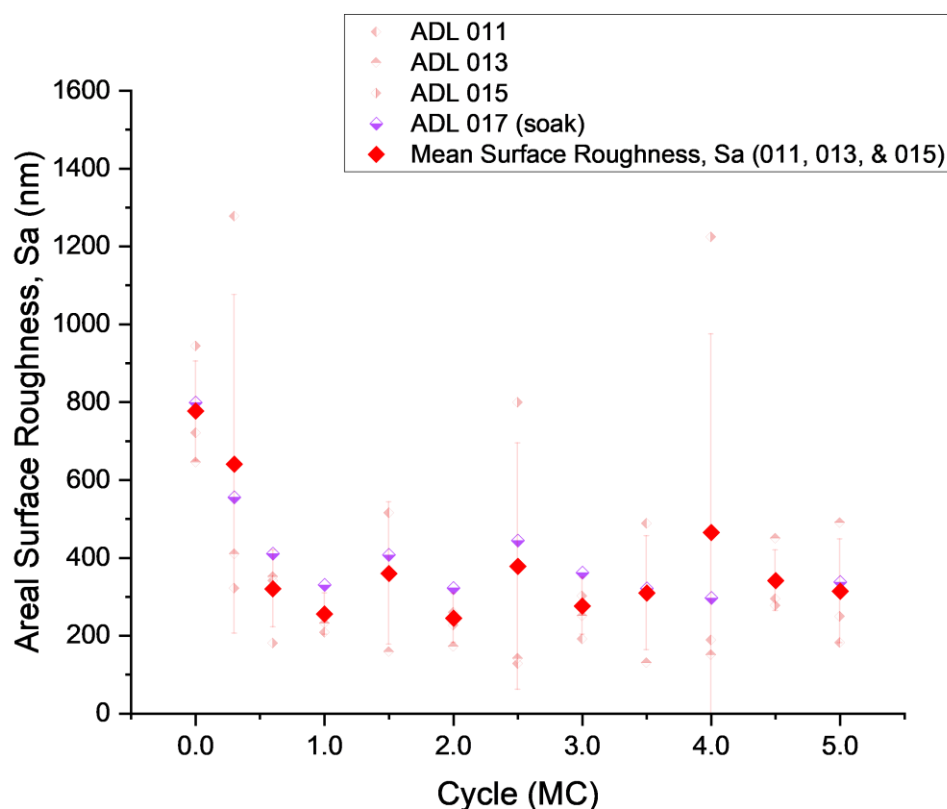


Figure 4.43 Average surface roughness of 1 mm² sampled bearing surface on UHMWPE convex parts during ADL Flexion/Extension wear simulation

4.3 Discussion

Two sets of wear simulations were successfully carried out in order to investigate the wear performance of cervical disc implant replicas under loads and motions that represent activities of daily living as well as under the prescribed parameters from the standard protocols. The first set of wear simulation involved parameters from ISO18192-1 [1] whereas the second simulation was based on one of the wear profiles formulated in Section 3.2.7. A comparison summary between these two simulations are illustrated in Table 4.6, Figure 4.44, and Figure 4.45 below.

| Parameters | Standard Cervical Wear Test | Cervical ADL Wear Test |
|----------------------------------|----------------------------------|------------------------------|
| Test Profile | ISO18192-1 [1] (Cervical) | ADL Flexion/Extension |
| <u>Angular Motion (°)</u> | | |
| Maximum Flexion | +7.5 | +1.9 |
| Maximum Extension | -7.5 | -5.8 |
| Maximum Lateral Bending (right) | +6.0 | +2.0 |

| | | |
|----------------------------------|------------|------|
| Minimum Lateral Bending (left) | -6.0 | +0.3 |
| Maximum Axial Rotation (left) | +4.0 | +0.1 |
| Minimum Axial Rotation (right) | -4.0 | -0.6 |
| <u>Loading Forces (N)</u> | | |
| Maximum Axial Loading | +150 | +347 |
| Minimum Axial Loading | +50 | +111 |
| Maximum Anteroposterior Loading | Not tested | +36 |
| Minimum Anteroposterior Loading | Not tested | 0 |

Table 4.6 Summary of input differences between the two sets of wear simulation carried out in this study

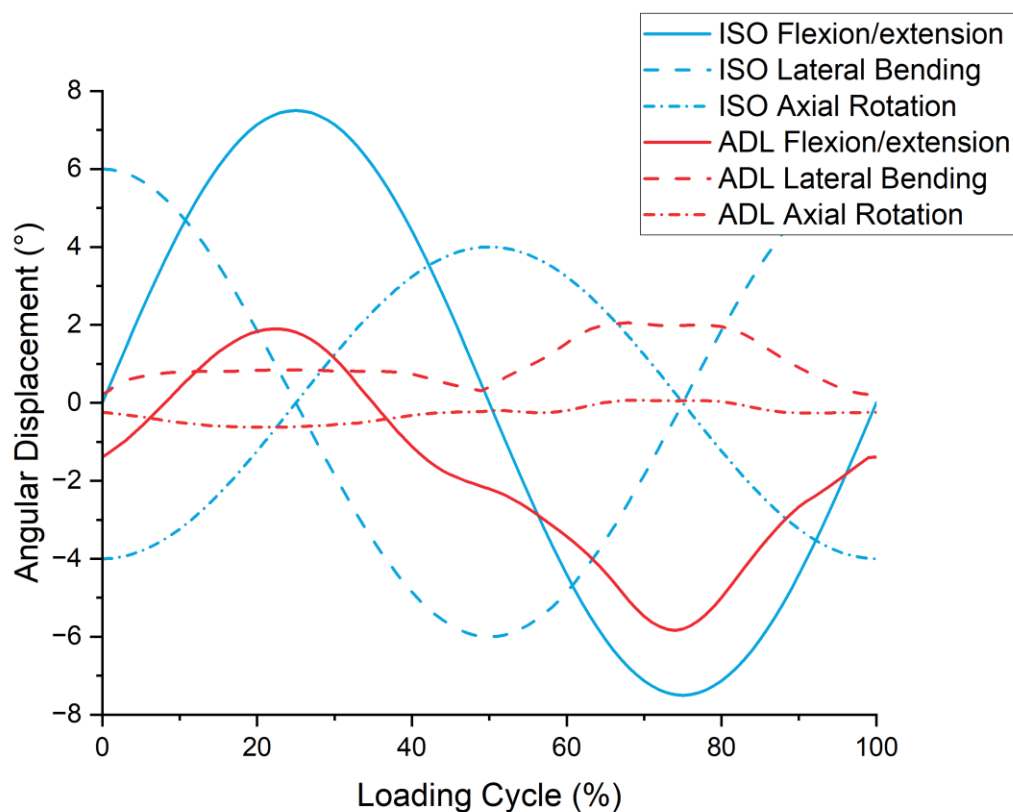


Figure 4.44 Graph showing the differences in magnitude and phasing of angular displacement between the two sets of wear simulations carried out

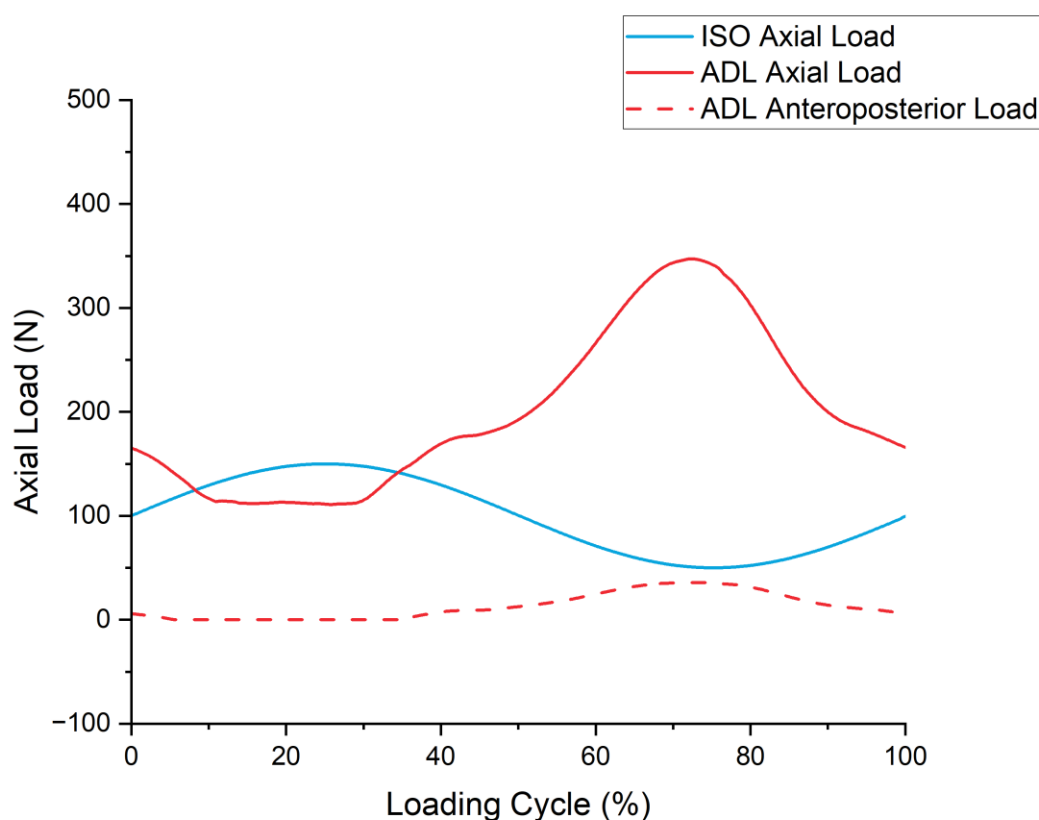


Figure 4.45 Graph showing the differences in magnitude and phasing of joint loadings between the two sets of wear simulations carried out

4.3.1 Cervical Spinal Disc Implant Replica Design

Eight pairs of UHMWPE convex and CoCrMo concave parts that represent an articulation in a typical cervical disc implant were successfully produced and used for mechanical wear simulation. The 7.5 millimetre-radius design for both concave and convex parts was replicated from previously published cervical disc wear study by Kraft *et al.* [252] albeit for PEEK-on-PEEK tribological pair simulation. A bigger, 13 millimetres, radial size also have been reported for a similar in-house production metal-on-polymer wear study [155]. In reality, all commercially available cervical disc implants come in different sizes to accommodate a range of population sizes and it is difficult to know the correlation between the implant size and the radius of the articulation for any manufacturers as it could be a well-guarded trade secrets.

From a tribological aspect, design of the manufactured implant replica in this study is far from achieving an ideal elastohydrodynamic lubrication regime

needed for an implant given its relatively small articulation radius (7.5 mm) and big radial clearance (0.40 mm at maximum). In a study on lubrication regimes of lumbar disc implant by Shaheen and Shepherd [109] concludes that a bigger convex radius or a smaller radial clearance will increase the lambda ratio, λ , and ultimately reduces the effect of wear, which is the opposite to the current study's design for the implant.

For the manufactured replicas, a theoretical calculation of lambda ratio in the worst-case scenario for the current study was estimated to be 0.0137 and 0.00739 for ISO18192-1 [1] and ADL Flexion/Extension wear simulations, respectively. Both values, which are less than one, are similar to ratio calculated by Kraft [111] for *in vitro* wear simulation of CoCrMo-UHMWPE lumbar disc implant, even though the diameter of the ball is bigger, radial clearance is smaller but the axial loading applied is higher compared to the current study. The lambda ratio calculation for the current study, using Hamrock-Dowson elasto-hydrodynamic equation for the theoretical minimum film thickness [109], is shown in Appendix F.

Two numerical simulation studies have shown that achieving a lambda ratio that is higher than 'unity' ($\lambda > 1$) in CoCrMo-UHMWPE spinal disc implant has been tricky at different angular velocities when altering the articulation radius and radial clearance of the implant [109, 111]. Clewlow *et al.* [110] theorised that a cervical disc implant could potentially achieve a fluid-film lubrication regime ($\lambda > 3$) when a soft layer bearing, such as elastomer, being introduced between a hard-backing convex and concave design. The current study, however, is trying to simulate the tribological pair that is commonly adopted design in commercially available cervical disc implants.

4.3.2 Output Verification During Pilot Simulations

As previously mentioned, the wear simulator was conceptualised to replicate the left hip where the range for axial loading in hip joint (experienced by the implant) is expected to be between 300 N to 3000 N. Therefore, the capability of the actuator motor to apply a load between 50 N to 400 N in axial loading, and 0 N to

40 N in medial-lateral direction, is beyond the precision it was initially designed. The simulator, nonetheless, is able to meet the tolerance demand very closely for kinematics as well as axial loading for both simulations due to its electromechanical controls, in which their performances also has been reported and vouched for previously [117]. In addition to that, the electromechanically-controlled simulator also has been known to be able to meet an input demand with unconventional curves, as seen in ADL wear profiles, as opposed to the traditional sinusoidal wave pattern seen in many wear profiles [253].

As the anteroposterior loading range of demand in ADL Flexion/Extension is relatively low (0 – 40 N), the tolerance for the magnitude, determined from $\pm 5\%$ of the maximum force value of the parameter, will also be significantly low, *i.e.* ± 2 N. The medial/lateral actuator motors were able to meet between 45-60% of the anteroposterior loading input demand in all three stations despite its limitation.

4.3.3 Bedding-in Phase

The length of bedding-in phase is based on the curve in cumulative net mass loss graphs (4.14 and 4.31) for each individual UHMWPE convex part. For ISO18192-1 [1] wear simulation, the slopes were stabled after 0.6 MC for UHMWPE Parts 012 and 016 whereas slope for UHMWPE Part 014 was only stabled after 1.0 MC. During ADL Flexion/Extension wear simulation, all three slopes for UHMWPE Parts 013, 015, and 017 were stabled after 1.0 MC. It is decided that the steady-state wear rate calculation period begins after 1.0 MC when the slopes representing all UHMWPE convex parts have reached a stable gradient and thus consistency is maintained for both simulations. A similar method also used by Smith and Unsworth [254] in which they have found a statistically significant higher wear rate of acetabular cup during the first 2.0 MC of wear simulation for hip implant, regardless of the biomaterial used for femoral head.

4.3.4 ISO18192-1 Gravimetric Wear Rate Validation

The mechanical wear simulation according to parameters outlined in ISO18192-1 [1] was successfully carried out for 5.0 million cycles on the surface replica of

cervical disc implant. The gravimetric wear rate for ISO18192-1 [1] after the bedding-in period in the current study is comparable with, commercially available, contemporary cervical disc implants of the same CoCrMo/UHMWPE biomaterial pairing.

| Device Name | Source | Wear Rate Reported (mg/MC) | Simulation Completed (MC) |
|-------------|----------------------------|----------------------------|---------------------------|
| ProDisc™-C | SSED [77] | 2.59 ± 0.36 | 10.0 |
| ProDisc™-C | Nechtow <i>et al.</i> [89] | 1.99 ± 0.15 | 6.0 |
| Mobi-C® | SSED [81] | 1.546 ± 0.075 | 10.0 |
| activ® C | Grupp <i>et al.</i> [73] | 1.0 ± 0.1 | 10.0 |
| This study | | 1.42 ± 0.071 | 5.0 |

Table 4.7 Comparison of wear rates under ISO18192-1 [1] between commercially available articulating cervical disc implants and replicas in the current study

Based on SSED submitted to FDA, the reported wear rate of ProDisc™-C and Mobi-C® are 2.59 ± 0.36 mg/million cycles and 1.546 ± 0.075 mg/million cycles, respectively [77, 81]. Nechtow *et al.* [89] has observed a lower wear rate for ProDisc™-C compared to its SSED value when a dynamic axial loading being applied instead of a constant loading. Meanwhile, a simulation study by Grupp *et al.* [73] has found the gravimetric wear rate of activ® C is 1.0 ± 0.1 mg/million cycles.

4.3.5 Statistical Comparison of Wear Rate between ISO18192-1 and ADL Flexion/Extension Simulations

Using the same biomaterial and design for the replicas, the mechanical wear simulation according to parameters from ADL Flexion/Extension wear profile concluded with a gravimetric wear rate of 1.26 ± 0.084 mg/million cycles during its steady-state period, lower than the rate observed during ISO18192-1 [1]’s steady-state period, which is 1.42 ± 0.071 mg/million cycles. However, the gravimetric wear rate from ADL Flexion/Extension profile is 1.57 ± 0.068 mg/million cycles, which is higher than observed value in ISO18192-1 [1], if the outlier measurements from UHMWPE Part 015 were excluded, as deduced from Friedman’s test in Section 4.2.2.4.

A statistical comparison on the coefficients (slopes) of the linear regression has shown that there is no significant difference in the steady-state wear rate of ADL Flexion/Extension when compared to ISO18192-1 [1]'s steady-state wear rate ($p = 0.066$), even when the outlier measurements were omitted ($p = 0.195$). As shown by the gradients of the linear fittings in Figure 4.46, the gravimetric wear rate from ADL Flexion/Extension wear simulation is almost match when compared to the gravimetric wear rate from ISO18192-1 [1] although its standard deviation at individual weighing time points is bigger compared to the latter due to the inclusion of UHMWPE Part 015 outlier. Similarly, Figure 4.47 shows the slopes of the linear fittings between wear simulations from ISO18192-1 [1] and ADL Flexion/ Extension are also closely matched when outliers are excluded. The standard deviations are, however, narrower at each measurement time point, for ADL Flexion/Extension due to smaller number of repeat measurements available.

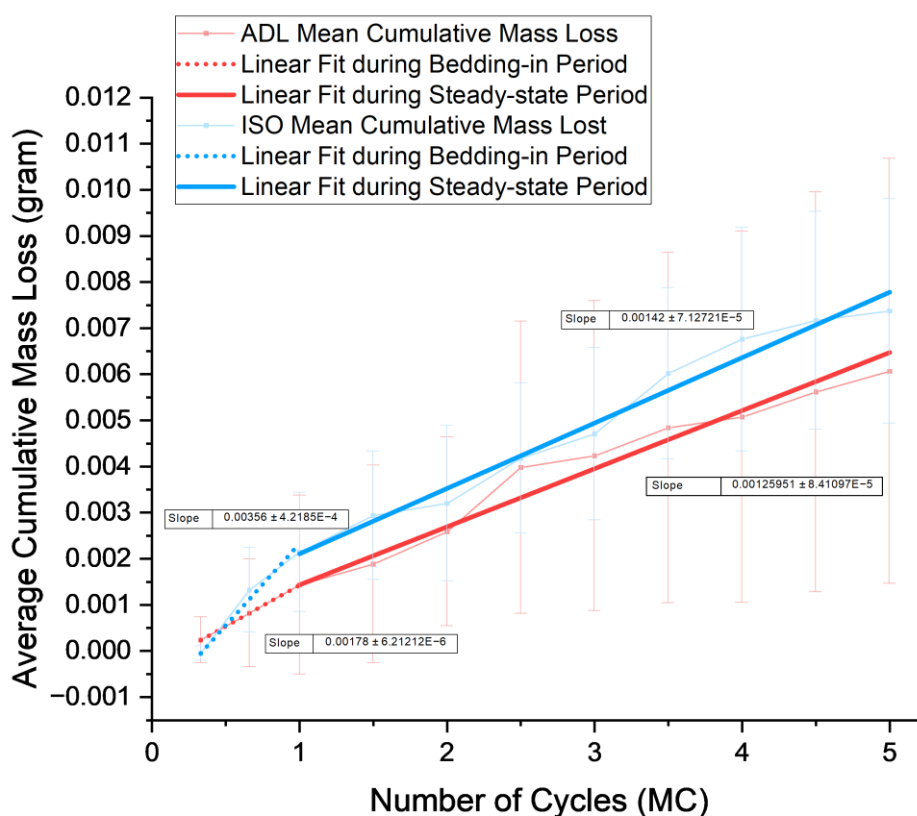


Figure 4.46 Comparison of wear rates between ISO18192-1 [1] (blue) and ADL Flexion/Extension (red) wear profiles

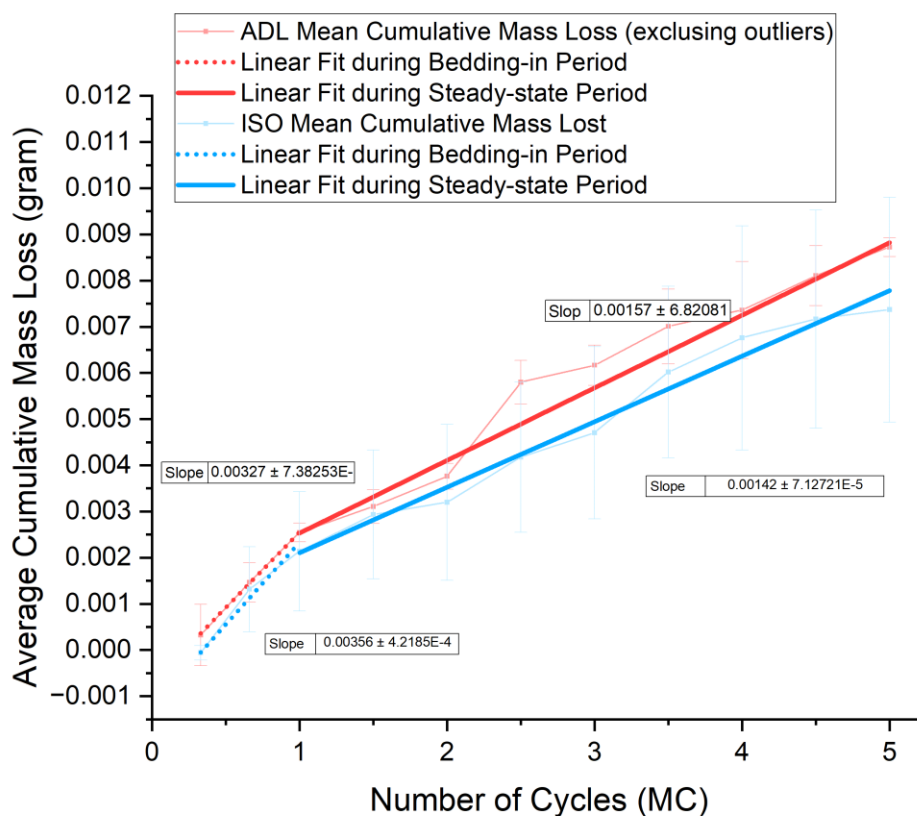


Figure 4.47 Comparison of wear rates between ISO18192-1 [1] (blue) and ADL Flexion/Extension (red) wear profiles without outliers

Analysis on each individual UHMWPE convex part's net mass loss (as opposed to cumulative mass loss), at each time point after bedding-in period, between the two wear simulations, reveals a statistically insignificant difference amongst the measurements ($p = 0.401$) when tested using non-parametric Kruskal-Wallis test, even when the outlier measurements were omitted ($p = 0.487$). Equally, the non-parametric analysis of variance on the average mass loss (between the repeats) at each measurement time point during steady-state period for both wear simulations using Mann-Whitney U test also reveals the difference to be insignificant ($p = 0.536$), even when the outliers are excluded ($p = 0.724$). Therefore, it can be concluded that simulation under ISO18192-1 [1] parameters and ADL Flexion/Extension parameters produce a comparable wear rate.

4.3.6 Tribological Regime

Although the wear rates between ADL Flexion/Extension and ISO18192-1 [1] are comparable, factors that influence the wear between these simulations can be explored tribologically using Archard's Volumetric Wear Equation, illustrated in Equation 2.1, which can be applied to both abrasive and adhesive wear mechanism models [87].

From the equation, normal load applied, W , and sliding distance, L , are the only variables that change between the two wear simulations. Each of these parameters, as well as the complex interplay it has in influencing the tribological system from these simulations, will be further discussed in Sections 4.3.6.1 and 4.3.6.2.

4.3.6.1 Normal (Axial) Load Applied, W

From the comparison graph shown in Figure 4.48, the axial load applied during ADL Flexion/Extension is, in general, higher than ISO18192-1 [1]. The axial load range in ADL Flexion Extension (110 N - 347 N) is more than twice than axial loading range in ISO18192-1 [1] (50 N - 150 N).

On top of that, the phasing of the axial loading in ISO18192-1 [1] is about π radian out of phase than what human is experiencing physiologically with respect to cervical vertebral motion in sagittal plane. From the outcome of cervical biomechanics study in Phase I, a higher axial loading is observed when the head is extended from its neutral position (drinking from a bottle) than when the head is flexing forward (looking at mobile) which is in total opposite than the curve produced in ISO18192-1 [1].

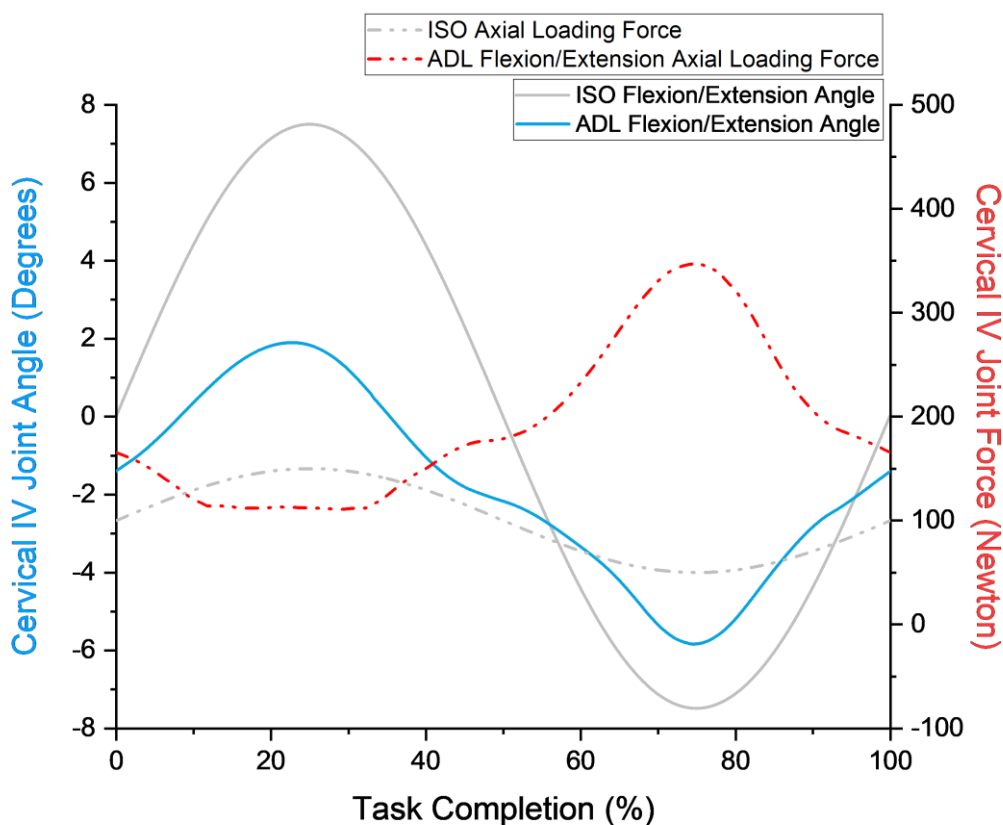


Figure 4.48 Comparison of flexion/extension angle and axial loading parameters between ISO18192-1 [1] (grey) and ADL Flexion/Extension (coloured) wear profiles

4.3.6.2 Sliding Distance, L

Based on the estimation of sliding distance for both wear simulations, the excursion length in ISO18192-1 [1] is longer than ADL Flexion/Extension for all 13 discrete tracking points. Table 4.8 shows that for the same tracking point on concave CoCrMo surface, sliding distance in ISO18192-1 [1] is more than twice the length traversed in ADL Flexion/Extension wear simulation and they are significantly different ($p < 0.01$).

| Point | Location of Point (viewed from top) | Sliding Distance (millimetres) | |
|---------------------------|--|--------------------------------|-----------------------|
| | | ISO18192-1 [1] | ADL Flexion/Extension |
| 1 | Pole | 5.56 | 2.18 |
| 2 | Inner ring – east | 5.47 | 2.08 |
| 3 | Inner ring – northeast | 5.82 | 2.13 |
| 4 | Inner ring – northwest | 5.82 | 2.18 |
| 5 | Inner ring – west | 5.47 | 2.15 |
| 6 | Inner ring – southwest | 5.15 | 2.17 |
| 7 | Inner ring – southeast | 5.15 | 2.15 |
| 8 | Outer ring – east | 5.23 | 1.85 |
| 9 | Outer ring – northeast | 5.91 | 2.03 |
| 10 | Outer ring – northwest | 5.91 | 2.15 |
| 11 | Outer ring – west | 5.23 | 2.00 |
| 12 | Outer ring – southwest | 4.66 | 2.10 |
| 13 | Outer ring – southeast | 4.66 | 2.09 |
| Mean | | 5.39 | 2.10 |
| Standard Deviation | | 0.43 | 0.09 |

Table 4.8 Table of comparison on sliding distance of thirteen discrete points between ISO18192-1 [1] and ADL Flexion/Extension wear profiles

4.3.6.3 Estimation of Wear Coefficients

Thus, using Equation 2.1, data from axial loading input (Figure 4.48), and sliding distance estimations (Table 4.8), the dimensionless wear coefficient of the tribological system in each simulation can be determined by rearranging the formula to have the coefficient as the subject, as shown in Equation 4.7 below.

$$K = \frac{V \times H_V}{W \times L}$$

Equation 4.7

If density of UHMWPE biomaterial is ρ g mm⁻³, the wear volume in one million cycles of ISO18192-1 [1] and ADL Flexion/Extension from this study are $1.42/\rho$ mm³ and $1.26/\rho$ mm³ (or $1.57/\rho$ mm³ when excluding the outliers) respectively. The integral values of axial load with respect to distance traversed ($W \times L$) for ISO18192-1 [1] and ADL Flexion/Extension after one million cycles are 5.45×10^8 N mm and 4.30×10^8 N mm, respectively (Figure 4.49). Therefore, the Archard's wear coefficient in these simulations after 1 million cycles are $2.60H_V\rho^{-1} \times 10^{-9}$

and $2.93H_{VP}^{-1} \times 10^{-9}$ for ISO18192-1 [1] and ADL Flexion/Extension, respectively (or $3.65H_{VP}^{-1} \times 10^{-9}$ when excluding the outliers in ADL Flexion/Extension).

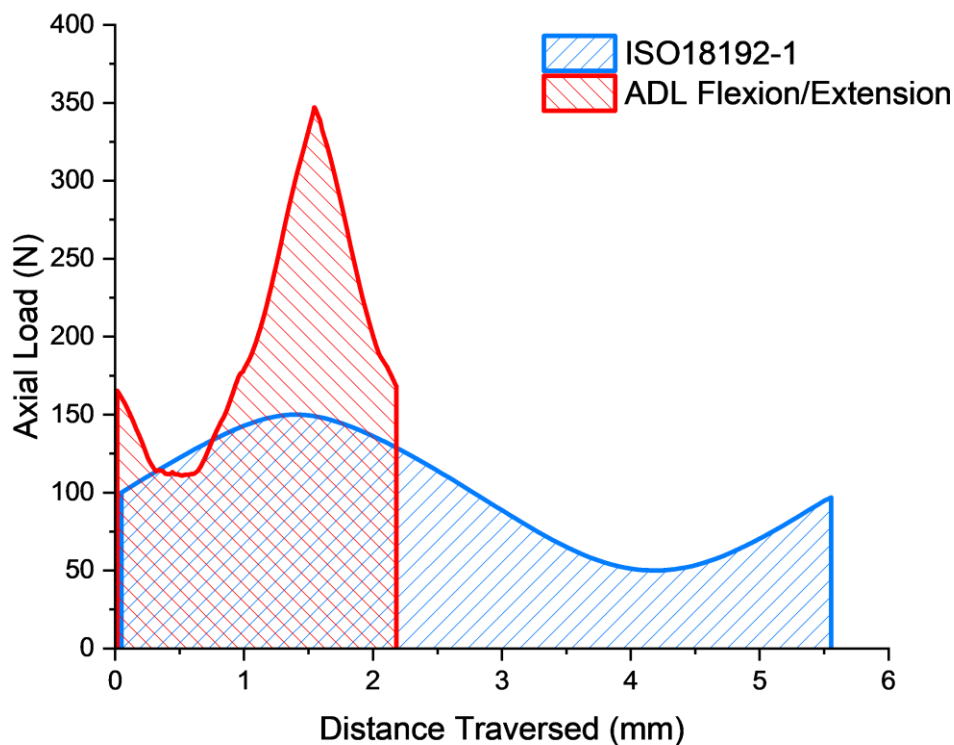


Figure 4.49 The comparison of integration between axial load and distance traversed curves at the pole (Point 1) between ISO18192-1 [1] (blue, 545 N mm) and ADL Flexion/Extension (red, 430 N mm) after one profile cycle

From here, it can be deduced that, under the same CoCrMo/UHMWPE biomaterials, ADL Flexion/Extension wear simulation is operating at a harsher tribological regime than ISO18192-1 [1] given the coefficient is higher, despite having a comparable wear rate.

The similarity in the wear rate observed, perhaps, could be attributed to the axial loading in ADL Flexion/Extension wear simulation is much higher ($> 2W$) whilst the sliding distance is less than half than the distance traverse during ISO18192-1 [1] ($< \frac{1}{2} L$). Therefore, the increase in axial loading in ADL Flexion/Extension wear profile is potentially offset by the decrease in sliding distance, making the volumetric wear approximately the same amount.

4.3.6.4 Estimation of Aspect Ratio for Individual Motion Path

It is also found that wear of a linear polymer, such as UHMWPE, is also affected by direction of sliding of a hip implant, where multidirectional motion will cause a higher wear rate than a unidirectional path [250]. The stark contrast in shape of motion path, and by extension the aspect ratio, between ISO18192-1 [1] and ADL Flexion/Extension can also be seen when the three-dimensional motion paths are projected into two-dimensional loci through zenithal equidistant projection as illustrated in Figure 4.50.

The degree of multidirectionality from these projected 2D loci is quantified from the aspect ratio of these motion paths, where the lower the ratio, the higher the degree [250]. Figure 4.51 illustrates graphically the comparison of the motion path for eleventh tracking point as well as the measurement of the aspect ratio for these paths. The aspect ratios for all 13 discrete motion paths between ISO18192-1 [1] and ADL Flexion/Extension are recorded in Table 4.9.

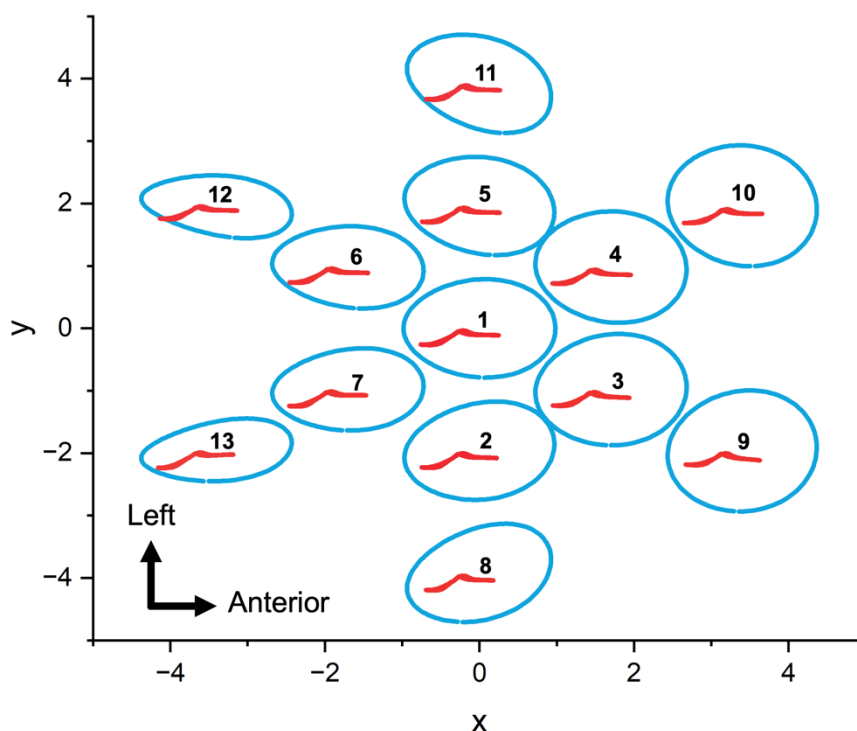


Figure 4.50 Two-dimensional projection of motion path for thirteen discrete points during ISO18192-1 [1] and ADL Flexion/Extension wear simulations

| Point | Location of Point (viewed from top) | Aspect Ratio | |
|---------------------------|--|----------------|-----------------------|
| | | ISO18192-1 [1] | ADL Flexion/Extension |
| 1 | Pole | 1.25 | 6.00 |
| 2 | Inner ring – east | 1.24 | 5.67 |
| 3 | Inner ring – northeast | 1.10 | 5.67 |
| 4 | Inner ring – northwest | 1.10 | 6.00 |
| 5 | Inner ring – west | 1.24 | 5.67 |
| 6 | Inner ring – southwest | 1.49 | 6.00 |
| 7 | Inner ring – southeast | 1.49 | 5.67 |
| 8 | Outer ring – east | 1.22 | 5.00 |
| 9 | Outer ring – northeast | 1.01 | 5.67 |
| 10 | Outer ring – northwest | 1.01 | 6.00 |
| 11 | Outer ring – west | 1.21 | 5.67 |
| 12 | Outer ring – southwest | 1.95 | 6.00 |
| 13 | Outer ring – southeast | 1.95 | 5.67 |
| Mean | | 1.33 | 5.74 |
| Standard Deviation | | 0.31 | 0.28 |

Table 4.9 Table of comparison on aspect ratio of the 13 discrete, tracking points between ISO18192-1 and ADL Flexion/Extension wear profiles

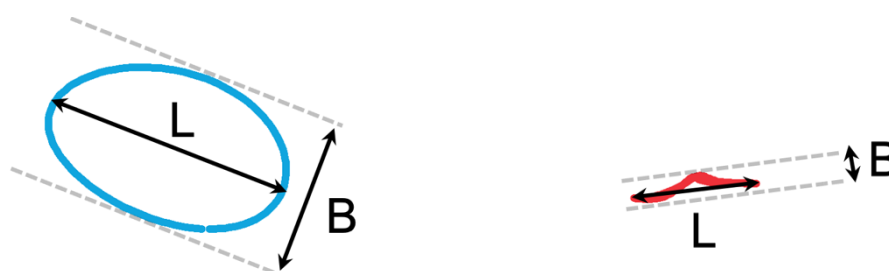


Figure 4.51 Comparison of calculation of motion path's aspect ratio on the eleventh point between ISO18192-1 [1] (blue, left) and ADL Flexion/Extension (red, right)

Table 4.9 shows that aspect ratio in ADL Flexion/extension is significantly higher ($p < 0.01$) than ISO18192-1 [1] for the same tracking point on concave CoCrMo surface which implies that ISO18192-1 [1] wear profile is more multidirectional than ADL Flexion/Extension. This, perhaps, contributes towards a marginally lower wear rate observed in ADL Flexion/Extension wear simulation than ISO18192-1 [1].

It can be argued that the motion in ADL Flexion/Extension wear profile is similar to protocol prescribed in ASTM F2423-11 [4] where each motion plane is tested

individually which ultimately producing only unidirectional, curvilinear wear motion path albeit with a higher axial load. Even when two motion planes are tested in combination but in-phase, the motion path it generates is still a curvilinear with high aspect ratio [255]. Nonetheless, the ADL Flexion/Extension wear profile only represents two of many neck movements within the scope of activities of daily living that were explored in Phase I. Although only a low degree of multidirectionality is present within each ADL tasks, the direction of motion amongst all ADLs are not necessarily in parallel with each other. Case in point, a wear profile generated from 'looking for traffic before crossing' (TRA) (Figure 3.11) has near-elliptical motion path in nine of the points whereas the other three points (2, 5, 8, and 11) have a curvilinear motion path with different direction. A 2D projection of the motion path for 'ADL Looking at Traffic' wear profile for the same 13 discrete points is shown in Figure 4.52 together with loci for ADL Flexion/Extension.

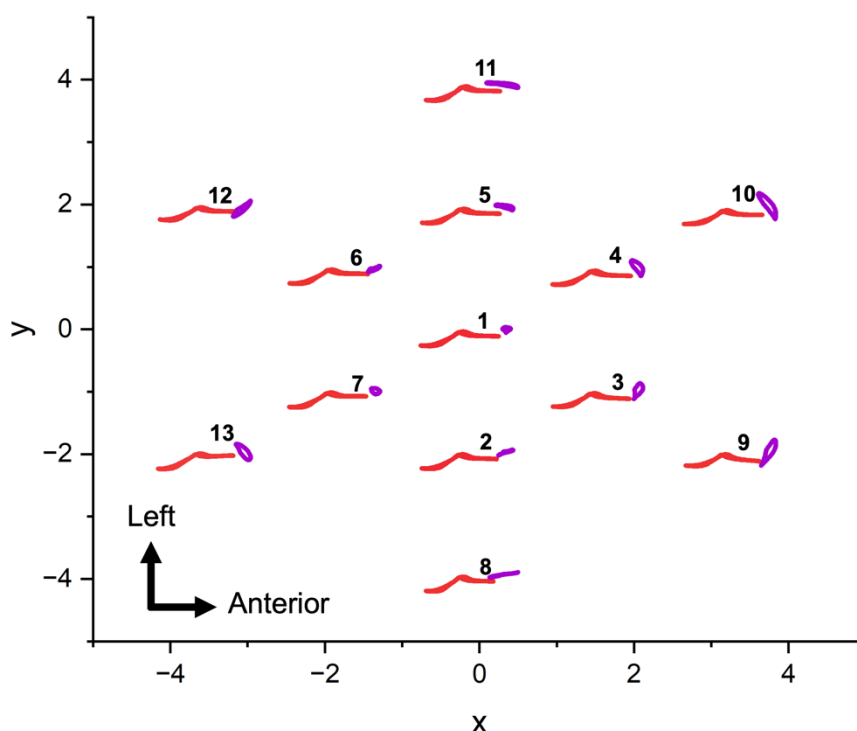


Figure 4.52 Comparison of two-dimensional projection of motion path for thirteen discrete points between ADL Flexion/Extension (red) and ADL Looking at Traffic (purple) wear profiles

Thus, it is recommended to have a suite of several ADL wear profiles to be employed when simulating *in vivo* wear condition on cervical disc implant. The inclusion of multiple ADL wear profiles is necessary in order to acknowledge the versatility of cervical spine movement. The heterogeneity of motion paths within ADLs also would introduce the cross-shear element which can influence the wear of the implant.

4.3.7 Surface Roughness Analysis

The wear scars observed during coarse visual assessment on UHMWPE convex surface for both wear simulations, Figure 4.21 and Figure 4.36, are comparable to the shape of theoretical motion paths plotted in Figure 4.16 and Figure 4.33, respectively. The elliptical wear scar seen during ISO18192-1 [1] wear simulation is also identical to the motion path characterised by Paré *et al.* [255] for the same wear profile. This is also true for the theoretical calculation of sliding distance at the pole (Point 1) from Table 4.4 based on radius-normalised ratio, $0.74r$, where r is the radius from centre of rotation, proposed by Paré *et al.* [255].

The qualitative visual assessment on the UHMWPE convex surface during ISO18192-1 [1] wear simulation yields a mixture of surface texture observations which also has been reported previously [126]. Polished appearance of the worn UHMWPE surface seen in Part 012 as well as roughened and raised texture in Part 016 are also present at the rim area and at the polar region, respectively, of UHMWPE insert from a wear simulation study by Hyde *et al.* [126]. Similarly, microscopic fine linear scarring described by Hyde *et al.* [126] from scanning electron microscopy also can be seen in Part 012 from the current study, even at 10× magnification, where the direction of the scars changes at every scanning time point (Table 4.3), over its otherwise generally smooth surface background. However, the macroscopic linear scarrings which can be seen during coarse visual examination throughout the course of wear simulation in both sets of wear test including the soak control are thought to be caused by handling of the UHMWPE parts during cleaning or assembling the test cell, rather than by the inherent wear process.

The trend seen from quantitative analysis of the surface roughness of the UHMWPE convex part during ISO18192-1 [1] wear simulation is comparable with the observation done by Hyde [256] on his study of semi-constrained (uni-articulation) ProDisc™-L lumbar disc implants. In the current study, the average surface roughness of the UHMWPE bearing surface at 4.0 MC is 71% from the average S_a value at the beginning of the simulation compared to 82% at 4.0 MC observed by Hyde [256]. Similarly, the percentage of surface roughness from initial analysis at the 1 mm² area sampled outside of the polar region is 40% in the current study compared to 17% recorded by Hyde [256], at an area analogue to the current study's sampling region which he defined as 'RIM'.

The change in overall average surface roughness of the soak control in the current study is 69% from its initial reading whereas the trend is almost unchanged as observed by Hyde [256] on his soak control with 97% from its initial value. Nonetheless, upon sampling at the 'RIM' region, the change in this study is closely matched with Hyde [256]'s observation with 34% and 32%, respectively. Summary of the quantitative analysis is shown in Table 4.10.

| Sampling Areas | Surface Roughness of Sliding Samples (nm) | | | | Surface Roughness of Soak Control (nm) | | | |
|----------------|---|------------|----------------------------------|------------|--|------------|----------------------------------|------------|
| | Overall / ALL | | 1 mm ² Sampling / RIM | | Overall / ALL | | 1 mm ² Sampling / RIM | |
| | Current Study | Hyde [256] | Current Study | Hyde [256] | Current Study | Hyde [256] | Current Study | Hyde [256] |
| 0.0 MC (a) | 557 | 1022 | 1139 | 1022 | 639 | 1022 | 1012 | 1022 |
| 4.0 MC (b) | 394 | 837 | 460 | 175 | 438 | 990 | 349 | 330 |
| % (b/a) | 71 | 82 | 40 | 17 | 69 | 97 | 34 | 32 |

Table 4.10 Table of comparison on change of surface roughness on UHMWPE convex part between current study and Hyde [256]

Caution, however, must be taken on these comparisons despite majority of the trends seen are similar. Although the materials of the implants are the same, simulation carried out by these studies is according to parameters for lumbar disc implant which have smaller angular displacements compared to cervical in all axes [126, 256]. On top of that, the modality used to measure surface roughness in the current study is non-contact, focus-variation, vertical optical scanning which provides a three-dimensional areal surface roughness, S_a . In contrast, the

modality employed by Hyde [256] was contact profilometry which gives a two-dimensional profile surface roughness, R_a .

The phenomenon of fluctuating surface roughness and texture throughout spinal disc simulation as seen in Figure 4.26 and Figure 4.43, also has been reported previously [124]. As highlighted by Prokopovich *et al.* [124], the analysis of bearing topography is not an indication of severity of wear; but can be a reflection of the wear mechanism, for example, abrasion and adhesion in this instance. Such the nature of disc implant to have a relatively small angular joint excursion compared to other joint implants, namely the hips and knees, has led to a belief that wear debris could be entrapped within bearing contact area or to be transplanted locally before it can be 'trafficked out' of the articulation surfaces by the lubricant. A 'short stroke' wear study by Hyde [256] using pin-on-plate does not provide enough evidence to support this theory but found that it decreases the lubrication regime of the system. Nonetheless, this finding is not replicated in his lumbar disc wear simulation study, nor in this current cervical wear simulation study, where the wear rate is reduced, rather than increased, when the sliding distance is reduced. He postulated that the lubrication regime was already poor to begin with that the reduction of sliding distance has little influence to the wear rate outcome, on top of other input variables at interplay during joint replacement wear simulation study that could also influence the result [256].

4.3.8 Phase II: Mechanical Wear Simulation Study Limitations

The GUR 1050 UHMWPE biomaterial used to make the convex surface of the disc implant replica in this study was not treated with any radiation. The purpose of irradiating UHMWPE at a high dose is to encourage cross-linkage of polyethylene fibres which can improve fatigue resistance and reduce wear [257]. However, a pin-on-disc study by Yao *et al.* [258] using the same tribological pair has shown that there is no statistical difference between mean coefficients of friction amongst non-irradiated, gamma-irradiated, or electron-beam irradiated GUR 1050 UHMWPE. It is postulated that the non-irradiated UHMWPE used in this study might have increased the wear rate in wear simulation based on ISO18192-1 [1] parameters due to the presence of cross shear as evidenced in

its motion path's aspect ratio. On the contrary, the non-irradiated UHMWPE might have little effect on the wear rate based on parameters from ADL Flexion/Extension as it has a high aspect ratio, provided that the principal motion of sliding is in parallel with the direction of its molecular chains.

As previously described, the control for flexion/extension, lateral bending (abduction/adduction), and axial (inward/outward) rotation on the joint simulator are located inferiorly and it is designed based on the functional motion of a femur in hip joint with respect to a static pelvic bone superiorly. This is in contrast to the requirement set in ISO18192-1 [1] where the angular motion has to happen on the superior component of the disc implant, to replicate the movement of the head with respect to a static torso. Nevertheless, the wear rate outcome from the current wear simulation studies under ISO18192-1 [1]'s parameters is still comparable to the published data from studies conducted on spine simulator.

The ISO18192-1 [1] wear simulation states that the minimum number of test repeat samples is six and it should be run for ten million cycles. Whereas, the wear simulation in the current study only have three repeat samples and were run for five million cycles. This is because of issues related to internal lab logistics as well as time constraint due to global pandemic. Having a greater size of data measurement would definitely improve statistical analysis robustness and possibly could impact the calculated probability value within the spectrum of the confidence interval in analysis of variance.

4.4 Summary

In this chapter, the experimental work on mechanical wear simulation of cervical disc implant has been presented and discussed in detail, guided by the three objectives outlined at the beginning. Two sets of wear simulation performed on replicas of cervical disc implants were successfully completed. The first set incorporates the standard test parameters prescribed in ISO18192-1 [1] for cervical disc implant whereas the second set of tests was based on physiological kinematics and loadings during head flexion/extension of the cervical spine in ADL, derived from Phase I of this research project.

From this wear simulation study,:-

- a) the wear rates between ISO18192-1 [1] and ADL Flexion/Extension profiles are found to be comparable with no statistical significant difference. Nonetheless, ADL Flexion/Extension profile operates at a harsher tribological regime, with higher wear coefficient, than ISO18192-1 [1] based on Archard's Volumetric Wear estimation.
- b) it is theorised that both higher axial load and reduced angular motion are instrumental in having a similar of wear rate between ADL Flexion/Extension and ISO18192-1 [1]. A higher aspect ratio in its motion path also contributed towards the low wear rate of ADL Flexion/Extension.
- c) calculated lambda ratio for both wear simulations is less than 1, which implies that both systems functions at boundary lubrication regime, where wear is amplified.
- d) ISO18192-1 [1] wear profile produces an elliptical wear scar whereas ADL Flexion/Extension has a wavy wear scar
- e) the areal surface roughness fluctuates throughout the simulation for both wear profiles. Surface texture varies across samples – polished as well as raised and roughened, which indicates abrasion and adhesion wear mechanisms.

This study has shown that wear testing of a cervical disc implant with a profile reflective of ADL could provide an insight how this device will behave under physiologically relevant loads and motions. The electromechanical hip joint simulator is capable of meeting the demands needed for testing a spinal disc implant despite its original intended purpose.

Chapter 5

Overall Discussion and Conclusion

5.1 Review of the Achievement on the Research Objectives

In Chapter 2, six objectives were outlined in order to achieve the aims of this research project. The first three objectives were accomplished in Phase I (Chapter 3) and the last three in Phase II (Chapter 4). Below are the reviews on the achieved objectives from this project.

Phase I

- a) to determine a list of everyday tasks that are thought to have an impact on the cervical spinal disc.

Objective (a) has been achieved through comparing the outcome from focus group discussion amongst patients with neck or cervical spine problems with the activities that are frequently reported in academic literature related to neck and cervical spine. From that comparison, eight activities of daily living involving the neck/cervical spine were chosen to be investigated for the study.

- b) to establish a catalogue of cervical joint loads and motions during several activities of daily living involving the cervical spine.

This objective has been achieved through the study of cervical biomechanics conducted in Chapter 3. Using optoelectronic equipment, motions from the chosen ADL were captured in the lab and processed before being further analysed using musculoskeletal multibody modelling for kinematics as well as inverse dynamics outputs. Outcomes for joint angles (flexion/extension, lateral bending, and axial rotation) and joint contact forces (superoinferior axial loading, anteroposterior, and mediolateral directions) for five cervical intervertebral levels (C3-C4, C4-C5, C5-C6, and C6-C7) from twelve subjects were aggregated and

averaged. Finally, a representative profile of loading and motion in cervical spine was defined for each of the eight ADL investigated .

- c) to formulate new wear testing profiles based on loads and motion of cervical spine during ADL as an input for wear simulation of cervical disc implants.

Objective (c) has been achieved by appropriating the representative ADL profiles for cervical loadings and motions derived from objective (b) into wear testing profiles for the simulator's input. The profiles formulated were harmonised according to the axes definition set by ISO18192-1 [1]. The curve of the parameters within the new profiles were also adjusted so the end of each cycle will have the same velocity as the beginning of a cycle. The newly formulated profiles have 1000 points, where it can be resampled according to the input size requirement of any wear simulators or any numerical wear simulation formula. One of the wear profiles formulated is ADL Flexion/Extension, which would be employed for objective (d).

Phase II

- d) to deploy the new wear testing profiles onto state-of-the-art electromechanical, three-station hip joint simulator.

The deployment of the new wear testing profile is to ensure the anatomical position of the cervical spine is aligned with the joint simulator's design as well as the tolerances for motion and loading are met. As the simulator was originally conceived for wear testing of hip joint implant, commissioned by LifeLongJoints consortium, objective (d) was achieved by having a deeper understanding on the working of the simulator and harmonising the research output from Phase I with the simulator inputs requirements. ADL Flexion/Extension, one of several wear profiles formulated in objective (c), was chosen to be deployed. Apart from the new ADL wear testing profile, the profile prescribed by ISO18192-1 [1] for cervical disc implant was also assimilated as an input for the joint simulator as it was never been uploaded onto this machine. Wear testing according to both profile conditions would be implemented in objective (e).

- e) to run mechanical wear simulations under the standard (ISO18192-1 [1]) and physiologically relevant data formulated in objective (c) on an electromechanical joint simulator for five million cycles, using replicas of articulating cervical disc implant bearing surfaces.

In this objective, ADL Flexion/Extension wear profile from objective (c) was selected to represent physiologically relevant loadings and motions on top of the standard test parameters from ISO18192-1 [1] for simulating the wear. This objective has been achieved by running both wear simulation profiles on replica bearings of an articulating cervical disc implant for five million cycles. Each wear profile took about twelve weeks to complete, interrupted by a weekly 24-hour cleaning and weighing session of the test samples as well as replacement of test serum lubricant.

- f) to analyse and compare gravimetric mass loss, as well as surface roughness of the bearing surfaces, throughout mechanical wear testing for both wear test conditions.

Whilst fulfilling objective (e), gravimetric as well as bearing surface roughness measurements were taken weekly on the UHMWPE parts of the implant replica. Data collected were analysed and graph were plotted to obtained wear rate from both wear simulations according to linear regression fit. The wear rate from ADL Flexion/Extension wear simulation has no significant difference to wear rate from ISO18192-1 [1] simulation.

5.2 Hypotheses Validation

In Chapter 2, three hypotheses were outlined as a steering direction for the research to find the answers based on the overall motivation of the project. The first two hypotheses were tested in Phase I (Chapter 3) and the last hypothesis was examined and discussed in detail in Phase II (Chapter 4). Following are reviews of each hypothesis analysed.

Hypothesis I

Cervical joint angle during activities of daily living is ***smaller*** than prescribed cervical joint angle in ISO18192-1 [1] in all movement directions (flexion/extension, lateral bending, and axial rotation) – *Hypothesis Supported.*

The analysis of results from Chapter 3 has shown that the cervical joint angle range is smaller than the ranges provided in ISO18192-1 [1] in all movement directions for all activities of daily living investigated in this project. The ISO18192-1 [1] document has cited the work by Panjabi *et al.* [162], which uses 16 sets of cadaveric cervical spines with all non-ligamentous soft tissue removed, as the source for its cervical motion parameters. Strangely, the study by Panjabi *et al.* [162] in 2001 reported a smaller mean RoM in all directions for all intervertebral joint levels between C3 to C7 than the supposedly angular displacement range prescribed in ISO18192-1 [1]. In a more recent study by Anderst *et al.* [161], which investigated the full cervical RoM from 29 subjects using a biplane x-ray, the mean cervical joint RoM between C3 to C7 reported to be even bigger than the ranges described in Panjabi *et al.* [162]. The range observed also agrees with the outcome from radiographic CT study by Salem *et al.* [160] during full RoM in axial rotation. These two radiographic studies, however, have its mean full cervical RoM value closer to the range prescribed by ISO18192-1 [1] for all directions of motion. Thus, the cervical joint angle range prescribed in ISO18192-1 [1] is, in actuality, a representative of a full cervical range of motion, rather than just an ‘average’ daily condition, given it is closer to ranges observed by Anderst *et al.* [161].

The discrepancies in cervical RoM reported amongst these studies sources could be attributed to the method of data collection employed. Given the motion in cadaveric study by Panjabi *et al.* [162] was conducted using a passive motion (with some of the cervical spine elements removed), the radiographic segmentation method employed by Anderst *et al.* [161] has a more credible, and possibly superior, outcome relating to the cervical RoM with its motion generated intrinsically by the muscles involved and other associated structures surrounding

the cervical spine are still intact, which could be either assisting or hindering the movement.

The results in Chapter 3 from the current project that uses multibody modelling technique also has shown that the cervical angular motion during ADL is a fraction (between 42-86%) of full cervical RoM reported by Anderst *et al.* [161], and, by extension, ISO18192-1 [1]. This observation fits into the hypothesis that cervical joint excursion during daily routines only covers a portion of full joint range afforded by the individual cervical joint levels, as opined by Anderson and Rouleau [76] and was later supported by observations made by Cobian *et al.* [163]. Table 5.1 compares the mean cervical intervertebral joint angle outcomes from studies by Panjabi *et al.* [162], Anderst *et al.* [161], Salem *et al.* [160], ISO18192-1 [1] as well as from this research project. All of this supported the hypothesis that is proposed at the beginning of this research project in which cervical joint angle during activities of daily living is smaller than prescribed cervical joint angle in ISO18192-1 [1] in all movement directions (flexion/extension, lateral bending, and axial rotation).

| Cervical Levels | | C3-C4 | C3-C4 | C3-C4 | C3-C4 |
|---|--|-------------------|-------------------|-------------------|-------------------|
| Mean (\pm SD) of Flexion-Extension ($^{\circ}$) | This study (ADL) | 3.4 (\pm 2.0) | | | |
| | ISO18192-1 [1] | 15.0 | | | |
| | Panjabi <i>et al.</i> [162] (RoM) | 7.7 (\pm 2.5) | 10.1 (\pm 4.0) | 9.9 (\pm 2.7) | 7.1 (\pm 2.0) |
| | Anderst <i>et al.</i> [161] (RoM) | 17.1 (\pm 3.3) | 19.5 (\pm 3.4) | 19.7 (\pm 3.7) | 15.8 (\pm 4.8) |
| Mean (\pm SD) of Unilateral Lateral Bending ($^{\circ}$) | This study (ADL) | 1.4 (\pm 1.0) | | | |
| | ISO18192-1 [1] | 12.0 | | | |
| | Panjabi <i>et al.</i> [162] (RoM) | 4.5 (\pm 1.9) | 4.7 (\pm 1.7) | 3.3 (\pm 1.5) | 2.7 (\pm 1.5) |
| | Anderst <i>et al.</i> [161] (Full RoM) | 14.3 (\pm 2.8) | 13.1 (\pm 3.2) | 12.3 (\pm 3.2) | 14.5 (\pm 3.9) |
| Mean (\pm SD) of Unilateral Axial Rotation ($^{\circ}$) | This study (ADL) | 2.1 (\pm 2.4) | | | |
| | ISO18192-1 [1] | 8.0 | | | |
| | Panjabi <i>et al.</i> [162] (RoM) | 2.6 (\pm 1.2) | 3.4 (\pm 1.3) | 2.5 (\pm 1.0) | 1.5 (\pm 0.8) |
| | Anderst <i>et al.</i> [161] (Full RoM) | 11.8 (\pm 2.1) | 11.3 (\pm 1.7) | 9.3 (\pm 1.9) | 6.5 (\pm 1.7) |
| | Salem <i>et al.</i> [160] (Full RoM) | 5.0 (\pm 2.0) | 5.5 (\pm 1.0) | 5.0 (\pm 2.0) | 4.0 (\pm 2.0) |

Table 5.1 Comparison of mean (and standard deviation) cervical intervertebral joint angles from C3 to C7 levels between studies

Hypothesis II

Cervical joint axial loading during activities of daily living is **higher** than prescribed cervical joint axial loading in ISO18192-1 [1] – Hypothesis Supported.

There is only one reference in ISO18192-1 [1] document that is related to the analysis of loading within the cervical spine. The work by Snijders *et al.* [157] in early 90's, which ISO18192-1 [1] has cited, employs a linked-body model that includes only a number of cervical muscles of substantial size with significant moment arm. It is worth noting that caution was advised by the authors on the conservative estimation of these forces due to several limitations of the analysis. Due to the redundancy nature of the model (more muscles are available than necessary), only three muscles are selected at any point of movement to stabilise the head, based on their optimisation algorithm. In addition, the cervical vertebrae C3 to C7 are modelled as single segment, to simplify the calculation, with only two analytical point of interests, C2-C3 and C7-T1 intervertebral joint levels, where the joint contact forces are calculated. These two cervical joint levels, however, are not suitable for disc prosthesis implantation. The joint contact forces calculated for C2-C3 intervertebral level by Snijders *et al.* [157] are ranging approximately between 25 – 75 N, 75 – 225 N, and 75 – 275 N in flexion/extension, axial rotation, and lateral bending, respectively. The values quoted here are only an approximation as they were obtained from graphs published by Snijders *et al.* [157] with its axes scale's uncertainty value of ± 25 N (Figure 5.1). It is speculated that the 50 – 150 N prescribed axial loading parameter in ISO18192-1 [1] might have been an adjusted value based upon the output data from Snijders *et al.* [157]'s C2-C3 joint contact force during flexion/extension only (25 – 75 N) to reflect the intervertebral levels where disc implant can be inserted.

Upon comparing the axial loading output with a more comprehensive model for the same flexion/extension head movement, it is evident that the magnitude computed by Snijders *et al.* [157] is grossly underestimated as the axial loading estimated by Anderst *et al.* [158] are much higher even at cervical intervertebral level above it (C1-C2). As a general rule, the axial loading is predicted to be increasing as the spinal intervertebral level is descending because it has to

support more structures above them when they are in parallel to the gravity's line of action.

Similarly, the calculated axial loading from the current research is also found to be higher than the estimated loading at C2-C3 level of Snijders *et al.* [157]'s model during flexion/extension head motion given a more comprehensive, discretised vertebral segments, with several additional non-elastic elements, is employed for the simulation. The simulation carried out in Phase I has a more sophisticated muscle modelling with synergistic muscle recruitment algorithm, which are absent in Snijders *et al.* [157]. For instance, the order of magnitude for the maximum axial loading estimated from the current research is more consistent in all directions whereas the maximum axial loading computed by Snijders *et al.* [157] during axial rotation and lateral bending of the head is over 200 N, a much higher force, with bigger loading range, than axial load calculated during flexion/extension motion (25 – 75 N). Therefore, it is assumed that the axial loading parameter prescribed in ISO18192-1 [1] has been considered only

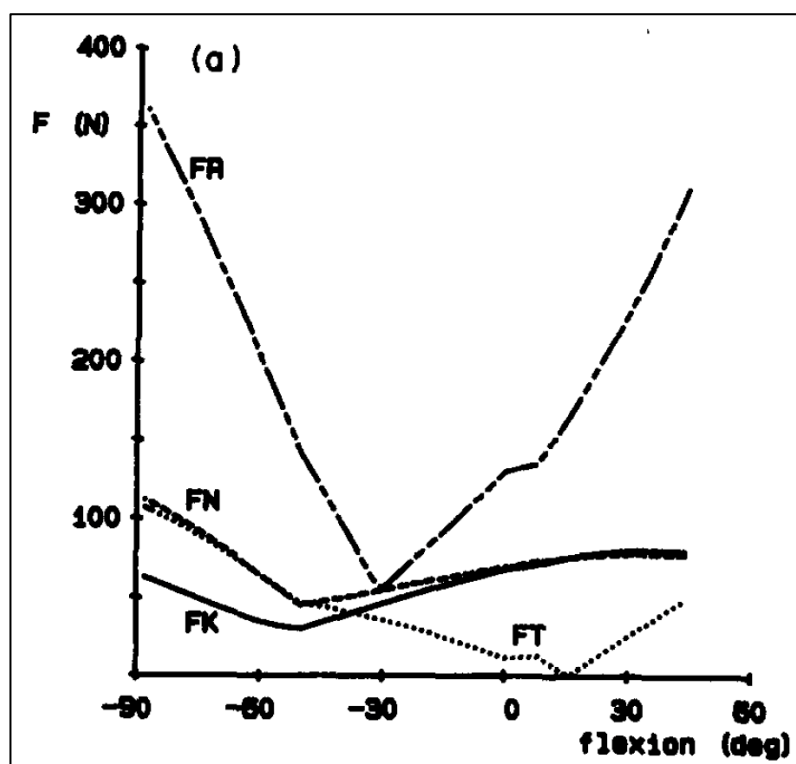


Figure 5.1 Joint contact forces calculated by Snijders *et al.* [157] during flexion/extension. Solid curve line labelled **FK** represents loading at C2-C3 level. The magnitude can be seen to be dipped lower than 50 N between (-)30° and (-)60° head extension.

from the flexion/extension movement in Snijders *et al.* [157], and not from lateral bending or axial rotation, as it is also the more dominant motion. Table 5.2 summarises the comparison described from these paragraphs.

| Head Movement | | Axial Loading Magnitude (N) | | | |
|-----------------|------------------------------|--------------------------------|--------------------------------|--------------------------------|--------------------------------|
| | | Flexion/Extension | | Axial Rotation | |
| Cervical Levels | Studies | Average (\pm SD) Minimum | Average (\pm SD) Maximum | Average (\pm SD) Minimum | Average (\pm SD) Maximum |
| C2-C3 | This study (ADL) | 76.2 (\pm 24.0) | 244.1 (\pm 47.0) | 92.4 (\pm 41.4) | 166.5 (\pm 33.8) |
| | Snijders <i>et al.</i> [157] | \approx 25 | \approx 75 | \approx 75 | \approx 275 |
| C1-C2 | This study (ADL) | 75.1 (\pm 28.1) | 276.2 (\pm 68.9) | - | - |
| | Anderst <i>et al.</i> [158] | \approx 50 | \approx 225 | - | - |
| ISO18192-1 [1] | | 50 | 150 | - | - |

Table 5.2 Comparison of axial loading estimation based from several studies at C2-C3 and C1-C2 cervical intervertebral levels during head flexion/extension and axial rotation as well as ISO18192-1 [1] wear test parameters (\approx indicates approximation value obtained from published graph with ± 25 N uncertainty error)

Arguably, the higher loading within the cervical intervertebral joint calculated in the current study could be resulted from a heavier skull mass employed by the musculoskeletal multibody modelling, as discussed in Section 3.3.6.3. To recap, the current study has the head mass averaging at 5.2 kg for male subjects and 4.0 for female subjects whereas Anderst *et al.* [158] head model is consistently set at 4.2 kg and 3.4 kg for male and female, respectively. Snijders *et al.* [157], on the other hand set the weight of the head at 45 N. Even though the heavier skull mass certainly adds towards the cervical joint loading, their contribution is only to a certain extent. Muscle contraction is still the major source for any joint loading force [174]. In the case of spinal intervertebral joint, the huge back muscle bulk, such as trapezius, is necessary to produce a large force in order to counterbalance the small moment arm it has with the spinal column, as illustrated by Stewart and Hall [259]. This is further evidenced by the compressive strength of the third cervical vertebra which has been reported to reach as high as 1300 N even at C3 vertebral level [259]. The tremendous magnitude of its compressive strength is a testament to its capability to withstand such a force as, according to Wolff's Law, the bone will only adapt its internal architecture as a response to constant exposure to the loading [260]. With a more comprehensive

multibody modelling, it is evidenced that the axial loading experienced by the cervical joint during activities of daily living has a higher estimation than ISO18192-1 [1] has suggested during flexion/extension which supported the original hypothesis proposed.

Hypothesis III

The wear rate of cervical disc implant under loads and motions that represent activity of daily living is **higher** than the wear rate of the implant under loads and motions prescribed in ISO18192-1 [1] – Hypothesis Rejected.

Although the axial loading is found to be more than twice in ADL Flexion/Extension wear simulation, the excursion from its sliding distance is lesser than half of the motion path distance for ISO18192-1 [1], as discussed in Chapter 4. Consequently, the increase in axial loading in ADL Flexion/Extension wear profile is offset by the decrease in sliding distance, making the theoretical volumetric wear should be approximately the same amount as ISO18192-1 [1]. This deduction is reflected in the results from the two mechanical wear simulations carried out in Phase II which have found the wear rate of ADL Flexion/Extension profile is comparable to ISO18192-1 [1] and the difference between them is statistically insignificant. This statistical difference, however, could be potentially improved by having a larger test sample data collected. In wear simulation, this could be achieved by increasing the number of bearing pairs being tested on the simulator as well as lengthening the period of the simulation study to ten million cycles. Currently, there are only three repeats for each of the simulation carried out for this study and they were run for only five million cycles.

The marginally lower wear rate from ADL wear profile, which is inconsequential in this case, perhaps can also be attributed to the notable discrepancy in the aspect ratio between the two wear profiles. Aspect ratio, which quantify the degree of multidirectionality of wear motion path, has been linked with higher wear rate when the ratio is lower and vice versa. The aspect ratio for ADL Flexion/Extension is significantly higher ($p < 0.01$) than ISO18192-1 [1], which explains the slightly lower wear rate in ADL Flexion/Extension compared to

ISO18192-1 [1] wear profile. More importantly, based on Archard's Volumetric Wear Equation, it has been estimated that ADL Flexion/Extension wear profile operates in a harsher tribological regime than ISO18192-1 [1].

Alternative Hypothesis III

The wear rate of cervical disc implant under loads and motions that represent activity of daily living in flexion/extension direction is **comparable** to the wear rate of the implant under loads and motions prescribed in ISO18192-1 [1].

The alternative hypothesis, where the wear rate of implant under loads and motions of activities of daily living is similar to the wear rate of ISO18192-1 [1], can be said to be true only for ADL Flexion/Extension wear profile. Although the axial loading is generally higher (Hypothesis I) and the sliding distance is generally shorter (Hypothesis II) for all ADL investigated in this research project, the wear coefficient and the aspect ratio for other ADL wear profiles were not analysed and it is uncertain how they would affect the wear rate ultimately. Nonetheless, it has been stated that for a simulation on a cervical disc implant to truly reflect the wear *in vivo*, a physiologically-relevant ADL wear profiles should be employed for its wear testing as they operate in a harsher tribological regime.

5.3 Scientific Advancements

The followings are some of the aspects from this research project that have contributed towards body of knowledge.

5.3.1 Catalogue of Cervical Intervertebral Joint Loadings and Motion during Different Activities of Daily Living

Outcome from Phase I of this research project has outlined of a catalogue of cervical intervertebral joint loads and motions during several activities of daily living which previously had been absent in the academic literature until now. Although there has been several musculoskeletal models as well as studies on

ADL involving the cervical spine before, the work from this research project have merged and utilised the knowledge from these two fields together in systemising physiologically-relevant loadings and motions at individual cervical spine levels that are routinely experience by the joints daily.

5.3.2 Mechanical Wear Simulation of Articulating Cervical Disc Implant under Loading and Motion that Represent Activities of Daily Living

Up until now, the outcome from wear simulation involving articulating cervical disc implant has always been reported according to the standard parameters, either by ISO18192-1 [1] or ASTM F2423-11 [4]. Outcome from Phase II of this research project allows us to ascertain the wear performance of the cervical disc implant when subjected to a more physiologically-relevant loadings and motions in which the device is experiencing routinely. Prior to this, it is not known how the articulating disc device would behave under this conditions. This is immensely important as the current standard parameters are lacking in a strong clinical basis or explant analysis justifications [16]. This research project has given a glimpse of the device's wear performance when tested under one of several ADL profiles drafted for evaluating the implants' wear.

5.4 Discussion and Review on the Overall Aims of the Research Project

As the title of this thesis suggests, the goal of this research project was to investigate the wear of cervical total disc replacement under loads and motions that represent activities of daily living. Through six research objectives outlined, the goal of this research project has been accomplished and the three hypotheses set at the beginning were also thoroughly explored.

Under loads and motions of ADL Flexion/Extension, the conservative estimate for wear rate of UHMWPE-CoCrMo cervical disc implant is 1.26 ± 0.084 mg/MC whilst the wear rate for ISO18192-1 [1] test protocol is 1.42 ± 0.071 mg/MC. The difference between the wear rates is, however, statistically insignificant. Based

on this outcome, the standard wear test from ISO18192-1 [1] might therefore not be necessarily inadequate in simulating the wear of a cervical disc implant. But it remains the case that ISO18192-1 [1] does not truly reflect the loads and motions that human cervical spine experience physiologically, which ultimately will influence the wear condition of the device. More importantly, it has been shown that ADL Flexion/Extension wear profile operates in a harsher tribological regime than ISO18192-1 [1] based on the wear coefficient estimation. The new testing protocol designed based on ADL also must match the duty cycle needed to compensate the low amplitude of the angular displacement of cervical spine observed during daily activities, where it has been estimated that a one-year implantation is equivalent between three to five million cycles under ADL wear test conditions [16]. This conclusion comes from a movement study by Cobian *et al.* [16] where they have shown that the neck moves in a more frequent manner with smaller joint amplitude annually than the suggested amount from ISO18192-1 [1] for one year (*i.e.* one million cycles). Therefore, to simulate a ten-year implantation from ADL Flexion/Extension wear profile, the wear testing must be carried out for at least 50 million cycles according to annual flexion/extension estimation from Cobian *et al.* [16]. Following on from this, the stark difference in mass loss of the UHMWPE part of the device after ten-year-implantation-equivalent also can be seen when extrapolated, which is 66.8 mg under ADL Flexion/Extension (using a conservative estimate from the lower wear rate observed in Section 4.3.5), as opposed to 14.2 mg according to ISO18192-1 [1]. This estimation is illustrated in Table 5.3.

| Disc Implant Wear Simulation | ISO18192-1 [1] | ADL Flexion/Extension (under duty cycle recommended by Cobian <i>et al.</i> [16]) |
|---|-----------------------|--|
| Estimation of annual cycle of movement | 1.0×10^6 | 5.3×10^6 [16] |
| Wear rate (mg/MC) | 1.42 ± 0.071 | 1.26 ± 0.084 (conservative value) |
| Estimation of number of cycles after ten years of device implantation | 10.0×10^6 | 53.0×10^6 |
| Estimated mass loss after ten years of device implantation (mg) | 14.2 | 66.8 |

Table 5.3 The estimation for mass loss of UHMWPE from cervical disc implant after ten years of device implantation based on outcomes from both simulations

Arguably, the ISO18192-1 [1] might have taken into consideration both the smaller cervical joint angle as well as more frequent cycles, and thus it was designed to have bigger angular displacement to reduce the duty cycle needed, to confine the wear simulation into a ten-million-cycle limit. This inference is certainly described in the movement study by Cobian *et al.* [16] which has found the overall yearly joint excursion measured in the cervical spine is nearly the same distance traversed by implant when subjected to ISO18192-1 [1] parameter for one million cycles, with 'Observation to Standard' ratio of 1.22, 1.09, and 1.04 for flexion/extension, lateral bending, and axial rotation, respectively. Nonetheless, the study has highlighted that the wear behaviour between ISO18192-1 [1] protocols and ADL conditions could potentially be different and warranted an investigation. In fact, differences in wear coefficients as well as aspect ratios exist between ISO18192-1 [1] and ADL Flexion/Extension wear profiles, enough to warrant a review of the standard wear testing.

The ADL wear simulation carried out in Phase II represents two of many daily living activities; and the movement is predominantly in the sagittal plane. There is also a clear need to simulate other ADL in other planes of motion for wear testing as head motion rarely occurs in a single isolated plane. Cobian *et al.* [16] also have estimated the yearly head movement counts in lateral bending and axial rotation directions to be 4.3 million and 2.8 million, respectively. This information could be the basis in determining the extent of other ADL wear profiles should be simulated for wear testing an articulating cervical disc implant in those directions. Case in point, the ADL wear profile for 'looking for traffic' (Figure 3.11) as formulated in Section 0 where the principal motion is in transverse plane, could be added into the wear testing suite, on top of the ADL Flexion/Extension wear profile as executed in Phase II, and run for another 28 million cycles to simulate a ten-year implantation of the implant. As well as recognising the wide-ranging movement of the neck, this would also incorporate the cross-shear element through heterogeneity of motion paths which ultimately contributes to the wear of the implant.

From these results, there is a strong case for pre-clinical wear testing of the cervical disc implant to be simulated based on activities of daily living and beyond the current standard parameters and requirements. The stylised sinusoidal wear

testing profile prescribed by the ISO has no clinical basis and therefore must be rectified with a more physiologically-relevant parameters [16]. The suite of ADL profiles, such as the set formulated in Phase I, ought to be incorporated into the testing regime for the implant. And these profiles will need to be tested according to its corresponding duty cycles based on observational studies, such as Cobian *et al.* [16].

Nevertheless, one also must acknowledge that simulating the wear testing using several ADL profiles at a higher duty cycle than the prescribed standard will require more time and effort being put in. This could be a critical factor for device manufacturers to consider as it would elongate their bench-testing timeline prior to regulatory approval and would delay the innovation being marketed and, ultimately, being utilised by patients. In this instance, a numerical wear simulation could potentially be a useful tool to have in their testing regime. *In silico* wear simulation has been gaining traction recently with several applications on total joint replacement implants, such as the hip and knee [15, 261]. de Jongh *et al.* [100] also have demonstrated the feasibility of *in silico* wear simulation for disc replacement devices, in which they employed parameters from a typical head movement range, as well as from ISO18192-1 [1]. For *in silico* testing to provide a more meaningful outcome than the traditional mechanical wear testing, the initial focus should be establishing an accurate loading during activities of daily living which could be derived from a comprehensive musculoskeletal multibody modelling, as reviewed by Affatato and Ruggiero [262]. And this research project has fulfilled that focus in Phase I. Fortunately, understanding of cervical biomechanics has been improved since the studies by Panjabi *et al.* [162] and Snijders *et al.* [157] on which ISO18192-1 [1] was based on and the knowledge is still continuously developing [156]. With the widespread availability of modern machine with better computational power, analysis using multibody modelling has become a relatively standard nowadays [158, 202, 263]. The pre-clinical testing of cervical disc implant is still rarely done according to loads and motions data based on activities of daily living from these studies although it has been broached several times within the academic literature [156, 168]. Nonetheless, the changing of tide can be seen as FDA has acknowledged the advantage of computational modelling towards as a tool in evaluating medical devices' performance, on top of the current animal studies and clinical trials [264].

5.5 Limitations of Current Research Project

Wear Simulation Profile for ADL

The analysis and discussion on the wear rate of cervical disc implant under loads and motion of activities of daily living only revolves around one wear testing profile: ADL Flexion/Extension which is derived from two ADL tasks – ‘looking at mobile’ (MOB) and ‘drinking from a bottle’ (WAT). This profile was designed and chosen because it is the most dominant movement by the cervical spine that has been reported, with its hourly average is almost twice as frequent as the other motions [171]. It is also meant to be an analogue to ISO18192-1 [1] wear profile.

There are six other ADLs being investigated and analysed in Phase I but they were not incorporated into the mechanical wear testing study in this research project due to time constraint. Therefore, it is unclear how these other ADLs might have affected the wear behaviour of cervical disc implant individually. Nonetheless, as stated in Section 5.4 earlier, the cervical disc device must be evaluated under a suite of several ADL profiles corresponded to its relevant duty cycles. As a testing regime, where these ADL profiles are combined, it is predicted that the wear rate would be higher and the wear performance of cervical disc implant would be inferior than the simulation under parameters prescribed by ISO18192-1 [1].

Temporal Parameter and Wear Test Frequency

The cycle of motion for cervical spine (flex-extend-flex) analysis is not as prescriptive as human gait. For the same motion in the neck, certain activities will take longer time to complete than the other *e.g.* extending the neck might be quicker for some people when looking at the clock on the wall than drinking water from a bottle. The temporal parameter for cervical spine movement has a greater variation than a typical human gait which is cyclical in nature as to maintain balance of the upper body during locomotion. Therefore, the temporal aspect of cervical spine biomechanics is not explored in Phase I nor it is being considered

as a variable to be manipulated (through cycle frequency) during the wear testing in Phase II.

Other Limitations from Individual Studies

Several other limitations relating to the experimental methods were also discussed in individual study chapters (Chapter 3 and Chapter 4). These limitations, reiterated in the following two paragraphs, should be considered on top of the limitations discussed above.

In Phase I, four main limitations were stated. Firstly, the issue surrounding the use of kinematic rhythm for the cervical spine model, which apportions the intervertebral joint angle motion between the head and thoracic cage equally at the level between C3 to C7. It is thought that this method reduces the accuracy in the calculation of joint angle. Secondly, the load transfer between rigid bodies that represent cervical spinal model employed in this project only has a single contact point when in reality it is known that the loadings between vertebrae are transmitted three-way due to the presence of facet joints. Thirdly, the oversimplification of hyoid-associated muscles modelled by the musculoskeletal model causes the LumpedHyoid muscle entity to be the preferred actuator for the motion at the joint due to its bulkier mass and shorter moment arm. This, consequently, produces an unrealistic loading of the cervical joint which prompted the omission of the muscle group entirely for the purpose of this research project. And lastly, the cubic polynomial muscle recruitment algorithm employed in this model also can cause an abrupt activation in subordinate muscles once the main muscle group has reached its contractility limit. The sudden activation of these muscles can produce a widely varying loading pattern throughout the cohort.

For Phase II, three main limitations were discussed. The first one is the UHMWPE biomaterial used was not treated with any radiation, which normally done to encourage cross-linkage of the polyethylene fibres. The non-irradiated UHMWPE might have caused an increased in wear rate during wear simulation under ISO18192-1 [1] parameters, but have little effect on the wear rate when used

during ADL Flexion/Extension wear simulation. This is based on the difference in their aspect ratio, which relates back to the individual profiles' cross shear. Secondly, the control of the rotational actuators for the joint simulator (flexion/extension, lateral bending, and axial rotation) are located inferior to the implant which is the opposite position required by ISO18192-1 [1], or even physiologically, where the motion should happen superiorly (*i.e.* by the head/skull). And thirdly, the wear simulations carried out in this study only has three repeat sample and were run for only five million cycles. The recommendation from ISO18192-1 [1] for the simulation is to have a minimum of six test specimens and run for ten million cycles. With more repeats and a longer simulation period, a larger data size would be made available for statistical analysis to be more robust, which could improve the probability value in the analysis of variance.

5.6 Potential Publications

Based on advancement of knowledge derived from this research project outlined in Section 5.3, the followings are two of potential manuscripts that will be submitted for publication in academic journals.

Catalogue of Cervical Intervertebral Joint Loadings and Motion during Different Activities of Daily Living

The first manuscript will cover the research work done in Phase I in general. The paper will outline the MoCap technique used to collect trajectory data of the cervical spine motion during ADL performed by the research participants and also the subsequent multibody simulations carried out using musculoskeletal modelling. The outcome from this manuscript will include a catalogue of cervical intervertebral joint loads and motions during several ADL tasks investigated in this research project which will be deposited in Research Data Leeds Repository and can be openly accessed by the research community as well as the public. The manuscript will be submitted to academic journal that focuses on biomechanics of the musculoskeletal system. These physiologically-relevant loadings and motions at individual cervical spine level dataset will hopefully stimulate further research on cervical spine biomechanics.

Mechanical Wear Simulation of Articulating Cervical Disc Implant under Loading and Motion that Represent Activities of Daily Living

The second manuscript, which will be submitted to journal for tribology of medical implant, will be describing the work on mechanical wear simulations performed on the articulating cervical disc implant, as outlined in Phase II of this research project. The paper will outline the wear testing carried out using parameters derived from cervical biomechanics study as well as parameters described in ISO18192-1 [1] as the standard test. Up until now, the outcome from wear simulation involving articulating cervical disc implant has rarely been reported beyond the standard parameters prescribed, either by ISO18192-1 [1] or ASTM F2423-11 [4]. The outcome from Phase II of this research project will report on the wear performance of the cervical disc implant when subjected to a more physiologically-relevant loadings and motions in which the device is experiencing routinely. The publication of this manuscript hopefully will shift the paradigm on cervical disc implant wear testing where it will be used to inform a revision to ISO18192-1 [1] as the current standard parameters are lacking in a strong clinical basis or explant analysis justifications [16].

5.7 Consideration for Future Research

Hyoid Bone and Hyoid-associated Muscle Modelling

As discussed in Chapter 3, hyoid-associated muscles are modelled as a single entity within the AMMR with the absence of the hyoid bone itself. Given that it is a suspended sesamoid bone with no articulation, modelling the hyoid bone for an inverse dynamic algorithm, which is based on Newton's Third Law, is challenging. With multibody modelling, this could be an advantage where it is capable of replicating the complex relationship of hyoid-associated suspensory muscles with its surrounding bones. Better understanding of the function of the hyoid within cervical spine would considerably improve the future iterations of the AMMR.

Spinal Kinematic Rhythm

The kinematics outputs from the musculoskeletal modelling utilised in Phase I are based on a spinal kinematic rhythm function where overall spinal segment motion is equally apportioned to each individual intervertebral joint levels within that spinal region. Given the availability of datasets from radiographic segmentation cervical spine studies, explorative work on proportional apportionment of spinal kinematic rhythm, as opposed to equal distribution, is possible. This research would improve kinematics output from musculoskeletal multibody modelling where it is almost impossible to track individual vertebral movements in the spine during a motion capture session.

Mechanical or Numerical Wear Simulation with Other Cervical ADL Profiles

Mechanical wear simulation carried out in Phase II of this research project only utilises one newly formulated ADL profile. This wear profile represented a typical flexion/extension activity carried out in daily routine. Although biomechanics output from other ADL tasks have been mapped out, they have not yet been incorporated into wear simulation. A mechanical or numerical wear simulation based on profiles from these ADL tasks could reveal the wear rate of the cervical disc implant under these conditions and, ultimately, predict the performance of a device after implantation. On top of that, a study that looked into the frequency of different ADL tasks being performed in a year would also be beneficial for a wear simulation that employs a suite of several ADL wear profiles so it can reflect real-world duty cycle demands.

5.8 Final Conclusions

5.8.1 Conclusions from Study of Cervical Spine Biomechanics During Activities of Daily Living

The investigation into the cervical spine loads and motions during activities of daily living concludes that:-

- the majority of activities of daily living affecting the cervical spine predominantly involve motion in flexion/extension and axial rotation more than lateral bending of the head. This is in contrast to the parameter set in ISO18192-1 [1].
- the cervical joint angle during ADL tasks consists of 42-86% of the total cervical range of motion. The joint excursion during ADL tasks is smaller than what is currently being prescribed in ISO18192-1 [1] because it is believed that angular range set within the standard is equivalent of full RoM for cervical spine.
- the cervical joint loadings during ADL tasks are higher than the value in ISO18192-1 [1] based on a comprehensive cervical musculoskeletal multibody modelling simulation. The magnitude prescribed by ISO18192-1 [1] might have been adjusted, insufficiently, from the C2-C3 cervical intervertebral joint level of a linked-body model which is not the indicated level for implantation of the disc replacement device.

5.8.2 Conclusion from Study of Mechanical Wear Simulation on Articulating Cervical Disc Implants

From the mechanical wear simulation of the cervical disc implant replicas, conclusions that have been drawn are:-

- the wear rate for ADL Flexion/Extension profiles is comparable to wear rate of ISO18192-1 [1] for the same biomaterial with no significant difference between them.
- the ADL Flexion/Extension wear simulation operates a harsher tribological regime compared to ISO18192-1 [1] wear simulation based their wear coefficients estimation.
- it is theorised that both higher cervical axial load and lower joint excursion contributes towards the similar wear rate between ADL Flexion/Extension

and ISO18192-1 [1]. The higher aspect ratio in its motion path also plays a role towards the low wear rate of ADL Flexion/Extension.

- the areal surface roughness fluctuates throughout the simulation for both wear profiles and shows polished as well as raised and roughened, which indicates abrasion and flow wear mechanisms.
- ISO18192-1 [1] wear profile produces an elliptical wear scar whereas ADL Flexion/Extension has a wavy wear scar.
- calculated lambda ratio for both wear simulations is less than one, which means the systems from both wear simulation tests are operating on boundary lubrication regime, where wear is amplified.

5.8.3 Overall Conclusion

Finally, this research project concludes that,

- the standard parameters from ISO18192-1 [1] might not be necessarily inadequate in simulating the wear of a cervical disc implant, but it remains the case that it does not truly reflect the physiological loads and motions that human cervical spine experience daily.
- in order to genuinely evaluate the wear performance of articulating cervical disc implant *in vivo*, the wear test is ought to be done according to the loading and motion experience by the device physiologically. This will be a meaningful shift from the current arbitrary, sinusoidal profile prescribed in ISO18192-1 [1] which is lack in clinical basis.
- wear performance of an articulating cervical disc implant has to be assessed under a suite of testing regime composed of several ADL profiles formulated from biomechanical musculoskeletal modelling outputs.

- each ADL profile has to be run for a period of time according to its appropriate duty cycle based on the number of frequency the motion is projected to annually.
- incorporating *in silico* method in assessing the wear performance is prudent for device manufacturers as the proposed new way of wear testing simulation can be costly and time consuming.

References

1. International Organization for Standardization. ISO 18192-1:2011. *Implants for surgery — Wear of total intervertebral spinal disc prostheses Part 1: Loading and displacement parameters for wear testing and corresponding environmental conditions for test*. Switzerland: International Organization for Standardization, 2011.
2. International Organization for Standardization. *Implants for surgery — Wear of total hip-joint prostheses Part 1: Loading and displacement parameters or wear-testing machines and corresponding environmental conditions for test*. Switzerland: International Organization for Standardization,, 2014.
3. International Organization for Standardization. ISO 14242-2:2016. *Implants for surgery — Wear of total hip-joint prostheses — Part 2: Methods of measurement*. Switzerland: International Organization for Standardization,, 2016.
4. ASTM International. F 2423 – 11. *Standard Guide for Functional, Kinematic, and Wear Assessment of Total Disc Prostheses*. United States: ASTM International, 2011.
5. Geisler, F.H. Surgical treatment for discogenic low-back pain: lumbar arthroplasty results in superior pain reduction and disability level improvement compared with lumbar fusion. *SAS J.* 2007, **1**(1), pp.12-19.
6. Pham, M.H., Mehta, V.A., Tuchman, A. and Hsieh, P.C. Material Science in Cervical Total Disc Replacement. *Biomed Res Int.* 2015, **2015**, p.719123.
7. Mills, E.S., Shelby, T., Bouz, G.J., Hah, R.J., Wang, J.C. and Alluri, R.K. A Decreasing National Trend in Lumbar Disc Arthroplasty. *Global Spine J.* 2022, p.21925682221079571.
8. Jain, N.S., Nguyen, A., Formanek, B., Alluri, R., Buser, Z., Hah, R. and Wang, J.C. Cervical Disc Replacement: Trends, Costs, and Complications. *Asian Spine J.* 2020, **14**(5), pp.647-654.
9. Nesterenko, S.O., Riley, L.H., 3rd and Skolasky, R.L. Anterior cervical discectomy and fusion versus cervical disc arthroplasty: current state and trends in treatment for cervical disc pathology. *Spine (Phila Pa 1976)*. 2012, **37**(17), pp.1470-1474.

10. Chang, H.K., Huang, W.C., Wu, J.C., Tu, T.H., Fay, L.Y., Chang, P.Y., Wu, C.L., Chang, H.C., Chen, Y.C. and Cheng, H. Cervical Arthroplasty for Traumatic Disc Herniation: An Age- and Sex-matched Comparison with Anterior Cervical Discectomy and Fusion. *BMC Musculoskelet Disord.* 2015, **16**, p.228.
11. Saifi, C., Fein, A.W., Cazzulino, A., Lehman, R.A., Phillips, F.M., An, H.S. and Riew, K.D. Trends in resource utilization and rate of cervical disc arthroplasty and anterior cervical discectomy and fusion throughout the United States from 2006 to 2013. *Spine J.* 2018, **18**(6), pp.1022-1029.
12. Anderson, P.A., Rouleau, J.P., Toth, J.M. and Riew, K.D. A comparison of simulator-tested and -retrieved cervical disc prostheses. Invited submission from the Joint Section Meeting on Disorders of the Spine and Peripheral Nerves, March 2004. *J Neurosurg Spine.* 2004, **1**(2), pp.202-210.
13. Kurtz, S., Ciccarelli, L., Harper, M.L., Siskey, R., Shorez, J. and Chan, F.W. Comparison of in vivo and simulator-retrieved metal-on-metal cervical disc replacements. *Int J Spine Surg.* 2012, **6**, pp.145-156.
14. Lunn, D.E., De Pieri, E., Chapman, G.J., Lund, M.E., Redmond, A.C. and Ferguson, S.J. Current Preclinical Testing of New Hip Arthroplasty Technologies Does Not Reflect Real-World Loadings: Capturing Patient-Specific and Activity-Related Variation in Hip Contact Forces. *J Arthroplasty.* 2020, **35**(3), pp.877-885.
15. Mattei, L., Tomasi, M., Artoni, A., Ciulli, E. and Di Puccio, F. Combination of musculoskeletal and wear models to investigate the effect of daily living activities on wear of hip prostheses. *Proceedings of the Institution of Mechanical Engineers, Part J: Journal of Engineering Tribology.* 2021, **235**(12), pp.2675-2687.
16. Cobian, D., Heiderscheit, B., Daehn, N., Anderson, P.A., Spenciner, D., Graham, J. and Dean, S.W. Comparison of Daily Motion of the Cervical and Lumbar Spine to ASTM F2423-11 and ISO 18192-1:2011 Standard Testing. *Journal of ASTM International.* 2012, **9**(1).
17. Grider-Potter, N., Nalley, T.K., Thompson, N.E., Goto, R. and Nakano, Y. Influences of passive intervertebral range of motion on cervical vertebral form. *Am J Phys Anthropol.* 2020.
18. Serhan, H.A., Varnavas, G., Dooris, A.P., Patwadhan, A. and Tzermiadianos, M. Biomechanics of the posterior lumbar articulating elements. *Neurosurg Focus.* 2007, **22**(1), p.E1.

19. Iorio, J.A., Jakoi, A.M. and Singla, A. Biomechanics of Degenerative Spinal Disorders. *Asian Spine J.* 2016, **10**(2), pp.377-384.
20. Watkins, J. *Structure and function of the musculoskeletal system.* 2nd ed. Champaign: Human Kinetics, 2010.
21. Ravindra, V.M., Senglaub, S.S., Rattani, A., Dewan, M.C., Hartl, R., Bisson, E., Park, K.B. and Shrimel, M.G. Degenerative Lumbar Spine Disease: Estimating Global Incidence and Worldwide Volume. *Global Spine J.* 2018, **8**(8), pp.784-794.
22. Davis, H. Increasing rates of cervical and lumbar spine surgery in the United States, 1979-1990. *Spine (Phila Pa 1976).* 1994, **19**(10), pp.1117-1123; discussion 1123-1114.
23. Cohen, S.P. and Hooten, W.M. Advances in the diagnosis and management of neck pain. *BMJ.* 2017, **358**, p.j3221.
24. McCartney, S., Baskerville, R., Blagg, S. and McCartney, D. Cervical radiculopathy and cervical myelopathy: diagnosis and management in primary care. *Br J Gen Pract.* 2018, **68**(666), pp.44-46.
25. Turner, D.A. BMJ Best Practice Degenerative cervical spine disease. [Online]. 2018. [Accessed 29 February 2020]. Available from: <https://bestpractice.bmj.com/topics/en-gb/577/emergingtxs>
26. McCormick, J.R., Sama, A.J., Schiller, N.C., Butler, A.J. and Donnally, C.J., 3rd. Cervical Spondylotic Myelopathy: A Guide to Diagnosis and Management. *J Am Board Fam Med.* 2020, **33**(2), pp.303-313.
27. Vonck, C.E., Tanenbaum, J.E., Smith, G.A., Benzel, E.C., Mroz, T.E. and Steinmetz, M.P. National Trends in Demographics and Outcomes Following Cervical Fusion for Cervical Spondylotic Myelopathy. *Global Spine J.* 2018, **8**(3), pp.244-253.
28. Upadhyayula, P.S., Yue, J.K., Curtis, E.I., Hoshida, R. and Ciacci, J.D. A matched cohort comparison of cervical disc arthroplasty versus anterior cervical discectomy and fusion: Evaluating perioperative outcomes. *J Clin Neurosci.* 2017, **43**, pp.235-239.
29. Dong, L., Xu, Z., Chen, X., Wang, D., Li, D., Liu, T. and Hao, D. The change of adjacent segment after cervical disc arthroplasty compared with anterior cervical discectomy and fusion: a meta-analysis of randomized controlled trials. *Spine J.* 2017, **17**(10), pp.1549-1558.

30. Cason, G.W. and Herkowitz, H.N. Cervical intervertebral disc replacement. *J Bone Joint Surg Am.* 2013, **95**(3), pp.279-285.
31. Hilibrand, A.S., Carlson, G.D., Palumbo, M.A., Jones, P.K. and Bohlman, H.H. Radiculopathy and myelopathy at segments adjacent to the site of a previous anterior cervical arthrodesis. *Journal of Bone and Joint Surgery - Series A.* 1999, **81**, pp.519-528.
32. Virk, S.S., Niedermeier, S., Yu, E. and Khan, S.N. *Adjacent segment disease.* Orthopedics. 2014, 37, pp.547-555.
33. Luo, J., Wang, H., Peng, J., Deng, Z., Zhang, Z., Liu, S., Wang, D., Gong, M. and Tang, S. Rate of Adjacent Segment Degeneration of Cervical Disc Arthroplasty Versus Fusion Meta-Analysis of Randomized Controlled Trials. *World Neurosurg.* 2018, **113**, pp.225-231.
34. Helgeson, M.D., Bevevino, A.J. and Hilibrand, A.S. Update on the evidence for adjacent segment degeneration and disease. *Spine J.* 2013, **13**(3), pp.342-351.
35. Menchetti, P.P.M. *Cervical Spine.* Cham: Springer International Publishing, 2016.
36. Richards, O., Choi, D. and Timothy, J. Cervical arthroplasty: the beginning, the middle, the end? *Br J Neurosurg.* 2012, **26**(1), pp.2-6.
37. Golish, S.R. and Anderson, P.A. Bearing surfaces for total disc arthroplasty: metal-on-metal versus metal-on-polyethylene and other biomaterials. *Spine J.* 2012, **12**(8), pp.693-701.
38. Hall, R.M., Brown, T.D., Fisher, J., Ingham, E., Mendoza, S.A. and Mayer, H.M. Introduction to lumbar total disc replacement: Factors that affect tribological performance. *Proceedings of the Institution of Mechanical Engineers, Part J: Journal of Engineering Tribology.* 2006, **220**(8), pp.775-786.
39. Ko, C.C., Feng, B.K., Kuo, Y.H., Kuo, C.H., Tu, T.H., Chang, C.C., Cheng, H., Huang, W.C. and Wu, J.C. Incidence and Risk Factor of Implant Dislocation After Cervical Disk Arthroplasty: A Retrospective Cohort Analysis of 756 Patients. *Neurosurgery.* 2023, **93**(2), pp.330-338.
40. Smucker, J.D. and Sasso, R.C. Anterior cervical disc replacement: Indications, techniques, and outcomes. *Seminars in Spine Surgery.* 2016, **28**(2), pp.97-106.

41. Malham, G.M., Parker, R.M., Ellis, N.J., Chan, P.G. and Varma, D. Cervical artificial disc replacement with ProDisc-C: clinical and radiographic outcomes with long-term follow-up. *J Clin Neurosci*. 2014, **21**(6), pp.949-953.
42. Yeh, C.-H., Hung, C.-W., Kao, C.-H. and Chao, C.-M. Medium-term outcomes of artificial disc replacement for severe cervical disc narrowing. *Journal of Acute Disease*. 2014, **3**(4), pp.290-295.
43. Gao, X., Yang, Y., Liu, H., Meng, Y., Zeng, J., Wu, T. and Hong, Y. A Comparison of Cervical Disc Arthroplasty and Anterior Cervical Discectomy and Fusion in Patients with Two-Level Cervical Degenerative Disc Disease: 5-Year Follow-Up Results. *World Neurosurg*. 2019, **122**, pp.e1083-e1089.
44. Ning, G.Z., Kan, S.L., Zhu, R.S. and Feng, S.Q. Comparison of Mobi-C Cervical Disc Arthroplasty Versus Fusion for the Treatment of Symptomatic Cervical Degenerative Disc Disease. *World Neurosurg*. 2018, **114**, pp.e224-e239.
45. Li, Y., Shen, H., Khan, K.Z., Fang, S., Liao, Z. and Liu, W. Comparison of Multilevel Cervical Disc Replacement and Multilevel Anterior Discectomy and Fusion: A Systematic Review of Biomechanical and Clinical Evidence. *World Neurosurg*. 2018, **116**, pp.94-104.
46. Jawahar, A., Cavanaugh, D.A., Kerr, E.J., 3rd, Birdsong, E.M. and Nunley, P.D. Total disc arthroplasty does not affect the incidence of adjacent segment degeneration in cervical spine: results of 93 patients in three prospective randomized clinical trials. *Spine J*. 2010, **10**(12), pp.1043-1048.
47. Shriver, M.F., Lubelski, D., Sharma, A.M., Steinmetz, M.P., Benzel, E.C. and Mroz, T.E. Adjacent segment degeneration and disease following cervical arthroplasty: a systematic review and meta-analysis. *Spine J*. 2016, **16**(2), pp.168-181.
48. Shehab, D., Elgazzar, A.H. and Collier, B.D. Heterotopic ossification. *Journal of Nuclear Medicine : official publication, Society of Nuclear Medicine*. 2002, **43**, pp.346-353.
49. Sandhu, F.A., Dowlati, E. and Garica, R. Lumbar Arthroplasty: Past, Present, and Future. *Neurosurgery*. 2020, **86**(2), pp.155-169.
50. Anderson, P.A., Nassr, A., Currier, B.L., Sebastian, A.S., Arnold, P.M., Fehlings, M.G., Mroz, T.E. and Riew, K.D. Evaluation of Adverse Events

in Total Disc Replacement: A Meta-Analysis of FDA Summary of Safety and Effectiveness Data. *Global Spine J.* 2017, **7**(1 Suppl), pp.76S-83S.

51. Noriega, D.C., Ramajo, R.H., Sanchez-Lite, I., Toribio, B., Delen, E. and Sahin, S. Heterotopic Ossification in Cervical Disk Surgery Is Still a Problem. What Are the Key Factors for a Solution? *World Neurosurg.* 2016, **96**, pp.585-590.
52. Zeng, J., Liu, H., Chen, H., Ding, C., Rong, X., Meng, Y. and Yang, Y. Comparison of Heterotopic Ossification After Fixed- and Mobile-Core Cervical Disc Arthroplasty. *World Neurosurg.* 2018, **120**, pp.e1319-e1324.
53. Chin, K.R., Pencle, F.J.R., Mustafa, L.S., Mustafa, M.S., Quijada, K.A. and Seale, J.A. Incidence of Fusion Across Total Disc Replacement With Heterotopic Ossification: Are Ball and Socket Disk Replacements Fusing With and Without Radiographic Evidence. *Clin Spine Surg.* 2019, **32**(10), pp.E469-E473.
54. Overley, S.C., McAnany, S.J., Brochin, R.L., Kim, J.S., Merrill, R.K. and Qureshi, S.A. The 5-year cost-effectiveness of two-level anterior cervical discectomy and fusion or cervical disc replacement: a Markov analysis. *Spine J.* 2018, **18**(1), pp.63-71.
55. Ament, J.D., Yang, Z., Nunley, P., Stone, M.B. and Kim, K.D. Cost-effectiveness of cervical total disc replacement vs fusion for the treatment of 2-level symptomatic degenerative disc disease. *JAMA Surg.* 2014, **149**(12), pp.1231-1239.
56. McAnany, S.J., Merrill, R.K., Overley, S.C., Kim, J.S., Brochin, R.L. and Qureshi, S.A. Investigating the 7-Year Cost-Effectiveness of Single-Level Cervical Disc Replacement Compared to Anterior Cervical Discectomy and Fusion. *Global Spine J.* 2018, **8**(1), pp.32-39.
57. Kim, J.S., Dowdell, J., Cheung, Z.B., Arvind, V., Sun, L., Jandhyala, C., Ukogu, C., Ranson, W., Jacobs, S., McAnany, S. and Cho, S.K. The Seven-Year Cost-Effectiveness of Anterior Cervical Discectomy and Fusion Versus Cervical Disc Arthroplasty: A Markov Analysis. *Spine (Phila Pa 1976)*. 2018, **43**(22), pp.1543-1551.
58. Lee, H., Kim, U.C., Oh, J.K., Kim, T., Park, S. and Ha, Y. Cost-Effectiveness Analysis of Cervical Anterior Fusion and Cervical Artificial Disc Replacement in the Korean Medical System. *J Korean Neurosurg Soc.* 2019, **62**(1), pp.83-89.

59. Traynelis, V.C., Leigh, B.C. and Skelly, A.C. Return to work rates and activity profiles: are there differences between those receiving C-ADR and ACDF? *Evid Based Spine Care J.* 2012, **3**(S1), pp.47-52.
60. Woods, B.I. and Hilibrand, A.S. Cervical radiculopathy: epidemiology, etiology, diagnosis, and treatment. *J Spinal Disord Tech.* 2015, **28**(5), pp.E251-259.
61. Boogaarts, H.D. and Bartels, R.H. Prevalence of cervical spondylotic myelopathy. *Eur Spine J.* 2015, **24 Suppl 2**, pp.139-141.
62. Park, C.K. and Ryu, K.S. Are Controversial Issues in Cervical Total Disc Replacement Resolved or Unresolved?: A Review of Literature and Recent Updates. *Asian Spine J.* 2018, **12**(1), pp.178-192.
63. Kurtz, S. Total Disc Arthroplasty. In: *Spine Technology Handbook.* 2006, pp.303-370.
64. Siemionow, K.B., Hu, X. and Lieberman, I.H. The Fernstrom ball revisited. *Eur Spine J.* 2012, **21**(3), pp.443-448.
65. Patwardhan, A.G. and Havey, R.M. Biomechanics of Cervical Disc Arthroplasty-A Review of Concepts and Current Technology. *Int J Spine Surg.* 2020, **14**(s2), pp.S14-S28.
66. Amoretti, N., Iannessi, A., Lesbats, V., Marcy, P.Y., Hovorka, E., Bronsard, N., Fonquerne, M.E. and Hauger, O. Imaging of intervertebral disc prostheses. *Diagn Interv Imaging.* 2012, **93**(1), pp.10-21.
67. Vital, J.M. and Boissiere, L. Total disc replacement. *Orthop Traumatol Surg Res.* 2014, **100**(1 Suppl), pp.S1-14.
68. Galbusera, F., Bellini, C.M., Brayda-Bruno, M. and Fornari, M. Biomechanical studies on cervical total disc arthroplasty: a literature review. *Clin Biomech (Bristol, Avon).* 2008, **23**(9), pp.1095-1104.
69. U.S. Food and Drug Administration. *Simplify® Cervical Artificial Disc. Summary of Safety and Effectiveness Data.* P200022. 2020.
70. Gomez, P.F. and Morcuende, J.A. A historical and economic perspective on Sir John Charnley, Chas F. Thackray Limited, and the early arthroplasty industry. *The Iowa Orthopaedic Journal.* 2005, **25**, pp.30-37.

71. Moghadas, P.M., Shepherd, D.E., Hukins, D.W. and Mahomed, A. Polymer-on-metal or metal-on-polymer total disc arthroplasty: does it make a difference? *Spine (Phila Pa 1976)*. 2012, **37**(21), pp.1834-1838.
72. U.S. Food and Drug Administration. *PRESTIGE® Cervical Disc System. Summary of Safety and Effectiveness Data*. P060018. 2007.
73. Grupp, T.M., Meisel, H.J., Cotton, J.A., Schwiesau, J., Fritz, B., Blomer, W. and Jansson, V. Alternative bearing materials for intervertebral disc arthroplasty. *Biomaterials*. 2010, **31**(3), pp.523-531.
74. Kölle, L., Ignasiak, D., Ferguson, S.J. and Helgason, B. Ceramics in total disc replacements: A scoping review. *Clin Biomech (Bristol, Avon)*. 2022, **100**, p.105796.
75. Hallab, N., Link, H.D. and McAfee, P.C. Biomaterial optimization in total disc arthroplasty. *Spine (Phila Pa 1976)*. 2003, **28**(20), pp.S139-152.
76. Anderson, P.A. and Rouleau, J.P. Intervertebral disc arthroplasty. *Spine (Phila Pa 1976)*. 2004, **29**(23), pp.2779-2786.
77. U.S. Food and Drug Administration. *ProDisc™-C total disc replacement. Summary of Safety Effectiveness Data*. P070001. 2007.
78. U.S. Food and Drug Administration. *BRYAN® Cervical Disc. Summary of Safety Effectiveness Data*. P060023. 2009.
79. U.S. Food and Drug Administration. *SECURE®-C Cervical Artificial Disc. Summary of Safety and Effectiveness Data*. P100003. 2012.
80. U.S. Food and Drug Administration. *PCM® Cervical Disc. Summary of Safety and Effectiveness Data*. P100012. 2012.
81. U.S. Food and Drug Administration. *Mobi-C® Cervical Disc Prosthesis. Summary of Safety and Effectiveness Data*. P110002. 2013.
82. U.S. Food and Drug Administration. *PRESTIGE® LP Cervical Disc. Summary of Safety and Effectiveness Data*. P090029. 2014.
83. Leven, D., Meaie, J., Radcliff, K. and Qureshi, S. Cervical disc replacement surgery: indications, technique, and technical pearls. *Curr Rev Musculoskelet Med*. 2017, **10**(2), pp.160-169.

84. U.S. Food and Drug Administration. *Simplify Cervical Artificial Disc - P200022*. [Online]. 2020. [Accessed 12 September 2022]. Available from: <https://www.fda.gov/medical-devices/recently-approved-devices/simplify-cervical-artificial-disc-p200022s003>
85. Williams, J. Introduction. In: *Engineering Tribology*. Cambridge: Cambridge University Press, 2005, pp.1-37.
86. Williams, J. Wear and Surface Damage. In: *Engineering Tribology*. 1st ed. Cambridge: Cambridge University Press, 2005, pp.166-199.
87. Kato, K. Classification of wear mechanisms/models. *Proceedings of the Institution of Mechanical Engineers, Part J: Journal of Engineering Tribology*. 2002, **216**, pp.349-356.
88. Archard, J.F. Contact and Rubbing of Flat Surfaces. *Journal of Applied Physics*. 1953, **24**(8), pp.981-988.
89. Nechtow, W., Bushelow, M., Hintner, M., Ochs, A. and Kaddick, C. Cervical Disc Prosthesis Polyethylene Wear Following The ISO Cervical Test. In: *54th Annual Meeting of the Orthopaedic Research Society, San Francisco*. 2008.
90. Wang, S., Liao, Z., Lu, J., Feng, P. and Liu, W. The Biotribological Behaviour of an Artificial Cervical Disc Model with Ball-on-Socket Contact Type Under Different Material Configurations. *Tribology Letters*. 2016, **65**(1).
91. Wang, S., Lu, J., Liao, Z., Feng, P. and Liu, W. Could Ti6Al4V be alternative as a bearing surface articulated with polymer in artificial cervical disc? *Biosurface and Biotribology*. 2017, **3**(2), pp.82-95.
92. Wu, W., Lyu, J., Liu, H., Rong, X., Wang, B., Hong, Y., Gong, Q., Li, T., Liu, L., Song, Y., Cai, Y. and Xu, W. Wear assessments of a new cervical spinal disk prosthesis: Influence of loading and kinematic patterns during in vitro wear simulation. *Proc Inst Mech Eng H*. 2015, **229**(9), pp.619-628.
93. Kienle, A., Graf, N., Kraiss, C. and Wilke, H.J. The MOVE-C Cervical Artificial Disc - Design, Materials, Mechanical Safety. *Med Devices (Auckl)*. 2020, **13**, pp.315-324.
94. Paré, P.E., Chan, F.W. and Powell, M.L. Wear characterization of the A-MAV™ anterior motion replacement using a spine wear simulator. *Wear*. 2007, **263**(7-12), pp.1055-1059.

95. Lee, J.L., Billi, F., Sangiorgio, S.N., McGarry, W., Krueger, D.J., Miller, P.T., McKellop, H. and Ebrahmdadeh, E. Wear of an experimental metal-on-metal artificial disc for the lumbar spine. *Spine (Phila Pa 1976)*. 2008, **33**(6), pp.597-606.
96. Moghadas, P., Mahomed, A., Hukins, D.W. and Shepherd, D.E. Wear in metal-on-metal total disc arthroplasty. *Proc Inst Mech Eng H*. 2013, **227**(4), pp.356-361.
97. U.S. Food and Drug Administration. *Premarket Notification 510(k) | FDA*. [Online]. 2023. [Accessed 20 May 2024]. Available from: <https://www.fda.gov/medical-devices/premarket-submissions-selecting-and-preparing-correct-submission/premarket-notification-510k>
98. Day, C.S., Park, D.J., Rozenshteyn, F.S., Owusu-Sarpong, N. and Gonzalez, A. Analysis of FDA-Approved Orthopaedic Devices and Their Recalls. *J Bone Joint Surg Am*. 2016, **98**(6), pp.517-524.
99. Strickland, M.A., Dressler, M.R. and Taylor, M. Predicting implant UHMWPE wear in-silico: A robust, adaptable computational–numerical framework for future theoretical models. *Wear*. 2012, **274-275**, pp.100-108.
100. de Jongh, C.U., Basson, A.H. and Scheffer, C. Predictive modelling of cervical disc implant wear. *J Biomech*. 2008, **41**(15), pp.3177-3183.
101. Bhattacharya, S., Goel, V.K., Liu, X., Kiapour, A. and Serhan, H.A. Models that incorporate spinal structures predict better wear performance of cervical artificial discs. *Spine J*. 2011, **11**(8), pp.766-776.
102. Wo, J., Lv, Z., Wang, J., Shen, K., Zhu, H., Liu, Y., Huang, Y., Sun, G. and Li, Z. Biomechanical Analysis of Cervical Artificial Disc Replacement Using Cervical Subtotal Discectomy Prosthesis. *Front Bioeng Biotechnol*. 2021, **9**, p.680769.
103. Rawlinson, J.J., Punga, K.P., Gunsallus, K.L., Bartel, D.L. and Wright, T.M. Wear simulation of the ProDisc-L disc replacement using adaptive finite element analysis. *J Neurosurg Spine*. 2007, **7**(2), pp.165-173.
104. Chen, W.C., Liu, Y.L., Lin, K.J., McClean, C.J., Lai, H.J., Chou, C.W., Chang, T.W., Yang, C.T., Huang, C.H., Lai, Y.S. and Cheng, C.K. Concave polyethylene component improves biomechanical performance in lumbar total disc replacement--modified compressive-shearing test by finite element analysis. *Med Eng Phys*. 2012, **34**(4), pp.498-505.

105. Williams, J. Boundary Lubrication and Friction. In: *Engineering Tribology*. 1st ed. Cambridge: Cambridge University Press, 2005, pp.348-380.
106. Beadling, A.R. *Biotribocorrosion of Hard-on-Hard Bearing Surfaces in Orthopaedic Hip Replacements*. PhD thesis, University of Leeds, 2017.
107. Stachowiak, G.W. *Wear – Materials, Mechanisms and Practice*. 2005.
108. Taylor, C.M. Automobile engine tribology—design considerations for efficiency and durability. *Wear*. 1998, **221**(1), pp.1-8.
109. Shaheen, A. and Shepherd, D.E. Lubrication regimes in lumbar total disc arthroplasty. *Proc Inst Mech Eng H*. 2007, **221**(6), pp.621-627.
110. Clewlow, J.P., Pyllos, T. and Shepherd, D.E.T. Soft layer bearing joints for spine arthroplasty. *Materials & Design*. 2008, **29**(10), pp.1981-1985.
111. Kraft, M. Investigation into the Lubrication Regime for Lumbar Total Disc Replacement of the Spine. *IOSR Journal of Engineering*. 2013, **3**(11), pp.21-29.
112. Xin, H., Shepherd, D. and Dearn, K. PEEK (Polyether-ether-ketone) Based Cervical Total Disc Arthroplasty: Contact Stress and Lubrication Analysis. *Open Biomed Eng J*. 2012, **6**, pp.73-79.
113. Williams, J. The Friction of Solids. In: *Engineering Tribology*. Cambridge: Cambridge University Press, 2005, pp.132-165.
114. Xin, H., Shepherd, D.E.T. and Dearn, K.D. A tribological assessment of a PEEK based self-mating total cervical disc replacement. *Wear*. 2013, **303**(1-2), pp.473-479.
115. Sonntag, R., Braun, S., Al-Salehi, L., Reinders, J., Mueller, U. and Kretzer, J.P. Three-dimensional friction measurement during hip simulation. *PLoS One*. 2017, **12**(9), p.e0184043.
116. Ali, M., Al-Hajjar, M., Partridge, S., Williams, S., Fisher, J. and Jennings, L.M. Influence of hip joint simulator design and mechanics on the wear and creep of metal-on-polyethylene bearings. *Proc Inst Mech Eng H*. 2016, **230**(5), pp.389-397.
117. Abdelgaied, A., Fisher, J. and Jennings, L.M. A comparison between electromechanical and pneumatic-controlled knee simulators for the

- investigation of wear of total knee replacements. *Proc Inst Mech Eng H*. 2017, **231**(7), pp.643-651.
118. Moghadas, P., Mahomed, A., Hukins, D.W. and Shepherd, D.E. Friction in metal-on-metal total disc arthroplasty: effect of ball radius. *J Biomech*. 2012, **45**(3), pp.504-509.
119. Scholes, S.C. and Unsworth, A. The effects of proteins on the friction and lubrication of artificial joints. *Proc Inst Mech Eng H*. 2006, **220**(6), pp.687-693.
120. Kurtz, S., Steinbeck, M., Ianuzzi, A., van Ooij, A., Punt, I.M., Isaza, J. and Ross, E.R. Retrieval analysis of motion preserving spinal devices and periprosthetic tissues. *SAS J*. 2009, **3**(4), pp.161-177.
121. Grupp, T.M., Yue, J.J., Garcia, R., Jr., Basson, J., Schwiesau, J., Fritz, B. and Blomer, W. Biotribological evaluation of artificial disc arthroplasty devices: influence of loading and kinematic patterns during in vitro wear simulation. *Eur Spine J*. 2009, **18**(1), pp.98-108.
122. Kettler, A., Bushelow, M. and Wilke, H.J. Influence of the loading frequency on the wear rate of a polyethylene-on-metal lumbar intervertebral disc replacement. *Eur Spine J*. 2012, **21 Suppl 5**, pp.S709-716.
123. Song, J., Xiang, D., Wang, S., Liao, Z., Lu, J., Liu, Y., Liu, W. and Peng, Z. In vitro wear study of PEEK and CFRPEEK against UHMWPE for artificial cervical disc application. *Tribology International*. 2018, **122**, pp.218-227.
124. Prokopovich, P., Perni, S., Fisher, J. and Hall, R.M. Spatial variation of wear on Charite lumbar discs. *Acta Biomater*. 2011, **7**(11), pp.3914-3926.
125. Hyde, P.J., Fisher, J. and Hall, R.M. Wear characteristics of an unconstrained lumbar total disc replacement under a range of in vitro test conditions. *J Biomed Mater Res B Appl Biomater*. 2017, **105**(1), pp.46-52.
126. Hyde, P.J., Tipper, J., Fisher, J. and Hall, R.M. Wear and biological effects of a semi-constrained total disc replacement subject to modified ISO standard test conditions. *J Mech Behav Biomed Mater*. 2015, **44**, pp.43-52.
127. Williams, J. Engineering surfaces. In: *Engineering Tribology*. Cambridge: Cambridge University Press, 2005, pp.38-72.

128. Teague, E.C., Scire, F.E., Baker, S.M. and Jensen, S.W. Three-dimensional stylus profilometry. *Wear*. 1982, **83**(1), pp.1-12.
129. Xu, X. and Hu, H. Development of Non-contact Surface Roughness Measurement in Last Decades. In: *2009 International Conference on Measuring Technology and Mechatronics Automation*. 2009, pp.210-213.
130. Davis, E.J. and Stout, K.J. Stylus measurement techniques: A contribution to the problem of parameter variation. *Wear*. 1982, **83**(1), pp.49-60.
131. Brabazon, D. Nanocharacterization Techniques for Dental Implant Development. In: *Emerging Nanotechnologies in Dentistry: Processes, Materials and Applications*. Elsevier, 2012, pp.307-331.
132. Rao, S. and Costa, K.D. Atomic Force Microscopy (AFM) in biomedical research. In: *Biomedical Imaging: Applications and Advances*. Elsevier, 2014, pp.41-64.
133. Murthy, N.S. 9 - Techniques for analyzing biomaterial surface structure, morphology and topography. In: Williams, R. ed. *Surface Modification of Biomaterials*. Woodhead Publishing, 2011, pp.232-255.
134. Deltombe, R., Kubiak, K.J. and Bigerelle, M. How to select the most relevant 3D roughness parameters of a surface. *Scanning*. 2014, **36**(1), pp.150-160.
135. Galbusera, F., Bellini, C.M., Zweig, T., Ferguson, S., Raimondi, M.T., Lamartina, C., Brayda-Bruno, M. and Fornari, M. Design concepts in lumbar total disc arthroplasty. *Eur Spine J*. 2008, **17**(12), pp.1635-1650.
136. Wennerberg, A., Ohlsson, R., Rosén, B.G. and Andersson, B. Characterizing three-dimensional topography of engineering and biomaterial surfaces by confocal laser scanning and stylus techniques. *Medical Engineering & Physics*. 1996, **18**(7), pp.548-556.
137. Ungersböck, A. and Rahn, B. Methods to characterize the surface roughness of metallic implants. *Journal of Materials Science: Materials in Medicine*. 1994, **5**(6-7), pp.434-440.
138. Green, N.C., Bowen, J., Hukins, D.W. and Shepherd, D.E. Assessment of non-contacting optical methods to measure wear and surface roughness in ceramic total disc replacements. *Proceedings of the Institution of Mechanical Engineers, Part H: Journal of Engineering in Medicine*. 2015, **229**(3), pp.245-254.

139. Hallab, N.J. A review of the biologic effects of spine implant debris: Fact from fiction. *SAS J.* 2009, **3**(4), pp.143-160.
140. Beatty, S. We Need to Talk about Lumbar Total Disc Replacement. *Int J Spine Surg.* 2018, **12**(2), pp.201-240.
141. Punt, I.M., Austen, S., Cleutjens, J.P., Kurtz, S.M., ten Broeke, R.H., van Rhijn, L.W., Willems, P.C. and van Ooij, A. Are periprosthetic tissue reactions observed after revision of total disc replacement comparable to the reactions observed after total hip or knee revision surgery? *Spine (Phila Pa 1976)*. 2012, **37**(2), pp.150-159.
142. Reeks, J. and Liang, H. Materials and Their Failure Mechanisms in Total Disc Replacement. *Lubricants*. 2015, **3**(2), pp.346-364.
143. Veruva, S.Y., Lanman, T.H., Isaza, J.E., MacDonald, D.W., Kurtz, S.M. and Steinbeck, M.J. UHMWPE wear debris and tissue reactions are reduced for contemporary designs of lumbar total disc replacements. *Clin Orthop Relat Res.* 2015, **473**(3), pp.987-998.
144. Gallo, J., Kaminek, P., Ticha, V., Rihakova, P. and Ditmar, R. Particle disease. A comprehensive theory of periprosthetic osteolysis: a review. *Biomed Pap Med Fac Univ Palacky Olomouc Czech Repub.* 2002, **146**(2), pp.21-28.
145. Gornet, M.F., Burkus, J.K., Harper, M.L., Chan, F.W., Skipor, A.K. and Jacobs, J.J. Prospective study on serum metal levels in patients with metal-on-metal lumbar disc arthroplasty. *Eur Spine J.* 2013, **22**(4), pp.741-746.
146. Hallab, N.J. Biological Responses to Spinal Implant Debris. *Spine.* 2017, **42**(7), pp.S4-S5.
147. Viceconti, M., Cavallotti, G., Andrisano, A.O. and Toni, A. Discussion on the design of a hip joint simulator. *Med Eng Phys.* 1996, **18**(3), pp.234-240.
148. Goldsmith, A.A. and Dowson, D. Development of a ten-station, multi-axis hip joint simulator. *Proc Inst Mech Eng H.* 1999, **213**(4), pp.311-316.
149. Saikko, V. A 12-station anatomic hip joint simulator. *Proc Inst Mech Eng H.* 2005, **219**(6), pp.437-448.

150. McIlff, T.E. and Pyk, P. The design and development of a six-degree-of-freedom loading and movement simulator for skeletal structures. *Journal of Biomechanics*. 1994, **27**(6).
151. Vicars, R. *Wear Simulation of Lumbar Total Disc Replacements*. PhD thesis, University of Leeds, 2009.
152. Wang, A. A unified theory of wear for ultra-high molecular weight polyethylene in multi-directional sliding. *Wear*. 2001, **248**(1-2), pp.38-47.
153. Nechtow, W., Hintner, M., Bushelow, M. and Kaddick, C. IVD REPLACEMENT MECHANICAL PERFORMANCE DEPENDS STRONGLY ON INPUT PARAMETERS. In: *52nd Annual Meeting of the Orthopaedic Research Society*. 2006.
154. Goreham-Voss, C.M., Hyde, P.J., Hall, R.M., Fisher, J. and Brown, T.D. Cross-shear implementation in sliding-distance-coupled finite element analysis of wear in metal-on-polyethylene total joint arthroplasty: intervertebral total disc replacement as an illustrative application. *J Biomech*. 2010, **43**(9), pp.1674-1681.
155. Wang, S., Song, J., Liao, Z., Feng, P. and Liu, W. Comparison of wear behaviors for an artificial cervical disc under flexion/extension and axial rotation motions. *Mater Sci Eng C Mater Biol Appl*. 2016, **63**, pp.256-265.
156. Newell, N., Little, J.P., Christou, A., Adams, M.A., Adam, C.J. and Masouros, S.D. Biomechanics of the human intervertebral disc: A review of testing techniques and results. *J Mech Behav Biomed Mater*. 2017, **69**, pp.420-434.
157. Snijders, C.J., Hoek van Dijke, G.A. and Roosch, E.R. A biomechanical model for the analysis of the cervical spine in static postures. *J Biomech*. 1991, **24**(9), pp.783-792.
158. Anderst, W.J., Donaldson, W.F., Lee, J.Y. and Kang, J.D. Subject-specific inverse dynamics of the head and cervical spine during in vivo dynamic flexion-extension. *J Biomech Eng*. 2013, **135**(6), pp.61007-61008.
159. Bayoglu, R., Galibarov, P.E., Verdonschot, N., Koopman, B. and Homminga, J. Twente Spine Model: A thorough investigation of the spinal loads in a complete and coherent musculoskeletal model of the human spine. *Med Eng Phys*. 2019, **68**, pp.35-45.

160. Salem, W., Lenders, C., Mathieu, J., Hermanus, N. and Klein, P. In vivo three-dimensional kinematics of the cervical spine during maximal axial rotation. *Man Ther.* 2013, **18**(4), pp.339-344.
161. Anderst, W.J., Donaldson, W.F., 3rd, Lee, J.Y. and Kang, J.D. Three-dimensional intervertebral kinematics in the healthy young adult cervical spine during dynamic functional loading. *J Biomech.* 2015, **48**(7), pp.1286-1293.
162. Panjabi, M.M., Crisco, J.J., Vasavada, A., Oda, T., Cholewicki, J., Nibu, K. and Shin, E. Mechanical properties of the human cervical spine as shown by three-dimensional load-displacement curves. *Spine (Phila Pa 1976)*. 2001, **26**(24), pp.2692-2700.
163. Cobian, D.G., Daehn, N.S., Anderson, P.A. and Heiderscheit, B.C. Active Cervical and Lumbar Range of Motion During Performance of Activities of Daily Living in Healthy Young Adults. *Spine.* 2013, **38**(20), pp.1754-1763.
164. Kurtz, S., Patwardhan, A., MacDonald, D., Ciccarelli, L., van Ooij, A., Lorenz, M., Zindrick, M., O'Leary, P., Isaza, J. and Ross, R. What is the correlation of in vivo wear and damage patterns with in vitro TDR motion response? *Spine (Phila Pa 1976)*. 2008, **33**(5), pp.481-489.
165. Vicars, R., Hyde, P.J., Brown, T.D., Tipper, J.L., Ingham, E., Fisher, J. and Hall, R.M. The effect of anterior-posterior shear load on the wear of ProDisc-L TDR. *Eur Spine J.* 2010, **19**(8), pp.1356-1362.
166. Vicars, R., Prokopovich, P., Brown, T.D., Tipper, J.L., Ingham, E., Fisher, J. and Hall, R.M. The effect of anterior-posterior shear on the wear of CHARITE total disc replacement. *Spine (Phila Pa 1976)*. 2012, **37**(9), pp.E528-534.
167. Kraft, M. Wear Performance of a Peek-on-Peek Bearing under Cervical Loading Conditions and at Different Test Frequencies. *Global Spine Journal.* 2017, **2**(1_suppl), pp.s-0032-1319995-s-1310032-1319995.
168. Harper, M.L., Dooris, A. and Pare, P.E. The fundamentals of biotribology and its application to spine arthroplasty. *SAS J.* 2009, **3**(4), pp.125-132.
169. Reinders, J., Sonntag, R. and Kretzer, J.P. How do gait frequency and serum-replacement interval affect polyethylene wear in knee-wear simulator tests? *J Mater Sci Mater Med.* 2014, **25**(11), pp.2463-2469.

170. Sterling, A.C., Cobian, D.G., Anderson, P.A. and Heiderscheit, B.C. Annual frequency and magnitude of neck motion in healthy individuals. *Spine (Phila Pa 1976)*. 2008, **33**(17), pp.1882-1888.
171. Cobian, D.G., Sterling, A.C., Anderson, P.A. and Heiderscheit, B.C. Task-specific frequencies of neck motion measured in healthy young adults over a five-day period. *Spine (Phila Pa 1976)*. 2009, **34**(6), pp.E202-207.
172. Lu, T.W. and Chang, C.F. Biomechanics of human movement and its clinical applications. *Kaohsiung J Med Sci*. 2012, **28**(2 Suppl), pp.S13-25.
173. Winter, D.A. *Biomechanics and motor control of human movement*. Fourth edition. ed. Hoboken, N.J: Wiley, 2009.
174. Kłodowski, A. and Rantalainen, T. Multibody Approach to Musculoskeletal and Joint Loading. *Archives of Computational Methods in Engineering*. 2014, **22**(2), pp.237-267.
175. Wang, J., Lui, Z., Qian, Z. and Ren, L. Soft tissue artifact evaluation of the cervical spine in motion patterns of flexion and lateral bending: a preliminary study. *PeerJ*. 2016, **4**, p.e1893.
176. Zemp, R., List, R., Gulay, T., Elsig, J.P., Naxera, J., Taylor, W.R. and Lorenzetti, S. Soft tissue artefacts of the human back: comparison of the sagittal curvature of the spine measured using skin markers and an open upright MRI. *PLoS One*. 2014, **9**(4), p.e95426.
177. Suzuki, Y., Inoue, T. and Nomura, T. A Simple Algorithm for Assimilating Marker-Based Motion Capture Data During Periodic Human Movement Into Models of Multi-Rigid-Body Systems. *Front Bioeng Biotechnol*. 2018, **6**, p.141.
178. Wu, S.K., Lan, H.H., Kuo, L.C., Tsai, S.W., Chen, C.L. and Su, F.C. The feasibility of a video-based motion analysis system in measuring the segmental movements between upper and lower cervical spine. *Gait Posture*. 2007, **26**(1), pp.161-166.
179. Shin, S., Yoon, D.M. and Yoon, K.B. Identification of the correct cervical level by palpation of spinous processes. *Anesth Analg*. 2011, **112**(5), pp.1232-1235.
180. Anderst, W.J., Baillargeon, E., Donaldson, W.F., 3rd, Lee, J.Y. and Kang, J.D. Validation of a noninvasive technique to precisely measure in vivo three-dimensional cervical spine movement. *Spine (Phila Pa 1976)*. 2011, **36**(6), pp.E393-400.

181. van der Horst, M.J. *Human head neck response in frontal, lateral and rear end impact loading : modelling and validation*. PhD thesis, Eindhoven University of Technology, 2002.
182. de Jager, M.K.J. *Mathematical head-neck models for acceleration impacts*. PhD thesis, Eindhoven University of Technology, 1996.
183. Marin, F., Hoang, N., Aufaure, P. and Ho Ba Tho, M.C. In vivo intersegmental motion of the cervical spine using an inverse kinematics procedure. *Clin Biomech (Bristol, Avon)*. 2010, **25**(5), pp.389-396.
184. Anderst, W.J., Donaldson, W.F., Lee, J.Y. and Kang, J.D. Cervical spine intervertebral kinematics with respect to the head are different during flexion and extension motions. *J Biomech*. 2013, **46**(8), pp.1471-1475.
185. Anderst, W.J. Bootstrap prediction bands for cervical spine intervertebral kinematics during in vivo three-dimensional head movements. *J Biomech*. 2015, **48**(7), pp.1270-1276.
186. Bogduk, N. and Mercer, S. Biomechanics of the cervical spine. I: Normal kinematics. *Clinical Biomechanics*. 2000, **15**(9), pp.633-648.
187. Lin, C.C., Lu, T.W., Wang, T.M., Hsu, C.Y., Hsu, S.J. and Shih, T.F. In vivo three-dimensional intervertebral kinematics of the subaxial cervical spine during seated axial rotation and lateral bending via a fluoroscopy-to-CT registration approach. *J Biomech*. 2014, **47**(13), pp.3310-3317.
188. Ishii, T., Mukai, Y., Hosono, N., Sakaura, H., Fujii, R., Nakajima, Y., Tamura, S., Iwasaki, M., Yoshikawa, H. and Sugamoto, K. Kinematics of the cervical spine in lateral bending: in vivo three-dimensional analysis. *Spine (Phila Pa 1976)*. 2006, **31**(2), pp.155-160.
189. Ishii, T., Mukai, Y., Hosono, N., Sakaura, H., Fujii, R., Nakajima, Y., Tamura, S., Sugamoto, K. and Yoshikawa, H. Kinematics of the subaxial cervical spine in rotation in vivo three-dimensional analysis. *Spine (Phila Pa 1976)*. 2004, **29**(24), pp.2826-2831.
190. Patwardhan, A.G., Havey, R.M., Ghanayem, A.J., Diener, H., Meade, K.P., Dunlap, B. and Hodges, S.D. Load-carrying capacity of the human cervical spine in compression is increased under a follower load. *Spine (Phila Pa 1976)*. 2000, **25**(12), pp.1548-1554.
191. Bell, K.M., Yan, Y., Debski, R.E., Sowa, G.A., Kang, J.D. and Tashman, S. Influence of varying compressive loading methods on physiologic motion patterns in the cervical spine. *J Biomech*. 2016, **49**(2), pp.167-172.

192. Colle, K.O., Butler, J.B., Reyes, P.M., Newcomb, A.G., Theodore, N. and Crawford, N.R. Biomechanical evaluation of a metal-on-metal cervical intervertebral disc prosthesis. *Spine J.* 2013, **13**(11), pp.1640-1649.
193. Ravary, B., Pourcelot, P., Bortolussi, C., Konieczka, S. and Crevier-Denoix, N. Strain and force transducers used in human and veterinary tendon and ligament biomechanical studies. *Clin Biomech (Bristol, Avon)*. 2004, **19**(5), pp.433-447.
194. Rohlmann, A., Gabel, U., Graichen, F., Bender, A. and Bergmann, G. An instrumented implant for vertebral body replacement that measures loads in the anterior spinal column. 2007, **29**(5), pp.580-585.
195. Otten, E. Inverse and forward dynamics: models of multi-body systems. *Philos Trans R Soc Lond B Biol Sci.* 2003, **358**(1437), pp.1493-1500.
196. Rasmussen, J., Damsgaard, M. and Voigt, M. Muscle recruitment by the min/max criterion -- a comparative numerical study. *J Biomech.* 2001, **34**(3), pp.409-415.
197. Damsgaard, M., Rasmussen, J., Christensen, S.T., Surma, E. and de Zee, M. Analysis of musculoskeletal systems in the AnyBody Modeling System. *Simulation Modelling Practice and Theory.* 2006, **14**(8), pp.1100-1111.
198. AnyBody Technology. *Muscle Models*. [Online]. 2024. [Accessed 31th May 2024]. Available from: https://anyscript.org/tutorials/Muscle_modeling/index.html
199. de Jager, M., Sauren, A., Thunnissen, J. and Wismans, J. A Three-Dimensional Head-Neck Model: Validation for Frontal and Lateral Impacts. In: *SAE Technical Paper Series*. 1994.
200. van Lopik, D.W. and Acar, M. Development of a multi-body computational model of human head and neck. *Proceedings of the Institution of Mechanical Engineers, Part K: Journal of Multi-body Dynamics.* 2007, **221**(2), pp.175-197.
201. de Zee, M., Falla, D., Farina, D. and Rasmussen, J. A Detailed Rigid-Body Cervical Spine Model Based on Inverse Dynamics. *Journal of Biomechanics.* 2007, **40**.
202. Diao, H., Xin, H., Dong, J., He, X., Li, D. and Jin, Z. Prediction of Cervical Spinal Joint Loading and Secondary Motion Using a Musculoskeletal Multibody Dynamics Model Via Force-Dependent Kinematics Approach. *Spine (Phila Pa 1976)*. 2017, **42**(24), pp.E1403-E1409.

203. Diao, H., Xin, H. and Jin, Z. Prediction of in vivo lower cervical spinal loading using musculoskeletal multi-body dynamics model during the head flexion/extension, lateral bending and axial rotation. *Proc Inst Mech Eng H*. 2018, **232**(11), pp.1071-1082.
204. Ignasiak, D., Dendorfer, S. and Ferguson, S.J. Thoracolumbar spine model with articulated ribcage for the prediction of dynamic spinal loading. *J Biomech*. 2016, **49**(6), pp.959-966.
205. Ignasiak, D., Ferguson, S.J. and Arjmand, N. A rigid thorax assumption affects model loading predictions at the upper but not lower lumbar levels. *J Biomech*. 2016, **49**(13), pp.3074-3078.
206. Ignasiak, D., Rueger, A., Sperr, R. and Ferguson, S.J. Thoracolumbar spine loading associated with kinematics of the young and the elderly during activities of daily living. *J Biomech*. 2018, **70**, pp.175-184.
207. Tsang, S.M., Szeto, G.P. and Lee, R.Y. Normal kinematics of the neck: the interplay between the cervical and thoracic spines. *Man Ther*. 2013, **18**(5), pp.431-437.
208. Goel, V.K. and Clausen, J.D. Prediction of load sharing among spinal components of a C5-C6 motion segment using the finite element approach. *Spine (Phila Pa 1976)*. 1998, **23**(6), pp.684-691.
209. Kumaresan, S., Yoganandan, N., Pintar, F.A. and Maiman, D.J. Finite element modeling of the cervical spine: role of intervertebral disc under axial and eccentric loads. *Med Eng Phys*. 1999, **21**(10), pp.689-700.
210. Bennett, S.E., Schenk, R.J. and Simmons, E.D. Active range of motion utilized in the cervical spine to perform daily functional tasks. *J Spinal Disord Tech*. 2002, **15**(4), pp.307-311.
211. Bible, J.E., Biswas, D., Miller, C.P., Whang, P.G. and Grauer, J.N. Normal functional range of motion of the cervical spine during 15 activities of daily living. *J Spinal Disord Tech*. 2010, **23**(1), pp.15-21.
212. Miller, C.P., Bible, J.E., Jegede, K.A., Whang, P.G. and Grauer, J.N. The effect of rigid cervical collar height on full, active, and functional range of motion during fifteen activities of daily living. *Spine (Phila Pa 1976)*. 2010, **35**(26), pp.E1546-1552.
213. Miller, C.P., Bible, J.E., Jegede, K.A., Whang, P.G. and Grauer, J.N. Soft and rigid collars provide similar restriction in cervical range of motion

- during fifteen activities of daily living. *Spine (Phila Pa 1976)*. 2010, **35**(13), pp.1271-1278.
214. Puttlitz, C.M., Rousseau, M.A., Xu, Z., Hu, S., Tay, B.K. and Lotz, J.C. Intervertebral disc replacement maintains cervical spine kinetics. *Spine (Phila Pa 1976)*. 2004, **29**(24), pp.2809-2814.
215. Patwardhan, A.G. and Havey, R.M. Prosthesis design influences segmental contribution to total cervical motion after cervical disc arthroplasty. *Eur Spine J*. 2020, **29**(11), pp.2713-2721.
216. AnyBody Technology. *Welcome to the AMMR documentation!* [Online]. 2019. [Accessed 29 February 2020]. Available from: <https://anyscript.org/ammr-doc/index.html>
217. AnyBody Technology. *The AnyMoCap Framework*. [Online]. 2019. [Accessed 29 February 2020]. Available from: <https://anyscript.org/ammr-doc/anymocap/index.html>
218. AnyBody Technology. *Introduction to Scaling*. [Online]. 2019. [Accessed 29 February 2020]. Available from: <https://anyscript.org/ammr-doc/Scaling/intro.html>
219. Gatton, M.L. and Pearcy, M.J. Kinematics and movement sequencing during flexion of the lumbar spine. *Clinical Biomechanics*. 1999, **14**(6), pp.376-383.
220. Beaudette, S.M., Zwambag, D.P., Graham, R.B. and Brown, S.H.M. Discriminating spatiotemporal movement strategies during spine flexion-extension in healthy individuals. *Spine J*. 2019, **19**(7), pp.1264-1275.
221. Shichang, L., Yueming, S., Limin, L., Lei, W., Zhongjie, Z., Chunguang, Z. and Xi, Y. Clinical and radiologic comparison of dynamic cervical implant arthroplasty and cervical total disc replacement for single-level cervical degenerative disc disease. *J Clin Neurosci*. 2016, **27**, pp.102-109.
222. Younus, A., Kelly, A. and van der Meulen, W. Motion preservation after cervical total disc replacement surgery-fact or fiction? *Interdisciplinary Neurosurgery*. 2021, **23**.
223. Kim, K.R., Chin, D.K., Kim, K.S., Cho, Y.E., Shin, D.A., Kim, K.N. and Kuh, S.U. Revision Surgery for a Failed Artificial Disc. *Yonsei Med J*. 2021, **62**(3), pp.240-248.

224. Wu, G., Siegler, S., Allard, P., Kirtley, C., Leardini, A., Rosenbaum, D., Whittle, M., D'Lima, D.D., Cristofolini, L., Witte, H., Schmid, O. and Stokes, I. ISB recommendation on definitions of joint coordinate system of various joints for the reporting of human joint motion—part I: ankle, hip, and spine. *Journal of Biomechanics*. 2002, **35**(4), pp.543-548.
225. Namwongsa, S., Puntumetakul, R., Neubert, M.S. and Boucaut, R. Effect of neck flexion angles on neck muscle activity among smartphone users with and without neck pain. *Ergonomics*. 2019, **62**(12), pp.1524-1533.
226. Zarkadis, N.J., Cleveland, A.W., Kusnezov, N.A., Dunn, J.C., Caram, P.M. and Herzog, J.P. Outcomes Following Multilevel Cervical Disc Arthroplasty in the Young Active Population. *Mil Med*. 2017, **182**(3), pp.e1790-e1794.
227. Zheng, B., Hao, D., Guo, H. and He, B. ACDF vs TDR for patients with cervical spondylosis - an 8 year follow up study. *BMC Surg*. 2017, **17**(1), p.113.
228. Zeng, J., Liu, H., Wang, B., Deng, Y., Ding, C., Chen, H., Yang, Y., Hong, Y. and Ning, N. Clinical and radiographic comparison of cervical disc arthroplasty with Prestige-LP Disc and anterior cervical fusion: A minimum 6-year follow-up study. *Clin Neurol Neurosurg*. 2018, **164**, pp.97-102.
229. Luo, H., Wang, X., Fan, M., Deng, L., Jian, C., Wei, M. and Luo, J. The Effect of Visual Stimuli on Stability and Complexity of Postural Control. *Front Neurol*. 2018, **9**, p.48.
230. Auvenshine Rc Dds, P. and Pettit Nj Dmd, M.S.D. The hyoid bone: an overview. *Cranio*. 2020, **38**(1), pp.6-14.
231. Sageshima, H., Pavlu, D., Dvorackova, D. and Panek, D. Onset Timing of Hyoid Muscles Activation during Cervical Flexion Is Position-Dependent: An EMG Study. *Life (Basel)*. 2022, **12**(7).
232. Mortensen, J.D., Vasavada, A.N. and Merryweather, A.S. The inclusion of hyoid muscles improve moment generating capacity and dynamic simulations in musculoskeletal models of the head and neck. *PLoS One*. 2018, **13**(6), p.e0199912.
233. Borst, J., Forbes, P.A., Happee, R. and Veeger, D.H. Muscle parameters for musculoskeletal modelling of the human neck. *Clin Biomech (Bristol, Avon)*. 2011, **26**(4), pp.343-351.

234. AnyBody Technology. *Polynomial Muscle Recruitment*. [Online]. 2023. [Accessed 4th May 2020]. Available from: <https://anyscript.org/tutorials/MuscleRecruitment/lesson4.html>
235. Falla, D., Jull, G., O'Leary, S. and Dall'Alba, P. Further evaluation of an EMG technique for assessment of the deep cervical flexor muscles. *J Electromyogr Kinesiol*. 2006, **16**(6), pp.621-628.
236. Cheng, C.H., Lin, K.H. and Wang, J.L. Co-contraction of cervical muscles during sagittal and coronal neck motions at different movement speeds. *Eur J Appl Physiol*. 2008, **103**(6), pp.647-654.
237. Disselhorst-Klug, C., Schmitz-Rode, T. and Rau, G. Surface electromyography and muscle force: limits in sEMG-force relationship and new approaches for applications. *Clin Biomech (Bristol, Avon)*. 2009, **24**(3), pp.225-235.
238. Roberts, T.J. and Gabaldon, A.M. Interpreting muscle function from EMG: lessons learned from direct measurements of muscle force. *Integr Comp Biol*. 2008, **48**(2), pp.312-320.
239. Choi, H. and Vanderby, R., Jr. Muscle forces and spinal loads at C4/5 level during isometric voluntary efforts. *Med Sci Sports Exerc*. 2000, **32**(4), pp.830-838.
240. Keshner, E.A., Campbell, D., Katz, R.T. and Peterson, B.W. Neck muscle activation patterns in humans during isometric head stabilization. *Exp Brain Res*. 1989, **75**(2), pp.335-344.
241. Yoganandan, N., Pintar, F.A., Zhang, J. and Baisden, J.L. Physical properties of the human head: mass, center of gravity and moment of inertia. *J Biomech*. 2009, **42**(9), pp.1177-1192.
242. Christophy, M., Faruk Senan, N.A., Lotz, J.C. and O'Reilly, O.M. A musculoskeletal model for the lumbar spine. *Biomech Model Mechanobiol*. 2012, **11**(1-2), pp.19-34.
243. Wong, K.W., Luk, K.D., Leong, J.C., Wong, S.F. and Wong, K.K. Continuous dynamic spinal motion analysis. *Spine (Phila Pa 1976)*. 2006, **31**(4), pp.414-419.
244. Rozumalski, A., Schwartz, M.H., Wervej, R., Swanson, A., Dykes, D.C. and Novacheck, T. The in vivo three-dimensional motion of the human lumbar spine during gait. *Gait Posture*. 2008, **28**(3), pp.378-384.

245. Fujii, R., Sakaura, H., Mukai, Y., Hosono, N., Ishii, T., Iwasaki, M., Yoshikawa, H. and Sugamoto, K. Kinematics of the lumbar spine in trunk rotation: in vivo three-dimensional analysis using magnetic resonance imaging. *Eur Spine J.* 2007, **16**(11), pp.1867-1874.
246. Stewart, T.D. and Hall, R.M. (iv) Basic biomechanics of human joints: Hips, knees and the spine. *Current Orthopaedics.* 2006, **20**(1), pp.23-31.
247. Anderst, W., Baillargeon, E., Donaldson, W., Lee, J. and Kang, J. Motion path of the instant center of rotation in the cervical spine during in vivo dynamic flexion-extension: implications for artificial disc design and evaluation of motion quality after arthrodesis. *Spine (Phila Pa 1976).* 2013, **38**(10), pp.E594-601.
248. Haider, H. Chapter 26 - Tribological Assessment of UHMWPE in the Knee. In: Kurtz, S.M. ed. *UHMWPE Biomaterials Handbook (Second Edition)*. Boston: Academic Press, 2009, pp.381-408.
249. Budenberg, S., Redmond, A., White, D., Grainger, A., O'Connor, P., Stone, M.H. and Stewart, T.D. Contact surface motion paths associated with leg length inequality following unilateral total hip replacement. *Proc Inst Mech Eng H.* 2012, **226**(12), pp.968-974.
250. Bennett, D., Orr, J.F., Beverland, D.E. and Baker, R. The influence of shape and sliding distance of femoral head movement loci on the wear of acetabular cups in total hip arthroplasty. *Proc Inst Mech Eng H.* 2002, **216**(6), pp.393-402.
251. Holland, M., Fleming, L., Walton, K., Cerquiglini, A., Hothi, H., Hart, A., Skinner, J. and Bills, P. Characterisation of wear areas on UHMWPE total knee replacement prostheses through study of their areal surface topographical parameters. *Surface Topography: Metrology and Properties.* 2018, **6**(3).
252. Kraft, M., Koch, D.K. and Bushelow, M. An investigation into PEEK-on-PEEK as a bearing surface candidate for cervical total disc replacement. *Spine J.* 2012, **12**(7), pp.603-611.
253. Viitala, R. and Saikko, V. Effect of random variation of input and various daily activities on wear in a hip joint simulator. *J Biomech.* 2020, **106**, p.109831.
254. Smith, S.L. and Unsworth, A. A comparison between gravimetric and volumetric techniques of wear measurement of UHMWPE acetabular cups against zirconia and cobalt-chromium-molybdenum femoral heads in a hip simulator. *Proc Inst Mech Eng H.* 1999, **213**(6), pp.475-483.

255. Pare, P.E., Chan, F.W., Bhattacharya, S. and Goel, V.K. Surface slide track mapping of implants for total disc arthroplasty. *J Biomech.* 2009, **42**(2), pp.131-139.
256. Hyde, P.J. *Bio-tribology of Total Disc Replacements of the Lumbar Spine*. PhD thesis, University of Leeds, 2012.
257. Cheng, C.K., Wang, X.H., Luan, Y.C., Zhang, N.Z., Liu, B.L., Ma, X.Y. and Nie, M.D. Challenges of pre-clinical testing in orthopedic implant development. *Med Eng Phys.* 2019, **72**, pp.49-54.
258. Yao, J.Q., Laurent, M.P., Johnson, T.S., Blanchard, C.R. and Crowninshield, R.D. The influences of lubricant and material on polymer/CoCr sliding friction. *Wear.* 2003, **255**(1-6), pp.780-784.
259. AnyBody Technology. *The Lumbar Spine Model*. [Online]. 2019. [Accessed 29 February 2020]. Available from: https://anyscript.org/ammr-doc/body/lumbar_spine_model.html
260. Izzo, R., Guarnieri, G., Guglielmi, G. and Muto, M. Biomechanics of the spine. Part I: spinal stability. *Eur J Radiol.* 2013, **82**(1), pp.118-126.
261. Burchardt, A., Abicht, C. and Sander, O. An efficient and robust simulator for wear of total knee replacements. *Proc Inst Mech Eng H.* 2020, **234**(9), pp.921-930.
262. Affatato, S. and Ruggiero, A. A Perspective on Biotribology in Arthroplasty: From In Vitro toward the Accurate In Silico Wear Prediction. *Applied Sciences.* 2020, **10**(18).
263. Huynh, K.T., Gibson, I., Jagdish, B.N. and Lu, W.F. Development and validation of a discretised multi-body spine model in LifeMOD for biodynamic behaviour simulation. *Comput Methods Biomech Biomed Engin.* 2015, **18**(2), pp.175-184.
264. Morrison, T.M., Pathmanathan, P., Adwan, M. and Margerrison, E. Advancing Regulatory Science With Computational Modeling for Medical Devices at the FDA's Office of Science and Engineering Laboratories. *Front Med (Lausanne).* 2018, **5**, p.241.
265. Malito, L.G., Arevalo, S., Kozak, A., Spiegelberg, S., Bellare, A. and Pruitt, L. Material properties of ultra-high molecular weight polyethylene: Comparison of tension, compression, nanomechanics and microstructure across clinical formulations. *J Mech Behav Biomed Mater.* 2018, **83**, pp.9-19.

266. Pasko, K.M. *Ceramic coatings for Cervical Total Disc Replacement*. PhD thesis, University of Leeds, 2017.

Appendices

Appendix A Ethics Approval from Engineering and Physical Sciences Ethics Committee (MEEC)

Tuesday, May 12, 2020 at 3:17:09 PM British Summer Time

Subject: MEEC 19-013 - Study Approval
Date: Tuesday, 12 May 2020 at 14:40:53 British Summer Time
From: John Hardy on behalf of EPSResearchEthics
To: Faizal Kamarol Zaman
CC: Richard M Hall [Mech Eng Staff], Michael Bryant, Anthony Redmond

Dear Faizal,

MEEC 19-013 - "Investigation of Wear in Cervical Total Disc Replacement under Loads and Motions that Represent Activities of Daily Living"

I am pleased to inform you that the above research ethics application has been reviewed by the Engineering and Physical Sciences Ethics Committee (MEEC) Committee and on behalf of the Chair, I can confirm a favourable ethical opinion based on the documentation received at date of this email.

Please retain this email as evidence of approval in your study file.

Please notify the committee if you intend to make any amendments to the original research as submitted and approved to date. This includes recruitment methodology; all changes must receive ethical approval prior to implementation. Please see <https://leeds365.sharepoint.com/sites/ResearchandInnovationService/SitePages/Amendments.aspx> or contact the Research Ethics Administrator for further information (EPSResearchEthics@leeds.ac.uk) if required.

Ethics approval does not infer you have the right of access to any member of staff or student or documents and the premises of the University of Leeds. Nor does it imply any right of access to the premises of any other organisation, including clinical areas. The committee takes no responsibility for you gaining access to staff, students and/or premises prior to, during or following your research activities.

Please note: You are expected to keep a record of all your approved documentation, as well as documents such as sample consent forms, risk assessments and other documents relating to the study. This should be kept in your study file, which should be readily available for audit purposes. You will be given a two week notice period if your project is to be audited.

It is our policy to remind everyone that it is your responsibility to comply with Health and Safety, Data Protection and any other legal and/or professional guidelines there may be.

I hope the study goes well.

Best wishes
John Hardy
On behalf of Matthew Campbell

Appendix B PPIE Notes from Cervical/Neck Problem Focus Group (ADL discussed are highlighted in grey)

- The group agreed that it's usually the load that causes problems for them, not the motion e.g. how long you have to stay in a position for.
- The group spoke about adapting activities based upon the required movement, they did this by moving the load elsewhere e.g. relying on mirrors when driving, not putting a seatbelt on whilst reversing so the full range of movement can be used, bringing their mobile phone to their face so they are looking straight at it rather than looking down, tilting the monitor/screen when using a computer/laptop, physically turning to face someone rather than just moving their neck.
- Static posture can be a problem, this is based upon load.
- Looking up and down is the hardest, swan neck rather than relying on shoulders to do so.
- Can't look down to make drinks, so spill a lot. The same for tilting head back to finish a drink.
- Balance can be thrown off. Prolonged loading can lead to dizziness, sickness, tiredness and falling.
- Heavy clothing can't be worn, as this adds to the load.
- One of the group said that she has changed a particular route when driving, as she can't comfortably see around the corner for oncoming traffic.
- Another member said similar, in that she has to move her entire body when crossing a road, as using her neck causes her such discomfort. Everyone agreed with this, saying that it puts pressure on their spine.
- When picking up heavy items, the group said that they have to rely on their knees which isn't good. The movement with going up and down can also cause dizziness.
- There was a discussion about pain when sleeping, or waking up in pain, and having to try out lots of different positions to get it right. This will also vary based upon the day's activities, so there is no set position each night. The group spoke about different pillows they had used, but again the use of the pillows varies based upon the strain that has been put on the neck during the day. One member said she had an inflatable pillow, which can be adjusted by taking stuffing in and out, as well as inflating/deflating.
- The group all agreed that the pain that is caused varies from activity to activity e.g. the pain caused by craning their neck to see a computer screen is different to the pain caused by walking.
- The group agreed that the problem is often made worse as it isn't isolated in the neck, as it has a knock-on effect to the shoulders and/or spine e.g. forward bending to pick up shopping can cause pain in the mid-spine and shoulders.
- Coming back up after tying laces can be a problem, as it causes dizziness. All agreed that the vertical to horizontal motion causes them dizziness. They discussed ways around this, sitting down to tie laces or propping their foot up on a wall.
- The group agreed that picking up something they have dropped causes the same problems for them. The same for looking up.
- The group said that it can be hard washing around the neck and under the chin, however they had work arounds for washing their hair e.g. leaning over bath. They all agreed that leaning back to have their hair washed in the hairdressers was a problem for them.
- They all said that they struggled to take things from high shelves, so tended to use their sticks or a grabber.
- Bad weather is a problem, as they tense up to shelter themselves from the wind/rain.
- A larger bust can cause problems in terms of the load.

Appendix C Programming Codes for Musculoskeletal Modelling in AnyBody Modeling System

(a) Simulation output pathway definition

```
#path ANYBODY_PATH_OUTPUT "Output/Subject_XX"
```

(b) C3D file input pathway definition

```
#path MOCAP_C3D_DATA_PATH "Input/Subject_XX"
```

(c) Configuration of the body model

```
Main = {
  #define BM_LEG_MODEL _LEG_MODEL_TLEM2_
  #define BM_LEG_MUSCLES_RIGHT _MUSCLES_3E_HILL_
  #define BM_LEG_MUSCLES_LEFT _MUSCLES_3E_HILL_

  #define BM_ARM_RIGHT ON
  #define BM_ARM_LEFT ON
  #define BM_ARM_MUSCLES_RIGHT _MUSCLES_3E_HILL_
  #define BM_ARM_MUSCLES_LEFT _MUSCLES_3E_HILL_
  #define BM_ARM_SHOULDER_RHYTHM ON

  #define BM_TRUNK_MUSCLES ON
  #define BM_TRUNK_CERVICAL_MUSCLES _MUSCLES_SIMPLE_
  #define BM_TRUNK_LUMBAR_MUSCLES _MUSCLES_SIMPLE_
  #define BM_TRUNK_CERVICAL_DISC_STIFNESS _DISC_STIFFNESS_NONLINEAR_
  #define BM_TRUNK_LUMBAR_DISC_STIFNESS _DISC_STIFFNESS_NONLINEAR_
  #define BM_TRUNK_CERVICAL_LIGAMENTS ON
  #define BM_TRUNK_LUMBAR_LIGAMENTS ON

  #define BM_SCALING _SCALING_LENGTHMASSFAT_
  #define BM_GLOBAL_REFERENCE_FRAME_SWITCH OFF
  #define BM_MANNEQUIN_DRIVER_DEFAULT OFF
  #define BM_MANNEQUIN_DRIVER_WEAK_SWITCH OFF
};
```

(d) Configuration of weak drivers for the mannequin

```

AnyFolder ExtraDrivers = {

    #define BM_MANNEQUIN_DRIVER_GLENOHUMERAL_ABDUCTION_LEFT ON
    #define BM_MANNEQUIN_DRIVER_GLENOHUMERAL_FLEXION_LEFT ON
    #define BM_MANNEQUIN_DRIVER_GLENOHUMERAL_EXTERNAL_ROTATION_LEFT ON
    #define BM_MANNEQUIN_DRIVER_ELBOW_FLEXION_LEFT ON
    #define BM_MANNEQUIN_DRIVER_ELBOW_PRONATION_LEFT ON
    #define BM_MANNEQUIN_DRIVER_WRIST_FLEXION_LEFT ON
    #define BM_MANNEQUIN_DRIVER_WRIST_ABDUCTION_LEFT ON

    #define BM_MANNEQUIN_DRIVER_GLENOHUMERAL_ABDUCTION_RIGHT ON
    #define BM_MANNEQUIN_DRIVER_GLENOHUMERAL_FLEXION_RIGHT ON
    #define BM_MANNEQUIN_DRIVER_GLENOHUMERAL_EXTERNAL_ROTATION_RIGHT ON
    #define BM_MANNEQUIN_DRIVER_ELBOW_FLEXION_RIGHT ON
    #define BM_MANNEQUIN_DRIVER_ELBOW_PRONATION_RIGHT ON
    #define BM_MANNEQUIN_DRIVER_WRIST_FLEXION_RIGHT ON
    #define BM_MANNEQUIN_DRIVER_WRIST_ABDUCTION_RIGHT ON

};

```

(e) Settings for LumpedHyoid muscle strength parameters

```

AnyFolder MuscleParametersCervicalSpineRight = {

    AnyVar StrengthScaleSpine = ...Scaling.StrengthScaling.Spine.StrengthScale;

    AnyMuscleModel LumpedHyoidT1C0Par = {
        AnyVar PCSA = 2.35*1.5; //Physiological Cross Sectional Area in cm2
        F0 = 0*.StrengthScaleSpine*PCSA *..StrengthRef.SpecificMuscleTensionSpine;
        //Maximum force output at optimum fibre length
    };

    AnyFolder MuscleParametersCervicalSpineLeft = {

        AnyVar StrengthScaleSpine = ...Scaling.StrengthScaling.Spine.StrengthScale;

        AnyMuscleModel LumpedHyoidT1C0Par = {
            AnyVar PCSA = 2.35*1.5; //Physiological Cross Sectional Area in cm2
            F0 = 0*.StrengthScaleSpine*PCSA *..StrengthRef.SpecificMuscleTensionSpine;
            //Maximum force output at optimum fibre length
        };
    };
};

```

(f) Setting for direction of gravity

```

Gravity = -9.81{0,0,1};

```

(g) Setup for force plates

```

Main.EnvironmentModel.ForcePlates = {

    ForcePlateAutoDetection Plate1(
        PLATE_NO=1,
        HeightTolerance = 0.07,
        VelThreshold = 2.2,
        ALLOW_MULTI_LIMB_CONTACT = OFF,
        FORCEPLATE_TYPE = 2
    ) = { };

    ForcePlateAutoDetection Plate2(
        PLATE_NO=2,
        HeightTolerance = 0.07,
        VelThreshold = 2.2,
        ALLOW_MULTI_LIMB_CONTACT = OFF,
        FORCEPLATE_TYPE = 2
    ) = { };

};

```

(h) Input setup for individual subject's height and weight

```

Main.HumanModel.Anthropometrics = {

    BodyMass = Z;
    BodyHeight = Y;
};

```

(i) Setup for trial file of the captured task

```

Main.ModelSetup.TrialSpecificData = {

    // The trial(s) from which segment scaling and marker parameters are loaded from.
    // This default to the current trial itself, if nothing is specified.
    LoadParametersFrom = {"ST"};

    // This is the name of the trial c3d file without extension.
    // Here we assume the c3d file has the same name as the main file directory.
    TrialFileName = "DT";

    // This the C3D frame where the analysis starts
    // If not specified it defaults to the first frame of the C3D file
    FirstFrame = .C3DFileData.Header.FirstFrameNo;

    // This the C3D frame where the analysis ends
    // If not specified it defaults the first frame of the C3D file
    LastFrame = .C3DFileData.Header.LastFrameNo;

};

```

(j) Optimisation setup for anthropometric measurement

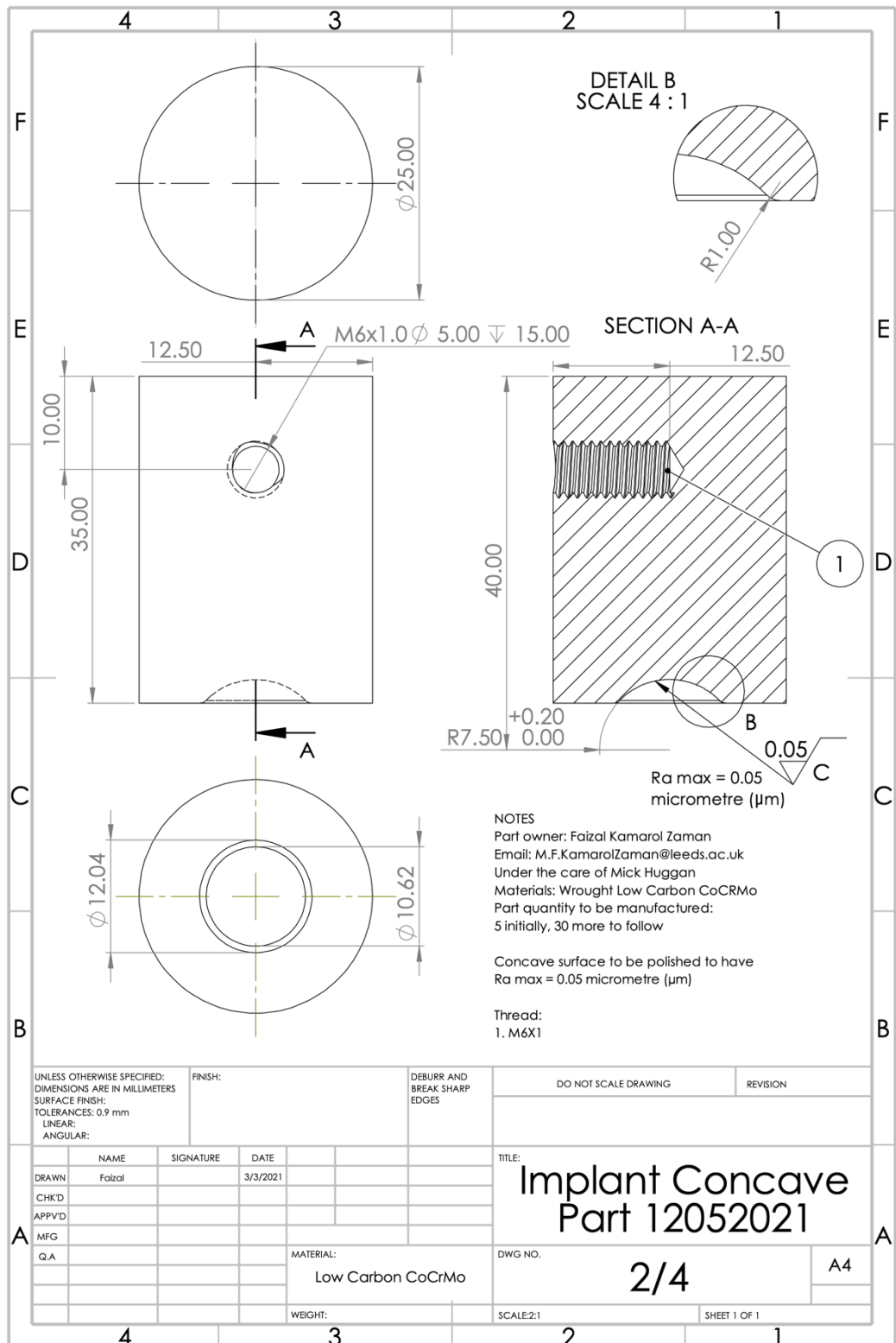
```
Main.ModelSetup.LabSpecificData = {  
  
  // This adds different segment length as design variables to the parameter identification  
  // study (Main.Studies.ParameterIdentification)  
  // This allows the segment length to be optimized in based on the markers/motion  
  
  OptimizeAnthropometricsOnOff OptimizeAntropometricsOnOff (  
    PELVIS_WIDTH = ON,  
    HEAD_HEIGHT = ON,  
    TRUNK_HEIGHT= ON,  
    RIGHT_THIGH_LENGTH= ON,  
    LEFT_THIGH_LENGTH = ON,  
    RIGHT_SHANK_LENGTH= ON,  
    LEFT_SHANK_LENGTH = ON,  
    RIGHT_FOOT_LENGTH= ON,  
    LEFT_FOOT_LENGTH = ON,  
    RIGHT_UPPERARM_LENGTH= ON,  
    LEFT_UPPERARM_LENGTH = ON,  
    RIGHT_LOWERARM_LENGTH= ON,  
    LEFT_LOWERARM_LENGTH = ON,  
    RIGHT_HAND_LENGTH= ON,  
    LEFT_HAND_LENGTH = ON,  
    LEFT_RIGHT_SYMMETRY = ON  
  ) = { };  
};
```

(k) Setup for MarkerFilterIndex value during Parameter Identification simulation study

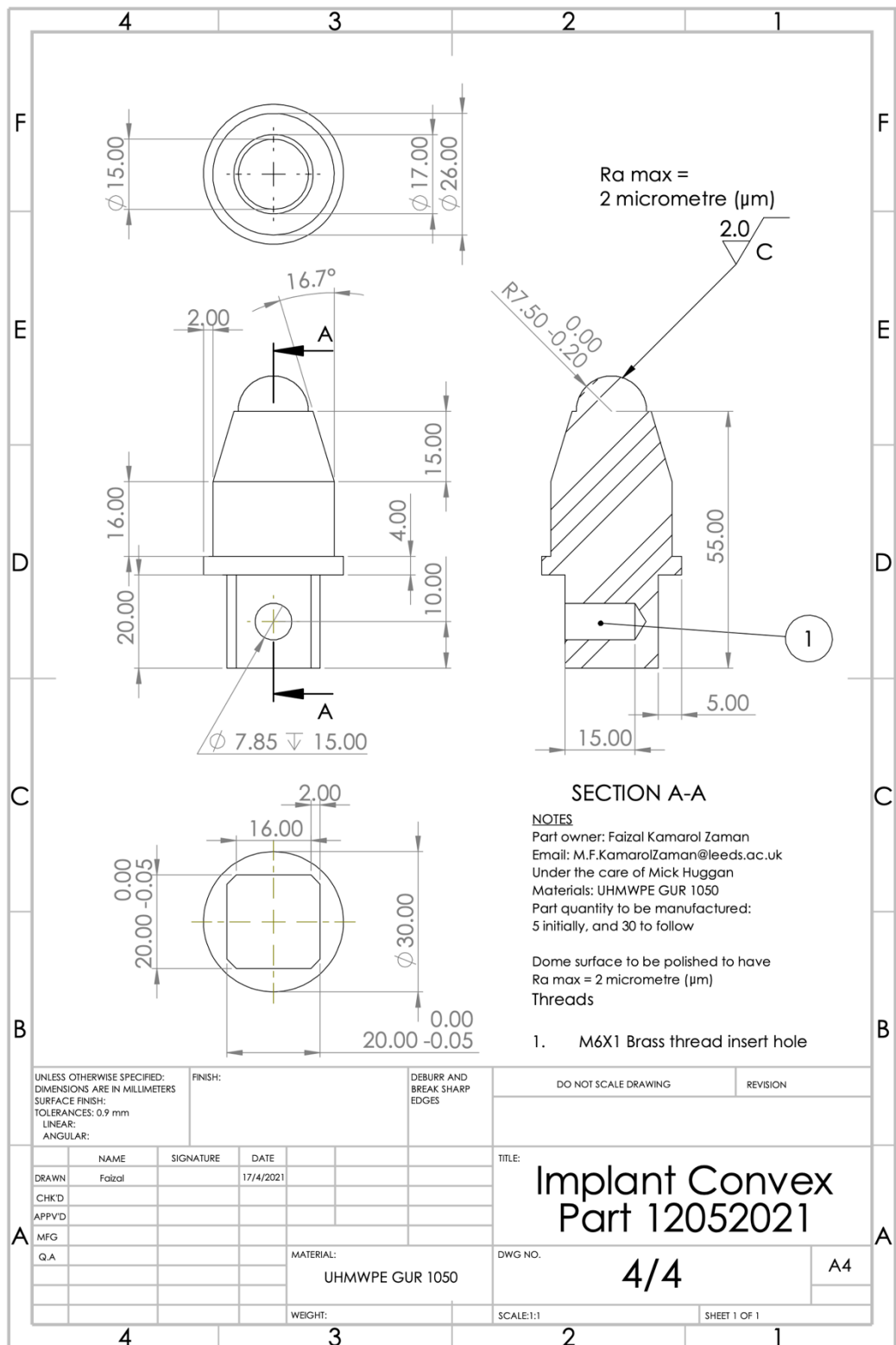
```
Main.ModelSetup.C3DFileData = {  
  
  MarkerFilterIndex = -1;  
};
```

Appendix D Engineering Drawings for Replica of Cervical Disc Implant

(a) Design for CoCrMo concave part



(b) Design for UHMWPE convex part



Appendix E 128-point Wear Profiles for LifeLongJoint Hip Simulator Input

(a) ISO18192-1 Cervical.txt

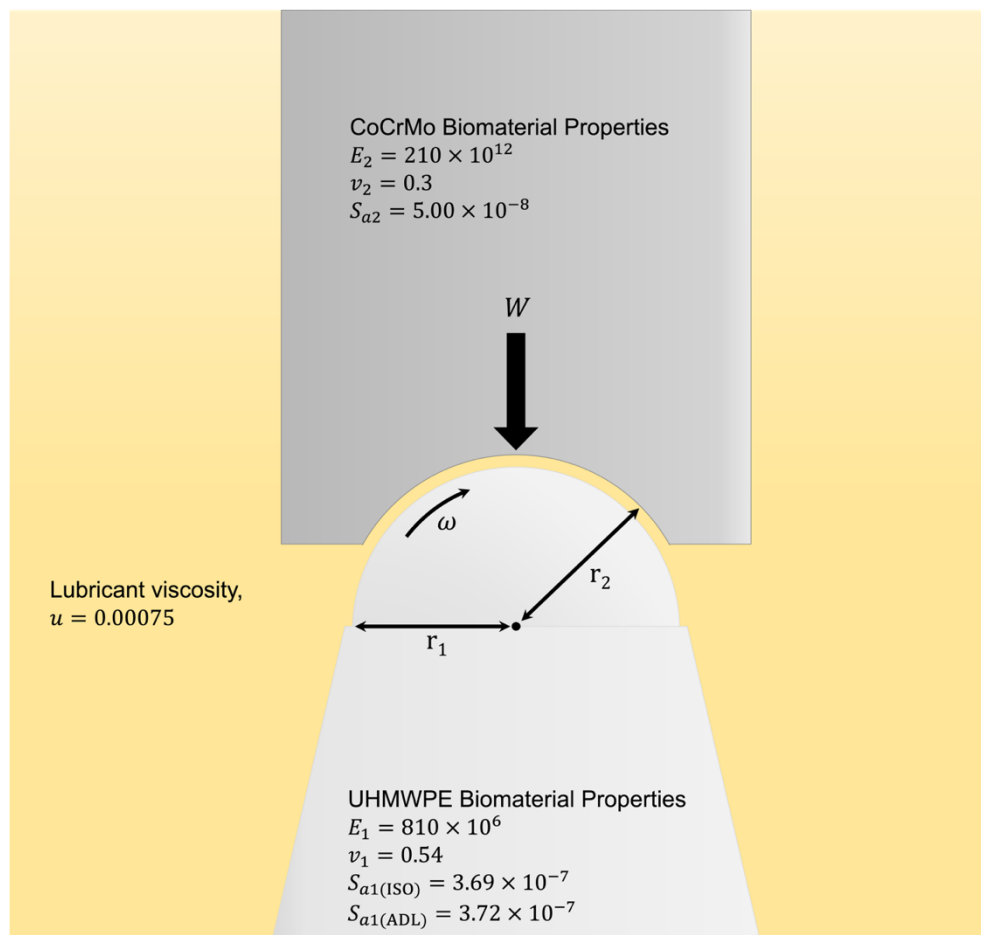
| Index | Axial Load | Flexion/ Extension | Lateral Bending | Axial Rotation | Index | Axial Load | Flexion/ Extension | Lateral Bending | Axial Rotation |
|-------|------------|--------------------|-----------------|----------------|-------|------------|--------------------|-----------------|----------------|
| 1 | 100.00 | 0.00 | 6.00 | -4.00 | 65 | 100.34 | 0.05 | -6.00 | 4.00 |
| 2 | 102.41 | 0.37 | 5.99 | -3.99 | 66 | 97.94 | -0.32 | -5.99 | 4.00 |
| 3 | 104.89 | 0.73 | 5.97 | -3.98 | 67 | 95.47 | -0.68 | -5.98 | 3.98 |
| 4 | 107.37 | 1.10 | 5.94 | -3.96 | 68 | 92.98 | -1.05 | -5.94 | 3.96 |
| 5 | 109.75 | 1.46 | 5.89 | -3.92 | 69 | 90.58 | -1.41 | -5.89 | 3.93 |
| 6 | 112.09 | 1.82 | 5.82 | -3.88 | 70 | 88.25 | -1.77 | -5.83 | 3.89 |
| 7 | 114.51 | 2.17 | 5.74 | -3.83 | 71 | 85.83 | -2.12 | -5.75 | 3.84 |
| 8 | 116.84 | 2.52 | 5.65 | -3.77 | 72 | 83.48 | -2.47 | -5.66 | 3.78 |
| 9 | 119.08 | 2.86 | 5.55 | -3.70 | 73 | 81.24 | -2.82 | -5.56 | 3.71 |
| 10 | 121.35 | 3.20 | 5.43 | -3.62 | 74 | 78.97 | -3.15 | -5.44 | 3.63 |
| 11 | 123.54 | 3.53 | 5.29 | -3.53 | 75 | 76.77 | -3.48 | -5.31 | 3.54 |
| 12 | 125.66 | 3.85 | 5.15 | -3.43 | 76 | 74.63 | -3.80 | -5.17 | 3.45 |
| 13 | 127.73 | 4.16 | 4.99 | -3.33 | 77 | 72.56 | -4.12 | -5.02 | 3.34 |
| 14 | 129.74 | 4.46 | 4.82 | -3.22 | 78 | 70.54 | -4.42 | -4.85 | 3.23 |
| 15 | 131.69 | 4.75 | 4.64 | -3.10 | 79 | 68.58 | -4.71 | -4.67 | 3.11 |
| 16 | 133.51 | 5.03 | 4.45 | -2.97 | 80 | 66.74 | -4.99 | -4.48 | 2.99 |
| 17 | 135.25 | 5.29 | 4.25 | -2.83 | 81 | 64.99 | -5.26 | -4.28 | 2.85 |
| 18 | 136.94 | 5.55 | 4.04 | -2.69 | 82 | 63.30 | -5.51 | -4.07 | 2.71 |
| 19 | 138.57 | 5.79 | 3.82 | -2.54 | 83 | 61.66 | -5.76 | -3.85 | 2.57 |
| 20 | 140.14 | 6.02 | 3.58 | -2.39 | 84 | 60.07 | -5.98 | -3.62 | 2.41 |
| 21 | 141.53 | 6.23 | 3.34 | -2.23 | 85 | 58.66 | -6.20 | -3.38 | 2.25 |
| 22 | 142.81 | 6.42 | 3.10 | -2.06 | 86 | 57.37 | -6.40 | -3.13 | 2.09 |
| 23 | 144.02 | 6.61 | 2.84 | -1.89 | 87 | 56.14 | -6.58 | -2.88 | 1.92 |
| 24 | 145.10 | 6.77 | 2.58 | -1.72 | 88 | 55.04 | -6.75 | -2.62 | 1.74 |
| 25 | 146.13 | 6.92 | 2.31 | -1.54 | 89 | 54.01 | -6.90 | -2.35 | 1.57 |
| 26 | 147.07 | 7.05 | 2.04 | -1.36 | 90 | 53.05 | -7.04 | -2.08 | 1.38 |
| 27 | 147.84 | 7.17 | 1.76 | -1.17 | 91 | 52.26 | -7.16 | -1.80 | 1.20 |
| 28 | 148.43 | 7.27 | 1.47 | -0.98 | 92 | 51.65 | -7.26 | -1.51 | 1.01 |
| 29 | 148.99 | 7.35 | 1.19 | -0.79 | 93 | 51.08 | -7.34 | -1.23 | 0.82 |
| 30 | 149.43 | 7.42 | 0.90 | -0.60 | 94 | 50.62 | -7.41 | -0.94 | 0.63 |
| 31 | 149.74 | 7.46 | 0.61 | -0.40 | 95 | 50.30 | -7.46 | -0.65 | 0.43 |
| 32 | 149.93 | 7.49 | 0.31 | -0.21 | 96 | 50.09 | -7.49 | -0.36 | 0.24 |
| 33 | 150.00 | 7.50 | 0.02 | -0.01 | 97 | 50.00 | -7.50 | -0.06 | 0.04 |
| 34 | 149.95 | 7.49 | -0.27 | 0.18 | 98 | 50.04 | -7.49 | 0.23 | -0.15 |
| 35 | 149.77 | 7.47 | -0.57 | 0.38 | 99 | 50.19 | -7.47 | 0.52 | -0.35 |
| 36 | 149.48 | 7.42 | -0.86 | 0.57 | 100 | 50.47 | -7.43 | 0.82 | -0.54 |
| 37 | 149.06 | 7.36 | -1.15 | 0.77 | 101 | 50.87 | -7.37 | 1.11 | -0.74 |
| 38 | 148.52 | 7.28 | -1.43 | 0.96 | 102 | 51.40 | -7.29 | 1.39 | -0.93 |
| 39 | 147.93 | 7.19 | -1.72 | 1.15 | 103 | 51.98 | -7.20 | 1.68 | -1.12 |
| 40 | 147.20 | 7.07 | -2.00 | 1.33 | 104 | 52.69 | -7.09 | 1.96 | -1.31 |
| 41 | 146.27 | 6.94 | -2.27 | 1.51 | 105 | 53.59 | -6.96 | 2.23 | -1.49 |
| 42 | 145.25 | 6.79 | -2.54 | 1.69 | 106 | 54.60 | -6.82 | 2.50 | -1.67 |
| 43 | 144.18 | 6.63 | -2.80 | 1.87 | 107 | 55.66 | -6.65 | 2.77 | -1.85 |
| 44 | 142.98 | 6.45 | -3.06 | 2.04 | 108 | 56.84 | -6.48 | 3.03 | -2.02 |
| 45 | 141.71 | 6.26 | -3.31 | 2.21 | 109 | 58.11 | -6.28 | 3.27 | -2.18 |
| 46 | 140.35 | 6.05 | -3.55 | 2.37 | 110 | 59.44 | -6.08 | 3.52 | -2.34 |
| 47 | 138.79 | 5.82 | -3.78 | 2.52 | 111 | 60.98 | -5.85 | 3.75 | -2.50 |
| 48 | 137.17 | 5.58 | -4.01 | 2.67 | 112 | 62.60 | -5.62 | 3.98 | -2.65 |
| 49 | 135.49 | 5.33 | -4.22 | 2.81 | 113 | 64.27 | -5.37 | 4.19 | -2.79 |
| 50 | 133.76 | 5.07 | -4.42 | 2.95 | 114 | 65.99 | -5.10 | 4.40 | -2.93 |
| 51 | 131.96 | 4.79 | -4.62 | 3.08 | 115 | 67.78 | -4.83 | 4.59 | -3.06 |
| 52 | 130.02 | 4.50 | -4.80 | 3.20 | 116 | 69.70 | -4.54 | 4.77 | -3.18 |
| 53 | 128.02 | 4.20 | -4.97 | 3.31 | 117 | 71.70 | -4.24 | 4.95 | -3.30 |
| 54 | 125.96 | 3.89 | -5.13 | 3.42 | 118 | 73.74 | -3.94 | 5.11 | -3.40 |
| 55 | 123.84 | 3.57 | -5.28 | 3.52 | 119 | 75.86 | -3.62 | 5.26 | -3.50 |
| 56 | 121.66 | 3.25 | -5.41 | 3.61 | 120 | 78.03 | -3.29 | 5.39 | -3.59 |
| 57 | 119.40 | 2.91 | -5.53 | 3.69 | 121 | 80.27 | -2.96 | 5.51 | -3.68 |
| 58 | 117.16 | 2.57 | -5.64 | 3.76 | 122 | 82.53 | -2.62 | 5.62 | -3.75 |
| 59 | 114.85 | 2.22 | -5.73 | 3.82 | 123 | 84.81 | -2.27 | 5.72 | -3.81 |
| 60 | 112.42 | 1.87 | -5.81 | 3.87 | 124 | 87.24 | -1.92 | 5.80 | -3.87 |
| 61 | 110.08 | 1.51 | -5.88 | 3.92 | 125 | 89.59 | -1.56 | 5.87 | -3.91 |
| 62 | 107.71 | 1.15 | -5.93 | 3.95 | 126 | 91.95 | -1.20 | 5.92 | -3.95 |
| 63 | 105.24 | 0.79 | -5.97 | 3.98 | 127 | 94.40 | -0.84 | 5.96 | -3.97 |
| 64 | 102.75 | 0.42 | -5.99 | 3.99 | 128 | 96.90 | -0.47 | 5.99 | -3.99 |

(b) ADL Flex/Ext Cervical.txt

| Index | Axial Load | Flexion/ Extension | Lateral Bending | Axial Rotation | Antero-posterior Load | Index | Axial Load | Flexion/ Extension | Lateral Bending | Axial Rotation | Antero-posterior Load |
|-------|------------|--------------------|-----------------|----------------|-----------------------|-------|------------|--------------------|-----------------|----------------|-----------------------|
| 1 | 165.34 | 1.39 | 0.31 | -0.26 | 5.94 | 65 | 192.48 | 2.55 | 0.8 | -0.22 | 12.61 |
| 2 | 163.03 | 1.27 | 0.36 | -0.26 | 5.20 | 66 | 196.17 | 2.64 | 0.88 | -0.23 | 13.25 |
| 3 | 160.52 | 1.16 | 0.41 | -0.28 | 4.59 | 67 | 200.24 | 2.73 | 0.96 | -0.24 | 13.95 |
| 4 | 157.58 | 1.03 | 0.48 | -0.29 | 3.92 | 68 | 204.67 | 2.82 | 1.03 | -0.24 | 14.68 |
| 5 | 154.18 | 0.90 | 0.55 | -0.31 | 3.17 | 69 | 209.42 | 2.92 | 1.11 | -0.25 | 15.45 |
| 6 | 150.31 | 0.75 | 0.62 | -0.34 | 2.31 | 70 | 214.60 | 3.03 | 1.19 | -0.24 | 16.26 |
| 7 | 146.06 | 0.59 | 0.68 | -0.36 | 1.23 | 71 | 220.34 | 3.13 | 1.28 | -0.24 | 17.11 |
| 8 | 141.43 | 0.43 | 0.72 | -0.39 | 0.17 | 72 | 226.59 | 3.23 | 1.37 | -0.22 | 18.00 |
| 9 | 137.13 | 0.26 | 0.74 | -0.41 | 0.00 | 73 | 232.98 | 3.34 | 1.46 | -0.21 | 18.98 |
| 10 | 132.65 | 0.09 | 0.76 | -0.44 | 0.00 | 74 | 239.49 | 3.45 | 1.55 | -0.18 | 20.06 |
| 11 | 127.61 | -0.09 | 0.77 | -0.46 | 0.00 | 75 | 246.22 | 3.56 | 1.64 | -0.16 | 21.25 |
| 12 | 122.63 | -0.26 | 0.78 | -0.48 | 0.00 | 76 | 253.28 | 3.67 | 1.72 | -0.13 | 22.48 |
| 13 | 118.99 | -0.44 | 0.79 | -0.51 | 0.00 | 77 | 260.58 | 3.79 | 1.79 | -0.10 | 23.78 |
| 14 | 116.05 | -0.61 | 0.8 | -0.53 | 0.00 | 78 | 268.30 | 3.92 | 1.86 | -0.07 | 25.01 |
| 15 | 113.66 | -0.77 | 0.8 | -0.55 | 0.00 | 79 | 275.99 | 4.06 | 1.92 | -0.05 | 26.28 |
| 16 | 114.39 | -0.93 | 0.81 | -0.56 | 0.00 | 80 | 283.58 | 4.21 | 1.96 | -0.02 | 27.51 |
| 17 | 113.93 | -1.08 | 0.81 | -0.58 | 0.00 | 81 | 291.06 | 4.36 | 2 | 0.00 | 28.67 |
| 18 | 113.62 | -1.23 | 0.81 | -0.59 | 0.00 | 82 | 298.69 | 4.53 | 2.02 | 0.02 | 29.79 |
| 19 | 112.02 | -1.36 | 0.81 | -0.60 | 0.00 | 83 | 305.92 | 4.69 | 2.04 | 0.04 | 30.86 |
| 20 | 111.97 | -1.47 | 0.81 | -0.61 | 0.00 | 84 | 312.81 | 4.86 | 2.04 | 0.05 | 31.85 |
| 21 | 111.87 | -1.58 | 0.82 | -0.62 | 0.00 | 85 | 319.12 | 5.04 | 2.04 | 0.06 | 32.72 |
| 22 | 111.94 | -1.67 | 0.82 | -0.62 | 0.00 | 86 | 325.07 | 5.20 | 2.04 | 0.06 | 33.49 |
| 23 | 112.04 | -1.75 | 0.82 | -0.62 | 0.00 | 87 | 330.59 | 5.34 | 2.03 | 0.07 | 34.18 |
| 24 | 112.36 | -1.81 | 0.83 | -0.63 | 0.00 | 88 | 335.42 | 5.48 | 2.02 | 0.07 | 34.73 |
| 25 | 112.86 | -1.86 | 0.84 | -0.63 | 0.00 | 89 | 339.33 | 5.59 | 2.01 | 0.06 | 35.12 |
| 26 | 113.21 | -1.89 | 0.84 | -0.63 | 0.00 | 90 | 342.29 | 5.68 | 2 | 0.06 | 35.24 |
| 27 | 112.69 | -1.90 | 0.84 | -0.63 | 0.00 | 91 | 344.40 | 5.75 | 2 | 0.06 | 35.36 |
| 28 | 112.67 | -1.90 | 0.85 | -0.62 | 0.00 | 92 | 345.68 | 5.80 | 1.99 | 0.06 | 35.47 |
| 29 | 112.29 | -1.88 | 0.85 | -0.62 | 0.00 | 93 | 347.03 | 5.83 | 1.99 | 0.06 | 35.58 |
| 30 | 112.01 | -1.83 | 0.85 | -0.62 | 0.00 | 94 | 347.17 | 5.83 | 1.99 | 0.06 | 35.65 |
| 31 | 111.57 | -1.77 | 0.84 | -0.61 | 0.00 | 95 | 346.07 | 5.80 | 1.99 | 0.06 | 35.65 |
| 32 | 111.80 | -1.69 | 0.84 | -0.60 | 0.00 | 96 | 344.22 | 5.75 | 2 | 0.06 | 35.56 |
| 33 | 111.28 | -1.59 | 0.84 | -0.59 | 0.00 | 97 | 341.63 | 5.68 | 2 | 0.06 | 35.44 |
| 34 | 110.81 | -1.46 | 0.83 | -0.58 | 0.00 | 98 | 338.75 | 5.58 | 2 | 0.06 | 35.34 |
| 35 | 111.34 | -1.32 | 0.83 | -0.57 | 0.00 | 99 | 331.98 | 5.47 | 2 | 0.06 | 34.40 |
| 36 | 111.35 | -1.17 | 0.82 | -0.56 | 0.00 | 100 | 327.16 | 5.34 | 1.99 | 0.05 | 34.13 |
| 37 | 111.88 | -0.99 | 0.82 | -0.55 | 0.00 | 101 | 320.91 | 5.19 | 1.97 | 0.04 | 33.56 |
| 38 | 112.02 | -0.81 | 0.82 | -0.54 | 0.00 | 102 | 313.65 | 5.02 | 1.95 | 0.03 | 32.70 |
| 39 | 113.90 | -0.62 | 0.81 | -0.52 | 0.00 | 103 | 305.59 | 4.84 | 1.92 | 0.01 | 31.73 |
| 40 | 117.01 | -0.40 | 0.81 | -0.50 | 0.00 | 104 | 296.82 | 4.66 | 1.88 | -0.01 | 30.59 |
| 41 | 121.54 | -0.20 | 0.81 | -0.48 | 0.00 | 105 | 287.60 | 4.47 | 1.82 | -0.04 | 29.32 |
| 42 | 126.55 | 0.00 | 0.81 | -0.46 | 0.00 | 106 | 278.02 | 4.29 | 1.76 | -0.06 | 27.88 |
| 43 | 131.82 | 0.20 | 0.81 | -0.44 | 0.00 | 107 | 268.27 | 4.10 | 1.69 | -0.09 | 26.34 |
| 44 | 136.89 | 0.40 | 0.8 | -0.42 | 0.00 | 108 | 258.46 | 3.92 | 1.61 | -0.12 | 24.80 |
| 45 | 141.20 | 0.60 | 0.79 | -0.39 | 0.00 | 109 | 249.17 | 3.75 | 1.53 | -0.14 | 23.23 |
| 46 | 145.36 | 0.79 | 0.78 | -0.37 | 0.57 | 110 | 240.31 | 3.58 | 1.44 | -0.17 | 21.64 |
| 47 | 148.58 | 0.97 | 0.75 | -0.34 | 1.89 | 111 | 231.92 | 3.41 | 1.35 | -0.19 | 20.14 |
| 48 | 152.56 | 1.14 | 0.72 | -0.32 | 3.35 | 112 | 224.02 | 3.25 | 1.27 | -0.21 | 18.81 |
| 49 | 157.19 | 1.30 | 0.69 | -0.30 | 4.48 | 113 | 217.31 | 3.10 | 1.18 | -0.23 | 17.35 |
| 50 | 161.44 | 1.44 | 0.65 | -0.28 | 5.59 | 114 | 211.06 | 2.96 | 1.09 | -0.24 | 16.17 |
| 51 | 165.41 | 1.57 | 0.6 | -0.27 | 6.68 | 115 | 205.39 | 2.82 | 1.01 | -0.25 | 15.12 |
| 52 | 168.83 | 1.69 | 0.56 | -0.26 | 7.52 | 116 | 200.32 | 2.70 | 0.93 | -0.26 | 14.17 |
| 53 | 171.71 | 1.79 | 0.5 | -0.25 | 8.10 | 117 | 195.93 | 2.59 | 0.85 | -0.26 | 13.32 |
| 54 | 174.00 | 1.87 | 0.45 | -0.24 | 8.51 | 118 | 192.15 | 2.50 | 0.77 | -0.26 | 12.61 |
| 55 | 175.64 | 1.94 | 0.41 | -0.24 | 8.80 | 119 | 189.03 | 2.41 | 0.7 | -0.26 | 12.02 |
| 56 | 176.61 | 2.00 | 0.38 | -0.23 | 9.00 | 120 | 186.49 | 2.32 | 0.62 | -0.26 | 11.52 |
| 57 | 177.00 | 2.06 | 0.37 | -0.22 | 9.10 | 121 | 184.60 | 2.23 | 0.55 | -0.26 | 10.92 |
| 58 | 177.39 | 2.12 | 0.38 | -0.21 | 9.09 | 122 | 182.57 | 2.13 | 0.48 | -0.26 | 10.55 |
| 59 | 178.68 | 2.17 | 0.41 | -0.21 | 9.21 | 123 | 180.37 | 2.03 | 0.41 | -0.25 | 10.14 |
| 60 | 180.30 | 2.22 | 0.46 | -0.21 | 9.64 | 124 | 178.03 | 1.92 | 0.35 | -0.25 | 9.59 |
| 61 | 182.09 | 2.27 | 0.51 | -0.21 | 10.11 | 125 | 175.59 | 1.82 | 0.31 | -0.25 | 8.93 |
| 62 | 184.03 | 2.33 | 0.57 | -0.21 | 10.65 | 126 | 173.08 | 1.71 | 0.28 | -0.25 | 8.20 |
| 63 | 186.22 | 2.40 | 0.64 | -0.21 | 11.39 | 127 | 170.54 | 1.61 | 0.28 | -0.25 | 7.45 |
| 64 | 189.17 | 2.47 | 0.72 | -0.22 | 11.99 | 128 | 168.01 | 1.50 | 0.29 | -0.25 | 6.69 |

Appendix F Estimation of Lubrication Regime Based on Replica of Implant during Worst-case Scenarios

(a) Schematic diagram of articulating surfaces and condition of the environment



(b) Biomaterial properties of replica parts

| | Convex UHMWPE (1) | Concave CoCrMo GUR1050 (2) |
|---------------------------------------|---|---|
| Radii, r_x (m) | Potential largest radius (including tolerances) = 0.075 - 0.02 = 0.073 | Potential smallest radius (including tolerances) = 0.075 + 0.02 = 0.077 |
| Elastic moduli, E_x (Pa) | 810.6×10^6 [265] | 210×10^{12} [109] |
| Poisson's ratios, ν_x | 0.540 [265] | 0.3 [109] |
| Areal surface roughness, S_{ax} (m) | Average $S_{a1(ISO)}$ after bedding-in period during ISO18192-1 [1] = 3.69×10^{-7} Average $S_{a1(ADL)}$ after bedding-in period during ADL Flexion/Extension = 3.72×10^{-7} | S_{a2} at the beginning = 5.00×10^{-8} Previous studies have shown no statistical significant changes of CoCrMo surface roughness after wear simulation [256]. |

(c) Wear simulation parameters

| | ISO18192-1 [1] (ISO) | ADL Flexion/Extension (ADL) |
|---|---|---|
| Lubricant viscosity, η_x (Pa.s) | | 0.00075 [258] |
| Angular velocity, ω_x (rad/s) | Angular velocity in flexion/extension direction = 0.00822 | Angular velocity in flexion/extension direction = 0.00455 |
| | N.B. For worst-case scenario, angular velocity values are chosen from the highest magnitude from second derivative of angular displacement ' time curve as well as its corresponding load, W_x , value (row below). Other values that have been used in academic literature are 0.3 and 4.5 [110, 266]. | |
| Load, W_x (N) | Load at maximum angular velocity = 100 N | Load at maximum angular velocity = 289.10 N |

(d) Formulated calculations

- (Reciprocal) Equivalent Radius, $\frac{1}{R'}$

$$\frac{1}{R'} = \frac{1}{r_1} - \frac{1}{r_2}$$

$$\frac{1}{R'} = \frac{1}{0.073} - \frac{1}{0.077}$$

$$\frac{1}{R'} = \mathbf{0.712}$$

- (Reciprocal) Equivalent Elastic Modulus, $\frac{1}{E'}$

$$\frac{1}{E'} = 0.5 \left(\frac{1 - \nu_1^2}{E_1} + \frac{1 - \nu_2^2}{E_2} \right)$$

$$\frac{1}{E'} = 0.5 \left(\frac{1 - 0.54^2}{810.6 \times 10^6} + \frac{1 - 0.3^2}{210 \times 10^{12}} \right)$$

$$\frac{1}{E'} = \mathbf{4.39 \times 10^{-10}}$$

- Entraining velocity, u

$$u_{\text{ISO}} = \frac{\omega_{\text{ISO}} r_1}{2}$$

$$u_{\text{ISO}} = \frac{0.00822 \times 0.073}{2}$$

$$u_{\text{ISO}} = \mathbf{3.00 \times 10^{-4}}$$

$$u_{\text{ADL}} = \frac{\omega_{\text{ADL}} r_1}{2}$$

$$u_{\text{ADL}} = \frac{0.00455 \times 0.073}{2}$$

$$u_{\text{ADL}} = \mathbf{1.66 \times 10^{-4}}$$

- Theoretical minimum film thickness, h_{min}

$$h_{\text{min(ISO)}} = 2.798R' \left(\frac{\eta u_{\text{ISO}}}{E'R'} \right)^{0.65} \left(\frac{W_{\text{ISO}}}{E'R'^2} \right)^{-0.21}$$

$$h_{\text{min(ISO)}} = \left(\frac{2.798}{0.712} \right) (0.00075 \times 3.00 \times 10^{-4} \times 0.712 \times 4.391 \times 10^{-10})^{0.65} (150 \times 0.712 \times 4.391 \times 10^{-10} \times 4.391 \times 10^{-10})^{-0.21}$$

$$h_{\text{min(ISO)}} = \mathbf{5.04 \times 10^{-9}}$$

$$h_{\text{min(ADL)}} = 2.798R' \left(\frac{\eta u_{\text{ADL}}}{E'R'} \right)^{0.65} \left(\frac{W_{\text{ADL}}}{E'R'^2} \right)^{-0.21}$$

$$h_{\text{min(ADL)}} = \left(\frac{2.798}{0.712} \right) (0.00075 \times 1.66 \times 10^{-4} \times 0.712 \times 4.391 \times 10^{-10})^{0.65} (289.10 \times 0.712 \times 4.391 \times 10 \times 10^{-10} \times 4.391 \times 10^{-10})^{-0.21}$$

$$h_{\text{min(ADL)}} = \mathbf{2.74 \times 10^{-9}}$$

- Compound Surface Roughness, σ

$$\sigma_{\text{ISO}} = \sqrt{S_{a1(\text{ISO})}^2 + S_{a2}^2}$$

$$\sigma_{\text{ISO}} = \sqrt{(3.66 \times 10^{-7})^2 + (5.00 \times 10^{-8})^2}$$

$$\sigma_{\text{ISO}} = \mathbf{3.69 \times 10^{-7}}$$

$$\sigma_{\text{ADL}} = \sqrt{S_{a1(\text{ADL})}^2 + S_{a2}^2}$$

$$\sigma_{\text{ADL}} = \sqrt{(3.68 \times 10^{-7})^2 + (5.00 \times 10^{-8})^2}$$

$$\sigma_{\text{ADL}} = \mathbf{3.72 \times 10^{-7}}$$

- Lambda Ratio, λ

$$\lambda_{\text{ISO}} = \frac{h_{\text{min (ISO)}}}{\sigma_{\text{ISO}}}$$

$$\lambda_{\text{ISO}} = \frac{5.04 \times 10^{-9}}{3.69 \times 10^{-7}}$$

$$\lambda_{\text{ISO}} = \mathbf{0.0137}$$

$$\lambda_{\text{ADL}} = \frac{h_{\text{min (ADL)}}}{\sigma_{\text{ADL}}}$$

$$\lambda_{\text{ADL}} = \frac{2.74 \times 10^{-9}}{3.72 \times 10^{-7}}$$

$$\lambda_{\text{ADL}} = \mathbf{0.00739}$$

Appendix G Permissions for Reproduction of Copyrighted Images

Figure 1.1 The national incidence of (a) lumbar and (b) cervical total disc replacements in the United States between 2005 to 2017 [7] is reproduced under the terms of Creative Commons Attribution-NonCommercial-NoDerivs 4.0 License.

Figure 2.6 Constraining classification for cervical disc implants; (a) non-conformal gliding surfaces, (b) different articulating couplings, and (c) deformable core [68]

| ELSEVIER LICENSE TERMS AND CONDITIONS | |
|--|---|
| | Jun 24, 2024 |
| This Agreement between Faizal Kamarol Zaman ("You") and Elsevier ("Elsevier") consists of your license details and the terms and conditions provided by Elsevier and Copyright Clearance Center. | |
| License Number | 5815450379417 |
| License date | Jun 24, 2024 |
| Licensed Content Publisher | Elsevier |
| Licensed Content Publication | Clinical Biomechanics |
| Licensed Content Title | Biomechanical studies on cervical total disc arthroplasty: A literature review |
| Licensed Content Author | Fabio Galbusera, Chiara M. Bellini, Marco Brayda-Bruno, Maurizio Fornari |
| Licensed Content Date | Nov 1, 2008 |
| Licensed Content Volume | 23 |
| Licensed Content Issue | 9 |
| Licensed Content Pages | 10 |
| Start Page | 1095 |
| End Page | 1104 |
| Type of Use | reuse in a thesis/dissertation |
| Portion | figures/tables/illustrations |
| Number of figures/tables/illustrations | 1 |
| Format | both print and electronic |
| Are you the author of this Elsevier article? | No |
| Will you be translating? | No |
| Title of new work | Investigation of wear in cervical total disc replacement under loads and motions that represent activities of daily living |
| Institution name | University of Leeds |
| Expected presentation date | Jul 2024 |
| Portions | Fig. 1 |
| The Requesting Person / Organization to Appear on the License | Faizal Kamarol Zaman |
| Requestor Location | Mohamad Faizal Kamarol Zaman University of Leeds Leeds, LS2 9JT United Kingdom Attn: Dr. Faizal Kamarol Zaman |
| Publisher Tax ID | GB 494 6272 12 |
| Total | 0.00 GBP |

Figure 2.13 Box-and-whisker plot of statistical analysis between ISO and ASTM wear testing protocols [121]

| SPRINGER NATURE LICENSE TERMS AND CONDITIONS | |
|--|---|
| Nov 23, 2023 | |
| <p>This Agreement between Dr. Faizal Kamarol Zaman ("You") and Springer Nature ("Springer Nature") consists of your license details and the terms and conditions provided by Springer Nature and Copyright Clearance Center.</p> | |
| License Number | 5675040857125 |
| License date | Nov 23, 2023 |
| Licensed Content Publisher | Springer Nature |
| Licensed Content Publication | European Spine Journal |
| Licensed Content Title | Biotribological evaluation of artificial disc arthroplasty devices: influence of loading and kinematic patterns during in vitro wear simulation |
| Licensed Content Author | Thomas M. Grupp et al |
| Licensed Content Date | Dec 3, 2008 |
| Type of Use | Thesis/Dissertation |
| Requestor type | academic/university or research institute |
| Format | print and electronic |
| Portion | figures/tables/illustrations |
| Number of figures/tables/illustrations | 1 |
| Will you be translating? | no |
| Circulation/distribution | 1 - 29 |
| Author of this Springer Nature content | no |
| Title of new work | Investigation of wear in cervical total disc replacement under loads and motions that represent activities of daily living |
| Institution name | University of Leeds |
| Expected presentation date | Dec 2023 |
| Portions | Fig. 5 |
| Requestor Location | Dr. Faizal Kamarol Zaman University of Leeds |
| | Leeds, LS2 9JT United Kingdom Attn: Dr. Faizal Kamarol Zaman |
| Total | 0.00 USD |

Figure 2.14 Intradiscal load at C5-C6 disc level from a kinematic simulation with superimposed ISO18192 [1] axial load input parameters in red (x-axis not to scale) [100]

ELSEVIER LICENSE TERMS AND CONDITIONS

Nov 23, 2023

This Agreement between Dr. Faizal Kamarol Zaman ("You") and Elsevier ("Elsevier") consists of your license details and the terms and conditions provided by Elsevier and Copyright Clearance Center.

| | |
|--|---|
| License Number | 5675040208432 |
| License date | Nov 23, 2023 |
| Licensed Content Publisher | Elsevier |
| Licensed Content Publication | Journal of Biomechanics |
| Licensed Content Title | Predictive modelling of cervical disc implant wear |
| Licensed Content Author | C.U. de Jongh,A.H. Basson,C. Scheffer |
| Licensed Content Date | Nov 14, 2008 |
| Licensed Content Volume | 41 |
| Licensed Content Issue | 15 |
| Licensed Content Pages | 7 |
| Start Page | 3177 |
| End Page | 3183 |
| Type of Use | reuse in a thesis/dissertation |
| Portion | figures/tables/illustrations |
| Number of figures/tables/illustrations | 1 |
| Format | both print and electronic |
| Are you the author of this Elsevier article? | No |
| Will you be translating? | No |
| Title of new work | Investigation of wear in cervical total disc replacement under loads and motions that represent activities of daily living |
| Institution name | University of Leeds |
| Expected presentation date | Dec 2023 |
| Portions | Fig. 1a |
| Requestor Location | Dr. Faizal Kamarol Zaman University of Leeds Leeds, LS2 9JT United Kingdom Attn: Dr. Faizal Kamarol Zaman GB 494 6272 12 |
| Publisher Tax ID | |
| Total | 0.00 USD |
| Terms and Conditions | |

Figure 2.15 Average of total force at C2 level from 16 subjects during head movement from full flexion to full extension and vice versa [158] and **Figure 3.25** Comparison of cervical axial joint loading at C1-C2 vertebral level from this study (dash lines) superimposed over results from Anderst *et al.* [158] (solid lines).



This is a License Agreement between Faizal Kamarol Zaman ("User") and Copyright Clearance Center, Inc. ("CCC") on behalf of the Rightsholder identified in the order details below. The license consists of the order details, the Marketplace Permissions General Terms and Conditions below, and any Rightsholder Terms and Conditions which are included below.

All payments must be made in full to CCC in accordance with the Marketplace Permissions General Terms and Conditions below.

| | | | |
|------------------|-------------|-------------------|------------------------------------|
| Order Date | 01-Dec-2023 | Type of Use | Republish in a thesis/dissertation |
| Order License ID | 1422482-1 | Publisher Portion | A S M E INTERNATIONAL |
| ISSN | 1528-8951 | | Chart/graph/table/figure |

LICENSED CONTENT

| | | | |
|-------------------|--|------------------|---|
| Publication Title | Journal of biomechanical engineering | Publication Type | e-Journal |
| Article Title | Subject-specific inverse dynamics of the head and cervical spine during in vivo dynamic flexion-extension. | Start Page | 61007 |
| Author/Editor | American Society of Mechanical Engineers. | End Page | 61008 |
| Date | 01/01/1977 | Issue | 6 |
| Language | English | Volume | 135 |
| Country | United States of America | URL | http://ojps.aip.org/ASMEjournals/Biomechanical |
| Rightsholder | American Society of Mechanical Engineers ASME | | |

REQUEST DETAILS

| | | | |
|--|-----------------------------|-----------------------------|----------------------------------|
| Portion Type | Chart/graph/table/figure | Distribution | Worldwide |
| Number of Charts / Graphs / Tables / Figures Requested | 1 | Translation | Original language of publication |
| Format (select all that apply) | Print, Electronic | Copies for the Disabled? | No |
| Who Will Republish the Content? | Author of requested content | Minor Editing Privileges? | Yes |
| Duration of Use | Life of current edition | Incidental Promotional Use? | No |
| Lifetime Unit Quantity | Up to 499 | Currency | GBP |
| Rights Requested | Main product | | |

NEW WORK DETAILS

| | | | |
|-----------------|--|----------------------------|---------------------|
| Title | Investigation of wear in cervical total disc replacement under loads and motions that represent activities of daily living | Institution Name | University of Leeds |
| Instructor Name | Faizal Kamarol Zaman | Expected Presentation Date | 2023-12-31 |

ADDITIONAL DETAILS

| | | | |
|-------------------------------|-----|--|----------------------|
| Order Reference Number | N/A | The Requesting Person / Organization to Appear on the License | Faizal Kamarol Zaman |
|-------------------------------|-----|--|----------------------|

REQUESTED CONTENT DETAILS

| | | | |
|--|--|---|--|
| Title, Description or Numeric Reference of the Portion(s) | Fig. 3 | Title of the Article / Chapter the Portion Is From | Subject-specific inverse dynamics of the head and cervical spine during in vivo dynamic flexion-extension. |
| Editor of Portion(s) | Anderst, William J; Donaldson, William F; Lee, Joon Y; Kang, James D | Author of Portion(s) | Anderst, William J; Donaldson, William F; Lee, Joon Y; Kang, James D |
| Volume / Edition | 135 | Issue, if Republishing an Article From a Serial | 6 |
| Page or Page Range of Portion | 61007-61008 | Publication Date of Portion | 2013-06-01 |

SPECIAL RIGHTSHOLDER TERMS AND CONDITIONS

Permission is granted for the specific use of the ASME Figure 3 ONLY as stated herein and does not permit further use of the materials without proper authorization. As is customary, we request that you ensure proper acknowledgment of the exact sources of this material, the authors, and ASME as original publisher.

Figure 3.16 Mean cervical intervertebral joint excursion during flexion/extension compared against normal cervical kinematics prediction bands between C1 to C4 [185], **Figure 3.17** Mean cervical intervertebral joint excursion during flexion/extension compared against normal cervical kinematics prediction bands between C4 to C7 [185], and **Figure 3.18** Mean cervical intervertebral joint excursion during axial rotation compared against normal cervical kinematics prediction bands between C3 to C7 [185]

ELSEVIER LICENSE TERMS AND CONDITIONS

Nov 23, 2023

This Agreement between Dr. Faizal Kamarol Zaman ("You") and Elsevier ("Elsevier") consists of your license details and the terms and conditions provided by Elsevier and Copyright Clearance Center.

| | |
|--|--|
| License Number | 5675060203880 |
| License date | Nov 23, 2023 |
| Licensed Content Publisher | Elsevier |
| Licensed Content Publication | Journal of Biomechanics |
| Licensed Content Title | Bootstrap prediction bands for cervical spine intervertebral kinematics during in vivo three-dimensional head movements |
| Licensed Content Author | William J Anderst |
| Licensed Content Date | 1 May 2015 |
| Licensed Content Volume | 48 |
| Licensed Content Issue | 7 |
| Licensed Content Pages | 7 |
| Start Page | 1270 |
| End Page | 1276 |
| Type of Use | reuse in a thesis/dissertation |
| Portion | figures/tables/illustrations |
| Number of figures/tables/illustrations | 2 |
| Format | both print and electronic |
| Are you the author of this Elsevier article? | No |
| Will you be translating? | No |
| Title of new work | Investigation of wear in cervical total disc replacement under loads and motions that represent activities of daily living |
| Institution name | University of Leeds |
| Expected presentation date | Dec 2023 |
| Portions | Fig. 1 and Fig. 2 |
| Requestor Location | Dr. Faizal Kamarol Zaman University of Leeds Leeds, LS2 9JT United Kingdom Attn: Dr. Faizal Kamarol Zaman |
| Publisher Tax ID | GB 494 6272 12 |
| Total | 0.00 USD |

Figure 3.22 Activation of deep cervical flexor (DCF, longi colli and longi capitis) during head flexion from neutral position as seen in EMG study [235]

| ELSEVIER LICENSE TERMS AND CONDITIONS | |
|--|--|
| Nov 23, 2023 | |
| <hr/> | |
| This Agreement between Mohamad Faizal Kamarol Zaman ("You") and Elsevier ("Elsevier") consists of your license details and the terms and conditions provided by Elsevier and Copyright Clearance Center. | |
| License Number | 5675071156153 |
| License date | Nov 23, 2023 |
| Licensed Content Publisher | Elsevier |
| Licensed Content Publication | Journal of Electromyography and Kinesiology |
| Licensed Content Title | Further evaluation of an EMG technique for assessment of the deep cervical flexor muscles |
| Licensed Content Author | D. Falla,G. Jull,S. O'Leary,P. Dall'Alba |
| Licensed Content Date | Dec 1, 2006 |
| Licensed Content Volume | 16 |
| Licensed Content Issue | 6 |
| Licensed Content Pages | 8 |
| Start Page | 621 |
| End Page | 628 |
| Type of Use | reuse in a thesis/dissertation |
| Portion | figures/tables/illustrations |
| Number of figures/tables/illustrations | 1 |
| Format | both print and electronic |
| Are you the author of this Elsevier article? | No |
| Will you be translating? | No |
| Title of new work | Investigation of wear in cervical total disc replacement under loads and motions that represent activities of daily living |
| Institution name | University of Leeds |
| Expected presentation date | Dec 2023 |
| Portions | Fig. 4 |
| Requestor Location | Mohamad Faizal Kamarol Zaman University of Leeds |
| Publisher Tax ID | Leeds, LS2 9JT United Kingdom Attn: Dr. Faizal Kamarol Zaman GB 494 6272 12 |
| Total | 0.00 USD |

Figure 3.23 Activation of sternocleidomastoids (SCM_l & _r) during head flexion from neutral position and return as seen in EMG study [236] and **Figure 3.24** Co-contraction ratio during head flexion from neutral position (left dashed box, 0.9) compared to flexed head back to neutral position (right dashed box, 0.1) [236]

| SPRINGER NATURE LICENSE TERMS AND CONDITIONS | |
|---|---|
| Nov 23, 2023 | |
| This Agreement between Mohamad Faizal Kamarol Zaman ("You") and Springer Nature ("Springer Nature") consists of your license details and the terms and conditions provided by Springer Nature and Copyright Clearance Center. | |
| License Number | 5675071456938 |
| License date | Nov 23, 2023 |
| Licensed Content Publisher | Springer Nature |
| Licensed Content Publication | European Journal of Applied Physiology |
| Licensed Content Title | Co-contraction of cervical muscles during sagittal and coronal neck motions at different movement speeds |
| Licensed Content Author | Chih-Hsiu Cheng et al |
| Licensed Content Date | May 14, 2008 |
| Type of Use | Thesis/Dissertation |
| Requestor type | academic/university or research institute |
| Format | print and electronic |
| Portion | figures/tables/illustrations |
| Number of figures/tables/illustrations | 2 |
| Will you be translating? | no |
| Circulation/distribution | 1 - 29 |
| Author of this Springer Nature content | no |
| Title of new work | Investigation of wear in cervical total disc replacement under loads and motions that represent activities of daily living |
| Institution name | University of Leeds |
| Expected presentation date | Dec 2023 |
| Portions | Fig. 1 and Fig. 3 |
| Requestor Location | Mohamad Faizal Kamarol Zaman University of Leeds Leeds, LS2 9JT United Kingdom Attn: Dr. Faizal Kamarol Zaman |
| Total | 0.00 USD |

Figure 5.1 Joint contact forces calculated by Snijders *et al.* [157] during flexion/extension. Solid curve line labelled FK represents loading at C2-C3 level. The magnitude can be seen to be dipped lower than 50 N between (-)30° and (-)60° head extension.

ELSEVIER LICENSE TERMS AND CONDITIONS

Jun 24, 2024

This Agreement between Faizal Kamarol Zaman ("You") and Elsevier ("Elsevier") consists of your license details and the terms and conditions provided by Elsevier and Copyright Clearance Center.

| | |
|---|---|
| License Number | 5815450746985 |
| License date | Jun 24, 2024 |
| Licensed Content Publisher | Elsevier |
| Licensed Content Publication | Journal of Biomechanics |
| Licensed Content Title | A biomechanical model for the analysis of the cervical spine in static postures |
| Licensed Content Author | C.J. Snijders,G.A. Hoek van Dijke,E.R. Roosch |
| Licensed Content Date | Jan 1, 1991 |
| Licensed Content Volume | 24 |
| Licensed Content Issue | 9 |
| Licensed Content Pages | 10 |
| Start Page | 783 |
| End Page | 792 |
| Type of Use | reuse in a thesis/dissertation |
| Portion | figures/tables/illustrations |
| Number of figures/tables/illustrations | 1 |
| Format | both print and electronic |
| Are you the author of this Elsevier article? | No |
| Will you be translating? | No |
| Title of new work | Investigation of wear in cervical total disc replacement under loads and motions that represent activities of daily living |
| Institution name | University of Leeds |
| Expected presentation date | Jul 2024 |
| Portions | Fig. 7a |
| The Requesting Person / Organization to Appear on the License | Faizal Kamarol Zaman |
| Requestor Location | Mohamad Faizal Kamarol Zaman University of Leeds Leeds, LS2 9(JT) United Kingdom Attn: Dr. Faizal Kamarol Zaman |
| Publisher Tax ID | GB 494 6272 12 |
| Total | 0.00 GBP |
| Terms and Conditions | |

INTRODUCTION

1. The publisher for this copyrighted material is Elsevier. By clicking "accept" in connection with completing this licensing transaction, you agree that the following terms and conditions apply to this transaction (along with the Billing and Payment terms and conditions established by Copyright Clearance Center, Inc. ("CCC"), at the time that you opened your RightsLink account and that are available at any time at <https://myaccount.copyright.com>).

GENERAL TERMS

- Elsevier hereby grants you permission to reproduce the aforementioned material subject to the terms and conditions indicated.
- Acknowledgement: If any part of the material to be used (for example, figures) has appeared in our publication with credit or acknowledgement to another source, permission must also be sought from that source. If such permission is not obtained then that material may not be included in your publication/copies. Suitable acknowledgement to the source must be made, either as a footnote or in a reference list at the end of your publication, as follows:
"Reprinted from Publication title, Vol /edition number, Author(s), Title of article / title of chapter, Pages No., Copyright (Year), with permission from Elsevier [OR APPLICABLE SOCIETY COPYRIGHT OWNER]." Also Lancet special credit - "Reprinted from The Lancet, Vol. number, Author(s), Title of article, Pages No., Copyright (Year), with permission from Elsevier."
- Reproduction of this material is confined to the purpose and/or media for which permission is hereby given. The material may not be reproduced or used in any other way, including use in combination with an artificial intelligence tool (including to train an algorithm, test, process, analyse, generate output and/or develop any form of artificial intelligence tool), or to create any derivative work and/or service (including resulting from the use of artificial intelligence tools).